[redacted]

MARTIN MARIETTA ENERGY SYSTEMS LIBRARIES
3 4456 0049748 8

LIBRARY
CTION

AEC RESEARCH AND DEVELOPMENT REPORT

ORNL-2057
Progress

cy. 8

DECLASSIFIED
CLASSIFICATION CHANGED TO:
BY AUTHORITY OF: E. J. Murphy 12-2-59
BY: J. Petska 2/25/59

HOMOGENEOUS REACTOR PROJECT

QUARTERLY PROGRESS REPORT

FOR PERIOD ENDING JANUARY 31, 1956

CENTRAL RESEARCH LIBRARY
DOCUMENT COLLECTION
LIBRARY LOAN COPY
DO NOT TRANSFER TO ANOTHER PERSON
If you wish someone else to see this document, send in name with document and the library will arrange a loan.

This document contains Confidential Restricted Data relating to Civilian Applications of Atomic Energy.

OAK RIDGE NATIONAL LABORATORY
OPERATED BY
UNION CARBIDE NUCLEAR COMPANY
A Division of Union Carbide and Carbon Corporation
UCC
POST OFFICE BOX P · OAK RIDGE, TENNESSEE

[redacted]

[redacted]

[redacted]

ORNL-2057

COPY NO. 8

Contract No. W-7405-eng-26

HOMOGENEOUS REACTOR PROJECT

QUARTERLY PROGRESS REPORT

For Period Ending January 31, 1956

Project Director – J. A. Swartout
Associate Director – C. E. Winters

Homogeneous Reactor Test – S. E. Beall
Reactor Design and Analysis – R. B. Briggs and J. A. Lane
Engineering Development – J. A. Lane
Corrosion and Materials – E. G. Bohlmann
Chemical Engineering Development – F. R. Bruce
Supporting Chemical Research – E. H. Taylor

Compiled by

H. F. McDuffie
V. K. Hill

DATE RECEIVED BY INFORMATION AND REPORTS DIVISION
(FEBRUARY 15, 1956)

DATE ISSUED

MAR 23 1956

OAK RIDGE NATIONAL LABORATORY
Operated by
UNION CARBIDE NUCLEAR COMPANY
A Division of Union Carbide and Carbon Corporation
Post Office Box P
Oak Ridge, Tennessee

[redacted]

SYSTEMS LIBRARIES

3 4456 0049748 8

[redacted]

[redacted]

[redacted]

INTERNAL DISTRIBUTION

1. C. E. Center
2. Biology Library
3. Health Physics Library
4. Metallurgy Library
5-6. Reactor Experimental Engineering Library
7-9. Central Research Library
10-18. Laboratory Records Dept.
19. Laboratory Records, ORNL R.C.
20. G. Adamson
21. R. Allen
22. S. Beall
23. D. Billington
24. E. Blizard
25. E. Bohlmann
26. C. Borkowski
27. G. Boyd
28. R. Briggs
29. F. Bruce
30. A. D. Callihan
31. W. Cardwell
32. L. Carter
33. H. Cottrell
34. A. Carpie
35. E. Cook
36. H. Cottrell
37. T. E. C
38. E. L. Compere
39. D. D. Cowen
40. S. Cromer
41. F. L. Culler
42. J. S. Culler
43. J. S. Dr
44. W. K. E
45. L. B. E (K-25)
46. D. E. F
47. W. J. F
48. J. H. F Jr.
49. J. L. G
50. W. R. G
51. H. E. G
52. C. B. G
53. J. C. G
54. P. N. H
55. J. W. H
56. C. J. H
57. A. Hollaender
58. A. S. Householder
59. H. K. J
60. G. H. J
61. W. H.
62. P. R.
63. C. P.
64. M. T.
65. R. B.
66. A. S.
67. K.
68. Lane
69. Leuze
70. Lind
71. Lindauer
72. Livingston
73. Lundin
74. N. Lyon
75. L. Marsh (C&CCC, South Charleston)
76. L. Marshall
77. F. McDuffie
78. P. McBride
79. A. McNees
80. R. McWherter
81. Menis
82. C. Miller
83. K. Morgan
84. E. Murphy
85. E. Nurmi
86. J. Murray (Y-12)
87. L. Parsly
88. H. Poppendiek
89. L. Quarles
90. P. Reyling
91. A. Rom
92. W. Ross
93. H. Savage
94. C. Secoy
95. C. Segaser
96. E. Shipley
97. M. Skinner
98. R. Stoughton
99. A. Snell
100. I. S
101. C.
102. J. A

[redacted]

[redacted]

103. E. H. Taylor
104. D. G. Thomas
105. R. F. Thomason
106. Tobias
107. S. Toomb
108. F. Unger
109. R. n Winkle
110. B. ver
111. A. M. inberg
112. T. A. ton
113. E. P. W r (consultant)
114. G. C. Will ns
115. C. Wilson
116. F. Winters
117. VonderLage
118. F. app
119. J. E. ker
120. H. O. D
121. W. J. Le d
122. M. L. Pick imer
123. ORNL – Y-12 echnical Library, Document Re ence Section
124. HRP Director's ce, Y-12

EXTERNAL DISTRIBUTION

125. AF Plant Representative, Burbank
AF Plant Representative, Marietta
127-12 AF Plant Representative, Seattle
129 F Plant Representative, Wood-Ridge
130. craft Laboratory Design Branch (WADC)
131. P Project Office, Fort Worth
132. A Products, Inc.
133-144. Ar ne National Laboratory
145. Arm Forces Special Weapons Project, Sandia
146. Arm Forces Special Weapons Project, Washington
147. Army emical Center
148-151. Atomi ergy Commission, Washington
152. Battell emorial Institute
153-158. Bettis P t (WAPD)
159-161. Brookhav National Laboratory
162. Bureau of s
163. Chicago Op tions Office
164. Chicago Pat Group
165. Chief of Nav esearch
166. Combustion E eering, Inc. (CERD)
167. Department of t Navy – Op-362
168-171. duPont Company iken
172. duPont Company, mington
173. Duquesne Light C any
174. Engineer Research Development Laboratories
175-176. General Electric Co y (ANPD)
177-184. General Electric Com , Richland
185. Hanford Operations Of
186. Headquarters, Air Force ecial Weapons Center
187. Iowa State College
188-191. Knolls Atomic Power Labo ry
192-195. Los Alamos Scientific Labo ry
196. Massachusetts Institute of T ology (Benedict)
197. Materials Laboratory (WADC)
198. Materials Laboratory Plans Offi WADC)
199. Mound Laboratory

[redacted]

[redacted]

[redacted]00. National Advisory Committee for Aeronautics, Cleveland
[redacted] National Advisory Committee for Aeronautics, Washington
202-2[redacted] Naval Research Laboratory
204-205. [redacted]w York Operations Office
206. N[redacted] American Aviation, Inc.
207. Nuc[redacted] Development Corporation
208. Nuclea[redacted]tals, Inc.
209. Office o[redacted] Quartermaster General
210. Patent Bra[redacted] Washington
211-217. Phillips Petr[redacted]n Company (NRTS)
218. Powerplant Lab[redacted]ry (WADC)
219. San Francisco Op[redacted]ons Office
220. Sylvania Electric Pr[redacted]ts, Inc.
221. USAF Project RAND
222. U. S. Naval Postgraduate [redacted]ol
223. University of California Ra[redacted]n Laboratory, Berkeley
224. University of California Radia[redacted] Laboratory, Livermore
225. Vitro Engineering Division
226. Vitro Laboratories
227. Division of Research and Developmen[redacted]C, ORO
228-542. Technical Information Extension, Oak Ri[redacted]ge

[redacted]

[redacted]

Reports previously issued in this series are as follows:

ORNL-527	Date issued, December 28, 1949
ORNL-630	Period Ending February 28, 1950
ORNL-730	Feasibility Report – Date Issued, July 6, 1950
ORNL-826	Period Ending August 31, 1950
ORNL-925	Period Ending November 30, 1950
ORNL-990	Period Ending February 28, 1951
ORNL-1057	Period Ending May 15, 1951
ORNL-1121	Period Ending August 15, 1951
ORNL-1221	Period Ending November 15, 1951
ORNL-1280	Period Ending March 15, 1952
ORNL-1318	Period Ending July 1, 1952
ORNL-1424	Period Ending October 1, 1952
ORNL-1478	Period Ending January 1, 1953
ORNL-1554	Period Ending March 31, 1953
ORNL-1605	Period Ending July 31, 1953
ORNL-1658	Period Ending October 31, 1953
ORNL-1678	Period Ending January 31, 1954
ORNL-1753	Period Ending April 30, 1954
ORNL-1772	Period Ending July 31, 1954
ORNL-1813	Period Ending October 31, 1954
ORNL-1853	Period Ending January 31, 1955
ORNL-1895	Period Ending April 30, 1955
ORNL-1943	Period Ending July 31, 1955
ORNL-2004	Period Ending October 31, 1955

[redacted]

[redacted]

HRP QUARTERLY PROGRESS REPORT

SUMMARY

PART I. HOMOGENEOUS REACTOR TEST

1. HRT Operations

During the past quarter the installation of blanket and fuel low-pressure systems was completed, and fewer than 1% of the welds were rejected in a total of approximately 1500 welds. A difficulty resulting from excessive tolerances in the specifications for ring-joint flanges was resolved by remachining 250 flanges. The reactor heat-removal system was completed by the contractor.

The results of tests conducted on the fuel and blanket low-pressure assemblies are reported. Entrainment during dumping was corrected, and entrainment during normal operations appears acceptable. Difficulties resulting from flooding of the recombiner-condenser appear to be correctable by installation of a valve downstream of the condenser. The effectiveness of aluminum foil insulation is less than was expected. As a result, additional layers of foil are recommended. The recombiners performed satisfactorily, although back flashes were not eliminated.

2. HRT Design

During this quarter, designs were completed for installation of HRT instrument cubicle piping, oxygen supply system, waste evaporator system, off-gas system, and electrical conduits. A new design for fuel and blanket pressurizers was completed, utilizing steam pressurization, and a study of a gas pressurization system was initiated. Two additional purge pumps were added to the system, and other minor revisions were made.

Tests were completed to determine procedures for placing barytes aggregate–water mixtures in the thermal shields and in the north wall. It was found that lateral pressures exerted by the mixture compare well with values predicted by adding hydrostatic head to Janssen's pressure based on submerged weight of the aggregate.

3. HRT Component Development

Thrust-bearing shoes made of cast Stellite were proved to be satisfactory in HRT fuel solution in the 400A-1 pump. The thermal-barrier and main-flange gaskets did not leak. Slight corrosion was noted on the thermal-barrier gasket and on the thermal barrier.

After serious leakage, the stainless steel thermal barrier was welded into the 300A-1 pump. No indications of trouble were noted during 150 hr of operation in the mockup.

The four reactor pumps were delivered. They have passed the thermal cycle and 200-hr operational tests at the factory.

Both heat exchangers were completed, and one was delivered to the reactor, after final cleaning at ORNL. The second unit will be cleaned and leak-tested before delivery to the reactor. Field inspection of the mockup (80 kw) heat exchanger indicated that it is in good condition.

The pressure relief valves for balancing pressures between the two HRT pressurizers did not seat properly in tests.

The test model of the HRT purge pump operated for 3600 hr without difficulty. This pump was then installed on the mockup.

Operation of the feed pump on the mockup was not entirely satisfactory. A new feed-pump test loop is being fabricated for further development and long-term operation.

A hinged, aluminum foil assembly was developed for use where insulation must be removed from pipe by remote means.

Operation of the HRT mockup loop for 375 hr, using a gas pressurizer, resulted in an average corrosion rate of 2 mpy. A 145-hr run with the newly designed steam pressurizer was apparently satisfactory, but longer operation is needed for conclusive evidence.

4. HRT Reactor Analysis

The pressure rise within the HRT core was calculated as a function of time following complete stoppage of core heat removal. With no fluid discharge from the high-pressure system, the pressure would reach 2800 psia in 38 sec and continue to rise until some safety device was actuated. A letdown rate of 2 gpm appears to be sufficient to prevent the pressure from reaching 2800 psia.

The core pressure-time relation during an HRT dump was calculated for various combinations of

[redacted]

[redacted]

heat-generation, heat-removal, and venting conditions. With no initial venting of the core system, the heat exchanger surface became exposed to vapor before the initial overpressure was relieved; this resulted in an extremely rapid drop in pressure to core saturation conditions. If vapor were initially vented from the pressurizer and if the dump valve opened after the overpressure was relieved, the maximum rate of core-pressure decrease would be much lower.

Shielding calculations were made to determine the protection required for the reactor off-gas lines, the charcoal adsorbers, the sampler, and the sample carrier.

Heat production in the thermal shield was recalculated because of design changes. The cooling system for the shield is adequate for all contemplated operating conditions.

5. HRT Controls and Instrumentation

The checking and calibration of components prior to installation are proceeding; tests to date indicate performance in accordance with the design specifications. Two prototype pressurizer-level controllers incorporating different damping mechanisms exhibited stability sufficient for control of the letdown valve. The documentation of design and test information is under way.

6. HRT Fuel Processing Plant

The HRT fuel processing plant will rely on the concentration, by centrifugation, of the insoluble rare-earth fission-product poisons and corrosion products precipitated in the reactor fuel and on a purge of 2 gal per week of reactor fuel to maintain fission-product poisons at a desirably low level. Hydraulic cyclones, operated on a small bypass stream around the reactor heat exchanger, will centrifugally separate the insoluble particles. These will be collected in a $2\frac{1}{2}$-gal accumulation receiver and discharged once each week; this represents the purge rate of the reactor fuel. The discharged purge will be accumulated in shielded carriers, evaporated to recover heavy water, and stored for decay, pending transfer to a solvent-extraction plant for recovery and decontamination of the associated uranium.

Provision is made in the processing facility for sampling the accumulation receiver before it is discharged; however, such sampling will be representative only if the solid particles are less than 20 μ in diameter. A special, heavily shielded carrier, provided to receive the contents from the solids-accumulation receiver, can be transported to a dissolving facility for solution of all the solids and for accurate sampling. The analysis of this sample will be compared with that of the samples taken from the slurry in the accumulation receiver to ascertain the representativeness of the latter sample.

Alternately, a dissolver may be installed in the chemical-processing cell, and each charge from the solids-accumulation receiver dissolved, sampled, and stored for decay as a solution. This procedure, however, would present a serious risk of cross-contamination between the heavy water of the reactor system and the light water of the dissolving equipment; furthermore, the corrosion products (primarily zirconium oxide) are soluble only with difficulty and the common solvents available (HNO_3-HF, H_2SO_4-Ce^{4+}) have not exhibited satisfactory dissolving rates.

The shop fabrication of process equipment components is approximately 50% complete. Process equipment design is approximately 85% complete. The installation of process services has begun.

PART II. REACTOR DESIGN AND ANALYSIS

7. Reactor Analysis

A study of fuel costs was made on power-only reactor systems fueled by UO_2SO_4-Li_2SO_4-D_2O solutions. One-region reactors operating at 330°C and delivering 1000 Mw of thermal energy and 300 Mw of electricity were considered. Fuel costs were obtained for both a 12% inventory charge with a \$40-per-pound cost for D_2O and a 4% inventory charge with a \$28-per-pound cost for D_2O. The minimum asymptotic fuel cost for the higher charge was 2.5 mills/kwhr, which is about the same as that found previously for UO_3-PuO_2-D_2O slurry reactors operating at 280°C. With the lower charge, the fuel cost was reduced by 0.8 mill/kwhr. The optimum reactor diameter was about 14 ft for the higher charge and about 17 ft for the lower charge. In both cases the optimum uranium concentration was about 200 g/liter, and the poison cross section was about 5% of the fission cross section.

Two-group nuclear calculations for two-region, cylindrical thorium breeder reactors were completed for a range of parameter values.

Nuclear calculations were performed for a series of D_2O-moderated thorium breeder reactors by

[redacted]

[redacted]

means of the multigroup, multiregion method. The results were compared with those obtained by the two-group, two-region method. The breeding ratios and critical concentrations obtained by the two methods were in good agreement down to core diameters of about 2.5 ft.

The effective extrapolation distance associated with a pressure vessel was calculated for one-region reactors containing D_2O, U^{235}, and U^{238}. The inside diameter of the pressure vessel, the pressure-vessel thickness, the operating temperature, and the uranium concentration were treated as parameters. The range of extrapolation distances found was 5 to 36 cm. The extrapolation distance decreased with increasing core diameter and increased with increasing pressure-vessel thickness. No simple variation with temperature and uranium concentration was found.

The reactivity change associated with settling of the ThO_2 slurry was calculated for the TBR. For a blanket initially containing 500 g of thorium per liter, an 8.7% increase in reactivity was obtained when the slurry settled to a uniform concentration of 1000 g of thorium per liter. Experimental measurements of settling rates indicate that no reactor safety problem would be involved; however, appreciable changes in operating conditions would accompany slurry settling.

Three Oracle codes were completed: one evaluates the Bessel functions I_0, I_1, J_0, J_1, K_0, K_1; another calculates the Fermi age of mixtures by use of the energy distribution curve for fission neutrons; and the third code calculates the time-dependent behavior of a batch-operated regenerative reactor and evaluates the economics of the associated system.

PART III. ENGINEERING DEVELOPMENT

8. Development of Fuel-System Components

The high-pressure recombiner loop was redesigned and was rebuilt with new pipe. Entrainment separators were installed in the gas-generating cells in order to prevent caustic buildup in the boiler.

Assembly of the flange-test system is complete except for part of the instrumentation.

Battelle Memorial Institute and Syracuse University are continuing their investigations on hydrogen-oxygen reactions.

The 2000-psi, 5-gpm, canned-rotor pump has accumulated over 4000 hr at 300°C with water. A 1000-psi, 5-gpm, canned-rotor pump has operated for about 11,300 hr at 250°C with water. The series-wound, 5-gpm, canned-rotor pump has accumulated 6600 hr of operation. The system was recently altered to permit studies of water injection to the rotor cavity.

Operation of the 4000-gpm loop with a UO_2SO_4 solution containing 5 g of uranium per liter was interrupted when it became impossible to maintain the condensate supply for the seal pump.

Specifications were prepared for purchase of a 500-gpm, canned-rotor pump.

The titanium-lined pipe sections and heat exchanger are in the final design stages. A test rig to subject the lined equipment to thermal and pressure cycles is in the preliminary design stage. A study of the feasibility of roll-cladding titanium to carbon steel is in progress at Armour Research Foundation.

9. Development of Blanket-System Components

Construction of the full-scale, high-pressure blanket mockup is essentially completed.

A statistical analysis of data on the attack of ThO_2 slurries on stainless steel circulating loops indicated that the following factors were important in attack, roughly in the order listed: particle size, velocity of the slurry, oxygen concentration, room temperature pH of the slurry, thorium oxide concentration, and thorium oxide calcination temperature. The results are tentative because of the limited amount of data available.

Modifications of Westinghouse pump 200A were made; tests have indicated that they will be effective in overcoming some of the difficulties encountered with the original pump, and possibly all of them.

A hard cake was deposited during operation of the 200A slurry loop. The characteristics of the cake have been determined, and the mechanism of its formation is being sought.

Study of the race-track type of dump tank indicated further promise; a model of a simpler, cone type of dump tank was designed and is being fabricated.

Very preliminary temperature-profile data indicated the presence, under some conditions, of a central, nonshearing plug in turbulent flow of Bingham plastics.

[redacted]

[redacted]

PART IV. CORROSION AND MATERIALS

10. Solution Corrosion

A number of loop runs were made in order to determine how much sulfuric acid is necessary to stabilize 0.04 *m* uranyl sulfate solutions containing 0.005 *m* copper sulfate at 300°C (HRT conditions) and to determine the corrosiveness of such solutions in the temperature range of 200 to 300°C. It was demonstrated that 0.01 *m* sulfuric acid is not sufficient to prevent hydrolytic precipitation of copper and uranium and that 0.02 *m* is sufficient. Future tests may indicate that less than 0.02 *m* sulfuric acid will be adequate. At 300°C corrosion of stainless steel is not serious, even with 0.02 *m* sulfuric acid, up to flow rates of 45 fps. However, at 200 to 250°C corrosion is more serious, and critical velocities as low as 15 to 20 fps were observed.

Preliminary corrosion tests in a uranyl carbonate–lithium carbonate system showed that the corrosion rates of austenitic and ferritic stainless steels were low, in most cases lower than the rates observed in comparable uranyl sulfate systems. In addition, carbon steel, which is completely dissolved by uranyl sulfate solutions, showed low corrosion rates, 3 to 5 mpy.

Further testing with highly concentrated uranyl sulfate solutions containing added lithium sulfate confirmed previous results concerning the beneficial effects of the lithium sulfate on the corrosion of stainless steel. One loop run was with 3.8 *m* uranyl sulfate and 3.8 *m* lithium sulfate at 350°C and showed the absence of a critical velocity up to 70 fps. Other runs made in toroids gave results similar to those obtained in loop runs. One series of toroid runs demonstrated that cesium sulfate was at least as effective as lithium sulfate and perhaps even more effective. However, both loop and autoclave tests failed to demonstrate the abnormally low vapor pressure previously reported for such solutions. At present, there is no explanation for the erroneous results given in the last quarterly report.

Static corrosion tests showed that type 1515N stainless steel has a corrosion resistance to uranyl sulfate solutions about equal to that of type 347 stainless steel. On the other hand, an antigalling type alloy, designated as Waukesha Metal No. 88, was badly attacked (43 mpy) by uranyl sulfate solutions at 300°C. In boiling 5% nitric acid, corrosion was also severe (32 mpy).

Studies with Iso-Elastic spring alloy which had been gold-plated were carried out. At imperfections in the gold plate, attack was severe enough to allow the gold to peel off. Preliminary tests with another spring alloy, Elgiloy, showed it to be much more resistant than Iso-Elastic and indicated that it may be superior to Iso-Elastic for use in the pressurizer liquid-level controller.

11. Slurry Corrosion

Corrosion data are presented for three slurry runs at 300°C on the 100A pump loop; three different preparations of thorium oxide were used. Average circulating concentrations ranged from 581 to 1075 g of thorium per kilogram of water. Operating problems, including some caking and plugging, are discussed. One water run was also made.

The attack rate by slurries in the pump loop on pin specimens of type 347 stainless steel appeared to be proportional to the slurry concentration and to the square of the flow velocity. Platinum, gold, Zircaloy-2, and titanium appeared to be attacked relatively less severely than stainless steel, which had a pin corrosion rate of 7 mpy at 20 fps and 1000 g of thorium per kilogram of water.

The attack of type 347 stainless steel, titanium 75A, and Zircaloy-2 by circulating slurries prepared from thorium oxide calcined at temperatures from 650 to 1600°C was studied over a range of slurry velocities in toroids. The study showed no correlation between oxide calcination temperature and attack rate.

12. Radiation Corrosion

12.1 In-Pile Loops. – The loop package components were redesigned so the completed loop will fit either beam hole (HB-2 or HB-4) by adjustment of the lengths of two connecting pipes. The new design also makes it possible to operate at pressures up to 2000 psia and at temperatures up to 300°C.

Loop L-4-12 was completed and is in operation in the LITR HB-4 facility. The core section of this loop was fabricated of titanium, type Ti-75A. Loop L-2-10, designed for operation in the LITR HB-2 facility, which will be completed next quarter, was completed and tested.

Approximately two thirds of the components of an in-pile loop to be fabricated entirely of titanium were completed.

The fifth in-pile loop experiment, L-4-8, was completed. The loop operated in-pile for a total

[redacted]

[redacted]

of 1637 hr, during which time the LITR energy output was 4377 Mwhr. The average fission power in the loop based on cesium analyses was 622 w when the LITR was at full power (3 Mw). Based on oxygen data the generalized corrosion rate for the first 300 hr was 4.0 mpy; the rate for the remaining 1337 hr was 0.7 mpy. The nickel data gave parallel results. The corrosion of the type 347 stainless steel, Zircaloy-2, and Ti-55AX coupons exposed in the core and in in-line holders was generally consistent with that observed in previous in-pile-loop experiments. Some differences were attributed to the fact that this was the first loop operated with 0.04 *m* H_2SO_4 present in the uranyl sulfate charge solution (0.17 *m* UO_2SO_4, 0.03 *m* $CuSO_4$).

Stress specimens, made from the alloys Zircaloy-2, 17-4 PH, and Ti-C-130-AM, were exposed in core, in-line, and pressurizer locations. Microscopic examination and average weight loss gave no indication of effects attributable to the stressed condition of the specimens.

12.2 LITR Bomb Tests. – The results of two type 347 stainless steel experiments at the LITR confirmed the results of the similar experiment, H-85, which was previously reported. For each experiment the observed rate was less than 1 mpy over the long periods of exposure. The solution employed with each of these experiments contained small amounts of sulfuric acid. Initial oxygen pressures of about 500 psi in one case and approximately 1500 psi in the other were employed with the experiments.

A corrosion rate of 5.2 mpy was determined from weight-loss data for two titanium 75A pins which were installed in a Zircaloy-2 bomb and exposed at 280°C and at an estimated power density of 17 w/ml.

The corrosion rate observed for two Zircaloy-2 experiments which employed a 1.4 *m* uranyl sulfate solution was appreciably less (8 mpy) than that observed (15 mpy) for an experiment which employed a 0.17 *m* solution; the test conditions for all three experiments were essentially the same, except for the solution concentration.

12.3 MTR Bomb Tests. – Exposure was completed in the MTR of an experiment designed as a test of the effect of reactor radiation alone on the corrosion of Zircaloy-2. The UO_2SO_4 enrichment was such that the power density in solution due to fission was less than 0.02 w/ml. The oxygen data indicate that the corrosion rate at the test temperature of 280°C was about 11 mpy.

12.4 Supporting Research. – A determination of the effect of irradiation by Van de Graaff electrons on the corrosion of Zircaloy-2 by uranyl sulfate solutions was completed. Weight-loss data indicate no significant acceleration of corrosion during a 104-hr exposure at an estimated power density of 20 to 30 w/ml in the solution adjacent to the specimen.

Experiments are in progress to determine the corrosion of type 347 stainless steel by uranyl sulfate solutions which are free of soluble corrosion products of the metal. Data are available from seven experiments at 250°C for which the exposure times ranged from 26 to 221 hr. The data indicate that the corrosion did not decrease from an initial rapid rate until after 96 hr and a penetration of about 0.1 mil.

13. Metallurgy

Spring-tempered Inconel-X stress-corrosion specimens showed no stress corrosion in boiling 42% $MgCl_2$ (154°C) in 316 hr at 70,000-psi stress followed by 196.5 hr at 90,000-psi stress. The tests were terminated by equipment failure.

The results of continued stress-corrosion testing of types 304L and 347 stainless steels at stress levels of 20,000 psi and lower showed a great amount of scatter in fracture times, as much as from 3.4 to 29.5 hr for type 304L at 16,000 psi and from 24 to 103 hr at 15,000 psi for type 347.

Zircaloy-2 specimens, cathodically charged in 1 *N* H_2SO_4 at 250°C for 100 hr, showed a definite accumulation of H_2 of from 50 to 100 ppm.

Metallographic-standard specimens of Zircaloy-2 HRT core-tank material, Zircaloy-2W, crystal-bar zirconium, and Zircaloy-3A, containing from 5 to 1000 ppm of H_2, were prepared. A metallographic technique (anodizing) for the identification and location by color of hydrides in the microstructure was developed. With the use of this technique and the metallographic standards prepared, it was concluded that the hydride forms preferentially in the grain boundaries of the zirconium alloys investigated and within the grains in crystal-bar zirconium.

Specimens of the Zircaloy-2 HRT core-tank material were heat treated to determine the grain-growth rates in the alpha, alpha-plus-beta, and beta fields; the effect of quenching rate on the alpha-prime structure; and the effects of time and

[redacted]

[redacted]

temperature on the annealing of the alpha-prime structure. The rate of grain growth of alpha and of beta is very slow. The beta grain size is apparently established during the heating through the alpha-plus-beta field. The alpha-prime structure is affected by quenching rate primarily in the size of the alpha needles formed – the faster the quenching, the finer the needles.

Fine-grained and randomly oriented, equiaxed alpha structure can be obtained by beta-quenching, cold-rolling, and alpha-annealing. The core-tank material was, as expected, found to have a very highly preferred orientation, such that the mechanical properties are isotropic within the plane of the rolled sheet, showing good ductility, but probably with very little if any ductility in the direction perpendicular to the plane of the sheet.

Subsize tensile specimens of Zircaloy-2, aged for 500, 1085, and 1585 hr at 250°C, were tested at room temperature and at 250°C at two different strain rates (0.01 and 0.1 in./in./min). Results of these tests do not indicate embrittlement due to the various aging cycles employed.

A satisfactory system by which titanium may be welded in air was developed. The protective blanket is obtained from the inert-gas atmosphere around the torch and from the internal purging gas.

Tentative procedures prepared for welding type 347 stainless steel permit the use of preplaced inserts for the root pass and call for the use of a modified rod which yields a fully austenitic deposit.

A technique yielding high-quality inert-gas-shielded arc welds in carbon steel was developed.

PART V. CHEMICAL ENGINEERING DEVELOPMENT

14. Thorium Oxide Slurry Development

Studies of the effect of in-pile irradiation on the properties of thorium oxide slurries continued. Four slurries of thorium oxide, 1000 g of thorium per kilogram of H_2O, containing 0.5 mole % of unenriched UO_3, were irradiated at 300°C in the LITR without apparent damage. Three similar slurries containing enriched uranium were irradiated at 300°C in the ORNL Graphite Reactor. One of these slurries, prepared from oxide previously circulated in a loop, could not be readily rinsed from the irradiation bomb, but the other two appeared to be unchanged by the irradiation. Relative viscosity measurements are being made of thorium oxide slurries in the dash-pot irradiation bomb. For in-pile slurry viscosity measurements a new model of the irradiation bomb, having a coaxial cylinder and a viscosity-sensitive, electromagnetically operated plunger, is under laboratory test. Thorium-uranium mixed oxides prepared by coprecipitation and subsequent thermal decomposition of the tetravalent oxalates had much lower surface areas than did mixed oxides prepared by wet-autoclaving, at 300°C, a mixture of the thorium and uranium oxides.

Oxides of palladium, molybdenum, vanadium, and cerium were studied as catalysts in thorium oxide slurries for the recombination of radiolytic gas. The palladium was the most effective; at 830 ppm concentration based on thorium it gave combination rates more than sufficient to recombine the radiolytic gases expected in the TBR blanket. Molybdenum and vanadium at 0.1 *m* concentration also gave rates sufficiently fast for TBR use. Cerium oxide showed negligible catalytic activity. Copper chromite was not significantly better than copper oxide as a catalyst.

In studies of the effect of pumping selected oxides, the average x-ray crystallite sizes appeared to be relatively unaffected. Particles greater than 1 μ in size were degraded. The hindered-settling rate, particle shape, and particle-size distribution in a slurry of oxide prepared by the thermal decomposition of oxalate, which had been precipitated at 10°C, did not appear to be affected by the pumping.

The function relating crystallite growth to calcination time and temperature was evaluated for the D-16 oxide. The growth results from the presence of a relic or ordered structure. An oxide preparation which had been pumped was heated at elevated temperature; failure of the crystallites to grow indicated that nearly complete degradation of the oxide particles to crystallite dimensions had occurred during pumping.

Slurry hindered-settling rates increased with increasing slurry temperature (to 98°C) and increasing oxide calcination temperature up to 1000°C. High-dispersion characteristics were obtained with oxide calcined at 1300°C.

15. Fuel Processing

Solid particles of neodymium sulfate, suspended in simulated fuel solution in quartz containers, showed no tendency to attach themselves to a hot Zircaloy-2 surface. In high-pressure loops (2000 psi and 300°C) precipitated neodymium sulfate was

[redacted]

[redacted]

found in both the heater and underflow pot, with 80% of the precipitated solids remaining in the heater. Praseodymium sulfate behaved like neodymium sulfate in that its solubility, at a given temperature, increased as the amount of uranyl sulfate in solution increased and decreased as the praseodymium percentage in the precipitating solids decreased.

In quartz tubes the solubility of ruthenium in simulated fuel solution was less than 5 ppm in the presence of air but was greater than 10 ppm with an overpressure of pure oxygen.

The solubility of molybdenum in simulated fuel solution at 265°C was 300 to 400 mg per kilogram of H_2O. In molybdic acid slurries of high concentration, various solid-phase changes were observed.

With improved techniques that gave iodine material balances of 85 to 95%, fuel iodine/iodate ratios were 9/1 at 250°C and 6/1 at 300°C. The ratio was lower in the presence of simulated fission and corrosion products. Dilute silver sulfate solution had a high capacity and an efficiency for scrubbing iodine from a D_2O vapor–oxygen gas stream at 300°C.

Dissolution of solids simulating those expected from HRT-CP operation required a treatment determined by the composition of the solid and its previous history. For solids containing only fission products, 70% HNO_3–0.1% HF was a good dissolvent; for "aged" solids consisting almost entirely of stainless steel corrosion products, HCl and HCl-$SnCl_2$ mixtures were better; when stainless steel and Zircaloy-2 corrosion products constituted the major fraction of the solids, 10.8 *M* sulfuric acid was the best dissolvent. The efficiency of the sulfuric acid solution was not lowered by heating the solids to 300°C prior to dissolution.

16. Plutonium-Producer Blanket Processing

The rate of plutonium adsorption on Zircaloy-2 and on titanium from uranyl sulfate solutions is markedly dependent on plutonium concentration and temperature. The rates of plutonium adsorption on Zircaloy-2 and on titanium from 1.26 *m* UO_2SO_4 containing 100 mg of plutonium per kilogram of H_2O at 250°C were 22 and 11 $\mu g/cm^2/hr$, respectively. When the plutonium concentration was 3 to 6 mg per kilogram of H_2O, adsorption rates for both metals varied between 0.008 and 0.04 $\mu g/cm^2/hr$. Based on these rates, 0.3 to 1.4% of the plutonium produced in a two-region reactor would adsorb on the metal walls. The rate of plutonium adsorption at 150°C from 1.4 *m* UO_2SO_4 containing 4 to 6 mg of plutonium per kilogram of H_2O was 0.008 $\mu g/cm^2/hr$ on titanium and 0.012 $\mu g/cm^2/hr$ on Zircaloy-2, but at 80°C the adsorption rates from a solution containing 13 mg of plutonium per kilogram of H_2O were only 9×10^{-5} $\mu g/cm^2/hr$ on titanium and 2×10^{-5} $\mu g/cm^2/hr$ on Zircaloy-2. At 150 and 250°C, plutonium adsorption was greater on Zircaloy-2 than on titanium but at 23 and 80°C it was greater on titanium.

The nature of plutonium adsorption at room temperature was different from that at elevated temperature: at room temperature the adsorption reaction reached equilibrium, PuO_2 was not present, and the plutonium could be desorbed.

Factors for concentration of PuO_2 from a water slurry at room temperature by centrifugation in a ¼-in.-dia hydroclone with a 35-ml underflow pot varied from 2.6 to 8.8.

When a 1.4 *m* UO_2SO_4 (0.3% U^{235}) solution containing no copper catalyst was irradiated in the LITR at 250°C, there was no significant buildup of radiolytic gas.

The solubility of Pu(IV) at 250°C in 1.3 *m* UO_2SO_4–1.3 *m* Li_2SO_4 solution in pyrex tubes was 5 to 6 mg per kilogram of H_2O; this is about twice the solubility noted in 1.3 *m* UO_2SO_4 solution containing no lithium. The solubility of Pu(IV) at 250°C in 4.0 *m* Li_2SO_4–4.0 *m* UO_2SO_4 solution was 7.8 mg per kilogram of H_2O.

17. Equipment Decontamination

Since fission products and plutonium are bound in the oxide corrosion film deposited on type 347 stainless steel by uranyl sulfate reactor solutions at 250°C, removal of this film is necessary for adequate decontamination and plutonium removal. A chromous sulfate solution appears to be the most applicable of several tested, since it dissolves the oxide film and effectively removes the plutonium and does not add objectionable foreign materials to the reactor system.

A solution containing 0.4 *M* $CrSO_4$–0.2 *M* K_2SO_4–1.0 *M* H_2SO_4 at 87°C (under 5 psig CO_2) dissolved the oxide corrosion film from type 347 stainless steel in 2 hr and dissolved a heavy golden oxide film from titanium in 10 hr. Plutonium decontamination factors for type 347 stainless steel, titanium, and Zircaloy-2 in the chromous sulfate solution at

[redacted]

[redacted]

87°C for 3 to 4 hr were 1.4×10^3, 1.7×10^3, and 1.9×10^3, respectively. Corrosion rates for type 347 stainless steel, titanium, and Zircaloy-2 in this solution at 87°C were 10, 7, and 2 mpy, respectively.

PART VI. SUPPORTING CHEMICAL RESEARCH

18. Aqueous Systems at Elevated Temperatures

18.1 Alkali Metal Carbonate–Uranium Trioxide Systems. – Data for the solubility of Li_2CO_3 in water disclosed the fact that the fourth power of the lithium ion concentration is proportional to the carbon dioxide pressure over a temperature range from 40 to 290°C and at CO_2 pressures from about 200 to 2500 psi. This observation indicates that the principal ionic species in solution are the lithium and the bicarbonate ions. The solubility of UO_3 in such solutions may be accounted for by assuming the existence of complex bicarbonate ions such as $UO_2(HCO_3)(CO_3)_2^{3-}$ and $UO_2(HCO_3)_2(CO_3)_2^{4-}$.

18.2 The Quaternary Systems CuO-UO_3-SO_3-H_2O and NiO-UO_3-SO_3-H_2O. – The 100°C isotherm for the base-saturated region of the system CuO-UO_3-SO_3-H_2O was completed. All solid phases, five in number, were identified, and the liquidus surface was completely defined.

18.3 Stabilization of ThO_2 Sols – Sol E. – A study of the physical and chemical properties of ThO_2 sols was initiated. A particular sol, 2.5 *M* in thorium and stabilized with $Th(NO_3)_4$, was characterized by measurement of its pH, density, and viscosity and by observations based on x-ray analysis and electron micrographs. The thermal stability of the sol decreased upon addition of more $Th(NO_3)_4$ solution. In no case was the thermal stability sufficient to make the sol of interest as a reactor blanket.

18.4 Adsorption of Water Vapor on ThO_2 at Elevated Temperatures. – The determination of isotherms from 260 to 360°C for the adsorption of water on ThO_2 disclosed no evidence for the existence of a stable hydrate.

19. Adsorption on Inorganic Materials

Study of the adsorptive properties of inorganic materials continued. During the last quarter, principal emphasis was centered on evaluation of the stability of the materials under a variety of conditions and on the development of techniques for the estimation of their ultimate capacity. Work is also under way on evaluation of the relative anion-exchange and cation-exchange properties of hydrous oxides, principally those of Zr(IV), Sn(IV), and Th(IV). Application of the hydrated oxides to the adsorption of fluorides from solutions appears to be promising, as well as their use for adsorption of chromates and for chromate analyses.

20. Radiation Studies of Thorium Nitrate Solutions

Preparations for bomb-type experiments for the reactor irradiation of thorium nitrate solutions are nearly complete. The back reaction between oxygen and nitrogen to re-form nitrate will be studied.

21. Protactinium Chemistry

The extraction of tracer Pa^{233} from aqueous solutions of hydrochloric acid by diisobutyl carbinol was found to be dependent strongly upon the molarity of the acid. This was also the case for a previously reported extraction from nitric acid. Measurements were made of the extraction of Pa^{233} from various aqueous solutions by di(2-ethylhexyl)phosphoric acid, a good extractant for uranium and also an extractant for thorium. In preliminary studies of the colloidal behavior of protactinium at very low concentrations, treatment in four different media followed by filtration gave indications that all particles were less than 0.5 μ in diameter.

[redacted]

[redacted]

CONTENTS

SUMMARY vii

PART I. HOMOGENEOUS REACTOR TEST

1. HRT OPERATIONS 3
   - 1.1 Construction 3
     - 1.1.1 Reactor 3
     - 1.1.2 Control Area 3
     - 1.1.3 Reactor Steam System 8
   - 1.2 Operations Testing 8
     - 1.2.1 Fuel Low-Pressure Assembly 8
     - 1.2.2 Blanket Low-Pressure System 10
   - 1.3 Operations Training 10

2. HRT DESIGN 11
   - 2.1 General Status of Design 11
   - 2.2 Zircaloy–Stainless Steel Transition Joint 11
   - 2.3 Steam Pressurization 11
   - 2.4 Gas Pressurization 12
   - 2.5 The Oxygen-Addition System 14
   - 2.6 Purge Pumps 15
   - 2.7 Waste System 15
   - 2.8 Installation of Air-Actuated Valves 15
   - 2.9 High-Pressure Valve Jig 15
   - 2.10 Barytes Aggregate–Water Placement Tests 16

3. HRT COMPONENT DEVELOPMENT 20
   - 3.1 Pump Development 20
     - 3.1.1 400A-1 Pump and Loop 20
     - 3.1.2 300A-1 Pump 20
     - 3.1.3 400A-2 Pump and Loop 22
   - 3.2 Reactor Fuel and Blanket Pumps 22
   - 3.3 HRT Heat Exchangers 22
     - 3.3.1 HRT Heat Exchanger Cleaning 22
     - 3.3.2 HRT Fuel Heat Exchanger Mockup 22
   - 3.4 Pressure-Relief Valves 23
   - 3.5 HRT Purge Pump 23
   - 3.6 HRT Feed Pump 23
   - 3.7 Glass Model of New HRT Pressurizer Design 23
   - 3.8 Removable Insulation 24
   - 3.9 HRT Mockup Loop 25
     - 3.9.1 Present Mockup Flowsheet 25
     - 3.9.2 Gas Pressurization Operation 27
     - 3.9.3 New Steam-Pressurizer Test 29

4. HRT REACTOR ANALYSIS 31
   - 4.1 Pressure Rise Following Stoppage of Heat Removal 31
   - 4.2 HRT Dump Analysis 31
   - 4.3 Miscellaneous Shielding Calculations 33
   - 4.4 Thermal-Shield Temperatures 34

[redacted]

[redacted]

5. HRT CONTROLS AND INSTRUMENTATION 35

5.1 General Status 35
5.2 Liquid-Level Transmitters 35
5.3 Valves and Operators 35
5.3.1 HRT Low-Pressure Valves 35
5.3.2 HRT High-Pressure Valves 38
5.3.3 Dump-Valve Operator 38
5.3.4 Small-Valve Operator 38
5.3.5 Valve-Trim Testing Program 38

6. HRT FUEL PROCESSING PLANT 41

6.1 High-Pressure System 45
6.1.1 Heater (H-3) 47
6.1.2 Screen (F-1) 47
6.1.3 Hydroclone and Underflow Receiver 47
6.1.4 Pump (P-1) 49
6.1.5 Valves, Flanges, and Freeze Plugs 49
6.1.6 Major Instrumentation 50
6.1.7 Sampling 50
6.2 Underflow Pot Cooling System 51
6.3 Low-Pressure System 53
6.3.1 Storage Vessels (Carrier C-1 and C-2) 55
6.3.2 Entrainment Separator (S-2 and S-3) 55
6.3.3 Superheater (H-7 and H-8) 55
6.3.4 Recombiner Condenser (H-1 and H-2) 55
6.3.5 Gage Tank (T-3 and T-4) 56
6.3.6 D_2O Receiver (T-2) 56
6.3.7 Meter Tank (T-5) 56
6.3.8 Sample Carrier (C-3) 56
6.4 Off-Gas Disposal System 57
6.5 Uranium Recovery System 59
6.6 Fuel Addition System 59

PART II. REACTOR DESIGN AND ANALYSIS

7. REACTOR ANALYSIS 63

7.1 Fuel Cost of Power Reactors Fueled by UO_2SO_4-Li_2SO_4-D_2O Solutions 63
7.2 Cylindrical-Reactor Studies 66
7.3 Multigroup, Multiregion Reactor Calculations 66
7.4 Extrapolation-Distance Estimates for Reactor Calculations 68
7.5 Reactivity Changes Associated with Slurry Settling in the TBR 68
7.6 Mathematics and Computations 69
7.6.1 Bessel-Function Code 69
7.6.2 Estimation of Fermi Age by Numerical Integration 69
7.6.3 Time-Dependence Studies 69

[redacted]

[redacted]

PART III. ENGINEERING DEVELOPMENT

8. DEVELOPMENT OF FUEL-SYSTEM COMPONENTS 73
- 8.1 Recombiner Development 73
  - 8.1.1 High-Pressure Recombiner Loop 73
  - 8.1.2 High-Pressure Flange Test 73
  - 8.1.3 Battelle and Syracuse Subcontracts 74
- 8.2 Small Reactor Components 74
  - 8.2.1 20-cfm Canned-Rotor Blower 74
  - 8.2.2 Small Circulating Pumps 74
- 8.3 Large Reactor Components 74
  - 8.3.1 4000-gpm Loop 74
  - 8.3.2 500-gpm Pump 74
- 8.4 Titanium-Lined Equipment 75

9. DEVELOPMENT OF BLANKET-SYSTEM COMPONENTS 76
- 9.1 Slurry Blanket Mockup 76
- 9.2 Attack of Circulating Aqueous ThO_2 Slurries on Stainless Steel Systems 76
- 9.3 Slurry Component Development and Loop Operation 78
  - 9.3.1 Westinghouse Slurry Pump 200A 78
  - 9.3.2 Caking During Operation of Slurry Loop 200A 80
  - 9.3.3 Dump-Tank Evaporator Tests 80
  - 9.3.4 Heat-Transfer Studies 81

PART IV. CORROSION AND MATERIALS

10. SOLUTION CORROSION 85
- 10.1 Pump Loops 85
- 10.2 Toroids 86
- 10.3 Laboratory Tests 86

11. SLURRY CORROSION 88
- 11.1 Pump Loops 88
- 11.2 Toroids 90

12. RADIATION CORROSION 91
- 12.1 In-Pile Loops 91
  - 12.1.1 Development and Construction 91
  - 12.1.2 General Description of In-Pile Loop Experiment, L-4-8 92
  - 12.1.3 Qualitative Results of Inspection and Evaluation of Loop L-4-8 94
  - 12.1.4 Quantitative Results of Inspection and Evaluation of Loop L-4-8 94
- 12.2 LITR Bomb Tests 96
- 12.3 MTR Bomb Tests 98
- 12.4 Supporting Research 98
  - 12.4.1 Van de Graaff Accelerator Tests 98
  - 12.4.2 Corrosion of Stainless Steel by Uranyl Sulfate Solutions Free of Stainless Steel Corrosion Products 99

[redacted]

[redacted]

13. METALLURGY 101

13.1 Physical Metallurgy 101
13.1.1 Effects of Hydrogen on Zirconium and Its Alloys 101
13.1.2 Development of Zirconium Alloys 102
13.1.3 Nature of Zirconium Oxide Films 104
13.1.4 Stress-Corrosion Testing 104
13.2 Mechanical Metallurgy of Titanium and Zirconium and Their Respective Alloys 104
13.2.1 Commercial Titanium 104
13.2.2 Zircaloy-2 105
13.3 Welding Development 105
13.3.1 Titanium Welding Development 105
13.3.2 Welding of Stainless Steel by Using Preplaced Inserts for the Root Pass 105
13.3.3 Inert-Gas-Shielded Arc Welding of Type 347 Stainless Steel with Fully Austenitic Filler Metal 105
13.3.4 Inert-Gas-Shielded Arc Welding of Carbon Steel 105
13.4 Effects of Radiation on Structural Metals and Alloys 106

PART V. CHEMICAL ENGINEERING DEVELOPMENT

14. THORIUM OXIDE SLURRY DEVELOPMENT 109

14.1 Thorium Oxide Slurry Irradiation Studies 109
14.1.1 Slurry Irradiations in the LITR 109
14.1.2 Slurry Irradiations in the Graphite Reactor 109
14.1.3 Postirradiation Examination of Slurries 109
14.1.4 Slurry Viscosity Measurements in the Irradiation Bombs 109
14.1.5 Preparation of Thorium-Uranium Mixed Oxides 112
14.2 Gas-Recombination Studies 113
14.3 Laboratory Studies on Thorium Oxide Slurries 115
14.3.1 Properties of Pumped Oxides 115
14.3.2 Crystallite Growth in Thorium Oxide 115
14.3.3 Hindered-Settling Properties of Thorium Oxide Slurries 118

15. FUEL PROCESSING 122
15.1 Fission- and Corrosion-Product Chemistry 122
15.1.1 Rare Earths 122
15.1.2 Zirconium 122
15.1.3 Ruthenium 122
15.1.4 Molybdenum 122
15.1.5 Iodine 123
15.2 Reactor Solids Dissolution 123
15.3 Test Equipment 124
15.3.1 Irradiation Bombs 124
15.3.2 Circulating Loop 124

16. PLUTONIUM-PRODUCER BLANKET PROCESSING 125

16.1 Adsorption of Plutonium on Metals 125
16.2 Separation of PuO_2 by a Hydroclone 126
16.3 In-Pile Chemistry of Plutonium and Neptunium 126
16.4 Solubility of Plutonium in Uranyl Sulfate–Lithium Sulfate Solutions 126
16.5 Test Equipment 127
16.5.1 Loop T-1 127
16.5.2 Loop P-1 127

[redacted]

[redacted]

17. EQUIPMENT DECONTAMINATION 128
17.1 Oxide Scale Removal 128
17.2 Plutonium Removal from Metal Walls 128

PART VI. SUPPORTING CHEMICAL RESEARCH

18. AQUEOUS SYSTEMS AT ELEVATED TEMPERATURES 131
18.1 Alkali Metal Carbonate–Uranium Trioxide Systems 131
18.2 The Quaternary Systems $CuO-UO_3-SO_3-H_2O$ and $NiO-UO_3-SO_3-H_2O$ 132
18.3 Stabilization of ThO_2 Sols – Sol E 133
18.3.1 Preparation 133
18.3.2 Composition 133
18.3.3 Description 133
18.3.4 Properties 134
18.3.5 Discussion 134
18.4 Adsorption of H_2O by ThO_2 at Elevated Temperatures 135

19. ADSORPTION ON INORGANIC MATERIALS 136
19.1 Cation-Exchange Properties of Zirconium Tungstate 136
19.1.1 Adsorptive Properties as a Function of Drying Temperature 136
19.1.2 Acid-Base Titrations: Uptake of Cesium and Stability as a Function of pH 136
19.2 Cation-Exchange Properties of Zirconium Phosphate 137
19.2.1 Stability in a Number of Media 137
19.2.2 Acid-Base Titrations: Cation Uptake and Stability as a Function of pH 137
19.3 Hydrous Zirconium Oxide 137
19.3.1 Apparent Solubility in a Number of Media 137
19.3.2 Stability in Fluoride Solutions: Fluoride Uptake 137
19.3.3 Use of Hydrous Zirconium Oxide in Chromate Analysis 138
19.3.4 Acid-Base Titrations: Anion-Exchange and Cation-Exchange Properties 138
19.4 Hydrous Stannic and Thorium Oxides 139
19.4.1 Acid-Base Titrations: Anion-Exchange and Cation-Exchange Properties 139
19.4.2 Dispersions of Hydrous Thorium Oxides: Degree of Polymerization 139

20. RADIATION STUDIES OF THORIUM NITRATE SOLUTIONS 140

21. PROTACTINIUM CHEMISTRY 141
21.1 Extraction of Protactinium 141
21.2 Colloidal Behavior of Protactinium 141

[redacted]

Part I

HOMOGENEOUS REACTOR TEST

S. E. Beall

1. HRT OPERATIONS

S. E. Beall

R. E. Brooksbank
W. D. Burch
C. C. Cardwell[1]
J. S. Culver
N. W. Curtis[2]
J. R. Engel
K. E. Estes
J. D. Flynn
J. L. Gory
J. J. Hairston
B. H. Hamling[3]
P. N. Haubenreich
J. W. Hill, Jr.
D. M. Johnson[4]
R. W. Jurgensen[5]
S. I. Kaplan
J. O. Kolb
W. L. Morgan
J. D. Perret
H. K. Search[2]
R. Van Winkle
H. E. Williamson

1.1 CONSTRUCTION

J. J. Hairston S. I. Kaplan W. L. Morgan

1.1.1 Reactor

A continuous labor force of approximately 60 craftsmen was kept busy installing reactor parts at the construction site. Approximately 50 other craftsmen were occupied in shop or test work directly associated with construction. It appears that the services of these people will be required for at least two more months before the first test phase can begin.

In the three-month period ending January 31, all the process equipment and service piping in both the fuel and blanket low-pressure systems was installed. These systems are complete except for electrical and thermocouple conduit and wires, air lines to valve operators, and leak-detector lines to valves. A total of almost 500 welds was made in ¼- to 3-in. process piping. Although inspection was on the basis of the rigid HRP specifications, only three welds were rejected. Furthermore, of the approximately 1000 socket welds made on ¼-in. leak-detector tubing, only 12 were rejected.

A major difficulty which arose during work on the process piping concerned the ring-joint flanges. The flanges for the HRT were purchased to ASA standards, which permit variations as great as ±0.005 in. in the pitch diameter of the ring groove. This tolerance, coupled with the gasket tolerance (±0.008 in.), made it impossible for many of the flanges to seal on both groove surfaces as required by the flange leak-detector design.[6] In the course of this work it was determined[7] that flanges would always seal satisfactorily if the tolerance on the pitch diameters of both ring and groove was not greater than ±0.002 in. Only 179 flanges of the 427 that were tested were found to be within this tolerance; the remaining 248 flanges were remachined.

As the low-pressure systems were completed, attention was turned to the high-pressure equipment. The thermal shield which surrounds the pressure vessel was completed first, and then the core-pressure-vessel assembly (see also Sec. 2.2) was prepared for installation. Figure 1.1 is a photograph which shows the assembly resting on the roof slabs covering the fuel-system equipment; in the foreground are the blanket low-pressure vessels and piping. Figure 1.2 shows the reactor assembly immediately after it was lowered inside the 2-ft-thick, cylindrical, thermal shield. The reactor was followed by the blanket heat exchanger, Fig. 1.3, and finally the blanket circulating pump. Figure 1.4 is a view of the inlet and discharge lines being welded to the volute of the pump. The prefabricated pipe lines which interconnect these components will be mounted next.

1.1.2 Control Area

The major activities in the control area were the wiring of the control system and installation of the instrument cubicles and of the refrigeration system.

---

[1]On loan from Babcock & Wilcox Co.

[2]On loan from Pennsylvania Power and Light Company.

[3]On loan from Union Carbide Nuclear Company, New York office.

[4]On loan from The Glenn L. Martin Co.

[5]On loan from American Gas and Electric Company.

[6]W. R. Gall *et al.*, *HRP Quar. Prog. Rep. Oct. 31, 1955*, ORNL-2004, p 14–15.

[7]*Sealing Characteristics of Ring-Joint Flanges*, memorandum from S. I. Kaplan to S. E. Beall (Jan. 23, 1956).

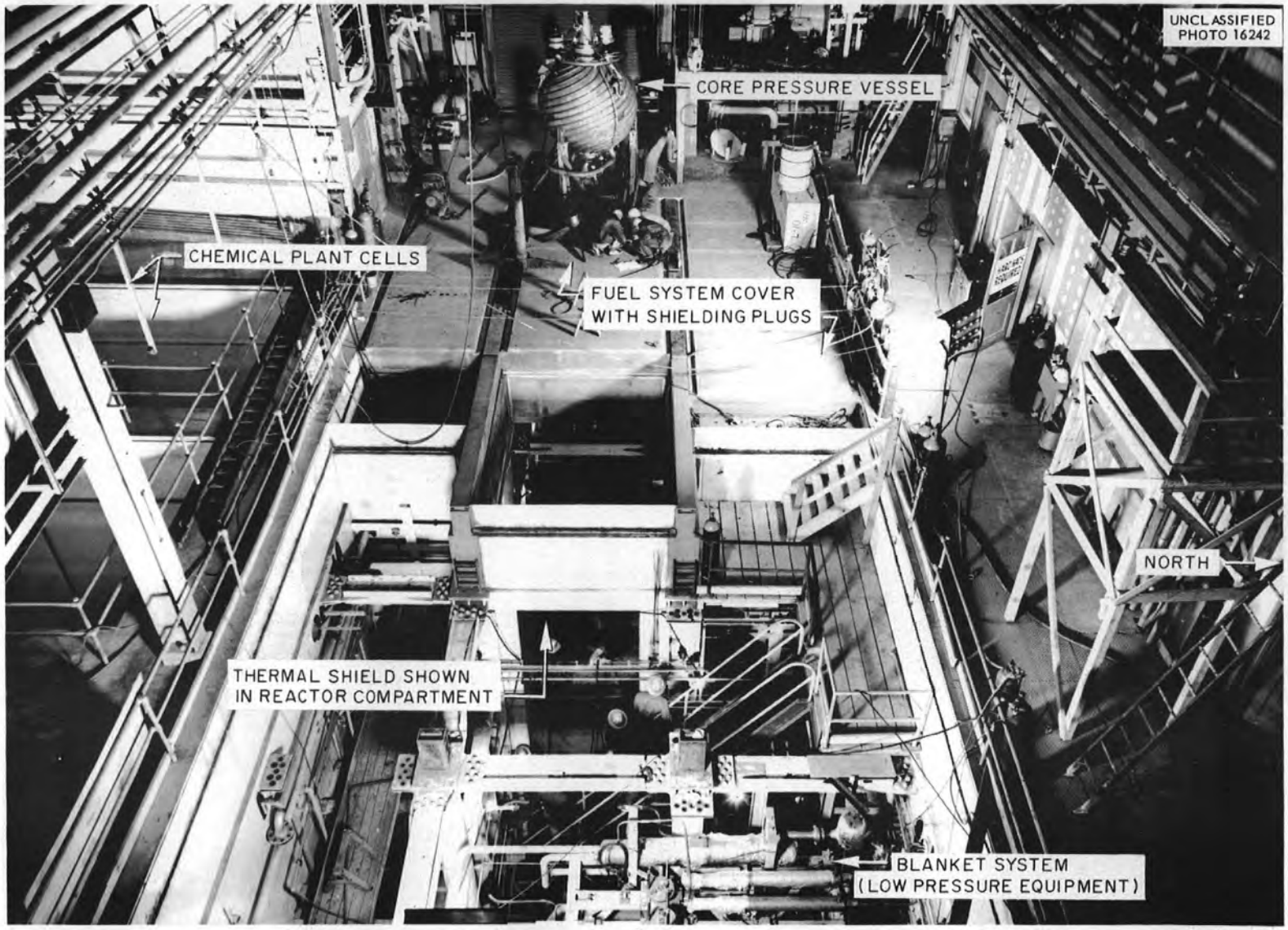

Fig. 1.1. View of HRT Building – Main Bay.

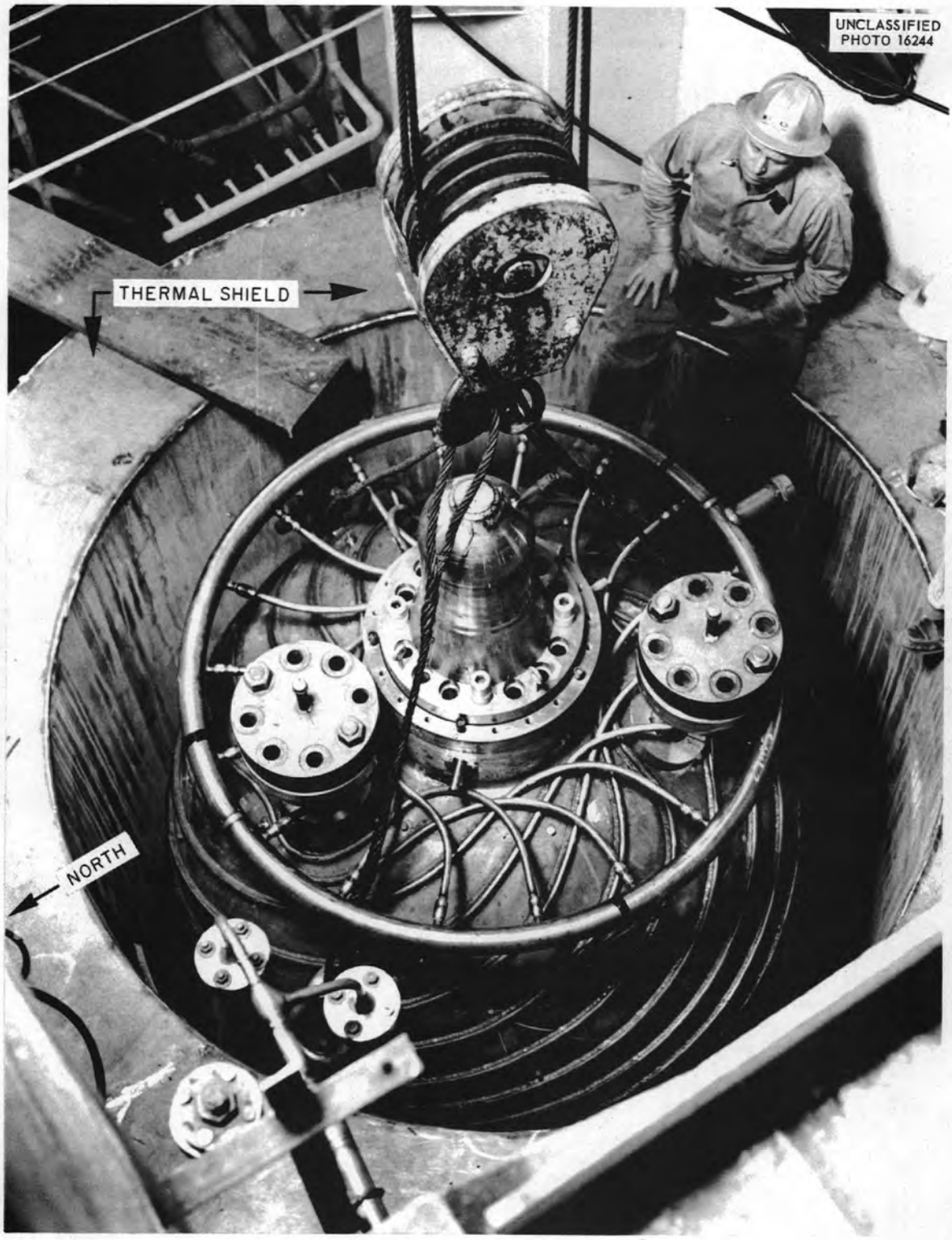

Fig. 1.2. Core-Pressure-Vessel Assembly Installed in Reactor Compartment.

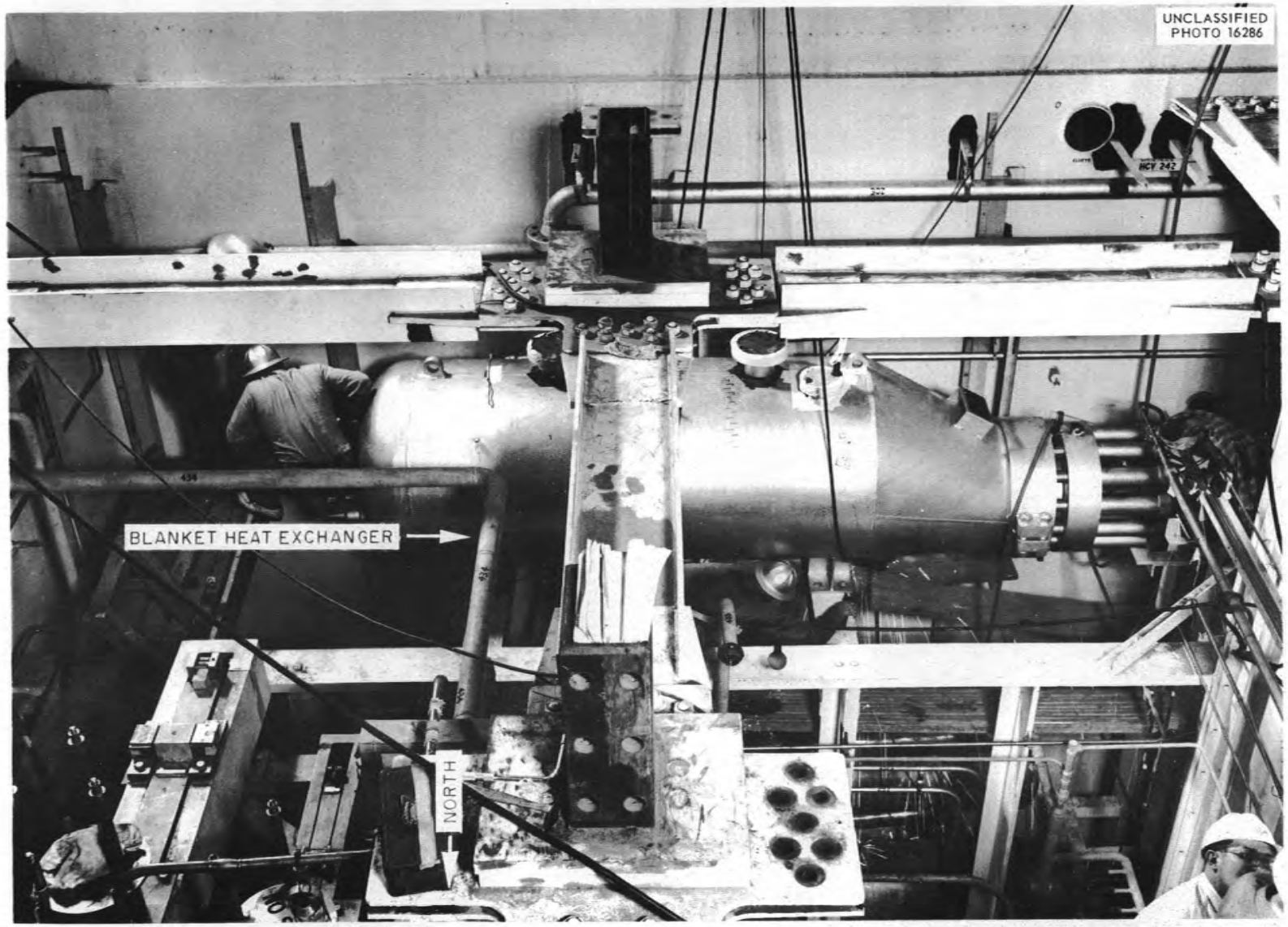

Fig. 1.3. Blanket Heat Exchanger.

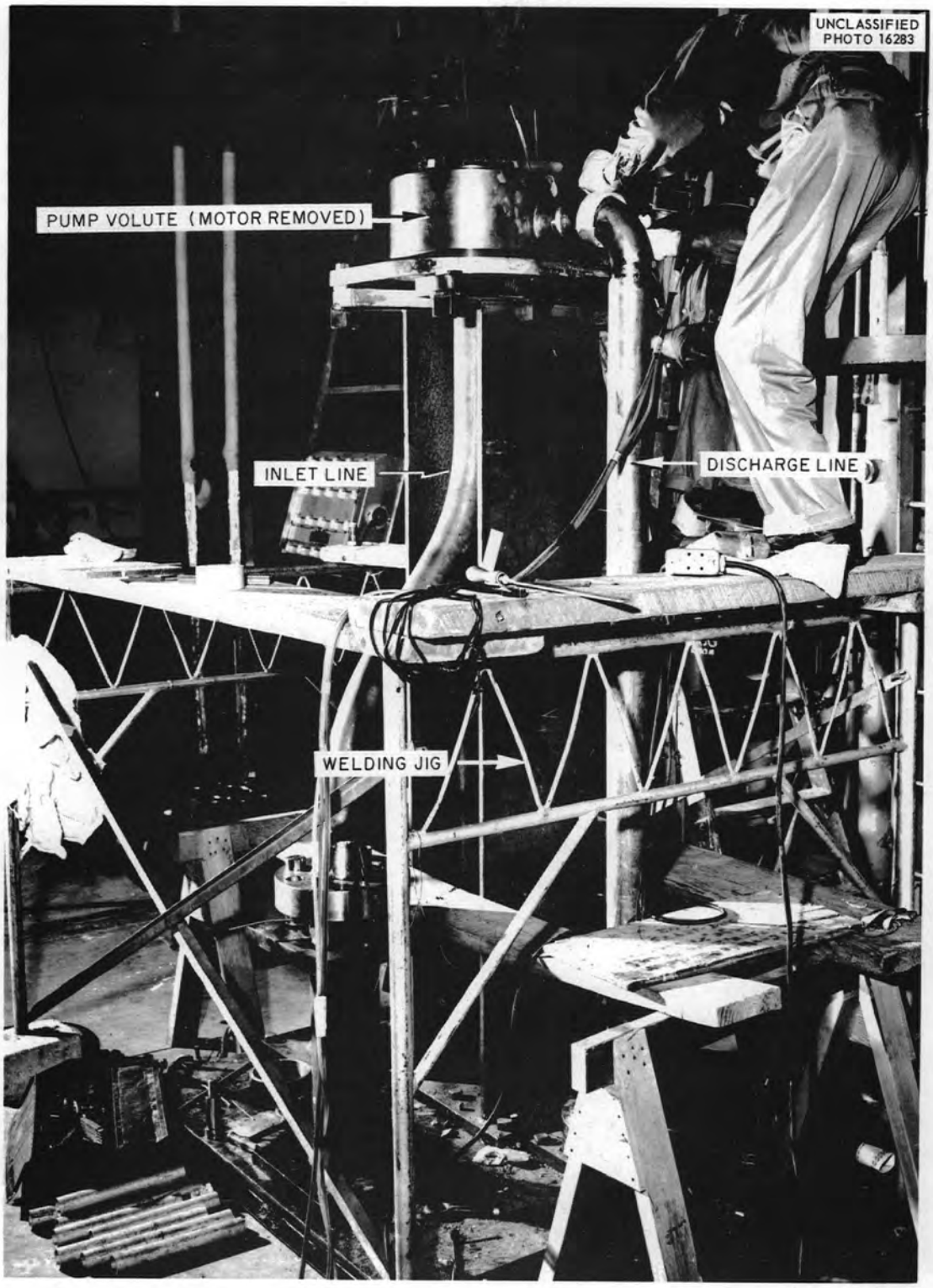

Fig. 1.4. Blanket Circulating Pump on Welding Jig.

The control system wiring is probably 75% complete. Much of the remaining work is associated with the three center panels which were revised to accomodate late changes in the process flowsheet.

The instrument cubicles are the 5-ft-dia welded tanks located in the east and west wings of the control area. They contain those instruments which are connected directly to process lines. Because the instruments may require relatively frequent attention and because it is not desirable to open the main reactor tank often, the instruments were located in the cubicles, which will be sealed and shielded to the same requirements as the reactor tank. Both cubicles were welded in place, and 60% of the instrument lines were completed.

1.1.3 Reactor Steam System

The reactor heat-removal system was completed by the contractor, and is pictured in Fig. 1.5. Although some instrumentation and electrical work remains to be done by ORNL forces, the checkout and startup of this system has begun.

1.2 OPERATIONS TESTING

T. E. Haynes J. O. Kolb
P. N. Haubenreich R. Van Winkle

1.2.1 Fuel Low-Pressure Assembly

Testing of the fuel low-pressure dump-tank assembly installed in its outdoor test stand was completed early in December.

Listed below are the significant findings from the test:

1. Moving the discharge end of the dump line from the entrainment separator to the top of the dump tanks appears to permit the entrainment separator to operate without flooding during simulated fuel dumps, provided that there is no flow through line 159 (the ½-in. dump line bypass that is provided to drain the low portion of the dump line). It was observed that when line 159 was open, jetting action at the end of the line caused heavy entrainment. Several methods of correcting this difficulty are being studied.

2. When the performance of the entrainment separator during normal operation of the dump tank evaporator was tested with solutions of trisodium phosphate, and the condensate analyzed for sodium, the observed decontamination factor, defined as the ratio of sodium concentration in the dump tank to that in the condensate, was in the range from 1,000 to 10,000 in all runs. There was considerable scatter of the data, and no clear relation was observed between the decontamination factor and either the evaporation rate or the dump tank liquid level. More entrainment tests will be performed with natural-uranium solutions.

3. In a study of condenser performance at various rates of cooling-water flow during simulated dumps, the condenser became flooded with from 75 to 250 lb of condensate – the amount varied with heat removal rate – when the pressure drop between the dump tank and the condenser prevented the normal gravity return of liquid to the dump tank. It was recommended that a valve be installed in line 116 between the condenser and the cold trap. This valve will close during a dump to prevent transfer of liquid to the cold trap.

4. The pressure drop was measured as a function of steam flow from the dump tank through the entrainment separator, line 115, and the catalytic recombiner to the condenser; the results were found to be correlated by

$$\Delta P = 4.1 \times 10^{-5} w^2 v \ ,$$

where ΔP is the pressure drop (psi), w the steam flow (lb/min), and v the specific volume (ft^3/lb). According to this result, all the piping between the dump tank and the condenser has a flow resistance equivalent to 111 ft of 3-in., sched-40 pipe. The actual length of line 115 is about 40 ft.

5. The aluminum foil insulation on the fuel dump-tank assembly was found to be less effective than had been predicted from earlier tests.[8] When six layers of 1.0-mil foil plus two additional layers of 2.0-mil foil were used, the insulation heat transfer coefficient was found to lie in the range 1.5 to 3.5 Btu/hr·ft^2·°F, which permitted a heat loss of about 48,000 Btu/hr during the outdoor tests. It was recommended that additional layers of 2.0-mil foil be installed after the cell-equipment installation is completed.

6. During a simulated dump with the relocated dump line, the recombiner appeared to recombine radiolytic gas continuously. In an earlier test of the recombiner during a dump (with the dump line

[8] I. Spiewak, *Aluminum Insulation (Report No. 2)*, ORNL CF-55-8-121 (Aug. 24, 1955).

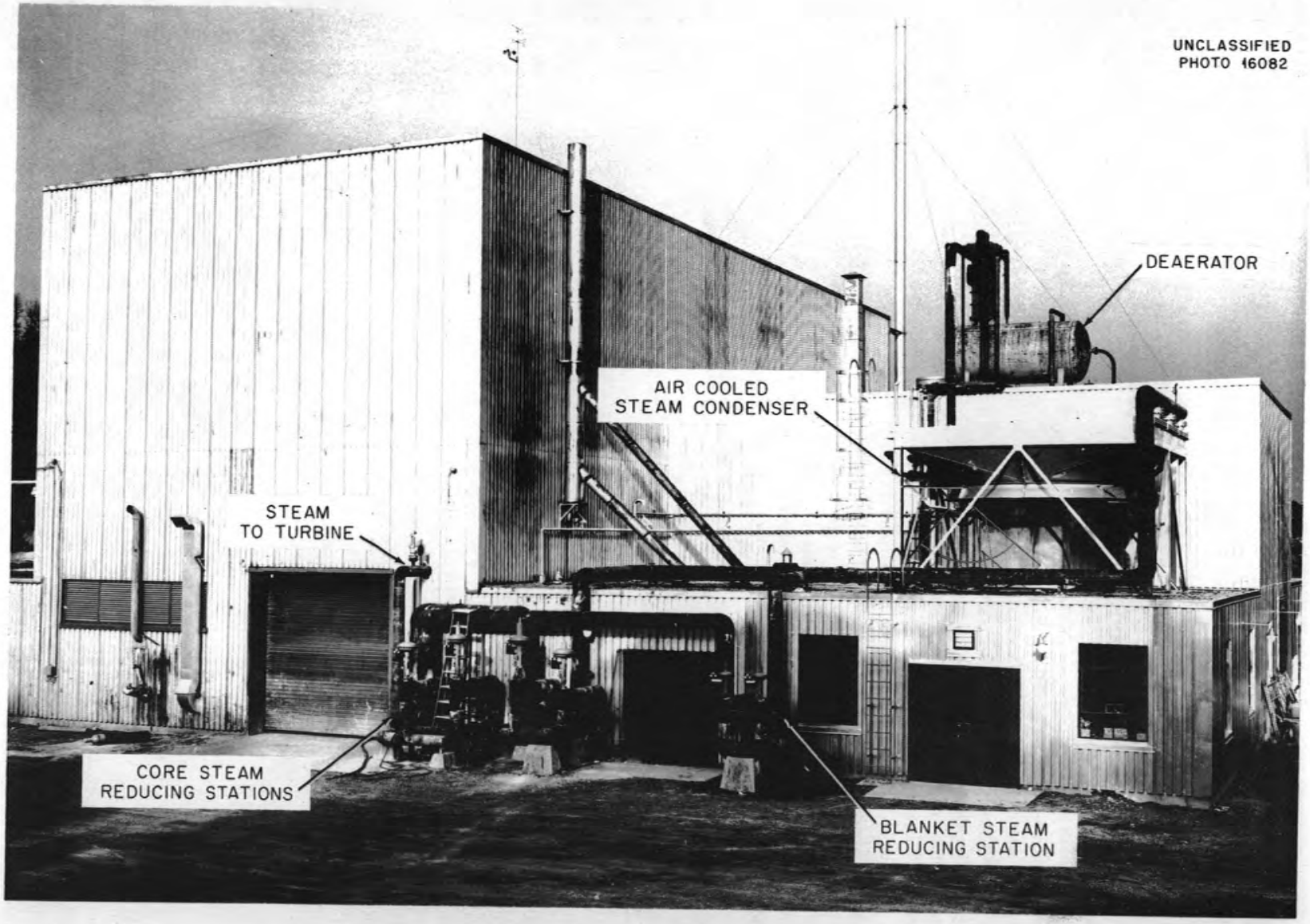

Fig. 1.5. Reactor Heat-Removal System.

discharging into the entrainment separator), some hydrogen and oxygen were unrecombined, as evidenced by two explosions within the system followed by a very rapid decrease in pressure immediately after the dump was stopped. Hydrogen was being injected into the system at a rate of 7.5 scfm, together with 3.75 scfm of oxygen.

Other testing work completed on the outdoor test stand included measurement of the evaporation rate as a function of steam pressure to the heating jacket of the dump-tank evaporators, calibration of the dump-tank and condensate-tank weighing mechanisms, volume measurements of the dump tanks and condensate tanks, observation of recombiner bed temperatures as a function of flows of radiolytic gas and diluent steam, measurement of head loss as a function of condensate flow through line 120 (returning condensate to the dump tank from the condenser), and measurement of off-gas residence time in the fuel low-pressure system as a function of gas flow, condenser cooling-water flow, and condenser heat load.

1.2.2 Blanket Low-Pressure System

The tests completed in the blanket dump-tank assembly were measurements of the dump-tank evaporation rates as a function of steam pressure, the heat loss from the blanket low-pressure system (which has aluminum foil insulation), and the recombination at normal evaporation rates. The results of these measurements were satisfactory and were similar to the information reported for the fuel system.

1.3 OPERATIONS TRAINING

J. W. Hill, Jr.

The training program for the first group of ten engineers continued along the lines outlined previously.[9] Another group of four engineers was initiated into the program, and preparations were completed to train ten technicians, starting January 30.

[9] J. W. Hill, Jr., *et al.*, *HRP Quar. Prog. Rep. Oct. 31, 1955*, ORNL-2004, p 7.

2. HRT DESIGN

W. R. Gall R. B. Korsmeyer

R. E. Aven
R. H. Chapman
C. J. Claffey
H. N. Culver[1]
R. F. Hughes[2]
R. W. Jurgensen[3]
J. E. Kuster[4]
M. C. Lawrence[5]
M. I. Lundin
R. G. McGrath[6]
C. Michelson[1]
R. C. Moren[6]
R. C. Robertson
J. N. Robinson
C. L. Segaser
W. F. Taylor[7]
W. Terry
T. H. Thomas
F. C. Zapp

2.1 GENERAL STATUS OF DESIGN

The following general items in the design of the HRT were completed during this quarter:

Instrument cubicle piping
Oxygen metering system
Electrical and thermocouple conduit drawings
Air lines to instruments, valves, and weigh cells
Waste evaporator and associated piping
Charcoal adsorbers and associated piping
Bulkhead penetrations and details
Outer dump-tank support and piping layouts
Injection pump drive unit installation
Pressurizer redesign
Thermal shield fill, vent, and cooling water systems

Approximately 95% of the working drawings for construction of the reactor have been completed. In the past quarter, some minor design revisions were made throughout the system as construction progressed, and a major redesign of the pressurizer was finished.

2.2 ZIRCALOY–STAINLESS STEEL TRANSITION JOINT

The HRT reactor vessel, as received from Newport News Shipbuilding & Dry Dock Co., had provisions for flanged connections with flat metal gaskets between the Zircaloy-2 core tank and the stainless steel portion of the vessel. Gaskets were not installed before shipment because a program for developing a satisfactory gasket or an improved joint design was still in progress.

Results of the development program have been outlined by Segaser.[8] The design finally developed for the Zircaloy-to-stainless-steel joint is shown by Fig. 2.1. It consists of a laminated, titanium A-55 cylinder fitted into a very closely confining machined groove in each of the mating flanges. A gold gasket, 0.005 in. thick, is placed in the bottom of each groove to effect a seal. The bolts and nuts are made of a titanium alloy of the following composition and room temperature properties: 6.18% aluminum, 4.15% vanadium, 0.25% iron, and the remainder, titanium; 155,000-psi yield strength (0.2% offset), 163,000-psi ultimate strength, 47.64% reduction in area.

2.3 STEAM PRESSURIZATION

Because of the unsatisfactory performance of the previous pressurizer during operation of the mockup loop,[9] the pressurizer was redesigned to eliminate contact of uranyl sulfate with heated surfaces. The new pressurizer, shown in Fig. 2.2, consists of a surge volume and a separate steam generator incorporated into one pressure vessel. The two parts are isolated by baffles to minimize the transfer of uranyl sulfate into the steam generator, which is supplied with condensate from the low-pressure system.

Four heated legs are installed on the steam generator, which has total capacity of 95,000 Btu/hr. This capacity is twice the calculated heat required to compensate for losses and to preheat the condensate feedwater at a rate of flow of 109 lb/hr. A prototype pressurizer of this

[1] On loan from TVA.

[2] On loan from Kaighin and Hughes, Inc.

[3] On loan from American Gas and Electric Company.

[4] On loan from Maxon Construction Co., Inc.

[5] On loan from General Dynamics Corp.

[6] On loan from Westinghouse Electric Corporation.

[7] On loan from Pioneer Service & Engineering Co.

[8] C. L. Segaser, *Zircaloy-to-Stainless Steel Transition Pipe Joint Design Study*, ORNL CF-55-12-72 (Dec. 5, 1955).

[9] C. B. Graham *et al.*, *HRP Quar. Prog. Rep. Oct. 31, 1955*, ORNL-2004, p 22.

UNCLASSIFIED
ORNL-LR-DWG 12029

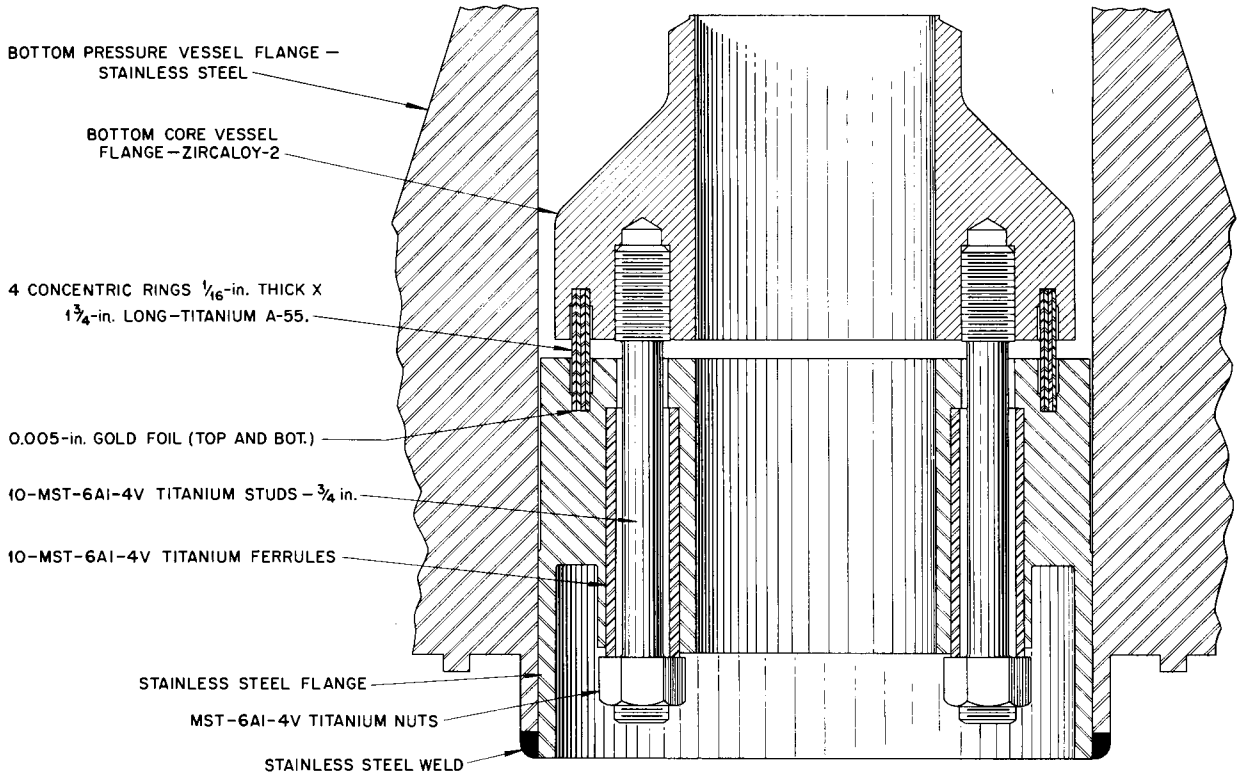

Fig. 2.1. Zircaloy–Stainless Steel Transition Joint.

design was constructed and is currently undergoing tests in the mockup loop.

In addition to the liquid level controller which maintains the fuel level in the pressurizer, a similar instrument is required to indicate the water level in the steam generator. The amount of water retained in the generator is sufficient for about 1 hr of operation after the feedwater supply has stopped. Feedwater in excess of pressurizing requirements overflows into the fuel leg and serves to purge the fuel leg. A liquid level indicator-controller with magnetic damping was tested in the shop and operated satisfactorily. At present the design is being modified to facilitate adjustment of the instrument after it is installed in the reactor.

2.4 GAS PRESSURIZATION

The feasibility of using gas to pressurize the HRT system is being studied as an alternate to D_2O vapor pressurization. A gas pressurizer would permit operation at temperatures no higher than the reactor fuel exit temperature and would allow the reactor to be pressurized faster than does a steam pressurizer. The major disadvantage of gas pressurization is the introduction of a noncondensable gas into the reactor system. If large quantities of gas were needed for normal reactor operation, the present off-gas system design would be inadequate.

A contract was awarded to Arthur D. Little, Inc., for the design of a gas pressurization system for the HRT. Their preliminary process flowsheet was reviewed and the specific problems were defined. Their present work consists in completing an engineering flowsheet, describing the equipment and the system operation, and estimating the experimental effort necessary to develop the information required for complete, detailed design of the system.

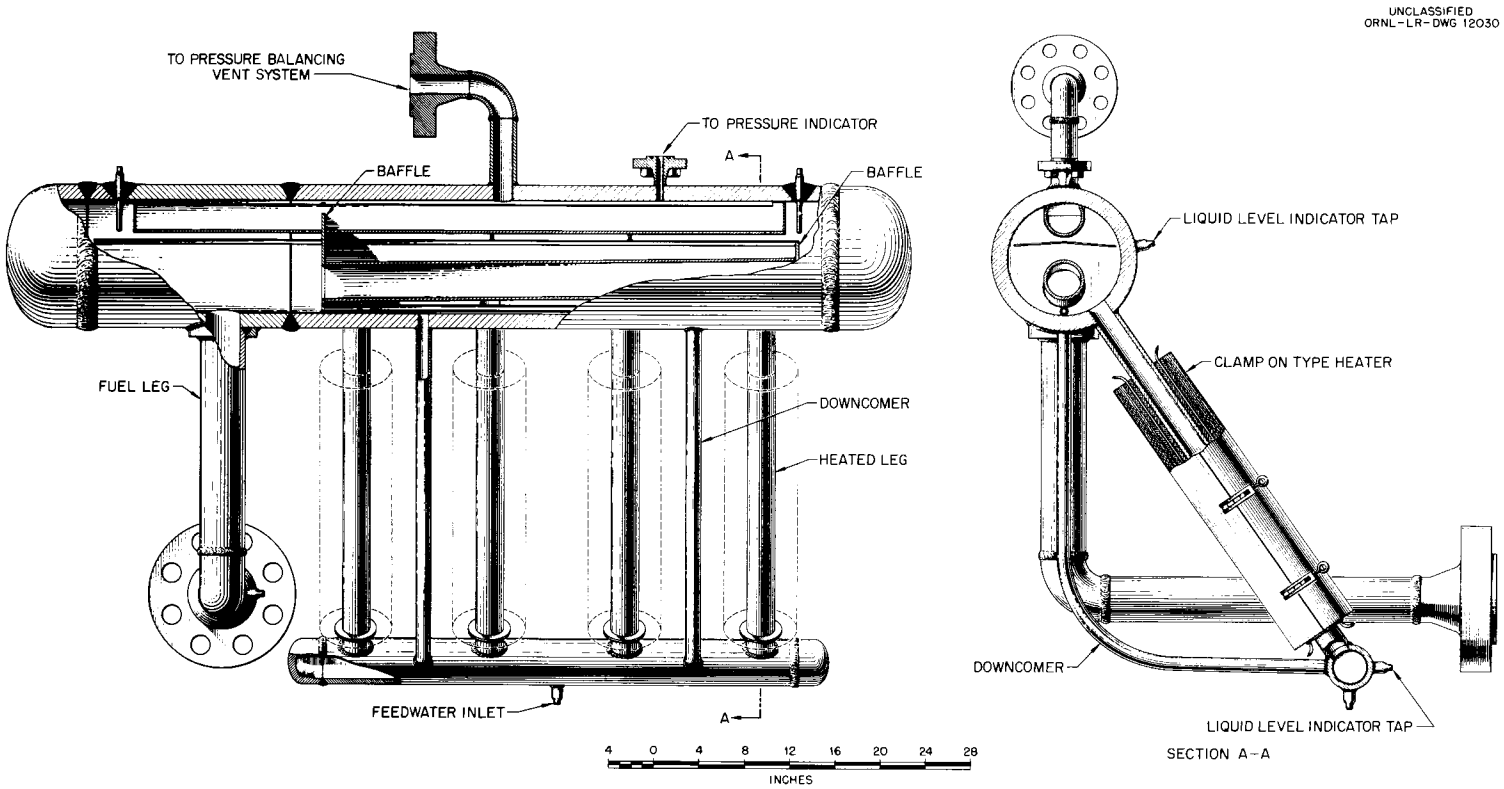

Fig. 2.2. HRT Steam Pressurizer (Revised).

The A. D. Little proposal is based on the use of oxygen, stored at about 3000 psi, as the pressurizing medium. The oxygen is taken from standard cylinders and compressed by diaphragm pumps to the storage pressure. Means are provided to prevent fuel solution from working back into the oxygen supply system and to prevent accumulation of explosive concentrations of radiolytic gases in the pressurizer during normal operation and in the reactor during a dump. Excess oxygen appearing in the low-pressure system is removed by burning it in hydrogen and removing the water formed, prior to passage of the gases into the charcoal beds. The presence of a substantial supply of oxygen to the charcoal beds is considered an unnecessary hazard, especially if there should be hot spots in the bed and rapid oxidation, which might release radioactive gases. By removing the oxygen with hydrogen, only the latter is used as a carrier through the charcoal.

2.5 THE OXYGEN-ADDITION SYSTEM

Oxygen will be added continuously to the HRT fuel systems to replace the oxygen consumed in the corrosion of metals and to prevent the reduction of uranyl ions. It is planned to add the oxygen to the low-pressure systems at the inlets of the high-pressure fuel and blanket feed pumps. Connections are also provided so that gas can be supplied to the high-pressure systems if oxygen concentrations greater than 100 ppm prove necessary. The design of the addition system is based on studies by Youngblood,[10] Visner,[11] and Van Winkle.[12]

The oxygen system will consist of: (1) a manifold arrangement utilizing standard gas cylinders for supplying gas at a pressure less than 100 psi and an oxygen evaporator, Fig. 2.3, for supplying pressures from 1000 to 3000 psi, (2) an oxygen-metering and valve station located in the east instrument cubicle, and (3) the accumulator tanks and piping to the pump lines within the cell.

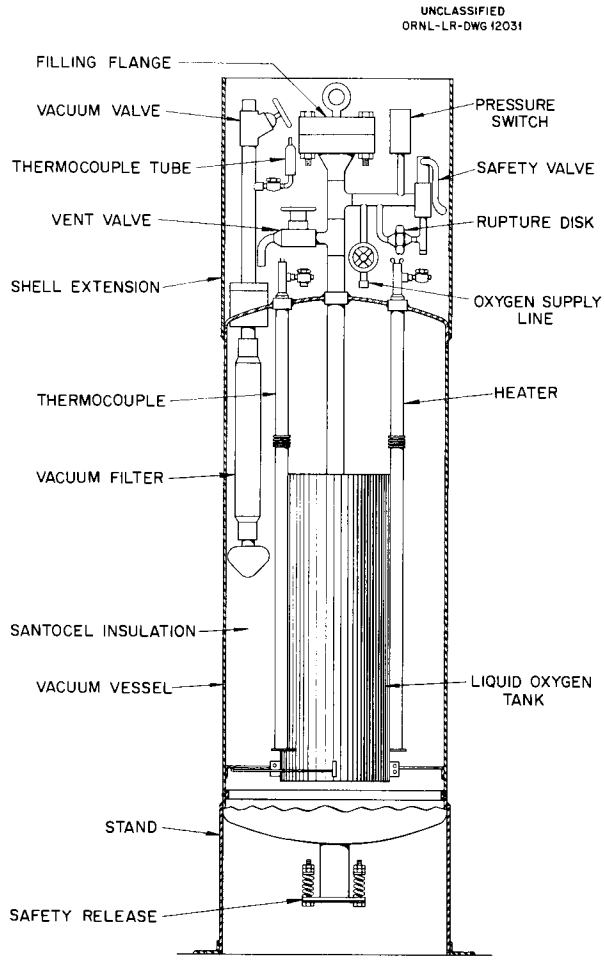

Fig. 2.3. Oxygen Converter.

Oxygen will flow from the manifold (located outside the building) to the accumulator tanks inside the reactor cell, from there to the instrument cubicle for metering and throttling, and then to the process lines within the cell.

Check valves and block valves have been incorporated to prevent a direct path for the escape of radioactive solution in case of an accident. All the system piping is of type 347 stainless steel. The accumulator tanks act as an intermediate storage volume, so that oxygen cylinders can be replaced during operation or the converter can be recharged. These tanks are always fully charged and are interlocked with a pressure switch and valve. The accumulators serve both the blanket and fuel systems, but the metering systems and piping within the reactor are separate.

---

[10] E. Youngblood, *Feed Pump Mockup*, ORNL CF-55-2-52 (Feb. 9, 1955).

[11] S. Visner, *Oxygenation of HRT Solution*, ORNL CF-54-7-34 (July 14, 1954).

[12] R. Van Winkle, *Specifications for the Fuel Oxygenation Systems*, ORNL CF-55-7-13 (July 1, 1955).

2.6 PURGE PUMPS

The flow diagram for the HRT process systems, as reported previously,[13] shows only two purge pumps, one in the fuel system and one in the blanket system. Two additional purge pumps have been added to the reactor systems. Each new pump will deliver a maximum flow of approximately 3.5 gph at 2000 psi. One will pump condensate to purge the rotor cavity and bearings of the fuel circulating pump, and the other will supply condensate for purging the blanket circulating pump.

The two purge pumps previously specified have a capacity of approximately 17 gph each at 2000 psi. They will be used to supply condensate to the fuel and blanket pressurizers. In this way the flow of feedwater to the newly designed steam pressurizers will not be affected by the needs of the circulating pumps.

2.7 WASTE SYSTEM

One waste evaporator and one entrainment separator are to be used in place of the two originally shown on the HRT flowsheets.[13] The evaporator has a capacity of $1\frac{1}{2}$ gpm, as compared with $\frac{3}{4}$ gpm for each of the earlier units; the entrainment separator and associated piping have been enlarged to handle this flow rate.[14] The revised unit (Fig. 2.4) now has three evaporator legs, and a bayonet-type heater is incorporated to evaporate the solution to a volume which can be handled by a shielded waste carrier. Two condensers are to be connected in parallel to obtain approximately 50 ft^2 of condensing area.

2.8 INSTALLATION OF AIR-ACTUATED VALVES

There are 44 air-actuated valves, ranging in nominal size from $\frac{1}{8}$ to 1 in., within the vapor-tight enclosure of the HRT cell. Since such valves and actuators are subject to failure, provisions have been made to facilitate their replacement. The drawing of a typical low-pressure valve installation, Fig. 2.5, illustrates how the mounting is accomplished in the cell. A fixture consisting of two steel angle guides is permanently mounted relative to the flanges to which the valve connects. With a stop suitably positioned to limit horizontal travel, the fixture positions the valve and actuator assembly in three planes relative to the cell flanges.

The valves are mounted between two piping flanges. To remove a valve, it will be necessary to remove the flange bolts which pass through slots machined in the valve body and are held by nuts tack-welded to the bottom flange. The valve-bellows leak-detector disconnect and the two valve-actuator air-line disconnects must be disengaged from mating members permanently located in the cell. With a hoist attached to the lifting bail located at the center of gravity of the valve and actuator assembly and with the flanges spread apart to clear the oval ring gaskets, the unit can be moved horizontally on the guide rails. When the valve body is clear of the flanges, the assembly can be removed vertically from the cell. The same procedure will be followed in reverse when a new valve and actuator assembly is being installed.

It is contemplated that removal and replacement will be accomplished with the cell flooded with water. Maintenance personnel will work from platforms at the top of the tank, 13 to 24 ft above the various valve locations. Freezer jackets are provided on the inlet and outlet piping to limit the light-water contamination of the system when the flanged joints are spread. Special tools such as wrenches, flange spreaders, and disconnect tools are being developed to facilitate the remote maintenance of valves. Care has been taken in the layout of the cell piping, equipment, and supports to ensure that all valves are accessible from above.

2.9 HIGH-PRESSURE VALVE JIG

The method of installing high-pressure valves in the HRT cell is similar to that used for the low-pressure valves. However, the valve bodies are welded into the piping instead of being directly flanged to the piping. Flanges are provided at some distance from each valve in both the inlet and outlet piping to facilitate replacement.

There are 16 different configurations of the valve body with respect to its piping and flanges. A universal jig has been developed which establishes the proper relation between the flange ring

[13] R. B. Briggs *et al.*, *HRP Quar. Prog. Rep. April 30, 1955*, ORNL-1895, p 3–15.

[14] W. L. Carter *et al.*, *Study of HRT-CP Waste Evaporator, Entrainment Separator, Condenser and Related Piping*, ORNL CF-55-11-143 (Nov. 25, 1955).

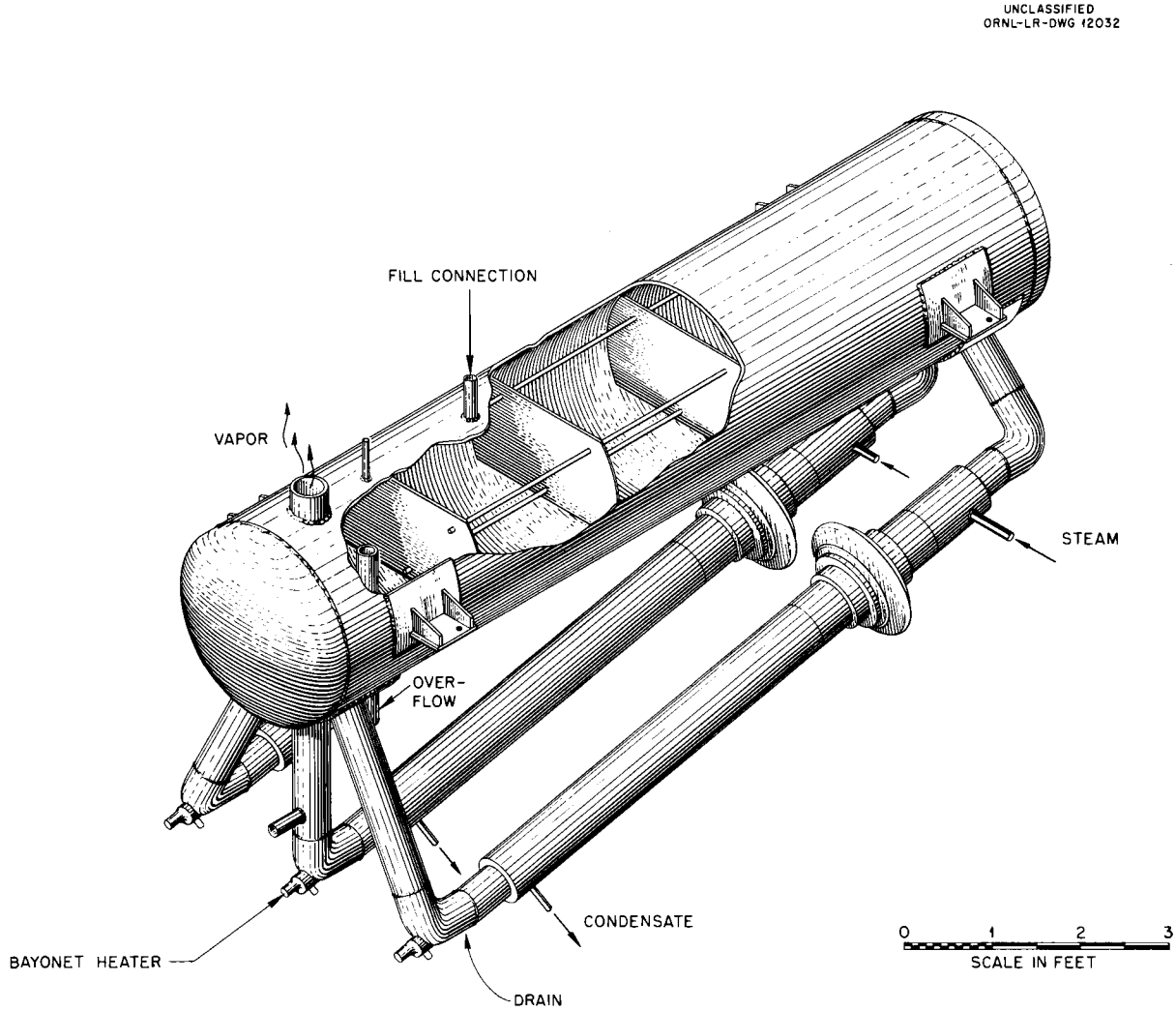

Fig. 2.4. Waste Evaporator.

grooves and the mounting points on the valve and actuator which mate with the fixture in the cell. The initial valve and flange configurations will be made on this jig. When it becomes necessary to replace a high-pressure valve, the jig will be utilized to make a duplicate of the original valve.

2.10 BARYTES AGGREGATE–WATER PLACEMENT TESTS

A series of tests[15] was conducted to determine the density attainable by the use of a mixture of barytes aggregate and water as a shielding medium, the lateral pressure exerted by such a mixture on the containing vessel, and practical placement procedures to be used in the field.

A steel tank (Fig. 2.6) was used in these tests; it was 2 × 2 × 12 ft high, and it was instrumented with strain gages. The strain gages, which were used to measure the lateral pressure (Fig. 2.7), were calibrated by filling the tank with water to produce a known pressure on the tank. Density measurements were achieved by weighing the tank, empty and full, and dividing the difference by the volume of the tank. Four tests were conducted in

[15] J. E. Kuster, *Lateral Pressure and Density of Barytes Aggregate and Water Mixture*, ORNL CF-55-10-61 (Oct. 14, 1955).

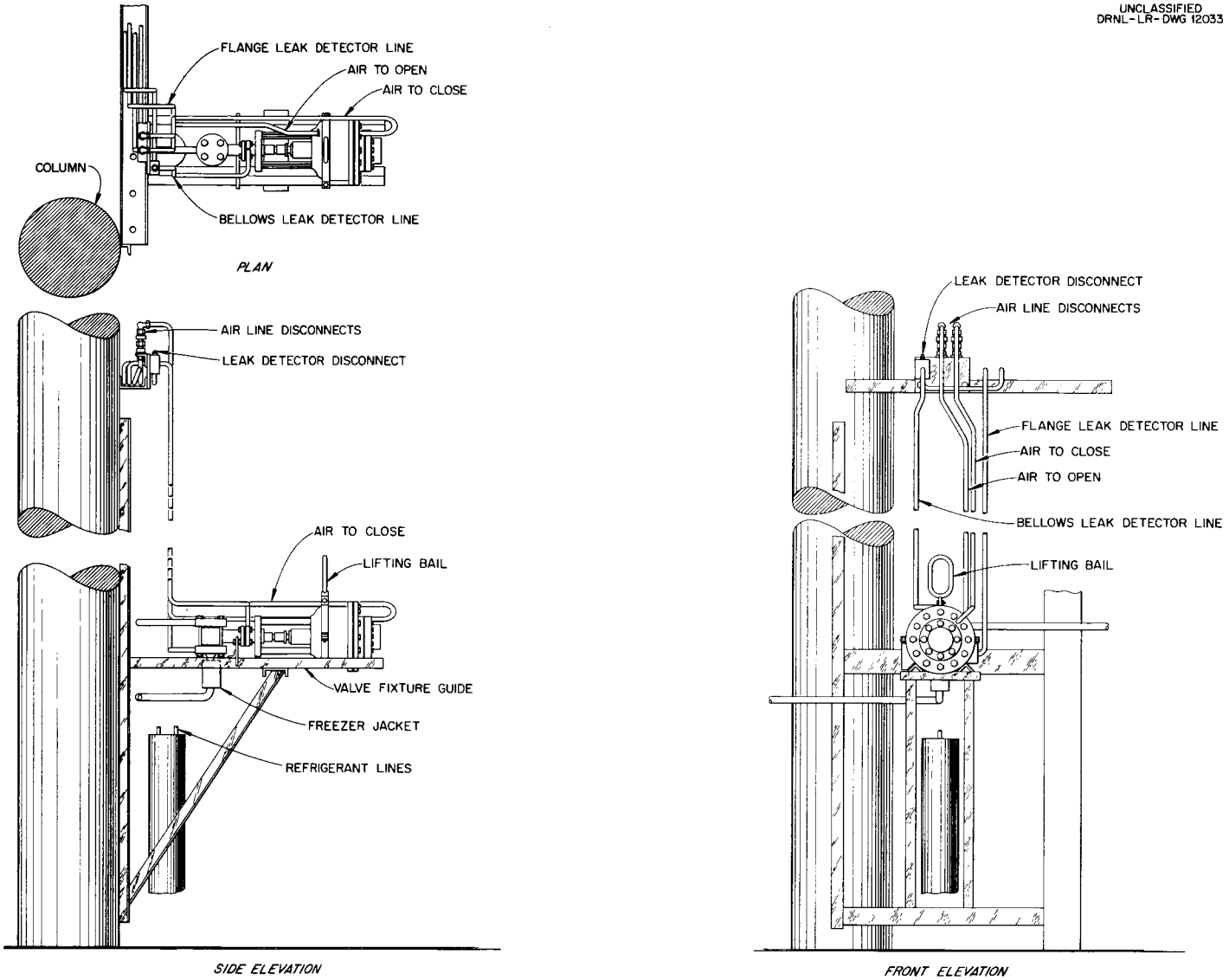

Fig. 2.5. Typical Low-Pressure Valve Installation.

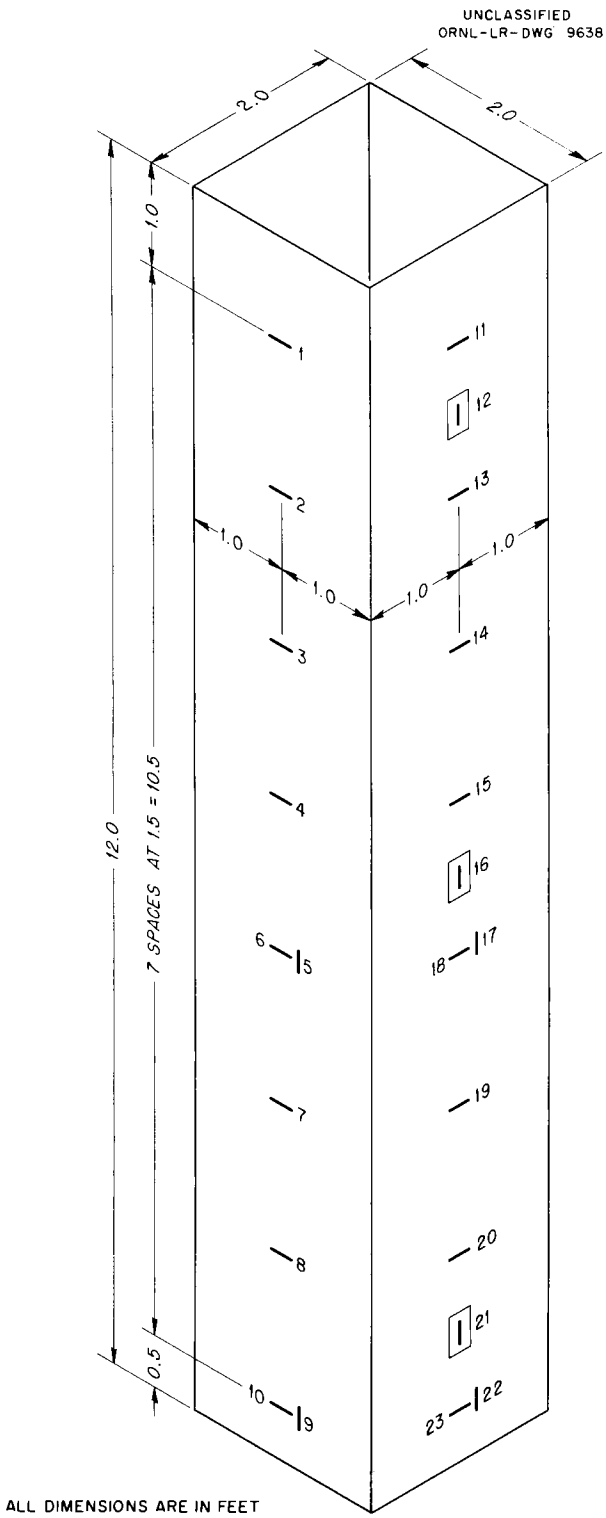

Fig. 2.6. Barytes-Sand–Water Test Tank.

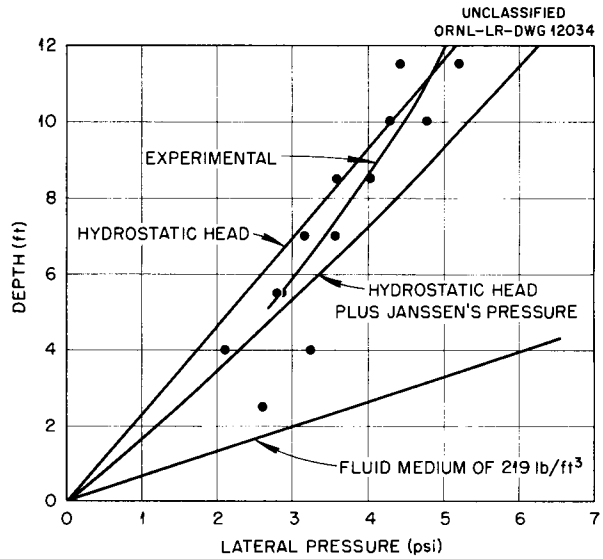

Fig. 2.7. Lateral Pressure of Barytes-Aggregate–Water Mixtures.

which different methods of placement and compaction were used. The maximum density obtained was 222 lb/ft^3.

Lateral pressures exerted by the mixture on the tank were about the same for all the tests and compared well with the values predicted by adding hydrostatic head to Janssen's pressure, based on the submerged weight of the aggregate. Janssen's pressure is given by the formula:[16]

$$P_h = \frac{wR}{\mu'}[1 - e^{-(\mu' k/R)h}] ,$$

where

P_h = lateral pressure, lb/ft^2,
w = weight of material, lb/ft^3,
h = depth at which pressure is calculated, ft,
R = A/U hydraulic radius, ft,
A = area of bin, ft^2,
U = perimeter of bin, ft,
μ' = tangent of ϕ',
ϕ' = angle of friction of material on wall,
k = $(1 - \sin\phi)/(1 + \sin\phi)$,
ϕ = angle of repose of material.

Curves of depth vs lateral pressure are shown in Fig. 2.7, with curves for a hydrostatic head and for a fluid medium with a density of 219 lb/ft^3. It

[16] M. S. Ketchum, *Design of Walls, Bins and Grain Elevators*, 3d ed., McGraw-Hill, New York, 1919.

is evident from these tests that satisfactory design values can be derived by using the procedure described above.

As a result of these tests a practical procedure for field placement of a barytes aggregate and water mixture may be summarized as follows:

1. The barytes should be mixed in the ratio of 57% coarse barytes and 43% fine barytes, by weight, plus such additional materials (colemanite) as are required for the specific application. No specification of gradation of the barytes is given, since the barytes as stockpiled at Sweetwater, Tennessee, will be used in the HRT.

2. The mixture should be thoroughly saturated with water by mixing either in a mortar box or in a concrete mixer. This minimizes the amount of entrained air carried into the fill and reduces the dusting problem.

3. The mixture should be placed in lifts of not more than 6 in., and a few inches of free water should be kept over the surface at all times.

4. The mixture should be placed with special care along the walls of the container and around any projections, tie bars, or struts so that no voids will be left under angles or other members having flat surfaces or projections.

3. HRT COMPONENT DEVELOPMENT

C. B. Graham

L. J. Bell
R. Blumberg
J. S. Culver
K. E. Estes
H. L. Falkenberry[1]
C. H. Gabbard
L. F. Goode
B. A. Hannaford
P. H. Harley
P. F. Pasqua[2]
W. L. Ross
I. Spiewak
D. S. Toomb
H. D. Willis
W. B. Wilson

3.1 PUMP DEVELOPMENT

3.1.1 400A-1 Pump and Loop

Three runs, for a total of 785 hr, with the 400A-1 Westinghouse pump circulating a solution containing 0.04 *m* UO_2SO_4, 0.005 *m* $CuSO_4$, and 50 mole % excess H_2SO_4 at 250°C were completed during this report period. The last run, 300 hr, was made with cast Stellite shoes in the thrust bearing, which are to be used in the HRT pumps and had not been run previously. The oxygen concentration was held at approximately 400 ppm.

At the end of the last run the pump was dismantled for inspection. The pump components were in good condition, except for corrosion on the thermal-barrier end of the pump-impeller hub and in the region of the thermal barrier. The metallic O-ring gasket under the thermal barrier showed attack at the line of contact with the mating flange. However, there was no indication of leakage across the O-ring or gold-plated stainless steel gasket in the main flange of the pump.

3.1.2 300A-1 Pump

Leakage at the main flange of the 300A-1 pump was reported earlier.[3] The leakage was stopped by seal-welding the pump casing to the stator flange. This solution to the flange-leakage problem will be adopted for the reactor pumps also. The pump was operated in the mockup test loop for 500 hr after seal-welding. Toward the end of the run, a high heat load, denoting a leak past the thermal-barrier O-ring seal, was measured in the cooling water to the pump jacket. The pump was dismantled, and its components were in good condition, with the exception of the thermal barrier and the thermal-barrier O-ring seal. The O-ring was corroded completely through in several places, and several cap screws were damaged, as shown in Fig. 3.1. As in the case of the 400A-1 pump discussed above, corrosion was evident in the wear ring section of the thermal barrier, as well as on the tip of the pump-impeller hub which fits into the thermal-barrier wear ring. This attack is shown in Figs. 3.2 and 3.3. The O-ring seating surfaces on both the thermal barrier and stator flange were badly pitted and corroded in several places, as may be seen in Figs. 3.4, 3.5, and 3.6.

In an attempt to prevent leakage of the hot fluid into the pump motor, a new thermal barrier was seal-welded into the stator flange. Cap screws are still used to hold the thermal barrier down, but caps are welded over the screws.

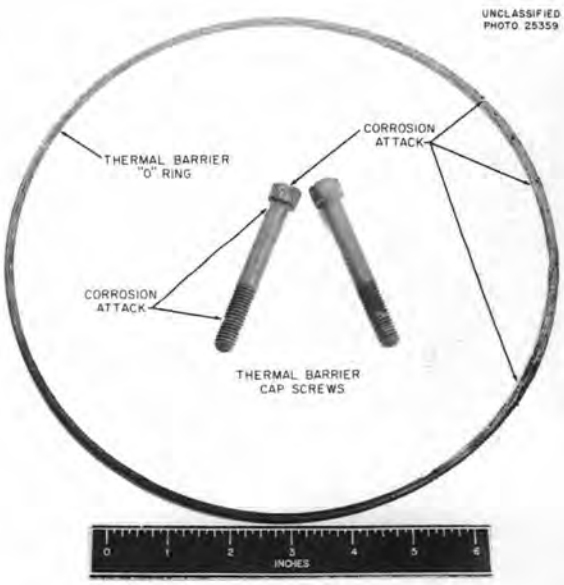

Fig. 3.1. 300A-1 Pump Parts – Thermal-Barrier O-Ring and Cap Screws.

[1]On loan from the TVA.

[2]Consultant from University of Tennessee.

[3]C. B. Graham *et al.*, *HRP Quar. Prog. Rep. Oct. 31, 1955*, ORNL-2004, p 22.

Fig. 3.2. 300A-1 Pump – Thermal-Barrier Front Side.

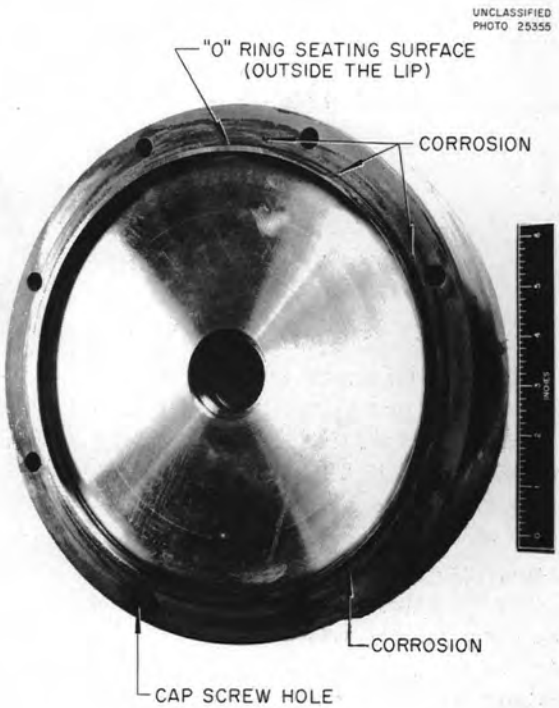

Fig. 3.4. 300A-1 Pump – Thermal-Barrier Back Side.

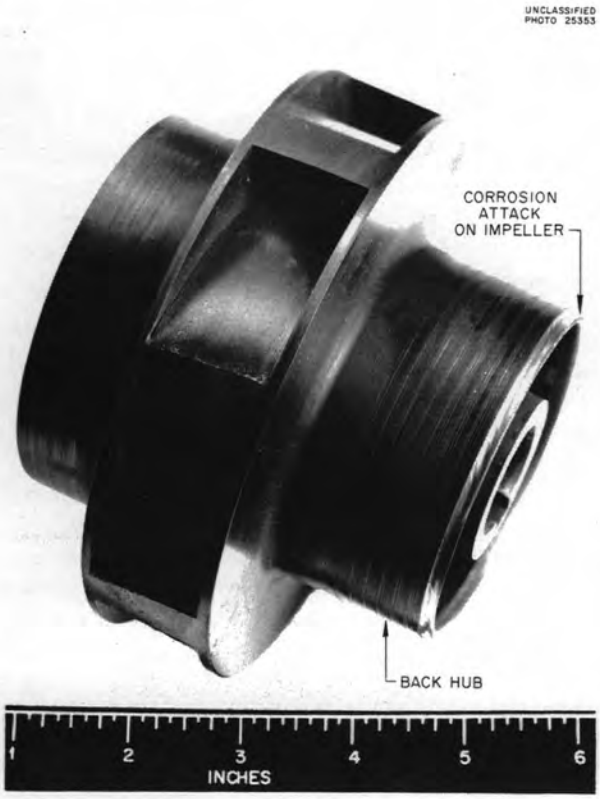

Fig. 3.3. 300A-1 Pump Impeller.

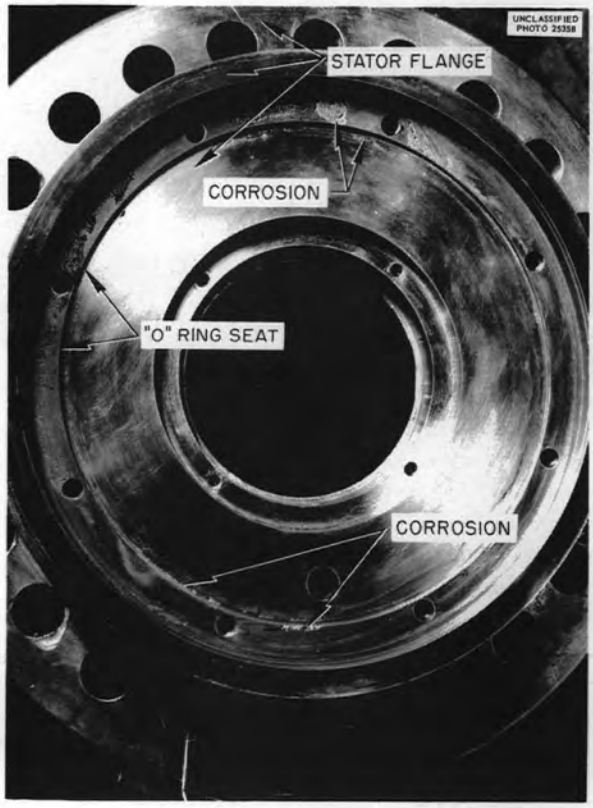

Fig. 3.5. 300A-1 Pump – Stator Flange.

Fig. 3.6. 300A-1 Pump – Stator Flange (Enlargement of Fig. 3.5).

3.1.3 400A-2 Pump and Loop

The 400A-2 pump was modified for use with the latest Westinghouse thermal barrier and was run for approximately 750 hr on water at 250°C. Unlike the 400A-1 and 300A-1 pumps, no leakage was observed across the thermal barrier or the main-flange gasket. The HRT pumps include this barrier design.

3.2 REACTOR FUEL AND BLANKET PUMPS

The two reactor pumps and two spares which had been on order were delivered. These four pumps were tested successfully at Westinghouse by thermal cycling, hydrostatic pressure, and helium leak testing. All were run for approximately 200 hr on water at 572°F and 2000 psi. They contain cast Stellite bearing shoes, such as have proved satisfactory in the 400A development loop tests. The 230-gpm, stainless steel, pump rotor assembly has a cast Stellite journal bearing at the lower end and a hard-faced Stellite journal at the upper end. The other three pumps have hard-faced journals.

3.3 HRT HEAT EXCHANGERS

The heat exchangers for the HRT were completed by the Foster Wheeler Corp. and shipped to the Nooter Corporation for installation of blast shields. The blanket exchanger was received at ORNL, subjected to final cleaning (see Sec. 3.3.1), and delivered to the reactor site for installation. The fuel exchanger was delivered to ORNL as this report period ended. This unit will be cleaned with hot water and UO_2SO_4. Although it passed the helium leak test specification (0.1 cc/day) at the fabricator's plant, a leak of approximately 0.01 cc/day was observed. For this reason, the unit will be retested after cleaning.

3.3.1 HRT Heat Exchanger Cleaning

Both heat exchangers failed the cleanliness requirement (no discoloration of surgical gauze) at the fabricator's plant. Slight deposits of organic material which could not be eliminated at the fabricator's plant were removed from the blanket heat exchanger by 250°C oxygenated water circulated for 48 hr. Under these conditions, the organic matter was oxidized to CO_2. Piping connections were made to test loop 400B to permit attachment of the heat exchangers for the cleaning aperations. Analytical results of the heat exchanger cleaning are shown in Fig. 3.7.

3.3.2 HRT Fuel Heat Exchanger Mockup

The small-scale heat exchanger in the fuel-mockup system was field inspected after about 2000 hr of operation. The primary-side end caps were removed to allow partial boroscopic examination of a majority of the tubes and visual examination of the tube sheets. No evidence of corrosion was seen on the tube-joint welds or the entrance regions of the tubes. Heavy scale was present on all primary-side surfaces; with the exception of several small areas in the exit regions of the tubes, the scale appeared uniform and continuous. The exit region of the tubes showed signs of either slight corrosion or irregular scale deposition, both at the inner edge of the tube ends and at the end of the rolled portion of the tubes.

UNCLASSIFIED
ORNL-LR-DWG 12035

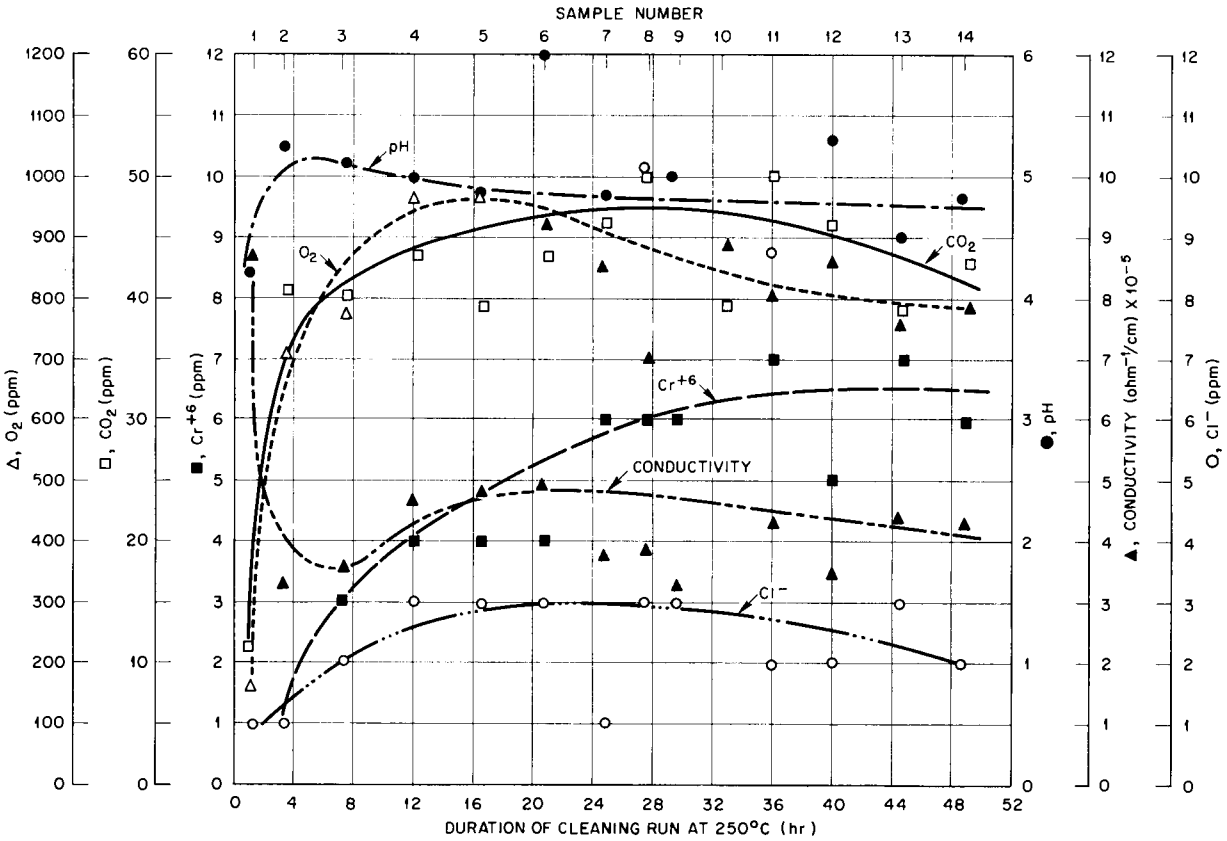

Fig. 3.7. Analytical Results of Heat Exchanger Cleaning.

3.4 PRESSURE-RELIEF VALVE

A pressure-relief valve was obtained from the Associated Valve & Engineering Co. for use in limiting the pressure difference between the core and blanket systems of the HRT. The valve has a spring-loaded poppet designed to relieve when the pressure difference is about 75 psi. In several tests with steam and air the valve failed to reseat after a few operating cycles. The leakage, during an air test, was 12 cc/min at 10 psi and increased to 1540 cc/min at 79 psi.

3.5 HRT PURGE PUMP

The test model of the HRT purge pump (used to supply cold condensate to the circulating pump bearings and the pressurizer) has been operated for 3600 hr without failure. At the present time, the drive unit is being modified to run at 30 strokes/min, in order to evaluate the operating characteristics at a discharge rate of 2 to 5 gph.

3.6 HRT FEED PUMP

Since the operation of the 1.5-gpm feed pump was not so satisfactory in the HRT mockup as it was on the original test stand, a new loop is being constructed to determine the pump performance on a system more closely duplicating the HRT piping. The principal trouble appears to be gas binding, which occurs when, through faulty operation or control, oxygen is injected into the pump suction at a rate approximately twice that specified for HRT operation. After the performance tests and other developments have been completed, the loop will be used for long-term endurance tests. The loop is approximately 60% complete.

3.7 GLASS MODEL OF NEW HRT PRESSURIZER DESIGN

A glass model of the connection between the circulating system and the pressurizer was tested for mixing characteristics. Cold water containing

gas and dye was circulated at 400 gpm, and hot water was injected to simulate a purge of 2.5 to 10 gph. There was a very stable interface between hot and cold water, as shown in Fig. 3.8. This interface could be broken up only by very rapid and violent surges, considerably more severe than those of the injection pump. Bubbles circulating in the main stream did not tend to travel into the pressurizer.

3.8 REMOVABLE INSULATION

In view of expected maintenance operations, a program was started to develop removable insulation for HRT piping and flanges. Various designs were built, tested, and appraised on considerations of ease of maintenance, insulating efficiency, and fabrication cost. The most suitable design (Figs. 3.9 and 3.10) uses layers of wrinkled aluminum foil as the insulating medium in a hinged open-ended can of 0.033-in.-thick aluminum sheet. Longitudinal flanges provide clamping surfaces.

Fig. 3.9. Remotely Replaced Thermal Insulation.

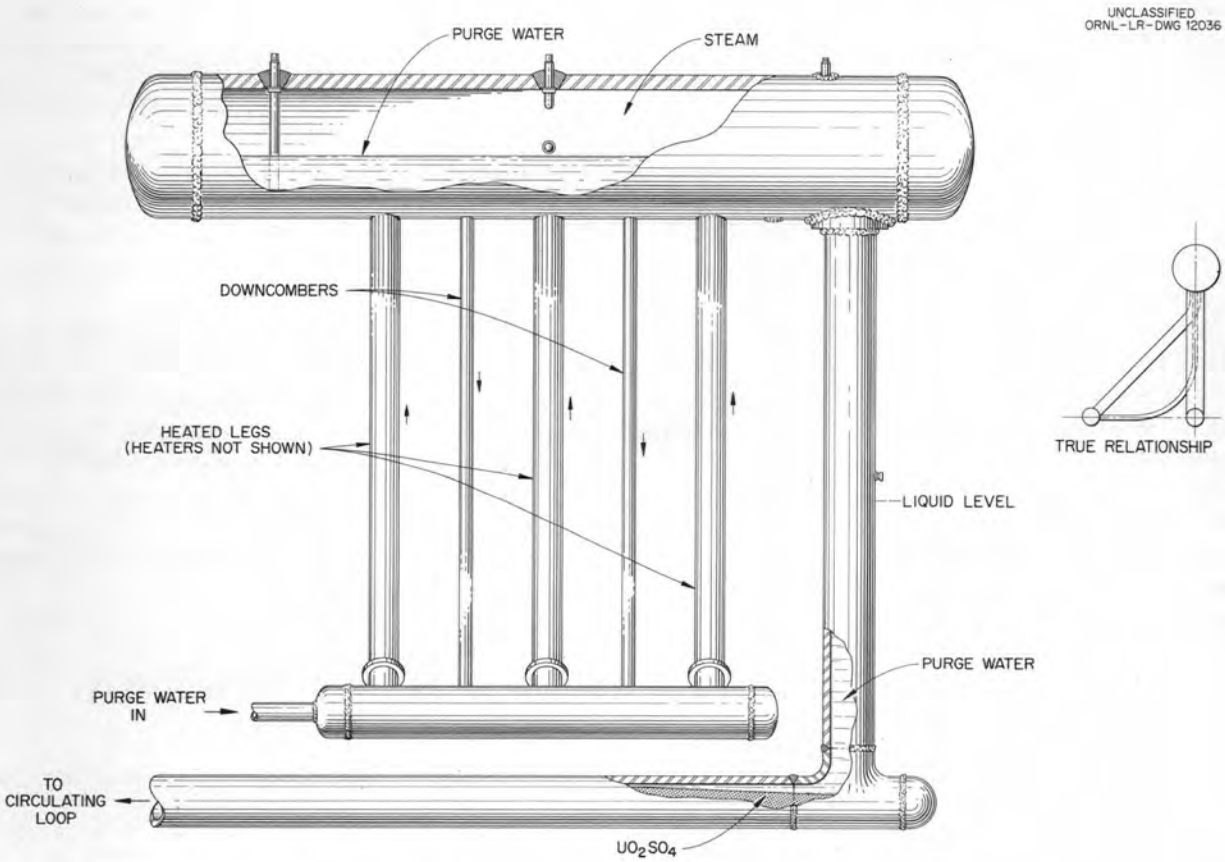

Fig. 3.8. Revised Mockup Pressurizer.

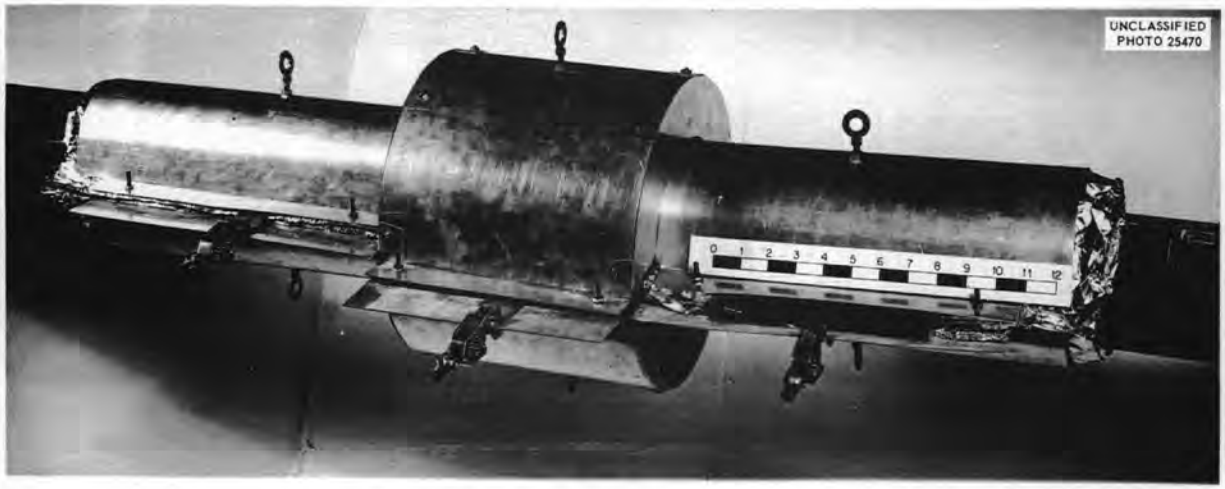

Fig. 3.10. Assembly Showing Insulation in Place Around Flange.

A standard toggle clamp is used to lock the insulation in place. In remote handling operations, two long-handled tools make it possible to lower, install, and lock the insulation in position. Heat losses are 10% of bare-pipe losses, as compared with 6% for stationary, wrapped-foil insulation.

3.9 HRT MOCKUP LOOP

3.9.1 Present Mockup Flowsheet

The flowsheet of the mockup in its present state is shown in Fig. 3.11. The high-pressure circulating loop contains a Westinghouse 300A circulating pump, a heat exchanger for heating the loop with high-pressure steam, a steam pressurizer, and a gas separator. These components are models or prototypes of HRT equipment. A continuous stream passes through the letdown heat exchanger and valve into the dump tank, simulating the HRT letdown system. In the dump tank, water is evaporated to feed 12 gph of condensate to the purge pump, which supplies pure water to the pressurizer and the back of the circulating pump. The remainder of the letdown stream is returned to the high-pressure loop with an HRT-prototype injection pump. To maintain the necessary oxygen content in the high-pressure system, oxygen is added to the injection pump suction stream.

Operation of the HRT mockup loop with water and four runs with UO_2SO_4 were previously summarized.[4–6] Difficulty was reported with the loop pressurizer, which supplies 2000-psi steam from three electrically heated legs.

Following the last run with the original pressurizer design, the pressurizer heater legs were cut out for examination. Two of the three legs were found to be plugged with solids which analyzed 4 to 5% U, 0.6 to 0.7% SO_4, 50% Fe, 6% Cr, 0.3% Ni, and 0.5% Cu. These two legs also showed severe pitting attack, as may be seen in the center leg of Fig. 3.12. The nonplugged east leg, shown in the same figure, was corroded to a lesser degree and contained a minor amount of U_3O_8 solids.

On subsequent examination of the pressurizer drum, it was observed that the condensate-distribution tube, which was to supply purge water equally to the three heater legs, had been bent during installation. As a result, it is probable that nearly all the purge water entered the east leg. It should be noted that, in spite of the excess purge water to the east leg, it did not adequately withstand the corrosive attack.

In the past quarter, the loop was operated for 759 hr, 550 hr of which was accumulated in two UO_2SO_4 runs (0.042 *M* UO_2SO_4, 0.023 *M* H_2SO_4, and 0.005 *M* $CuSO_4$).

[4] J. A. Hafford *et al.*, *HRP Quar. Prog. Rep. April 30, 1955*, ORNL-1895, p 33–37.

[5] C. B. Graham *et al.*, *HRP Quar. Prog. Rep. July 31, 1955*, ORNL-1943, p 28–31.

[6] C. B. Graham *et al.*, *HRP Quar. Prog. Rep. Oct. 31, 1955*, ORNL-2004, p 22–25.

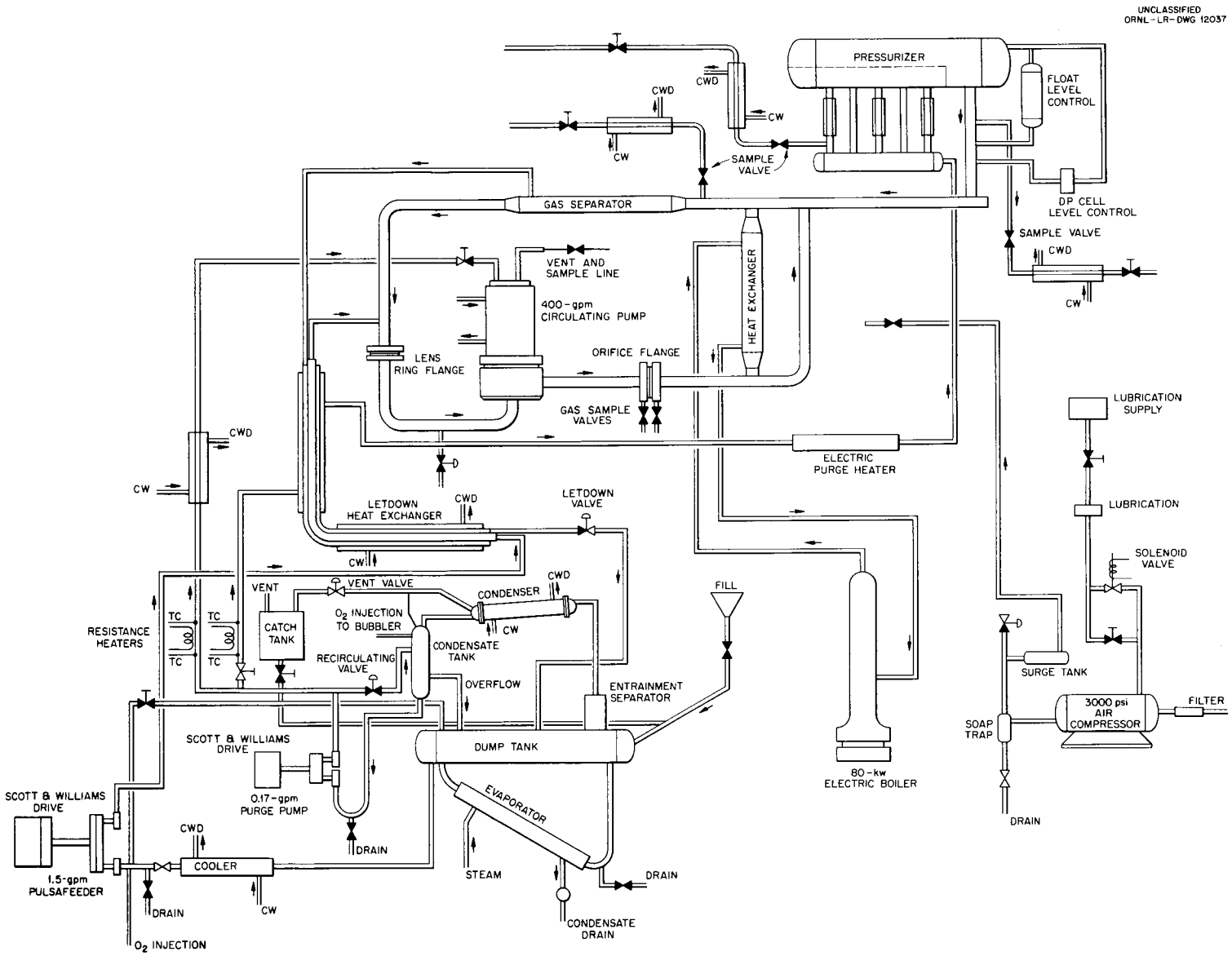

Fig. 3.11. Present Mockup Flowsheet.

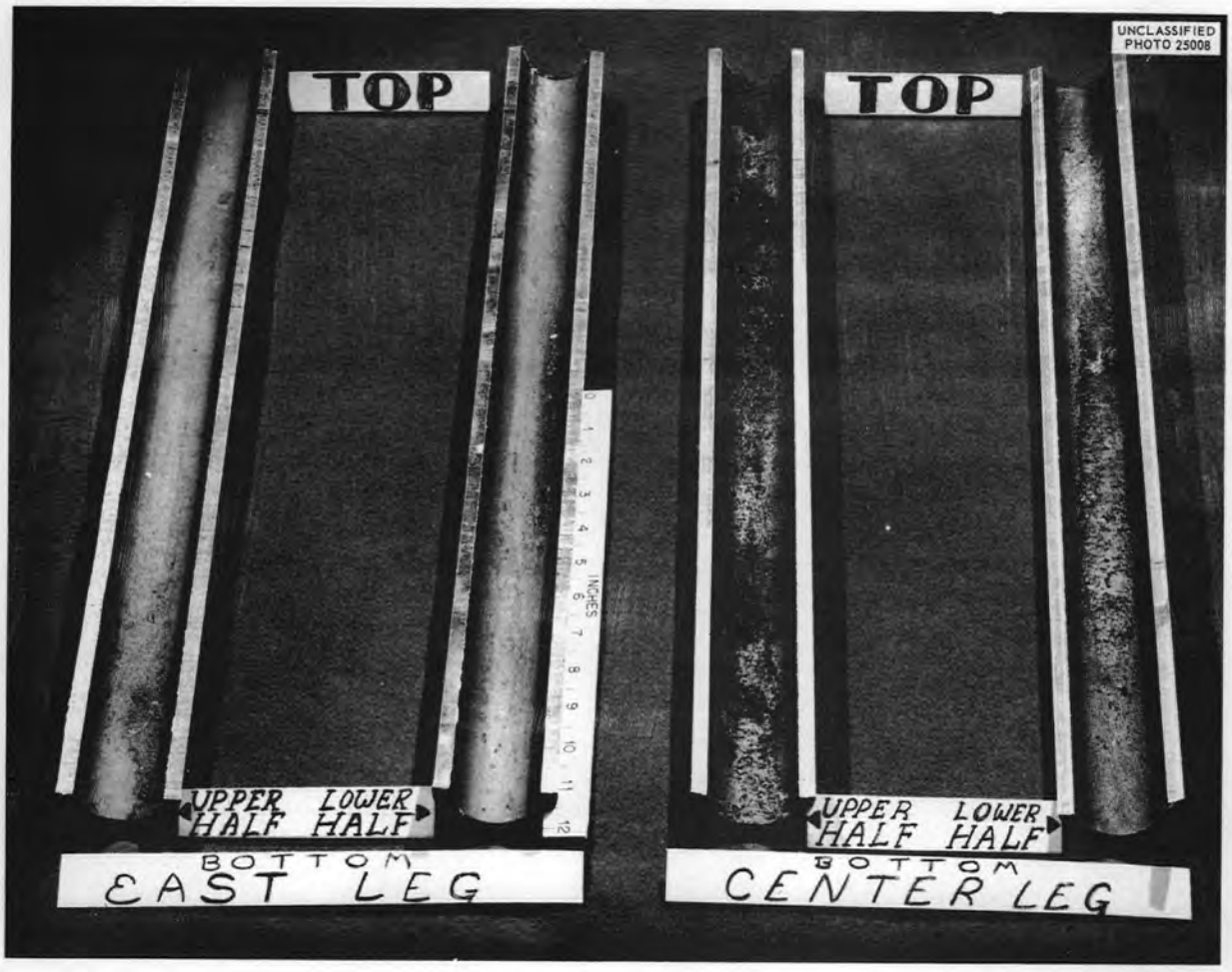

Fig. 3.12. Mockup Pressurizer Heater Legs in Original Pressurizer Design.

3.9.2 Gas Pressurization Operation

Following the unfavorable experience with steam pressurization described above, it was decided to explore the possibilities of gas pressurization, as well as to redesign the steam pressurizer to eliminate the obvious faults. While this redesign was in progress, new legs were installed in the original pressurizer, and a run was made with 2000-psi air to provide the overpressure. Corrosion and fuel stability data are presented in Fig. 3.13. The average corrosion rate over the run was 2 mpy; for the last 200 hr, it was 1.3 mpy. A photograph of one heater leg (Fig. 3.14) shows no significant corrosive attack. It was concluded from this run that gas pressurization would present no chemical problems in the HRT. This is consistent with corrosion-loop observations.

The above run covered a period of 375 hr before it was terminated in order for the loop to be modified for operation with the new steam-pressurizer design. During the run, two leaks developed in the stainless steel jacket of the letdown heat exchanger through which the purge water flows. Metallographic examination showed that stress-corrosion cracking was responsible for the failures. Signs of cracking were also observed in the inner pipe where it contacted the purge annulus. (The cracks were in no way related to the experiment with gas pressurization.)

The normal content of the purge jacket was condensate of pH varying from 2.5 to 6.1. On one occasion, UO_2SO_4 at a concentration of 5 g/liter was present for about 24 hr. The condensate had a chloride concentration (often responsible for

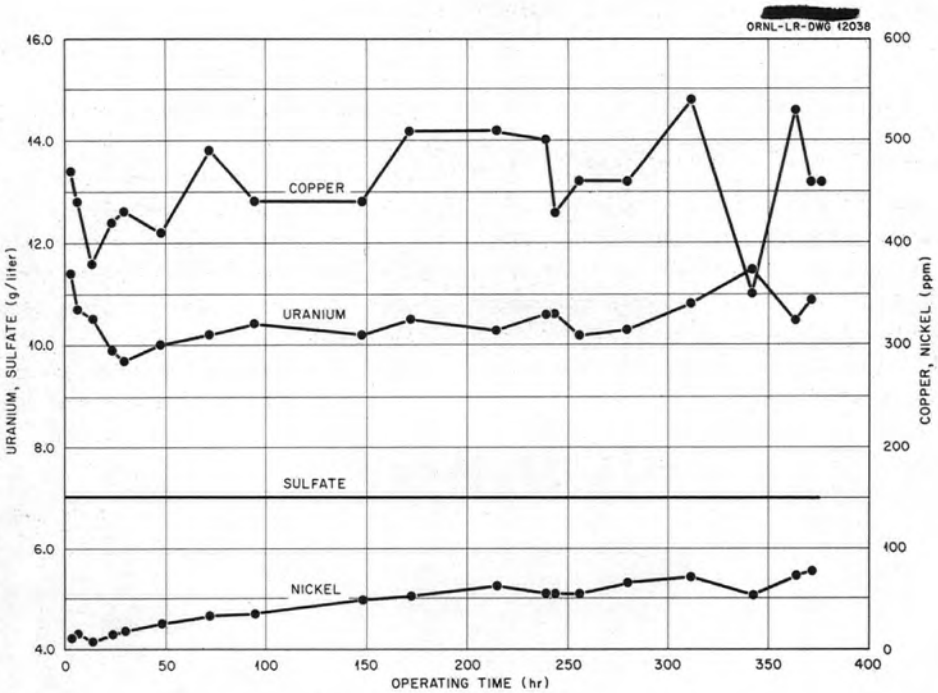

Fig. 3.13. Chemical Analyses of HRT Mockup Fuel During Gas-Pressurization Run – Nov. 19 to Dec. 4, 1955. All analyses corrected to a constant sulfate concentration of 7.0 g/liter.

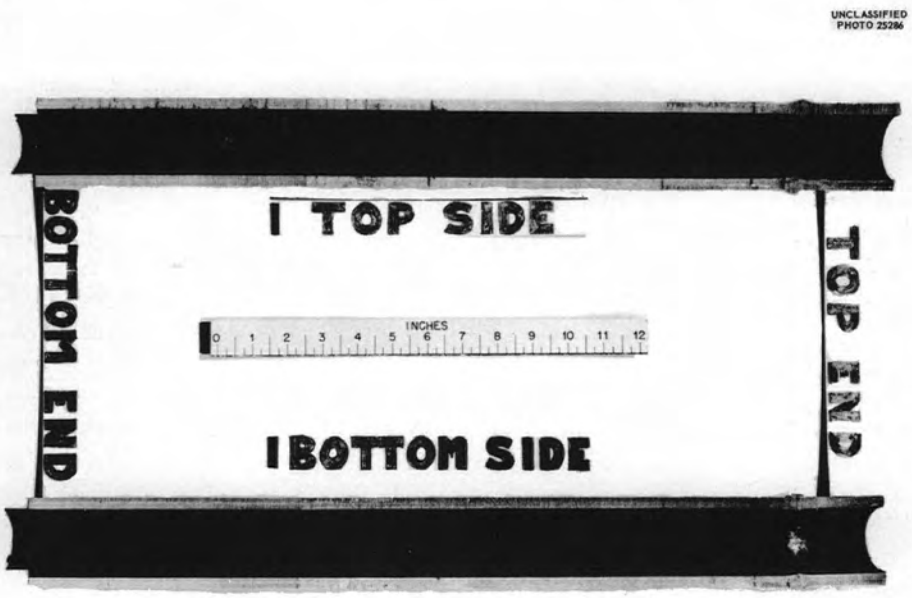

Fig. 3.14. Mockup Pressurizer Heater Leg, Gas-Pressurized Run.

cracking) below 1 ppm in the two samples checked. However, the chloride concentration was 2 ppm in the UO_2SO_4, and sampled corrosion products contained 19 to 400 ppm Cl.

3.9.3 New Steam-Pressurizer Test

Following the gas-pressurized operation, the letdown exchanger was replaced and the pressurizer rebuilt to conform to the new HRT design (Fig. 3.8). In this installation, water is pumped through the electrically heated legs into the pressurizer drum. Excess water and condensate from the drum overflow into the pipe which connects the drum to the circulating loop. As this water flows through the connecting pipe, it cools and mixes with fuel solution. Thus, only water is at the high temperature (~335°C) of the pressurizer.

The loop was operated with UO_2SO_4 for 145 hr; during this time the average corrosion rate was 5 mpy. Corrosion and fuel stability data are presented in Fig. 3.15. The relatively high corrosion rate is believed to be due principally to a leak around the thermal barrier of the circulating pump.

When the pump was disassembled, the O-ring gasket was found to be partly destroyed and the metal in the vicinity of the gasket severely attacked. The pump was repaired by seal-welding the barrier to the stator assembly.

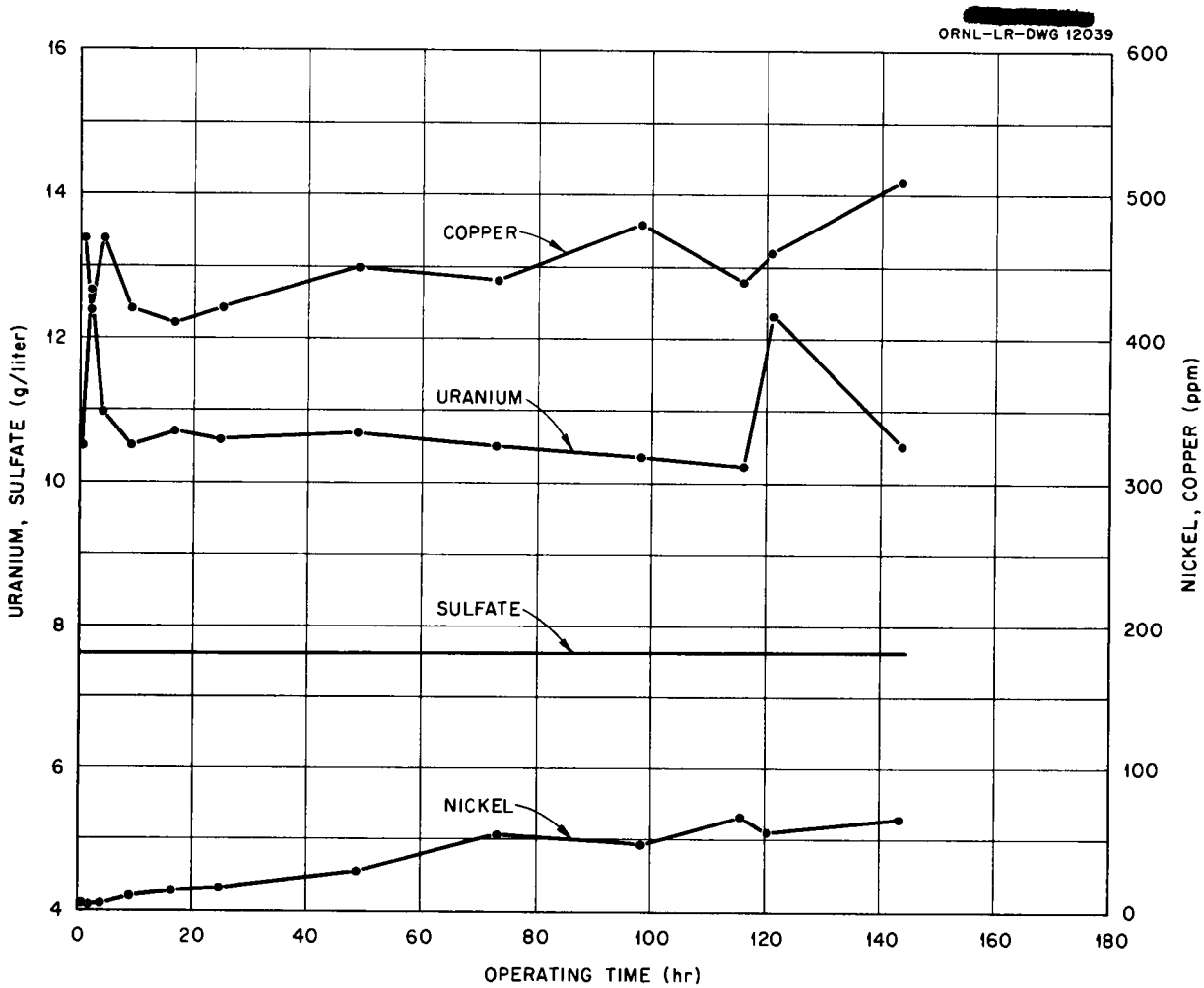

Fig. 3.15. Chemical Analyses of HRT Mockup Fuel During Steam-Pressurization Run with Modified Pressurizer Design – Dec. 29, 1955, to Jan. 4, 1956. All analyses corrected to a constant sulfate concentration of 7.6 g/liter.

The pressurizer system and the corrosion samples in it were examined, and no localized attack was found. A slight precipitate of $(UO_2)_3(PO_4)_2 \cdot 4H_2O$ was observed in the lower half of the horizontal pipe connecting the pressurizer to the loop. However, the phosphate was present because of contamination from a previous cleaning of the loop. Since no copper or uranium oxides were present in the solids removed from the pressurizer system, preliminary indications are that the revised pressurizer design will be suitable for the HRT. The location of solids indicated that the purge stream–solution boundary was as shown in Fig. 3.8, confirming model tests (see Sec. 3.7).

Following repair of the circulating pump and conversion to an HRT-prototype purge pump, the test of the revised pressurizer was resumed.

[redacted]

4. HRT REACTOR ANALYSIS

P. R. Kasten

H. C. Claiborne
P. N. Haubenreich
M. K. Hullings
D. M. Johnson[1]
J. O. Kolb
M. W. Rosenthal

4.1 PRESSURE RISE FOLLOWING STOPPAGE OF HEAT REMOVAL

M. W. Rosenthal H. C. Claiborne

Following sudden and complete stoppage of heat removal from the core system, energy will continue to be generated throughout the fuel solution by fission-product decay and to some extent by the fission process. This situation would be approximated if the liquid on the shell side of the heat exchanger were quickly removed or if the core fluid flow were suddenly and completely stopped. If there were no heat removal from the system, the generated energy would raise the temperature of the fuel solution and cause it to expand. Fluid expansion would reduce the free volume in the pressurizer and raise the operating pressure unless fluid were removed from the core system.

The pressure rise as a function of time was evaluated[2] for the above situation; calculations were made for several rates of liquid discharge through the letdown valve and of vapor discharge through the pressurizer vent line. The results are given in Fig. 4.1 for various discharge rates. The fluid expansion rate as a function of time was obtained from calculations by Hill[3] in which stoppage of flow was assumed after long-term operation at 5 Mw. The pressure-rise calculation was based on the assumption of adiabatic compression of the vapor in the pressurizer.

As shown in Fig. 4.1, with no fluid discharge, the pressure would reach 2800 psia in 38 sec and continue to rise until some safety device was actuated. However, a total discharge rate of 2 gpm appears to be sufficient to prevent the pressure from reaching 2800 psia.

[1]On loan from The Glenn L. Martin Co.

[2]M. W. Rosenthal and H. C. Claiborne, *Effects of Heat Generation and Heat Removal on HRT Shutdown and Dump*, ORNL CF memorandum (to be issued).

[3]J. W. Hill, Jr., *HRT Power and Fuel Temperature After Fuel Circulation Stops*, ORNL CF-54-9-64, (Sept. 9, 1954).

4.2 HRT DUMP ANALYSIS

M. W. Rosenthal H. C. Claiborne M. K. Hullings

The pressure-time relation during an HRT dump was calculated[2] for various combinations of heat-generation, heat-removal, and venting conditions. The results, presented in Figs. 4.2 and 4.3, represent cases where reactor after-heat and vapor condensation in the heat exchanger were, and were not, considered. The results in Fig. 4.2 are based upon the assumption that the dump valve opened when the core pressure was initially 2000 psi, while for Fig. 4.3 it was assumed that vapor was initially vented from the pressurizer and that the dump valve opened when the pressure had dropped to the level corresponding to saturation conditions in the core.

Since some heat-transfer surface in the heat exchanger becomes exposed as soon as 28 liters of liquid has been discharged from the high-pressure system, it was necessary to consider heat removal by vapor condensation within the heat exchanger. Four different models were used to obtain the rate of heat removal from the core. These were based on two different heat-transfer coefficients for vapor condensation inside the heat exchanger tubes and on two different volume heat capacities for the heat exchanger. For these cases the condensing coefficient was assumed to be either infinite or 1000 Btu/hr·ft^2·°F. In both instances a tube-wall resistance and shell-side boiling coefficient were considered. The volume heat capacity was assumed to be either infinite or the capacity associated with the tube metal plus a given mass of fluid on the shell side of the heat exchanger. For both cases the minimum shell-side pressure was assumed to be 520 psia.

With no initial venting, the pressure decreased rapidly as the overpressure was relieved, as shown in Fig. 4.2. When heat removal was considered, the subsequent high rate of pressure drop resulted from the rapid condensation of vapor as the heat exchanger surface was exposed. With heat removal

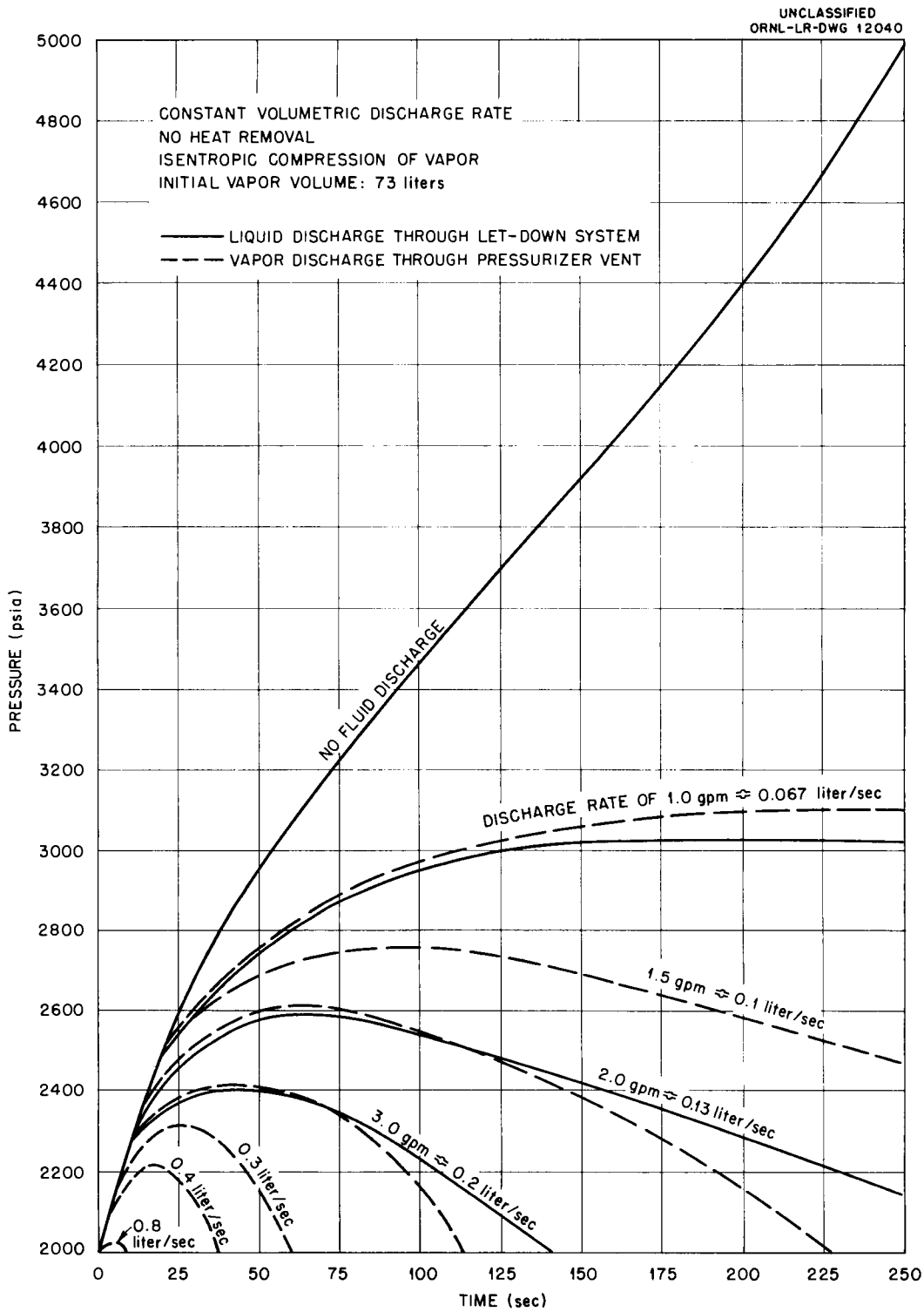

Fig. 4.1. Pressure in HRT Following Flow Stoppage in the Absence of Heat Removal or Venting.

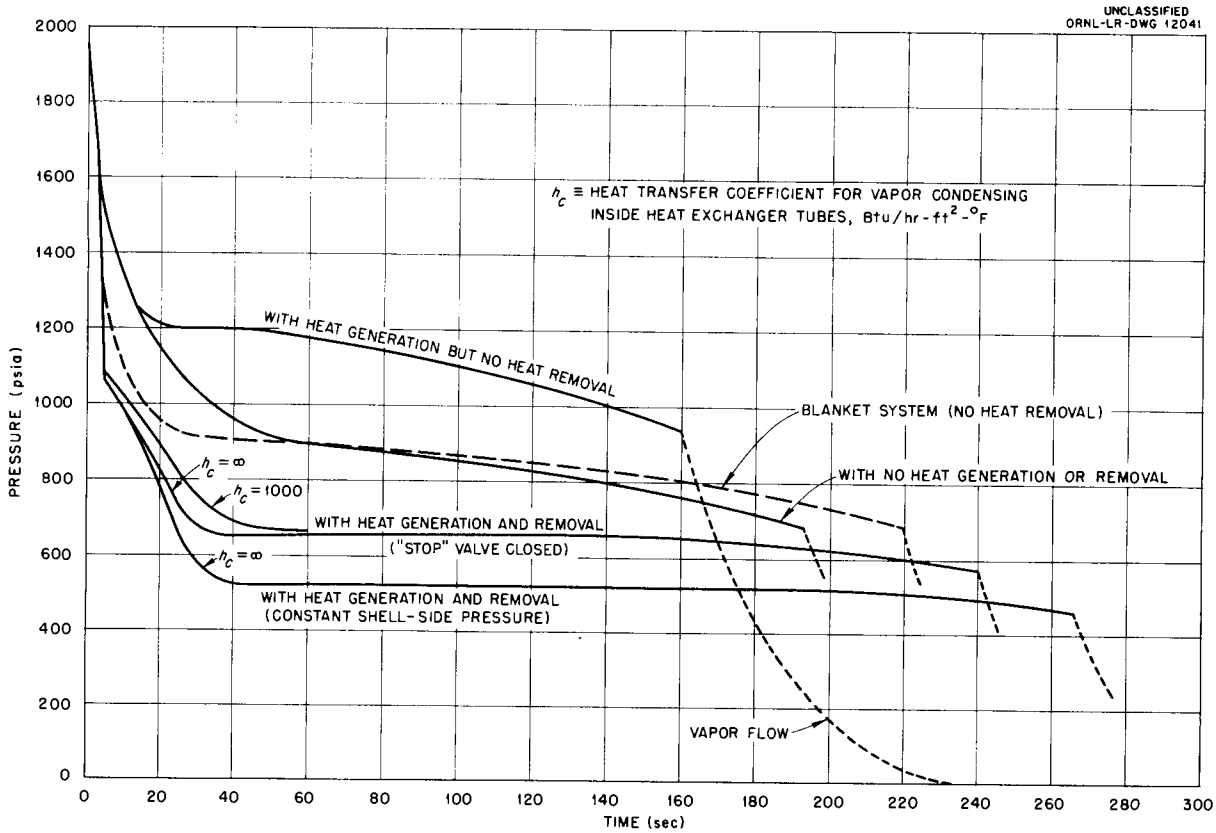

Fig. 4.2. Effects of Heat Generation and Heat Removal on Pressure-Time Relation During HRT Dump *Without* **Initial Venting.** Dump of core system following operation at 5 Mw.

and constant shell-side pressure, the core pressure leveled off at slightly above 520 psia. When the heat exchanger pressure increased with time, the core pressure curve was displaced upward.

A 30-sec vent period was assumed for those cases in which venting was considered. Since no vapor would be exposed to a condensing surface until the overpressure had been relieved, the pressure would not decrease so rapidly (Fig. 4.2 vs Fig. 4.1). The dashed line in Fig. 4.2 represents the blanket pressure-time behavior and was based on calculations by Pasqua.[4]

4.3 MISCELLANEOUS SHIELDING CALCULATIONS

P. N. Haubenreich J. O. Kolb D. M. Johnson

A number of shielding calculations were carried out during the past quarter. Calculations for the off-gas lines and the charcoal adsorbers were revised to include the recent information on decay schemes of some of the fission products involved and to take into account revised estimates of delay time of gas inside the reactor cell. Eight feet of earth, or an equivalent weight of denser material, will be required over the off-gas line. Ten feet of earth, or its equivalent, will be placed over the pit containing the charcoal adsorbers.

The original design of the samplers included a shield plug 25 in. thick containing lead shot in water.[5] Because the sample valves are longer than had been expected, the plug must be somewhat thinner. Calculations indicate that the thickness could be safely reduced by as much as 4 in., which is more than enough to accommodate the longer valves.

---

[4]P. F. Pasqua, *Report on Analysis of Data Obtained from HRT Dump Test, Phase I*, ORNL CF-55-10-14, (Oct. 6, 1955).

[5]W. R. Gall *et al.*, *HRP Quar. Prog. Rep. July 31, 1955*, ORNL-1943, p 13–15.

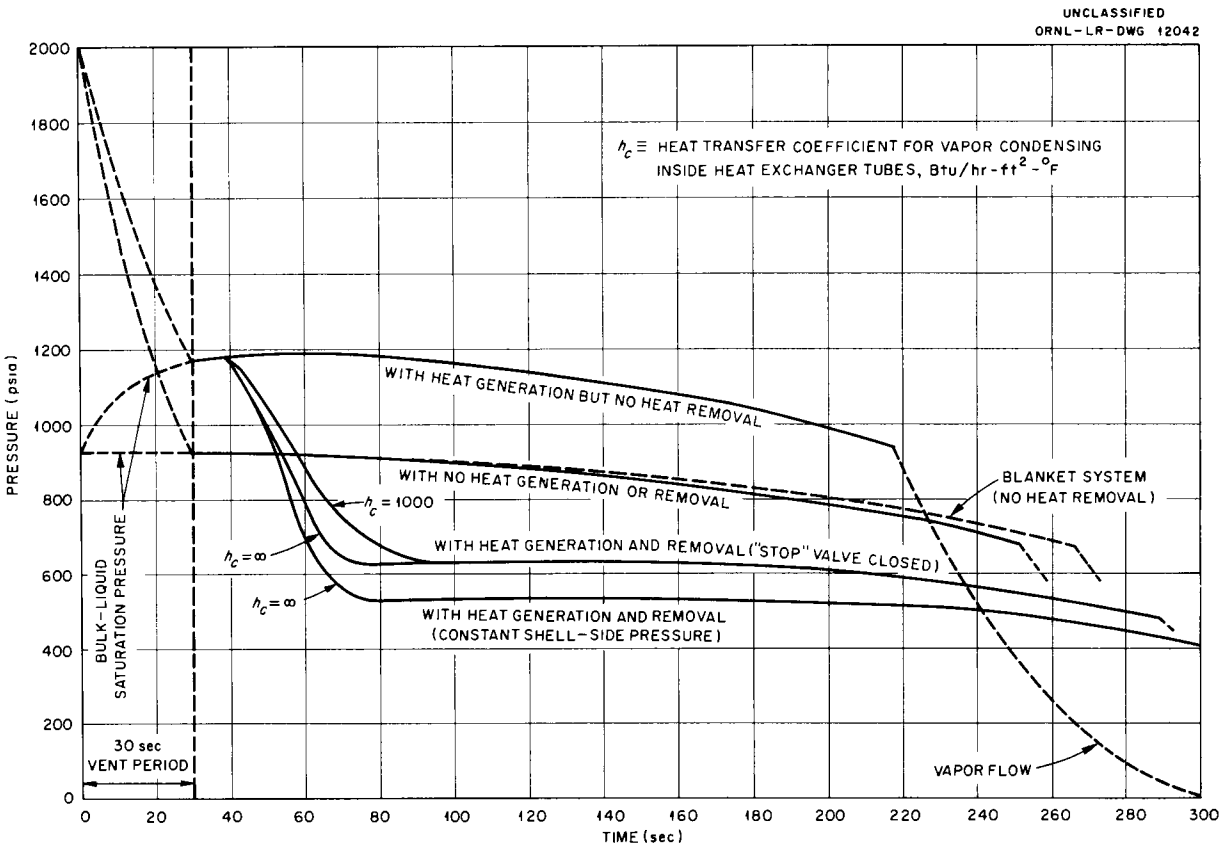

Fig. 4.3. Effects of Heat Generation and Heat Removal on Pressure-Time Relation During HRT Dump *With* Initial Venting. Dump of core system following operation at 5 Mw.

The carrier in which samples are to be transported will have 6 in. of lead on the sides, 5.5 in. on the top, and 5 in. on the bottom. Calculations show this shielding to be adequate for carrying 5-ml samples from the fuel high-pressure system; these samples will be the most radioactive ones taken from the reactor.

4.4 THERMAL-SHIELD TEMPERATURES

P. N. Haubenreich J. O. Kolb

The diameter and spacing of the cooling-water passages in the thermal shield were determined by calculations in which the cooled region was approximated by a cylinder in which there was uniform volumetric heat source.[6] The cooling system was designed to maintain temperatures in the shield at values below the boiling point of water at the cell pressure at reactor powers up to 10 Mw. More detailed calculations of the distribution of the heat source in the shield indicate that this shield temperature criterion will be met when the reactor is operated with a D_2O reflector.[7] If, however, the reactor is operated with a natural-uranium blanket, the heat production in the inner portions of the shield will be much more intense as a result of the fast-neutron leakage from the blanket. Calculations of temperature distributions in the side walls by a relaxation procedure indicate that the temperature at some points will reach the boiling point of water if the core power is above 6 Mw. This is not considered to be a serious limitation, because operation at higher powers is not planned and, in any case, would only result in vapor pockets at hot spots; this would not significantly reduce the average shield density.

[6] W. R. Gall *et al.*, *HRP Quar. Prog. Rep. Oct. 31, 1955*, ORNL-2004, p 8.

[7] P. N. Haubenreich and J. O. Kolb, *Further Calculations of Heating and Temperature Distributions in HRT Thermal Shield*, ORNL CF memorandum (to be issued).

5. HRT CONTROLS AND INSTRUMENTATION

D. S. Toomb

A. M. Billings
J. R. Brown
C. H. Gabbard
J. C. Gundlach
R. L. Moore
L. R. Quarles[1]
R. E. Toucey
W. P. Walker[1]
K. W. West

5.1 GENERAL STATUS

The construction of the instrumentation and control system and the checkout of completed circuits are continuing. Wiring in the main and auxiliary control rooms is complete, and the interconnections are now being made. Valves and instrument components are being bench-tested as they are received from vendors; tests, to date, indicate performance in agreement with the design specifications.

Materials ordered now total $184,000, of which $75,000 is for the reactor core- and blanket-system valves and $29,000 is for steam- and auxiliary-system valves.

The instrument-application index tabulation, which relates the process flowsheets to the instrument specification sheets and the reactor installation drawings, was issued.

Explosion-proof screw-type cover Condulets have been selected for the reactor-cell electrical-conduit installation. Covers and joints will be seal-welded for final waterproofing.

A heater-thermocouple-type liquid-level alarm probe was constructed and tested as part of the liquid-level instrument development program; it was found to have excessive time lag and poor reproducibility. A unit utilizing smaller thermocouple heater assemblies will be built in an effort to improve this instrument.

5.2 LIQUID-LEVEL TRANSMITTERS

Two prototype pressurizer-level controllers, incorporating different damping mechanisms, have exhibited stability sufficient for control of the letdown valve, which throttles a mixture of reactor liquids and gases from the high-pressure piping to the low-pressure dump tanks.

The hydraulically damped model now installed on the HRT mockup loop is shown in Fig. 5.1. Movement of the soft-iron core is sensed through the wall of the float housing by a differential transformer. The suspension springs are Iso-Elastic[2] alloy with a 3-mil gold plate. The gold plate is desirable for corrosion protection but unfortunately affects the constant-temperature-modulus characteristics of the alloy. Titanium plating of Iso-Elastic is being investigated. Elgiloy[3] spring alloy has shown excellent corrosion resistance without plating and will be tested as soon as suitable quantities are received.

With a radial clearance of $\frac{1}{32}$ in. around the damping disks, a vibration of 0.015 in. is reduced almost to zero in 16 sec. Instrument full-scale deflection at the test temperature of 636°F was approximately 0.020 in.

The second type of level controller, which is magnetically damped, is shown in Fig. 5.2. It utilizes the same springs and electric motion transmitter as the hydraulically damped unit. Float motion is damped by the action of the magnetic field on a copper ring, which is encased in stainless steel for corrosion resistance. The field of the permanent magnets acts through the nonmagnetic stainless steel pressure housing, thus permitting damping action without small clearances between the housing and moving float extensions. Damping oscillograms for this unit are shown in Fig. 5.3. The initial float displacement was 0.040 in., and the vibration decreased almost to zero in 2 sec with the magnet assembly in place.

5.3 VALVES AND OPERATORS

5.3.1 HRT Low-Pressure Valves

Delivery and testing of the HRT low-pressure valves are 90% complete. Elimination of leakage between plug and seat of the air-operated valves gave some difficulty due to a slight out-of-

[1]Consultant, University of Virginia.

[2]John Chatillon & Sons, New York 38, N. Y.

[3]Elgin National Watch Co., Elgin, Ill.

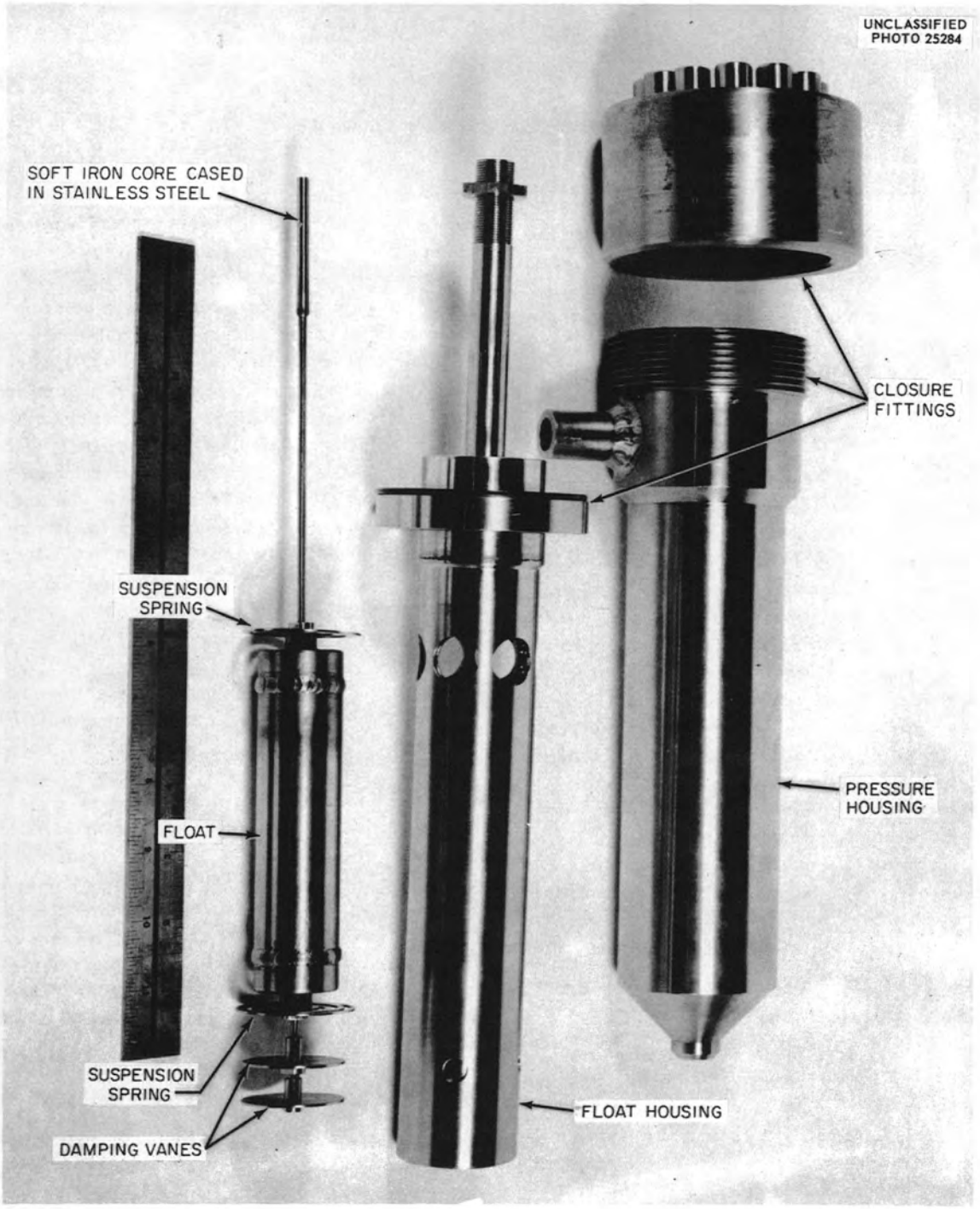

Fig. 5.1. Prototype Hydraulically Damped Liquid-Level Controller.

UNCLASSIFIED
PHOTO 25285

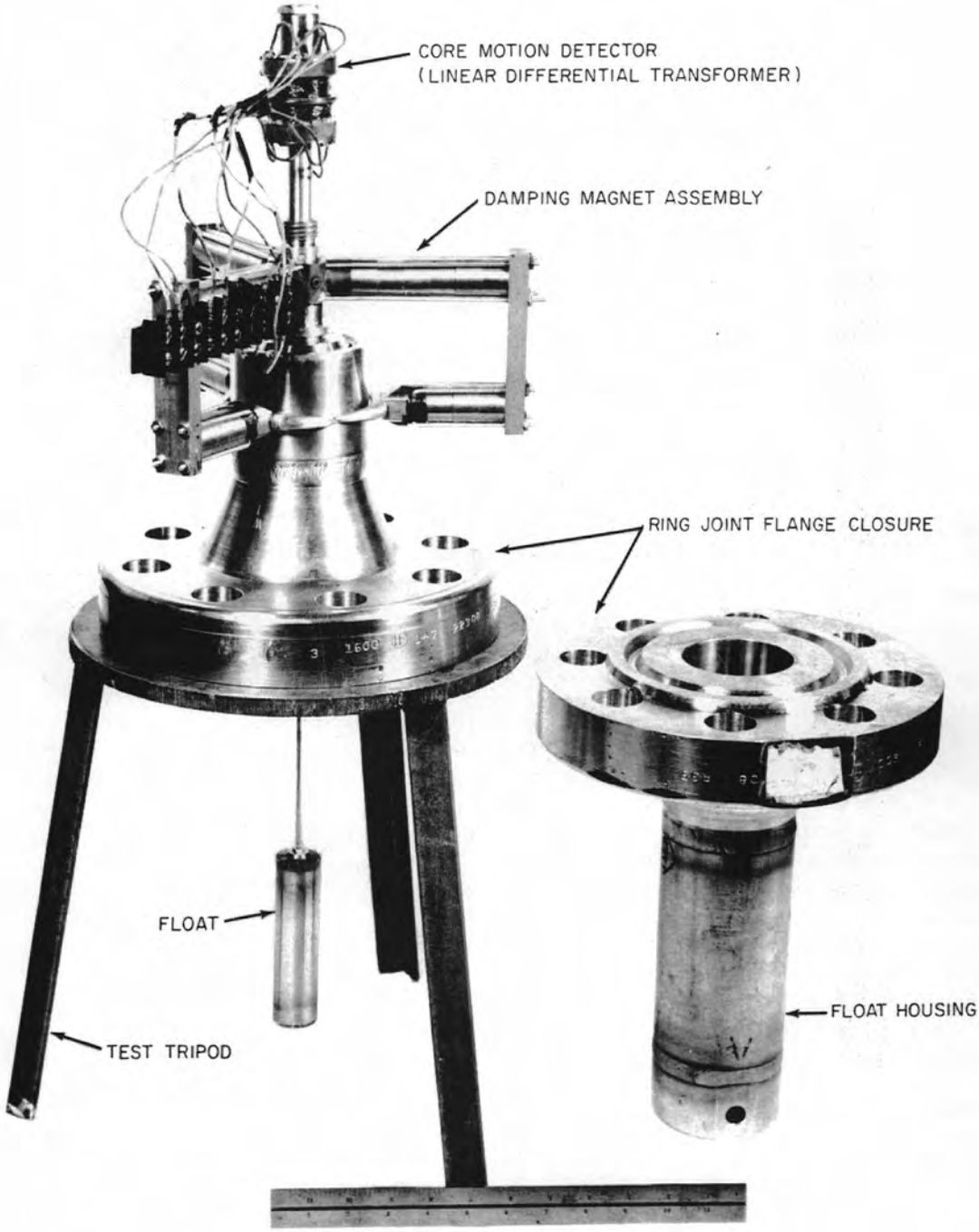

Fig. 5.2. Prototype Magnetically Damped Liquid-Level Controller.

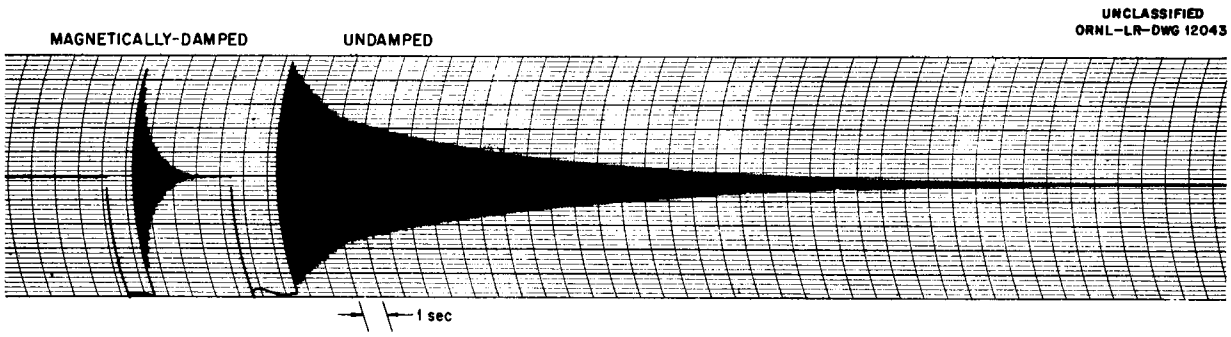

Fig. 5.3. Damping Action of Assembly Shown in Fig. 5.2.

roundness of the bore of the precision-cast and -ground Stellite No. 12 seats. However, satisfactorily low leakage rates were achieved by hand-lapping.

5.3.2 HRT High-Pressure Valves

Sixty per cent of the HRT high-pressure valves are now on hand, and the remainder should be delivered by February 1. Radiographs, leak tests, and hydrostatic tests have all been satisfactory. An HRT-model letdown valve was installed on the HRT mockup for performance tests under simulated reactor-operating conditions.

5.3.3 Dump-Valve Operator

A prototype model of the dump-valve operator shown in Fig. 5.4 was cycled 20,000 times without failure. This operator has an effective area of 68 in.^{2}, will operate with air pressures up to 80 psi, and has a maximum stroke of $\frac{3}{4}$ in. Its construction is suitable for high-temperature operation in nuclear radiation fields. Four such operators are to be delivered by the vendor[4] by February 1.

5.3.4 Small-Valve Operator

The operator for the small valves is shown in Figs. 5.5 and 5.6. This operator has an effective area of 48 in.^{2}, is rated to 60-psi operating pressures, and has a maximum stroke of $\frac{1}{2}$ in. Prototypes have been cycled 60,000 times in the vendor's plant[5] and 20,000 times by ORNL without failure.

5.3.5 Valve-Trim Testing Program

Eight trim-material combinations have been tested in the valve-trim-material testing program, utilizing the valve-test loop.[6-8] Best performance was obtained with a set of trim fabricated from titanium alloy Ti-130A. Leakage before testing resulted in a pressure-rise rate of 6 μ/min, and, after 404 "dump" cycles, this had increased to 16 μ/min. Appearance of the trim after testing was excellent. The plug showed a weight loss of 0.0086 g, and the weight loss of the seat was negligible. Other samples of trim were obtained from several manufacturers for testing.

---

[4]Fulton-Sylphon Division, Robertshaw-Fulton Controls Company, Knoxville, Tenn.

[5]The Annin Company, Los Angeles 23, Calif.

[6]C. B. Graham *et al.*, *HRP Quar. Prog. Rep. Oct. 31, 1954*, ORNL-1813, p 109.

[7]D. S. Toomb *et al.*, *HRP Quar. Prog. Rep. Oct. 31, 1955*, ORNL-2004, p 31.

[8]A. M. Billings, *HRP Experimental Valve Program*, ORNL CF-56-2-42 (Feb. 14, 1956).

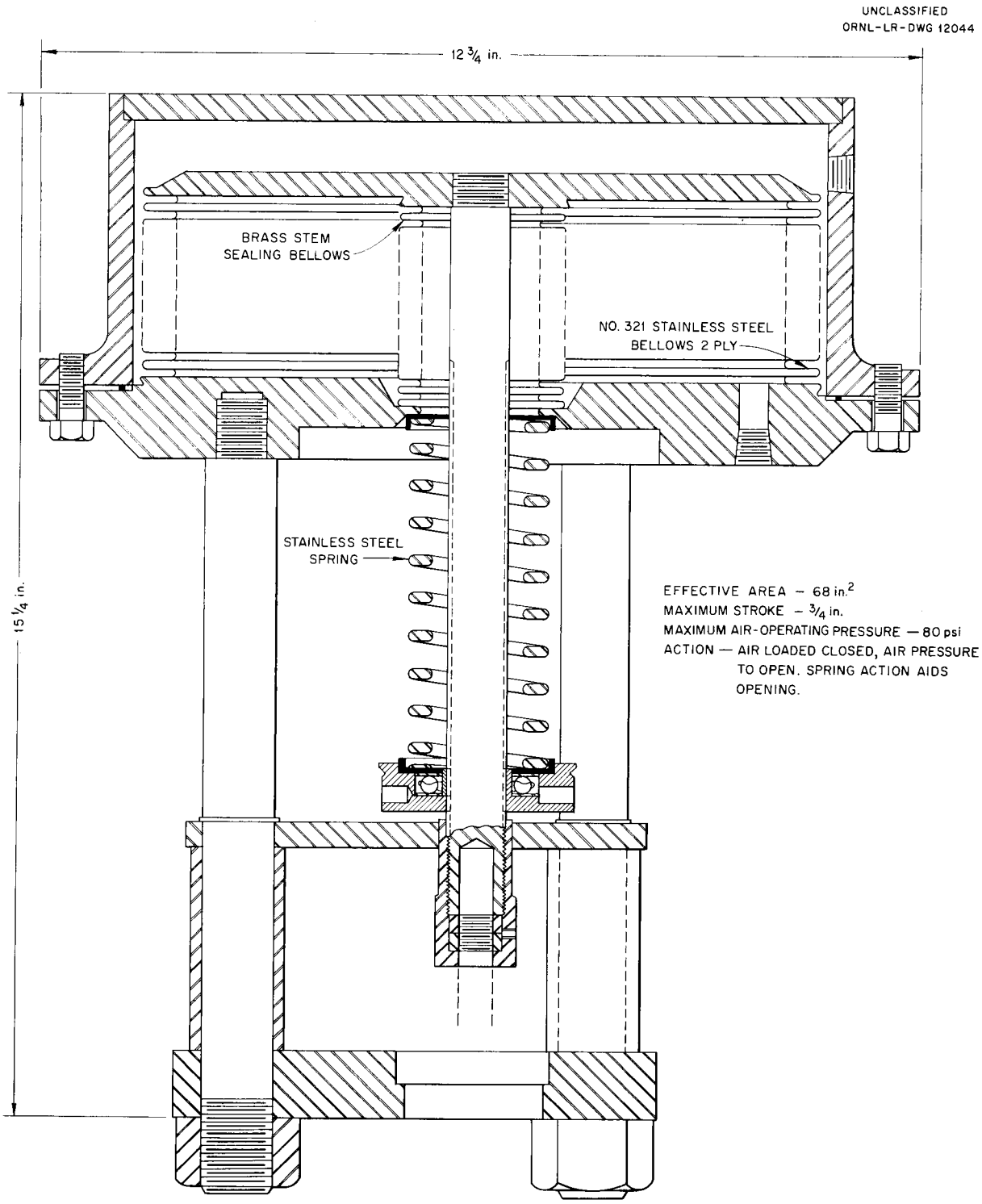

Fig. 5.4. Dump-Valve Operator.

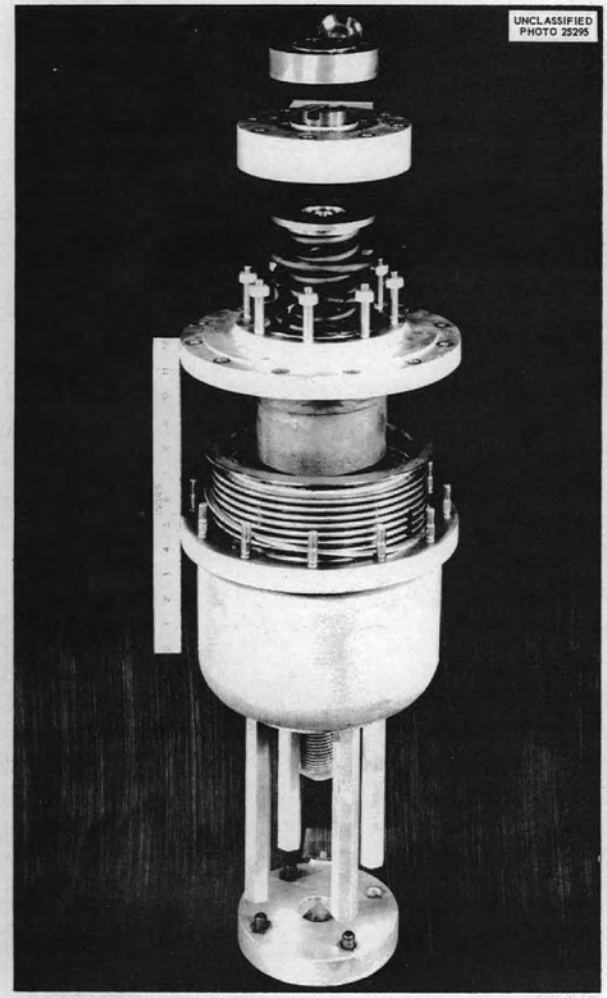

Fig. 5.5. Disassembled Small-Valve Operator.

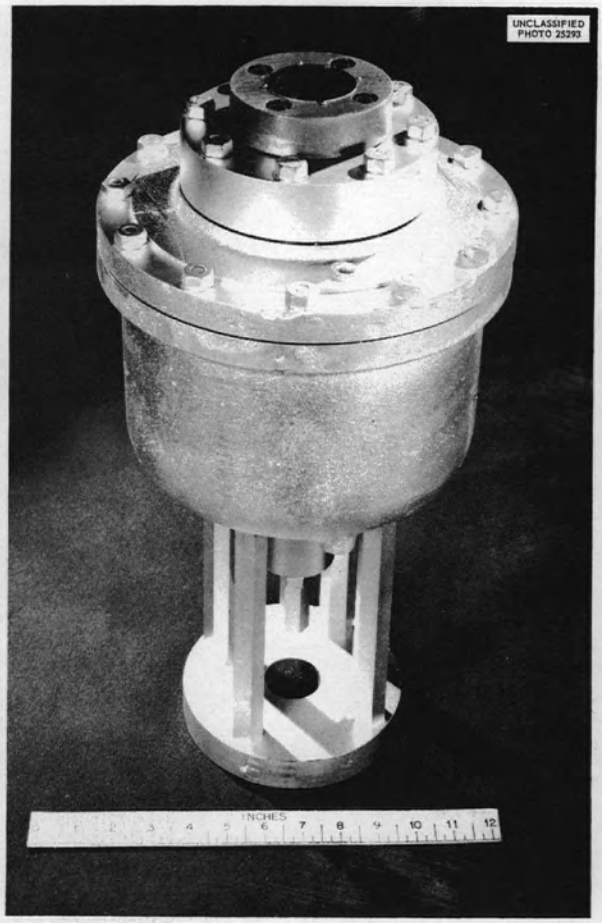

Fig. 5.6. Assembled Small-Valve Operator.

6. HRT FUEL PROCESSING PLANT

F. R. Bruce W. E. Unger E. O. Nurmi
W. D. Burch R. B. Lindauer
W. L. Carter F. C. McCullough
G. W. Gray P. E. Novak
C. E. Guthrie A. M. Rom
P. A. Haas H. O. Weeren
C. C. Haws H. E. Williamson
R. O. Ivins R. H. Winget

Although the fuel processing plant for the HRT has been in the course of design for about a year, there has not yet been a comprehensive report on the entire plant. The discussion which follows is intended to present matters which have not been completely reported previously and to delineate and interrelate the various problems.

During operation of the HRT, fission and corrosion products will be formed and will accumulate in the fuel solution. In the scheduled demonstration the concentrations of these poisons will not build up sufficiently to interfere seriously with reactor operation. However, in a large power-producing facility, continuous removal of foreign atoms would be essential for high neutron efficiency. The most serious poisons are the rare-earth fission products, with corrosion and other fission products being secondary.

The HRT system will be provided with a chemical plant to demonstrate a method for continuous removal of fission and corrosion products from the reactor fuel solution. A portion of the circulating-fuel stream will be bypassed through this plant (abbreviated HRT-CP) for cleanup and will be returned to the reactor fuel system. Fortunately, the solubility of the rare-earth sulfates decreases as the temperature increases, and at the operating temperature of the reactor (300°C) they are 500 to 1000 times less soluble than at room temperature. Some of the corrosion products (zirconium, iron, and chromium) hydrolyze at this temperature to form insoluble oxides. This condition is favorable for use of solid-liquid separation methods on the bypassed fuel stream.

At 5-Mw power about 1.3 g of insoluble rare-earth fission products per day would be produced. Laboratory data indicate that at 300°C a rare-earth solubility of 0.03 to 0.09 g/liter can be expected. The reactor will operate from two to four weeks before the fuel solution is saturated and rare-earth fission products begin to precipitate.

Corrosion products, being less soluble than fission products, will appear earlier as solids. At corrosion rates of 10 mpy for the zirconium core tank and 1 mpy for the stainless steel parts, the solids accumulated in the reactor fuel will be preponderantly corrosion products (Table 6.1).

TABLE 6.1. PREDICTED SOLIDS PRODUCTION IN THE HRT

Core power: 5 Mw
Corrosion rates: stainless steel, 1 mpy
zirconium core, 10 mpy

Compound Expected	Production Rate (g/day)	Total Solids Composition (wt %)
ZrO_2	24	44
Fe_2O_3	22	41
Cr_2O_3	6.8	13
$(RE)_2(SO_4)_3$*	2.6	2

*An approximately equal quantity of insoluble fission products other than rare earths (alkaline earths, zirconium, ruthenium, rhodium, palladium, and probably molybdenum) is expected to precipitate from the reactor fuel solution.

The HRT is being installed in Building 7500 (Figs. 6.1 and 6.2), which originally housed the HRE. Space for the HRT-CP has been provided adjacent to and just south of the reactor cells. The facility consists of an office and operating area above grade and four cells below grade (Fig. 6.3). The surrounding earth supplies some of the support and shielding. Access to the cells is from the top only. The cells are separated from each other by 4-ft walls of barytes concrete and from the reactor cell by 5 ft of colemanite-concrete radiation

ORNL-LR-DWG 2784
REVISION 1 4-6-55

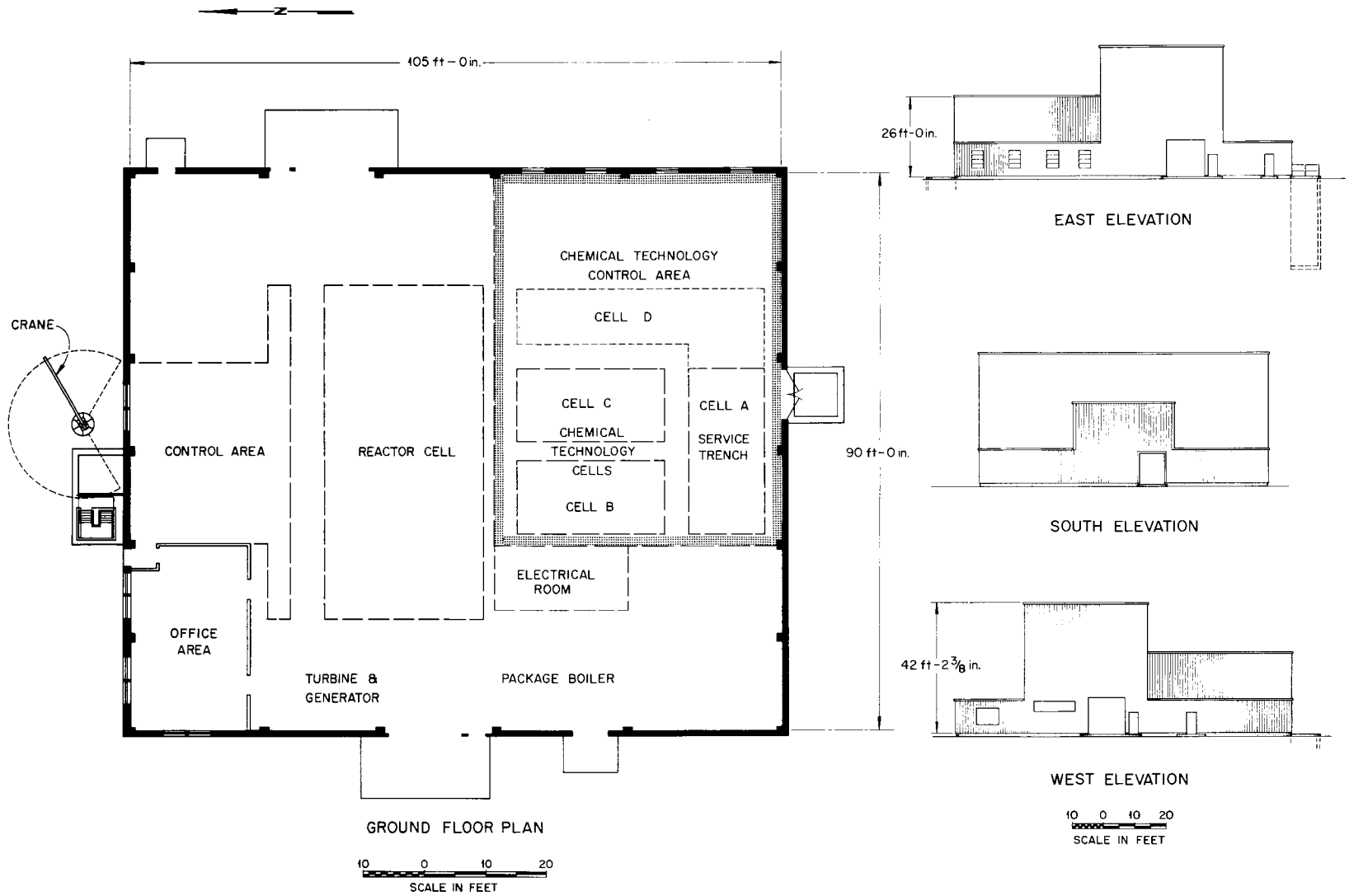

Fig. 6.1. Plan and Elevation of Building 7500.

[redacted]

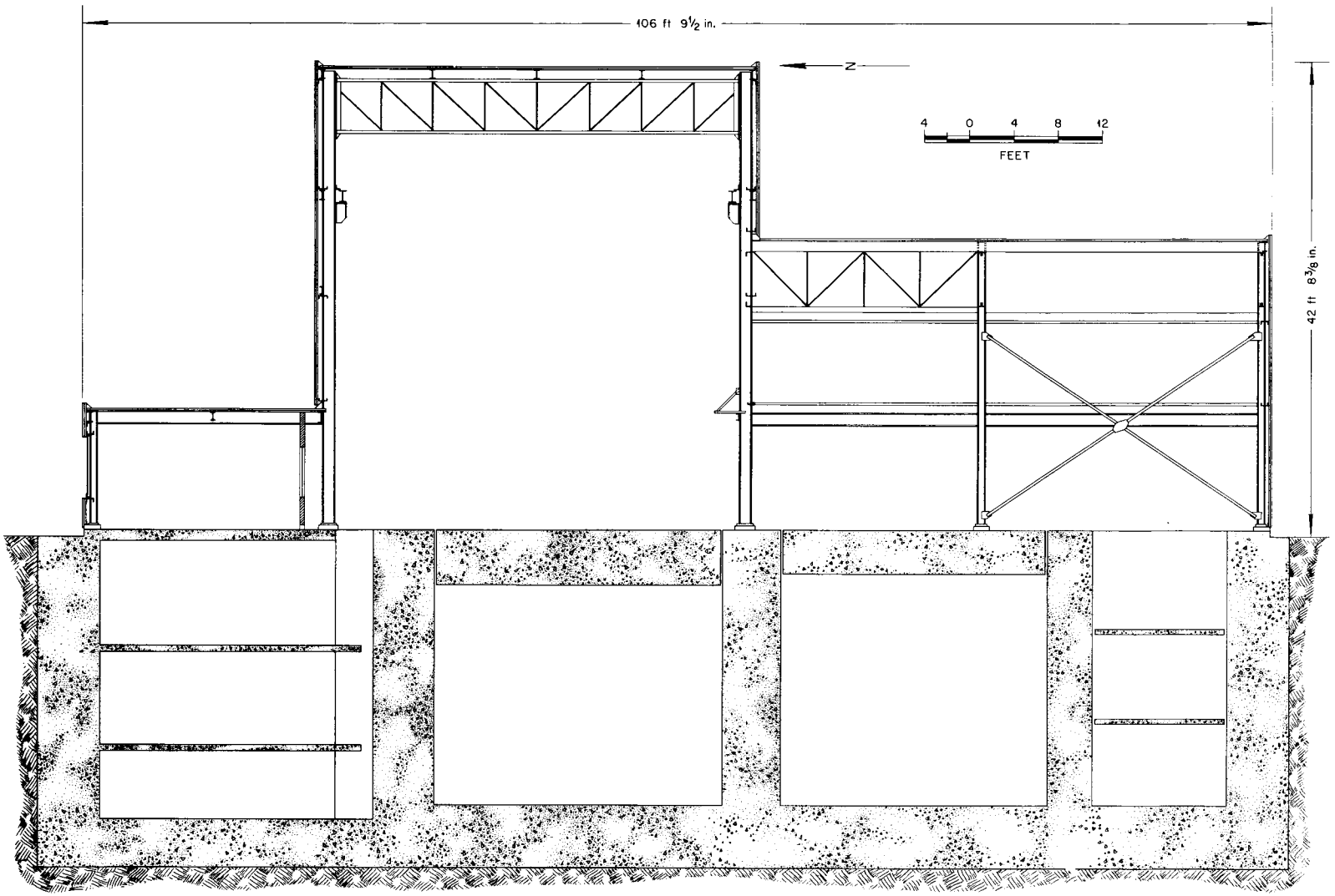

Fig. 6.2. Structural Details for Building 7500.

[redacted]

DWG. 19918A

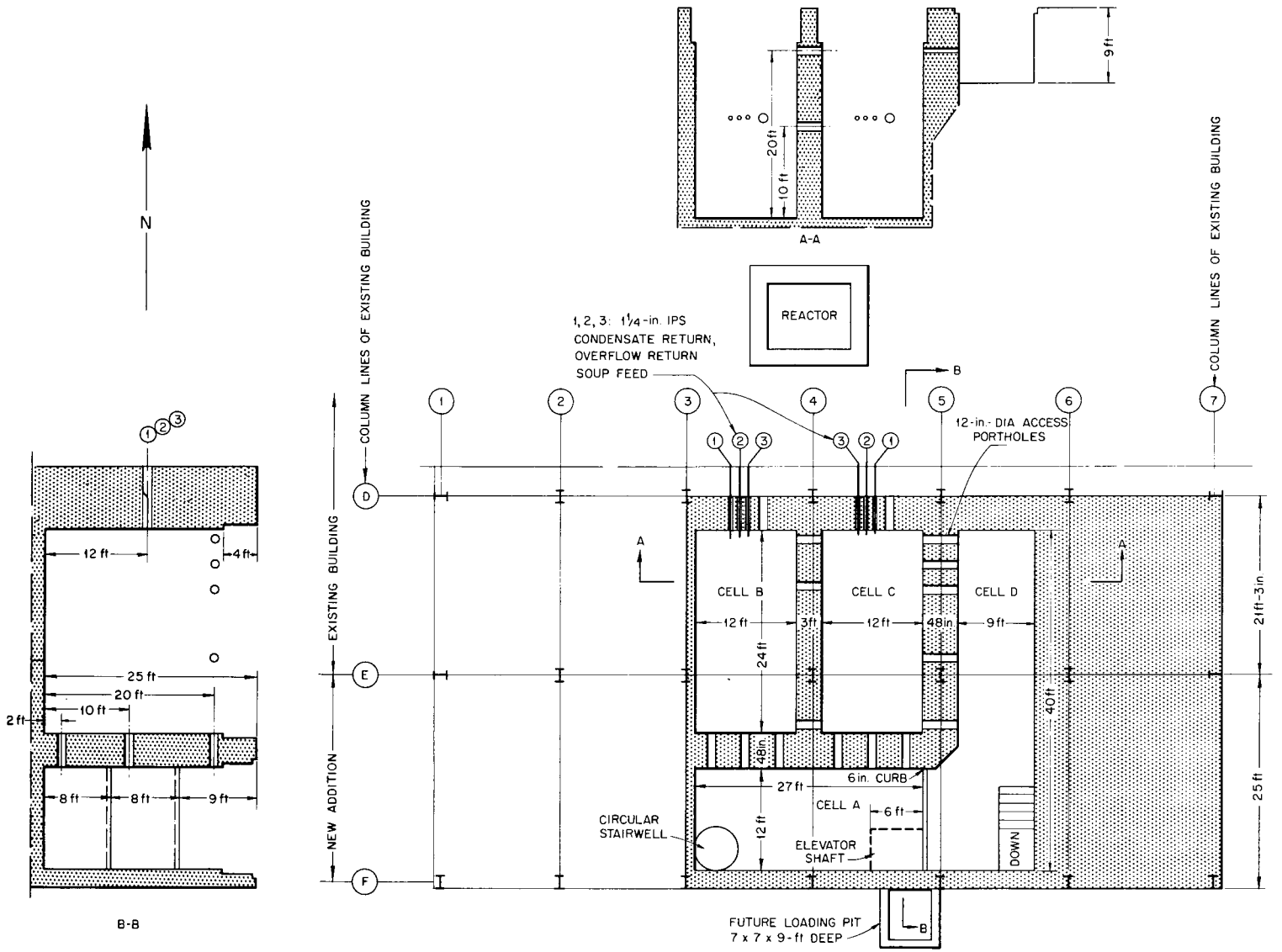

Fig. 6.3. Chemical Processing Facilities for HRT Core and Blanket.

shields. Pipe-line connections passing through the shield will connect the chemical plant area with the reactor fuel and blanket systems. The main processing equipment will be in cell C, cells A and D are for auxiliary equipment and instrumentation required by the process, and cell B is reserved for future blanket processing equipment.

Cells A and B are rectangular tanks fabricated from $\frac{3}{4}$-in.-thick steel plate. The lower 4 ft and the bottom of the tanks are clad with $\frac{1}{16}$-in. type 304 stainless steel. Five coats of Amercoat were used to protect the steel above the clad portion. Concrete walls up to 4 ft thick back up the steel walls structurally and provide shielding.

The main processing cells, B and C, are 24 ft long, 12 ft wide, and 20 ft deep. Auxiliary cell A is 27 ft long, 12 ft wide, and 25 ft deep and is broken into three levels by permanent floors. Cell D is 40 ft long, 9 ft deep, and 9 ft wide. The process equipment inside the shielded cells will be operated from cells A and D; hence, only equipment which will not be radioactive is located in these cells.

Cells B and C are designed for a maximum internal pressure of 50 psia and will normally be operated at 7.5 psia. The tops of the cells (or tanks) will be covered with two layers of concrete plugs similar to the arrangement of the reactor plugs. Between the plug layers a thin steel membrane welded at its periphery to the tank will hermetically seal the cell. The maximum acceptable leakage rate of air into or out of the cells has been set at 200 cc/min STP, dictated by the severity of the radioactivity hazards that would result from vapor leaks of process solution exceeding this figure.

Access of instrument, cooling water, steam, and other similar lines to the main cells B and C will be through 12-in.-dia sleeves cast into the walls. The sleeves will be prefabricated and installed in place, and continuation lines will then be run from each end of the sleeve. Lead shot will be used for sleeve shielding, and the sleeve itself will be welded into the tank wall to maintain the leak tightness. Use of sleeves in this manner allows flexibility in design and also ease in future modifications. Some lines connecting the reactor equipment with the chemical plant and various drain lines and vent lines were cast into the wall during construction.

The chemical plant (Fig. 6.4) is divided into high- and low-pressure sections. A small portion of the reactor circulating-fuel stream is bypassed through the high-pressure section, where solids are concentrated in a small volume of fuel solution by a solid-liquid hydroclone and then removed, the bulk of the fuel being returned to the reactor. Operation of the high-pressure system is continuous for a specified period, which is normally two days each week. At the end of this time the high-pressure system is isolated from the reactor and then cooled to reduce its pressure. The concentrate is sampled, then discharged to the low-pressure system, where it is stored for decay of radioactive material.

Only about 1% of the reactor fuel is burned each week, and each batch removed will contain about 85 g of U^{235}. Recovery of the uranium will require a dissolving step followed by solvent extraction. Dissolution of the solids is very difficult because the chief component, ZrO_2, resists attack by conventional solvents. Fluoride ion appears to be successful in dissolving ZrO_2, but materials of construction resistant to corrosion by fluorides are largely limited to the noble metals. Nitric acid containing 1% HF shows promise of dissolving ZrO_2 and is not intolerably corrosive to type 309 SCb stainless steel. Dissolving equipment has not been designed, but space for it is reserved in the shielded cell. No difficulty is anticipated in the solvent-extraction step, which will be carried out in existing facilities.

6.1 HIGH-PRESSURE SYSTEM

The high-pressure system is composed of a heater, screen, hydroclone, underflow receiver, and pump. It operates at reactor temperature and pressure conditions (300°C and 2000 psia) continuously during any particular period of operation.

From the main circulating loop of the reactor downstream of the gas separator, 0.75 gpm of fuel solution is removed and passed through the high-pressure equipment in the order specified in Sec. 6. The same quantity of purged fuel is returned to the main circulating loop just upstream of the canned-rotor pump (type 400A) used to circulate the reactor fuel. In its passage through the chemical plant the fuel bypasses the main heat exchanger. This provides feed of maximum temperature and takes advantage of the pressure drop across the reactor

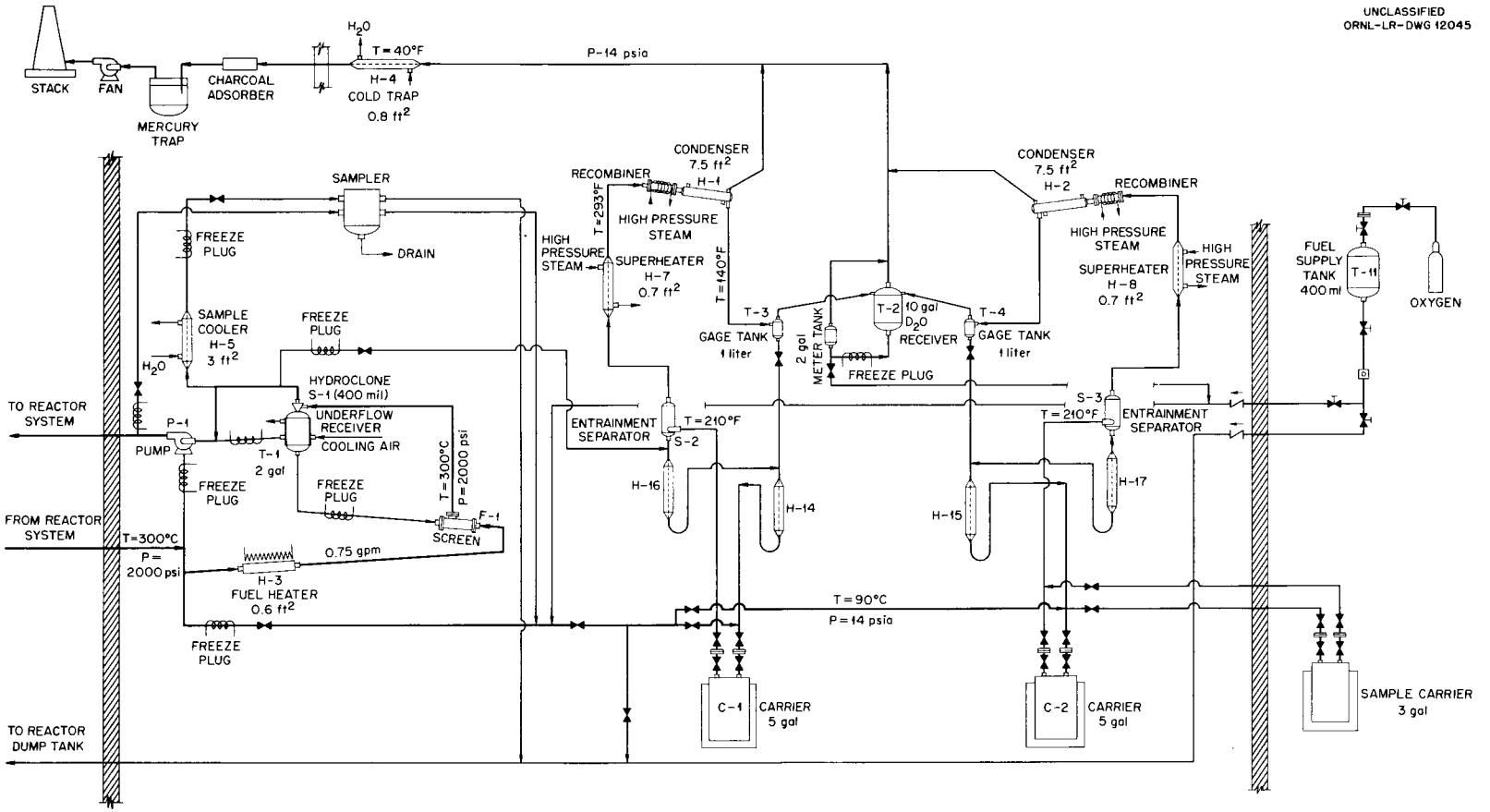

Fig. 6.4. Schematic Flow Diagram of HRT Chemical Processing Plant.

heat exchanger to furnish a portion of the energy needed to move the stream through the chemical plant. The effect of this bypassed stream on the power efficiency of the reactor is negligible, since it is only 0.75 gpm of a total reactor circulation rate of 400 gpm.

The retrograde solubility of rare-earth solids with temperature makes it important that the solution be removed from the reactor at the hottest point. For this reason the take-off point is located upstream from the heat exchanger and downstream of the gas separator to obtain a gas-free feed. There is a possibility that a gas-laden feed might introduce flow disturbances that would adversely affect the efficiency of the hydroclone.

Insoluble fission and corrosion products are separated by the hydroclone and collected in the underflow receiver. The hydroclone divides the bypassed stream into an underflow and an overflow stream, causing solids to report to the underflow. The concentration of solids in the underflow is thereby made 25 to 50 times higher than that in the fuel solution. From the receiver the insolubles are removed in batches by closing valves to isolate the underflow receiver from the reactor, then reducing the pressure to atmospheric by cooling and draining the contents to the low-pressure system.

6.1.1 Heater (H-3)

The heater in the high-pressure loop adjusts the temperature and provides a possible collection point for particulate matter. A few degrees of temperature will be lost in the lines between the reactor and the HRT-CP, and at the lower temperature the solubility of the particulates is increased, the rare earths being about twice as soluble at 275°C as they are at 300°C.

Loop experiments performed at about 300°C and 2000 psia have shown that both fission and corrosion products have an affinity for a hot surface. These products tend to deposit on a hot wall even though the wall temperature may be only a degree or two higher than the bulk temperature of the fluid. It has been theorized that inverse solubility causes precipitation in the hot film on the wall surface and that the particles continue to accumulate at this point. The heater will be used to test the deposition of solids on a hot surface, and, in this sense, the heater may serve as a solid-liquid separator. Reversing the condition – making the heater walls colder than the bulk of the solution – causes the precipitate to return to the solution, although redissolution may not be complete. Provisions are made in the design to permit back-flushing the heater with cold fuel solution to facilitate solids removal.

At temperatures of 330°C and above, $UO_2SO_4 \cdot D_2O$ solutions at reactor concentrations of 10 g of uranium per kilogram of D_2O separate into two liquid phases (Fig. 6.5). Since the heavier liquid phase contains the bulk of the uranium, it is not desirable to feed such a stream to the hydroclone where uranium can be concentrated in the underflow receiver, and careful control must be maintained on the heat input to the heater.

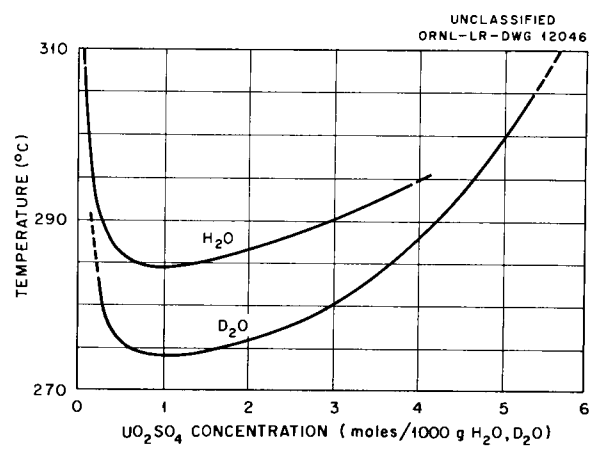

Fig. 6.5. Two-Liquid-Phase Region of Uranyl Sulfate in H_2O and D_2O.

6.1.2 Screen (F-1)

The screen, which protects the hydroclone from plugging, is constructed of a ¼-in.-OD, 30-in.-long titanium tube which has been perforated with a number of 3/32-in.-dia holes, slightly smaller than the smallest opening (0.10-in. dia) in the hydroclone. The screen will retain particles larger than can be accommodated by the hydroclone. Provisions are made for flushing solids off the screen.

6.1.3 Hydroclone and Underflow Receiver

The hydroclone is a cyclonic device which makes use of an induced centrifugal field to separate solids from liquids. There are no moving parts in the unit; the centrifugal field is obtained

by a tangential entry of the feed stream under pressure into a conical interior. The hydroclone was selected in preference to a filter, which would have to be cleaned and maintained remotely, and to a centrifuge, whose moving parts would introduce maintenance problems. Further, a centrifuge would have to be a canned-rotor, continuous-discharge type to comply with the no-leakage requirement; such a centrifuge has not been developed. After operation for 1366 hr in a corrosion test loop[1] the dimensions of the overflow and underflow ports of an experimental 0.4-in.-dia titanium-lined hydroclone were not detectably changed. The erosion rate at a point about ¼ in. above the underflow port was estimated to be about 50 mpy.

In the hydroclone the feed stream is divided into an underflow and an overflow (Fig. 6.6). The proportion of the feed that reports to each of these streams affects the efficiency of solids removal from the clarified overflow and the concentration of solids in the underflow. In the HRT-CP the hydroclone design is such that about 2% of the feed stream reports to the underflow. This provides the necessary high ratio of the concentration in the underflow receiver to that in the feed.

[1] *Reactor Handbook*, vol. 2, p 649, TIS, Oak Ridge, May 1955.

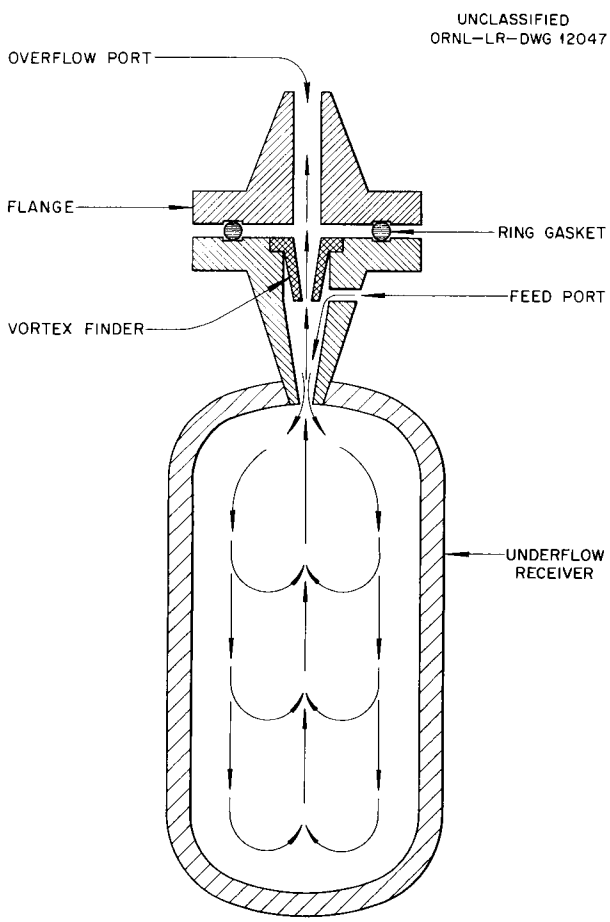

Fig. 6.6. Hydroclone and Induced-Underflow Receiver.

Hydroclones operated with an integral underflow receiver have no net underflow but an induced circulating underflow that provides the high concentration factor desired. The solids content of the underflow receiver would increase as a logarithmic function, approaching a maximum value which is a function of the feed stream concentration. The unit would be operated long enough to approach that equilibrium and then shut down to discharge the underflow receiver contents. The significance of such an installation in the HRT-CP is that the unit can be run for extended periods to process a bypassed stream from the reactor and that the fuel inventory in the underflow receiver will be small and constant.

One characteristic of the hydroclone is the large throughput for even small units. Small-diameter, ¼ in., hydroclones remove submicron particles more effectively than do larger hydroclones; they have a smaller capacity but a higher pressure drop. Efficiencies greater than 95% were observed for separation of particles 1 μ and larger; for the 0.2-μ particles, efficiencies are about 30%. The throughput capacity of this device is about 0.25 gpm with a pressure drop of 40 psi. Even this small capacity is about three times that needed for the HRT-CP.

The possibility of the hydroclone ports becoming plugged argues strongly in favor of the largest unit consistent with adequate efficiency. The 400-mil-dia by 2.4-in.-long hydroclone can separate particles of the order of 0.5 μ with efficiencies of about 50%. The capacity of this hydroclone is 0.75 gpm with a 20-psi pressure drop; its port sizes are three times as large as those of the ¼-in.-dia hydroclone.

The HRT-CP hydroclones are to be operated intermittently to compensate for their excessive throughput capacity. A study[1] was made which indicated that it probably would be of little value to operate more than two continuous days out of each seven. In the two days of being on stream, essentially all solids produced in the previous

five days are removed; further operation would only keep the removal rate the same as the production rate, which is small. The solids concentration in the reactor can be lowered by extending the operating cycle (Fig. 6.7).

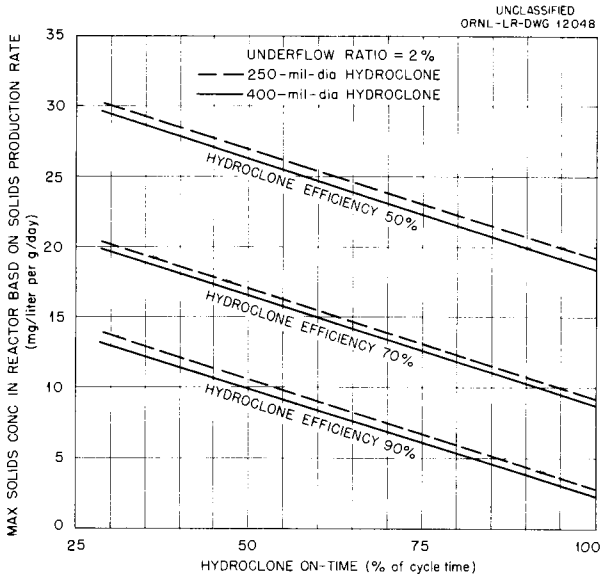

Fig. 6.7. Solids Concentration in Circulating Reactor Fuel as a Function of Hydroclone Operating Time.

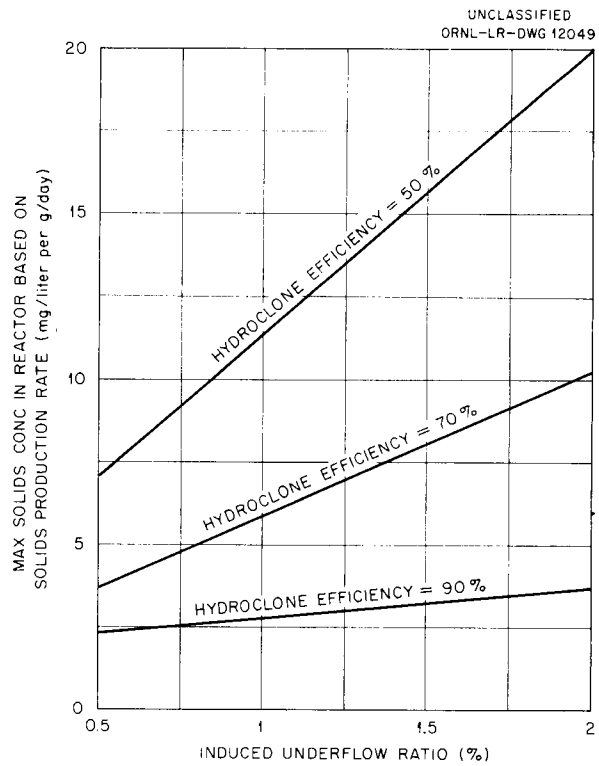

Fig. 6.8. Reactor Solids Concentration as a Function of Induced-Underflow Ratio. Hydroclone operated 90% of cycle time.

The size and shape of the underflow pot also affect the concentration of solids in the reactor. As the ratio of underflow to feed increases, the concentration to which solids in the reactor can build up also increases (Fig. 6.8).

6.1.4 Pump (P-1)

The only piece of mechanically operated equipment in the plant is a canned-rotor pump, which supplies part of the energy for moving 0.75 gpm of fuel solution through the plant. A vertically-installed, canned-rotor pump of ORNL design is still running smoothly in loop A after 2100 hr of operation.

The total pressure drop through the high-pressure system is of the order of 40 psi, of which about 16 psi is furnished by the pressure drop across the main heat exchanger in the reactor fuel system, with the balance made up by the pump. Since the high-pressure system operates completely flooded, that is, without any gas space, the pump may be placed in either the feed or the clarified overflow line. The overflow line is preferred to minimize particle attrition of the pump parts.

The pump is designed to operate from a variable frequency power supply of 30 to 80 cps for control of pump speed and thereby fuel throughput through the plant. In the tests of an ORNL canned-rotor pump the a-c electrical supply frequency was varied from 26 to 90 cps. The observed heads can be represented by

$$H = 0.0122\, D^{1.3}\, f^{1.6} ,$$

where

H = output head in feet of liquid for 0 to 2 gpm flow,
D = impeller diameter, in.,
f = a-c electrical supply frequency, cps.

6.1.5 Valves, Flanges, and Freeze Plugs

The processing plant will use valves ordered to the same specifications as those procured for the reactor for corresponding service. HRP-grade,

type 347 stainless steel trim on test valves survived 24,000 open-close cycles against a 500-psi cold-water head before developing a leakage rate of 100 ml/min; Stellite-6 trim developed that leakage rate in 10,000 cycles.

Flanges tend to leak at operating temperatures because of the expansion of the flange bolts. When the flanges are not insulated, the flange bolts are cooled by the ambient air, and the threat of leakage is minimized. Equipment tests are in progress to ascertain the rate of heat lost from uninsulated flanges and to ascertain the effectiveness of spring-loading to accommodate the thermal expansion of the flange bolts.

Freeze plugs will be used in the process plant to ensure against leakage from high-pressure valves and, where feasible, to replace a valve that would otherwise be required. With 0.04 *M* UO_2SO_4 solutions freeze plugs (Fig. 6.9) were pressure-tight up to 7600 psi. Plugs could be formed in a ¼-in.-IPS pipe under a fluid flow of up to 6 ml/min. These tests were made on apparatus attached to loop B, operating at 300°C and 2000 psi.

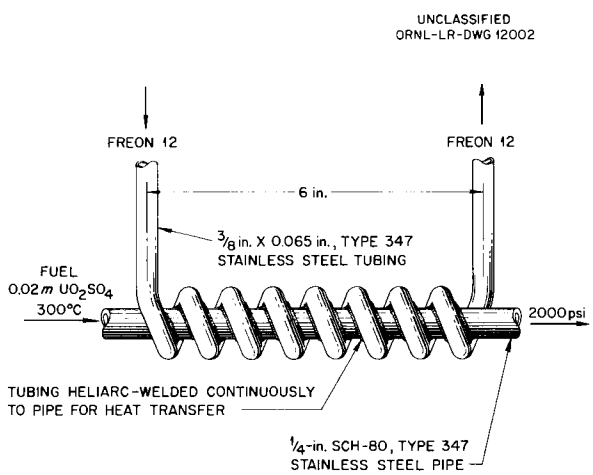

Fig. 6.9. Freeze Plug.

6.1.6 Major Instrumentation

Four types of measurements will be made in the high-pressure system: flow, temperature, pressure, and radiation. Whenever an element inside the cell is required to transmit a signal outside the cell, an electrical impulse will be used to avoid the hazard of shield penetration by process lines.

The flow rate in the high-pressure loop will be determined by measuring the pressure drop across the hydroclone, since this is a function of the flow rate. The pressure drop will be sensed by a differential-pressure cell, connected between the feed and overflow lines. The signal from the differential-pressure cell will control the flow in the plant by controlling the variable frequency of the current generator which supplies power to the canned-rotor pump.

Stainless-steel-jacketed thermocouples are used throughout the system to measure process pipe temperatures up to 325°C and freeze plug temperatures as low as −35°F. Temperature control is required in the underflow receiver (T-1) and the heater (H-3). The underflow receiver is maintained at 300°C by circulating hot air around the tank. The air temperature, in turn, is controlled by electrical heaters operated by a temperature signal from the underflow receiver. The heater (H-3) output is controlled by a hand-operated Variac; however, a temperature signal from the unit protects against overheating and equipment damage.

One absolute pressure measurement is made on the supply line from the reactor system. This impulse is not used for control but for actuating certain safety devices protecting against transfers of fluids and vapors between the reactor and the chemical plant.

Several radiation measurements are made in the HRT-CP, but only one instrument, a radiation-intensity measuring instrument called the "gamma eye," is specifically for use in the high-pressure system. It is a pipe set in the shielding wall in alignment with the underflow receiver (T-1) and terminating in a radiation chamber. The chamber will indicate the gamma-radiation intensity of the underflow receiver.

6.1.7 Sampling

Two samples must be obtained from the HRT-CP for evaluation of the effectiveness of the plant for separating solids, one from the hydroclone overflow stream and one from the underflow receiver. Sampling of the hydroclone feed is not necessary, since such a sample would be identical to one of the reactor fuel samples being taken as part of reactor operation. The samples will be analyzed for the entire fission-product spectrum, uranium,

acid, copper, and the corrosion products zirconium, tin, iron, chromium, and nickel. Since corrosion products are being concentrated in the chemical plant, analysis of the underflow receiver contents will indicate the lower limit of the rate of corrosion of the reactor materials of construction.

The overflow sample is taken while the plant is operating at 2000 psia and 300°C and is removed just downstream of the hydroclone overflow port. Sampling will consist in isolating about 5 ml of a representative portion of this stream. In this procedure about 0.2 gpm of the overflow is diverted through a heat exchanger, pressure-reducing valve, and isolation chamber. From here the stream is routed to a dump tank in the reactor low-pressure system. The stream is allowed to flow in this manner until representativeness is assured; then a sample is trapped in the isolation chamber. By remote means the isolation chamber is emptied into a sample carrier and transported to the laboratory for analysis. The overflow stream gradually changes in solids content during the course of the two-day operating cycle because of the nature of the hydroclone operation. The cleanest overflow is at initial startup, and at shutdown the overflow solids content approaches that of the feed. Therefore for overflow sample data to be significant in measuring hydroclone efficiency, this sample will be taken concurrently with a sample of the reactor fuel system.

The underflow sample will be taken only once during the two-day operating period, at the end of the run. The sample is a measure of the total accumulation of fission and corrosion products for a one-week period. This sample is withdrawn from the underflow receiver after the high-pressure loop has been isolated from the reactor, cooled to 90°C or lower, and reduced in pressure to 1 atm. The content of the receiver is really a slurry of solids in uranyl sulfate solution, from which it will be rather difficult to obtain a representative sample. Provisions have been made to agitate the tank by circulating its contents via the pump through the sampler. A circulation rate of 3 gpm can be maintained as long as necessary to reach a high degree of homogeneity. Since the fluid has been circulating through the sample chamber, a small portion (5 ml) can be isolated at any time.

Since it cannot be said for certain that an underflow sample obtained by this method will be representative, the design includes a means of removing the entire contents of the underflow receiver for use as a sample. Connections will be provided between the underflow receiver and a shielded carrier of about 3-gal capacity that can be removed from the area after receiving the underflow and distilling heavy water for storage. The approximately 400 g of solids left in the carrier will be dissolved and an aliquot removed for analysis. If the analysis agrees with that of the sample removed before dissolving, the practice of using the entire receiver contents for the sample can be discontinued.

6.2 UNDERFLOW POT COOLING SYSTEM

Unlike the other parts of the high-pressure chemical plant system, the underflow pot contains an appreciable amount of relatively stagnant reactor solution. The heat generated by the decay of fission products in this solution is greater than that lost by the underflow pot to the surroundings, and, unless the excess heat is removed, the solution temperature will rise considerably above the system operating temperature. This would lead to separation of the uranium solution into two phases, one considerably heavier and much richer in uranium than the other. Any such separation of a heavier uranium phase would, over a period of time, increase the uranium content in the underflow receiver. Since the formation of the two phases occurs at about 330°C, an upper temperature limit of 320°C was selected.

It is almost equally important that the underflow-pot temperature not be allowed to drop much below 275°C, because most of the precipitated fission products, which have inverse solubilities, would redissolve and be carried back to the reactor. The underflow pot is designed to be maintained at or near 300°C during a processing run.

The cooling system should also be able to cool the pot and its contents from operating temperature to about 90°C before the charge is dumped to the low-pressure system and to heat the pot from cell temperature to operating temperature before the start of the next processing cycle. The cooling system chosen to perform these functions uses air as the coolant and regulates the temperature of the underflow pot by adjusting the temperature of the air. The underflow pot is so designed that the air does not come in direct contact with the pot surface but passes through tubes spaced along the side of the pot. These tubes are cast in aluminum billets strapped to the underflow pot. A drawing

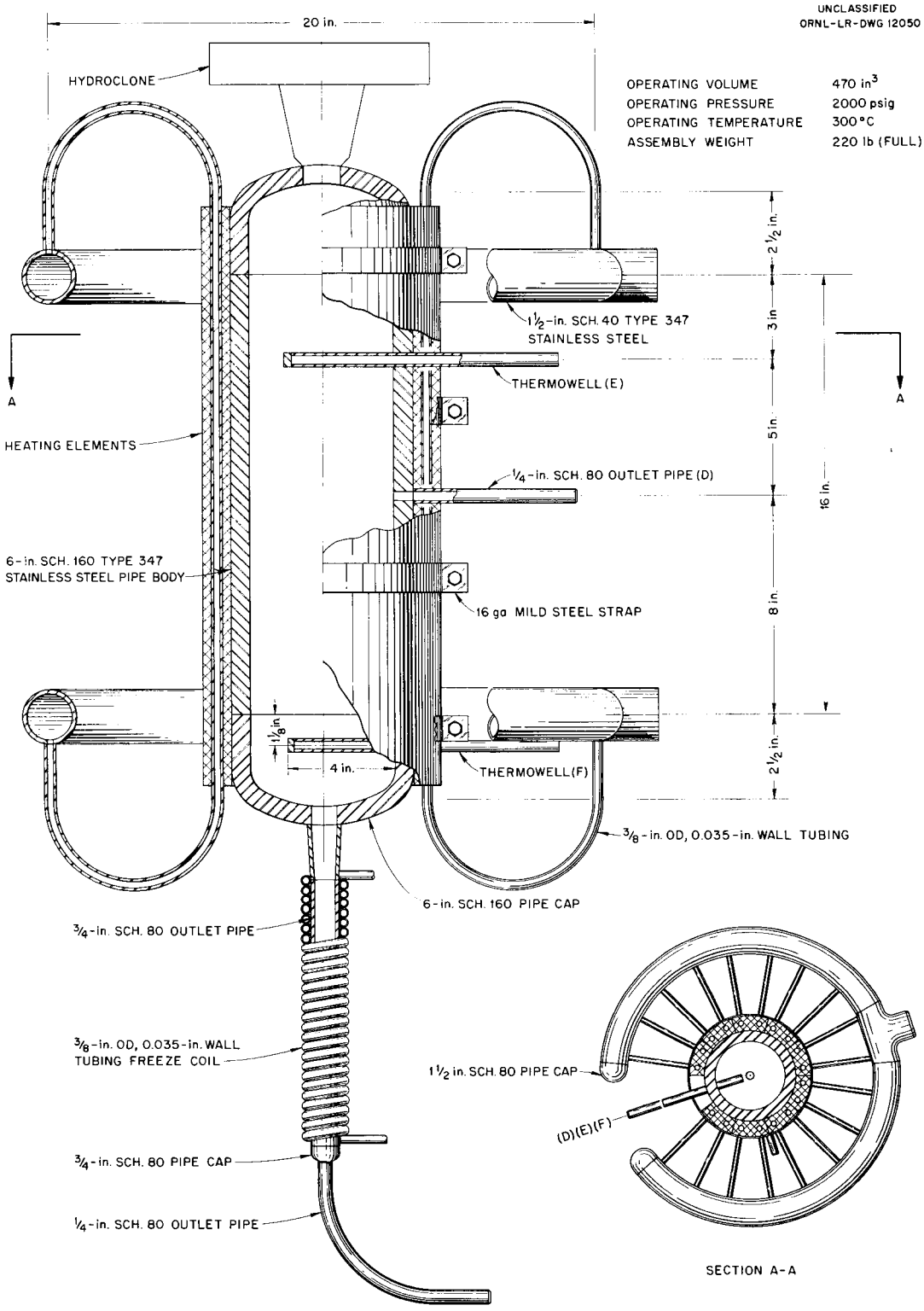

Fig. 6.10. HRT Core Processing Experimental Underflow Pot.

of the underflow pot is shown in Fig. 6.10. The air-cooling system and the high-pressure chemical processing system are separated by two thicknesses of pipe instead of one so that any leak in the underflow pot will discharge into the cell rather than into the air line leading outside the cell. With the danger of the escape of highly radioactive process solution through the air lines thus obviated, the heater, blower, and controls of the air system can be located outside the cell for ease of operation and maintenance.

The air blower that will be used has a capacity of 250 lb/hr of air at 6 psi head. So much area on the underflow pot is available for heat transfer that it is necessary at this air flow rate to keep the inlet air at a fairly high temperature in order to avoid having a large temperature gradient along the underflow pot. The exact air temperature that is necessary will have to be determined by experience during actual operation of the system. Normal operating conditions should not be far from those shown in Fig. 6.11, however.

At the end of the process cycle, the air system will be used to cool the underflow pot and its contents to below 200°F. This will be done by shutting off the heater and blowing outside air through the system. The sensible heat to be removed from the underflow pot and solution is calculated to be 18,700 Btu; the fission heat that must also be removed decreases through the cooling cycle from 2790 to about 2400 Btu/hr.

The cooling cycle must be relatively short to eliminate the possibility of an explosion as a result of ignition of the radiolytic deuterium and oxygen during the cooling cycle. Most of the dissolved deuterium and oxygen present at the end of the processing cycle will be recombined by the copper catalyst in the solution in the few minutes that elapse between the shutting off of the flow from the reactor solution and any significant drop in the temperature of the underflow pot. However, the recombination rate is strongly temperature-dependent, and very little of the gases produced during the cooling cycle will be recombined.

Fresh uranium solution will be charged to the reactor before each processing run by feeding the solution to the underflow pot, heating the pot and contents to 300°C, and then opening the reactor valves and feeding reactor solution to the underflow pot to displace the feed solution. The air system will be used to supply the necessary heat. The heater will heat the incoming air to 700°F. After some loss of heat to the surroundings the air should reach the underflow pot at about 640°F. Over a period of 4 hr the underflow pot will be heated to operating temperature. Figure 6.12 shows the temperature curves predicted for the heating operation.

Some design calculations were made for a regenerator which would considerably reduce the heater requirements by using the exit gas stream to heat the inlet stream before it is sent to the heater. The conclusion was reached that a regenerator is feasible but not economical on an installation of this size.

6.3 LOW-PRESSURE SYSTEM

A storage vessel in the low-pressure area receives the material from the high-pressure loop after each two-day operating period and stores it until radioactive materials have decayed sufficiently to be acceptable as feed to a solvent extraction plant for recovery of the associated uranium.

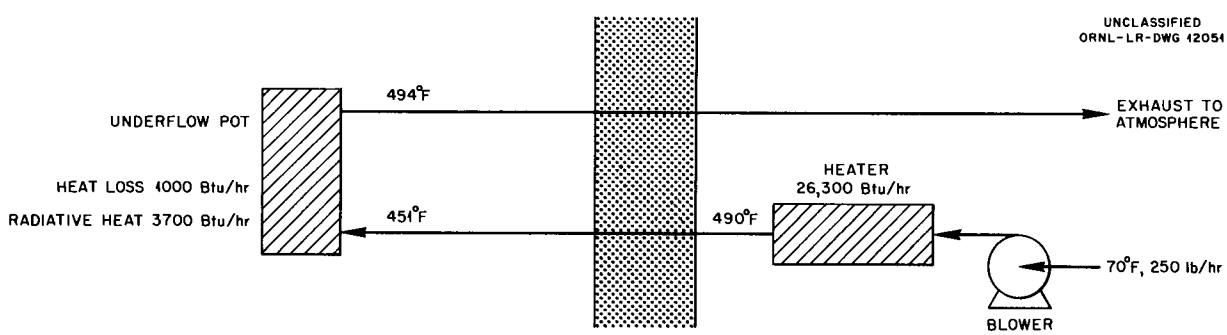

Fig. 6.11. Schematic Flow Diagram of Air System for Maintaining Underflow Pot at Operating Temperature.

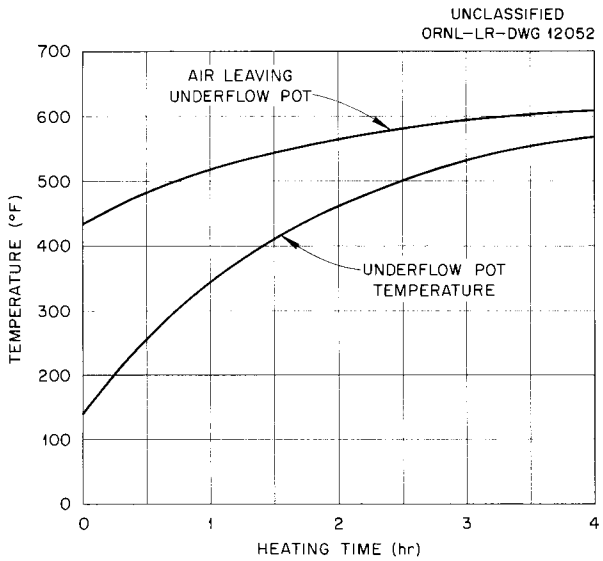

Fig. 6.12. Temperatures of Underflow-Pot System During Heating Cycle.

About one week is required for decay of one batch from the initial radioactive energy of about 1.7 kw to one of 0.5 kw (Fig. 6.13). It is planned to collect a number of volumes from the underflow receiver in one tank until sufficient material has been accumulated to justify solvent extraction processing. If weekly batches are collected for six months, a second six months of decay will be required to reduce the activity to 0.5 kw.

In the low-pressure area is also located equipment for heat dissipation, D_2 and O_2 recombination, heavy-water recovery, and off-gas disposal (Fig. 6.14). Two complete assemblies are provided to permit one storage vessel to be in the six-month decay cycle while the second is collecting batches from the high-pressure system. Each batch from the underflow receiver is drained into the carrier, where the solution is allowed to boil by heat from decay of radioactivity. This energy is dissipated in the condenser to the cooling water, and the heavy-water condensate is returned to the

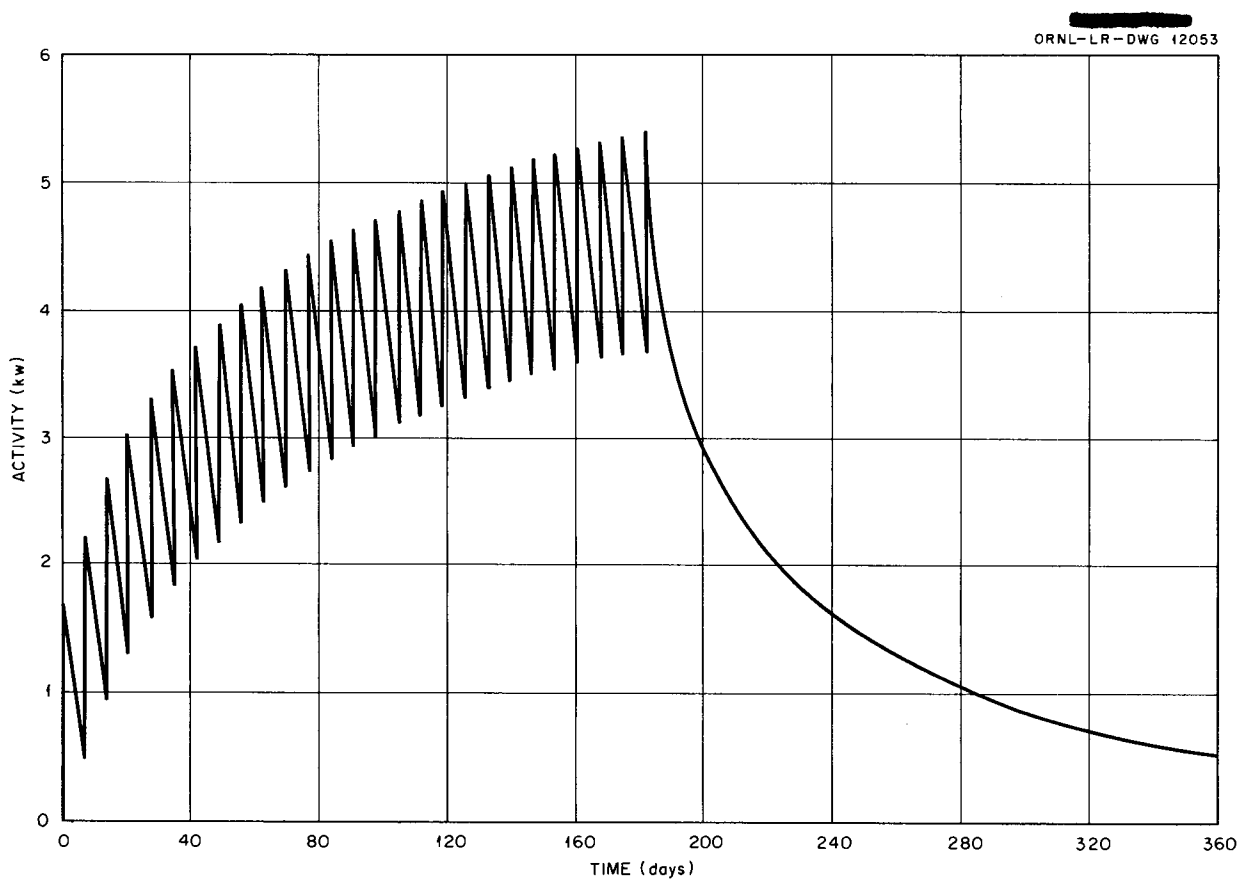

Fig. 6.13. Rate of Release of Radioactive Decay Energy in Carriers C-1 and C-2.

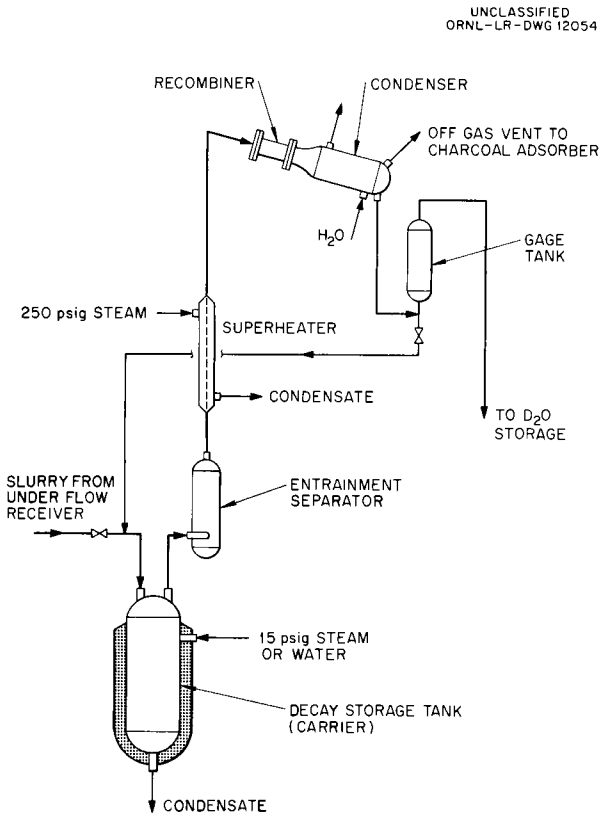

Fig. 6.14. Typical Low-Pressure-System Installation.

carrier as reflux. A large storage vessel is not required to contain these weekly batches, because the solution is concentrated by distilling off heavy water. A water balance is maintained with the reactor by returning D_2O to the fuel system with fresh fuel makeup.

Normal operating pressure in the low-pressure system is 1 atm, but all vessels are designed for 500 psia internal pressure to contain possible explosions.

6.3.1 Storage Vessels (Carrier C-1 and C-2)

The storage vessels, two of which have been provided, are designed to be critically safe, which limits their diameter to that of a standard 6-in. pipe; the total volume is 5 gal. Each tank will be arranged in the cell layout so that it can be disconnected remotely from the system, placed in a lead shield, and removed from the cell for transportation of the contents to the solvent extraction plant. Each vessel is provided with coils on the outside so that either cooling water or low-pressure steam may be supplied. Sufficient heat transfer area is available to admit 10,000 Btu/hr of heat to assist in evaporating heavy water.

6.3.2 Entrainment Separator (S-2 and S-3)

An entrainment separator is provided for each storage vessel. The platinized alumina catalyst used for recombination of D_2 and O_2 is rendered ineffective by moisture and certain foreign metallic atoms such as uranium, and it is essential to remove these materials before the vapor reaches the recombiner. The design provides three methods of entrainment separation: first, the vapor enters tangentially to provide a swirling movement and make use of centrifugal force to throw out particles; second, it passes through a series of baffles to provide a number of reversals of flow and impingements; and third, two sections of wire mesh made of 0.011- and 0.0045-in.-dia wire deentrain remaining moisture. As a precaution against plugging, a small coil condenser is inserted in the top of the entrainment separating unit to provide condensate for washing down the internals. The design of this separator is similar to that of the separators on the reactor dump tanks.

6.3.3 Superheater (H-7 and H-8)

Each superheater receives vapor at 210°F from the entrainment separators and increases the vapor temperature to 293°F. It ensures that the stream will be sufficiently above its dew point so that no condensation will occur in the recombiner. Superheated vapor feed to the recombiner should not be required once D_2 and O_2 recombination has begun, because sufficient heat of reaction is released to keep the catalyst dry. Nevertheless, as a safety measure the superheater will be operated continuously. Heat is supplied by 250-psig steam in the jacket.

6.3.4 Recombiner Condenser (H-1 and H-2)

Superheated steam and decomposed water at a rate of 10.3 lb/hr are fed to the recombiner to carry out the reaction $2D_2 + O_2 \rightarrow 2D_2O$. The reactive gas portion of the mixture is maintained at less than 1 vol % to preclude flashbacks and explosive concentrations. Radioactive decay energy will normally boil enough water to maintain a safe composition; however, if needed, assistance can be obtained from the heating jacket on

the carrier. Heavy water does not decompose at a very rapid rate (Fig. 6.15), but, if it were not recombined, losses could be appreciable over an extended period of time. Furthermore, the gases would constitute an explosive hazard in the off-gas system.

The recombiner chamber is a piece of 3-in.-dia by 5-in.-long pipe filled with platinized alumina pellets; the platinum content is 0.3 wt %. A coil, through which is passed 250-psig steam, supplies heat to the catalyst bed and will be used to keep the catalyst dry during periods of inactivity.

Intimately connected with the recombiner is the condenser which refluxes steam from the recombiner to the carrier. This unit dissipates the heat of radioactive decay plus any heat added via the steam jacket of the decay storage vessel. The equipment is a conventionally designed shell-and-tube type of exchanger.

6.3.5 Gage Tank (T-3 and T-4)

The gage tank is sized at 1 liter so that this quantity of heavy water can be gaged and added to the carrier. Before the carrier is transported, it may be necessary to add this small volume of water to its contents to prevent solidification and possible fusion.

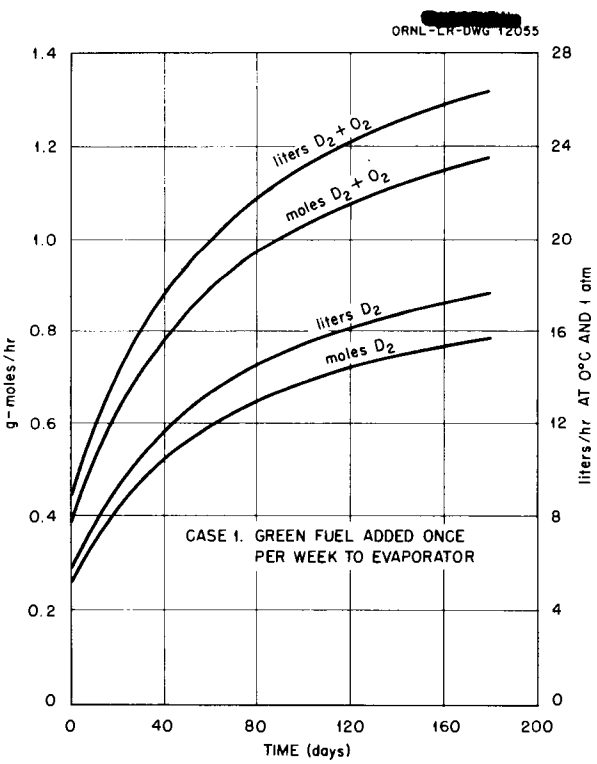

Fig. 6.15. Rate of Decomposition of D_2O in Evaporator-Decay Tank in HRT-CP.

6.3.6 D_2O Receiver (T-2)

The heavy-water receiver is an accumulator for water that has been boiled off the carriers during concentration. The vessel is common to the two storage systems. It is from level measurements on this tank that an inventory of heavy water is obtained.

6.3.7 Meter Tank (T-5)

The meter tank measures a specified volume of D_2O into the fuel makeup concentrate. The tank will be made to the required size after the high-pressure system has been fabricated and calibrated and will contain exactly 72.7% of the high-pressure volume at room temperature. This allows for expansion as the D_2O is heated to 280°C. The tank is located with reference to the D_2O receiver (T-2) so that it can be flooded as long as the receiver has sufficient inventory.

6.3.8 Sample Carrier (C-3)

The 2-gal carrier and its associated equipment will be located outside the chemical processing cell and in the adjacent access cell (cell A) to avoid the necessity for removing the roof plugs, cutting the cell membrane, and flooding the cell for each 2-gal batch. The carrier will be in a cubicle to shield it from the working area. The equipment must be partly below the floor level of the processing cell to permit gravity flow. This arrangement will permit ready removal of the sample for dissolution of the solids so that a homogeneous aliquot may be analyzed. If results of analyses agree with those of samples of the underflow receiver contents taken at the end of each processing cycle, dissolution of the 2-gal batch may be discontinued. Whether or not the sample of the underflow receiver contents is representative of the material depends on the particle-settling velocity. Calculations indicate that 10-μ particles will be represented in the sample with 90% accuracy.

The samples will be used to determine such data as rate of corrosion of the zirconium core tank, efficiency of the hydroclone, and behavior of the fission product particles.

It will be necessary to shield the process lines and the sample can with a considerable thickness

of lead to avoid overexposure of personnel to the radiation. A calculated thickness of 14 in. will be needed at all points in line with the sample can; a lesser thickness can be used to shield the process lines.

An operational mishap or equipment failure during processing could divert the reactor solution directly to the sample station and thereby expose the sample can to a pressure of 2000 psi. It is not feasible to design the sample can to withstand this pressure; therefore, the can and the connecting process lines must be enclosed in a leaktight box that will discharge through a rupture disk to the processing cell at any pressure in excess of 50 psia.

The cubicle (Fig. 6.16) will be installed partly above and partly below the floor level of cell A and will measure 7 ft long by 5 ft wide by 7 ft 1 in. high, 3 ft 5 in. of this being below grade. The cubicle will contain two main areas, a loading pit for inserting and removing the carrier and a loading station where the 2-gal batch will be charged to the carrier can. The can will be moved between the two areas on a trolley installed in the cubicle for the purpose.

When the carrier is to be connected in the cubicle, the cover will be removed from the loading pit. Connecting the cubicle to a vacuum pump will maintain an inward flow of air and thus prevent the escape of any minor contamination from the cubicle. The carrier will then be lowered into the loading pit with the cell crane. The carrier cover will be suspended by lugs in the top of the loading pit; the bulk of the carrier will be lowered another 8.5 in. to rest on the trolley in the bottom of the loading pit. The crane will then be disengaged and the cubicle cover will be put back in place and bolted down. The trolley is next moved into position beneath the processing lines by means of a chain drive. With the carrier can in this position, the flange connections between it and the processing lines can be made from above the cubicle by lowering threaded rods through positioned holes in the shielding and bolting the flanges together. In a somewhat similar manner the other necessary connections are made; service lines are connected to the jacket of the carrier can, a thermocouple is positioned in the thermocouple well of the carrier can, and valves on the process lines and the carrier can are opened. The holes in the shielding, through which the connections were made, are then sealed, and the carrier can is ready to receive a charge.

After the 2 gal of solution has reached the carrier can from the underflow pot, it is refluxed for a time. The reflux condenser is located in cell C; therefore the vapor from the sample can will be returned to cell C, condensed, and refluxed to the carrier can through the process charge line to wash the process charge line relatively clean. After a period of refluxing, the solution in the carrier can will be boiled to dryness and be left to bake for a number of hours. The baking will remove all traces of water from the carrier can; otherwise, during the transit of the carrier to a processing station, these traces of water would be decomposed by fission product activity and would produce a considerable gas pressure within the carrier. Since this gas is explosive, it would represent a considerable hazard.

The procedure for removing the sample carrier is the reverse of the procedure for loading it. The holes in the shielding are unsealed, the various valves are closed, the service lines are disconnected, the thermocouple is removed, and the flanges connecting the carrier can and the process lines are disconnected. The trolley is then cranked back into position in the loading pit beneath the carrier cover. The cubicle cover is removed and the crane is lowered into the loading pit to engage the lugs on the carrier. As the carrier is raised it automatically engages the carrier cover, which settles into position, and the completely shielded carrier is hoisted from the loading pit.

The carrier cubicle will contain a sump and sump jet for drainage, provision for washing down the cubicle in the event of a spill, and associated instrumentation. The cubicle will be made of stainless steel for ease in decontamination. Design of the cubicle and carrier is estimated to be 40% complete.

6.4 OFF-GAS DISPOSAL SYSTEM

The inert gases that collect at various points are vented through a common off-gas system, consisting of a cold trap, to remove the bulk of the D_2O vapor, an activated charcoal adsorber to remove the xenon and krypton, and a seal pot to prevent outside air from backing into the system. The cold trap, a 4-ft length of jacketed $\frac{3}{4}$-in. pipe, condenses the bulk of the water vapor in the

UNCLASSIFIED
ORNL-LR-DWG 12056

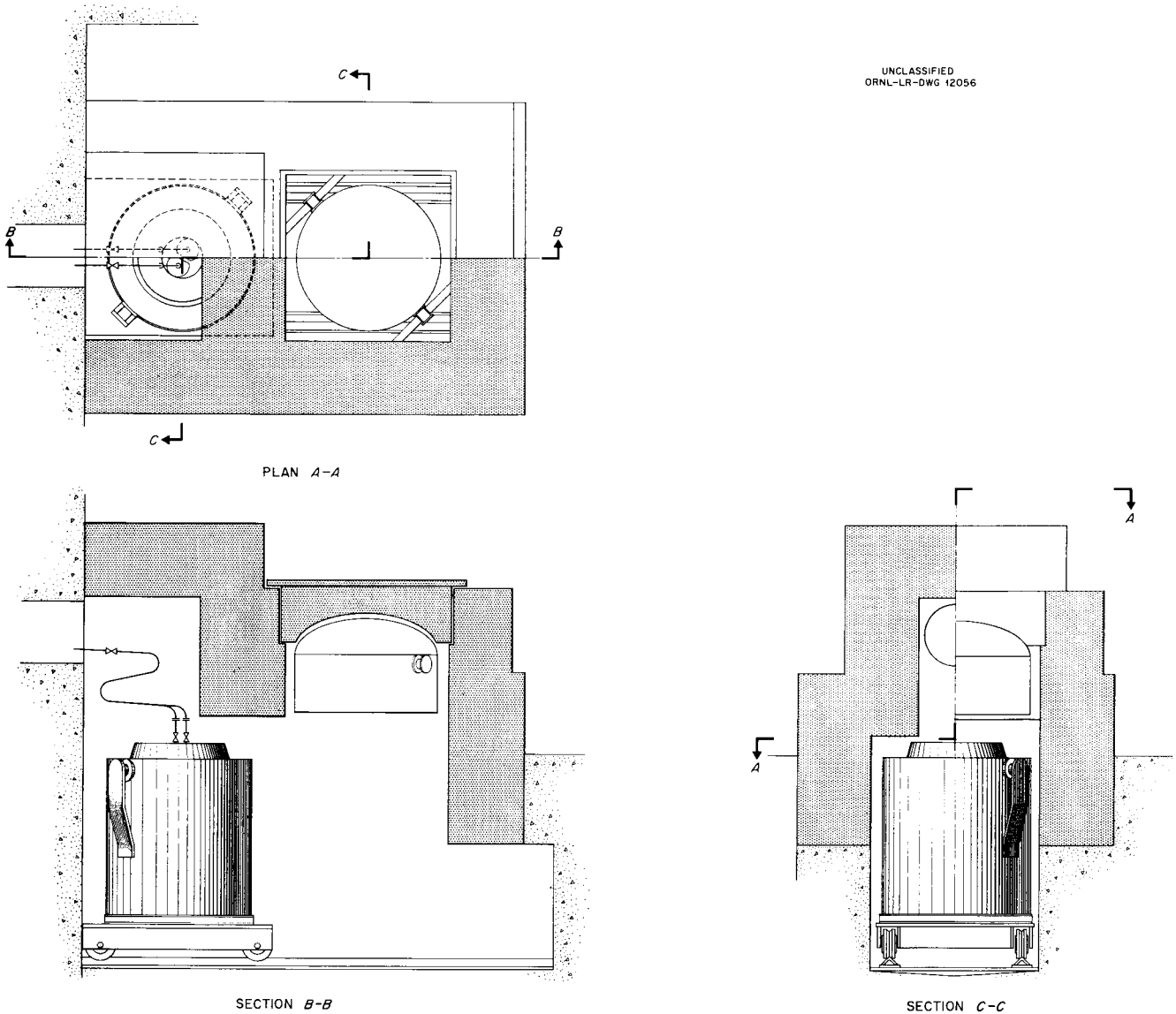

Fig. 6.16. Sample Carrier and Shield.

off-gases and returns it to the low-pressure system. This is accomplished by cooling the off-gas to a low temperature (40°F) by means of chilled water and allowing the condensate to drain to the D_2O receiver.

The charcoal adsorber is installed primarily to adsorb the fission-product rare gases xenon and krypton and to hold them until the isotopes with short half lives have had time to decay. The adsorber is identical in design to the reactor beds and is buried underground to reduce the shielding requirements. Cooling is provided to remove the radioactive heat; it is expected that the temperature can be kept below 140°F. The bed can be regenerated periodically by reducing the pressure on the adsorber with a vacuum pump until the gases have been desorbed. The quantity of off-gas produced by the chemical plant is so low that such a regeneration will probably not be necessary during the operating life of the HRT.

The seal pot serves to prevent outside air from backing into the vent system when the pressure in the chemical processing system falls below atmospheric. The seal pot consists merely of a dip leg and a mercury seal.

After passing through the seal pot, the off-gases pass through a filter cartridge for the removal of particulate matter and thence to the dispersal stack.

6.5 URANIUM RECOVERY SYSTEM

Associated with each weekly batch of fission and corrosion products will be about 85 g of enriched uranium valuable enough to warrant separation from the mixture. The proposed procedure is to remove the carriers from the chemical processing cell at the end of the six-month collection plus the six-month decay period and then dissolve and process the contents through an existing ORNL solvent extraction facility to remove and decontaminate the uranium. The quantity of uranium involved is small, and a number of batches will be accumulated to justify operation of the recovery plant.

6.6 FUEL ADDITION SYSTEM

At 5-Mw power level the HRT will fission about 6.7 g of uranium per day; more uranium will be withdrawn through the chemical plant with the fission and corrosion products concentrate. Sufficient fresh fuel is required to compensate for these losses, which total about 117 g of uranium per week. Fresh uranyl sulfate fuel solution will be prepared, at a concentration of 500 g of uranium per kilogram of D_2O, and added to the reactor dump tank through the fuel addition system. This system is located outside the shield of the chemical processing facility and connected to it by pipes through the shield. The two vessels in this area are a concentrated fuel supply tank and a heavy-water storage tank; each has a capacity of 300 ml. The prescribed quantity of fuel is gravimetrically determined by weighing the fuel supply tank and its contents before they are drained into the cell. The heavy-water vessel furnishes flush water for washing the fuel supply tank. Both vessels may be pressurized with an oxygen cylinder.

Alternately fresh fuel for the reactor may be added through the chemical plant high-pressure system. In this case, uranyl sulfate concentrate is allowed to flow from the fuel supply tank into the high-pressure system (underflow receiver) instead of to the reactor dump tanks. Additional heavy water necessary to dilute the solution to the reactor fuel concentration, 10.4 g of uranium per kilogram of D_2O, is added from the meter tank (T-5), which is designed so that a flooded tank supplies the proper volume. The resulting quantity of makeup amounts to 2.0 gal in a loop which contains a total volume of 2.75 gal; the difference corresponds to the expansion of the fuel when heated to the reactor temperature of 300°C.

The temperature of the contents of the high-pressure loop is raised (with an accompanying increase in pressure) by the hot air system to 300°C. At this point the volume of fresh fuel charged has increased to fill the entire loop, and the system is ready to begin another two-day run of HRT-CP operation as soon as the isolation valves in the connecting lines between the reactor and chemical plant are opened. During operation the fresh fuel in the underflow receiver is displaced by the hydroclone underflow into the reactor system.

Part II

REACTOR DESIGN AND ANALYSIS

R. B. Briggs J. A. Lane

7. REACTOR ANALYSIS

P. R. Kasten

H. C. Claiborne
T. B. Fowler
D. C. Hamilton
M. K. Hullings
C. W. Nestor, Jr.
M. W. Rosenthal
M. Tobias

7.1 FUEL COST OF POWER REACTORS FUELED BY UO_2SO_4-Li_2SO_4-D_2O SOLUTIONS

H. C. Claiborne T. B. Fowler

A study of fuel costs was made for power-only reactor systems fueled by UO_2SO_4-Li_2SO_4-D_2O solutions.[1] It was assumed that all plutonium remained in solution or suspension and was continuously fed back to the reactor. The molar ratio of Li_2SO_4 to UO_2SO_4 was considered to be unity. The purpose of the study was to compare the fuel costs of this solution system (stable at temperatures as high as 350°C) with those obtained for a UO_3-PuO_2-D_2O slurry system investigated previously.[2] The results of this study also complement those obtained previously[3] for similar systems in which a premium price was assigned to plutonium.

As a result of plutonium feedback, the equilibrium concentrations of the plutonium isotopes were high enough for resonance absorptions and fission to have an appreciable effect. A six-group method[1] was therefore used for the nuclear calculations in an effort to account properly for the resonance effects in uranium and plutonium.

The results, shown in Figs. 7.1 through 7.3, are for spherical one-region reactors operating at an average temperature of 330°C, producing 1000 Mw of thermal energy, and delivering 300 Mw of electricity to a power grid. All cost results in the figures are shown in terms of the asymptotic fuel cost, which includes only a minimum Purex processing charge, calculated for a central processing plant serving a very large number of reactors.

In all cases the optimum fission-product poison concentration, which is a function of the chemical process cycle time, was very close to the equivalent of 5% of the macroscopic fission cross section.

The optimum uranium concentration was about 200 g/liter; it was slightly lower with a 12% inventory charge and $40-per-pound D_2O (Fig. 7.1) and slightly higher with a 4% inventory charge

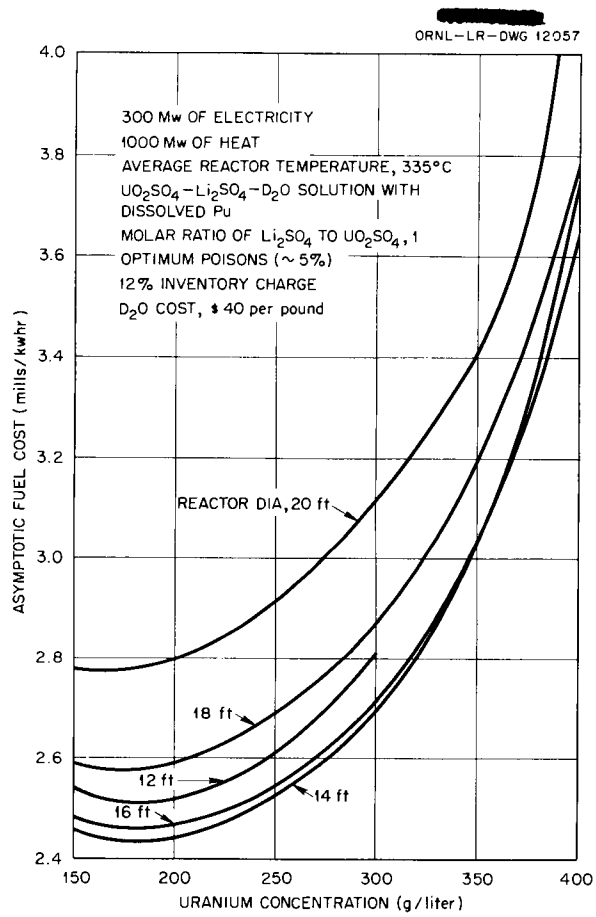

Fig. 7.1. Effect of Uranium Concentration on Fuel Cost.

[1] H. C. Claiborne and T. B. Fowler, *Fuel Cost of Power Reactors Fueled by UO_2SO_4-Li_2SO_4-D_2O Solution*, ORNL CF-56-1-145 (Jan. 30, 1956).

[2] R. B. Briggs, *Aqueous Homogeneous Reactors for Producing Central-Station Power*, ORNL-1642 (May 4, 1954).

[3] H. C. Claiborne, *HRP Quar. Prog. Rep. Oct. 31, 1955*, ORNL-2004, p 53.

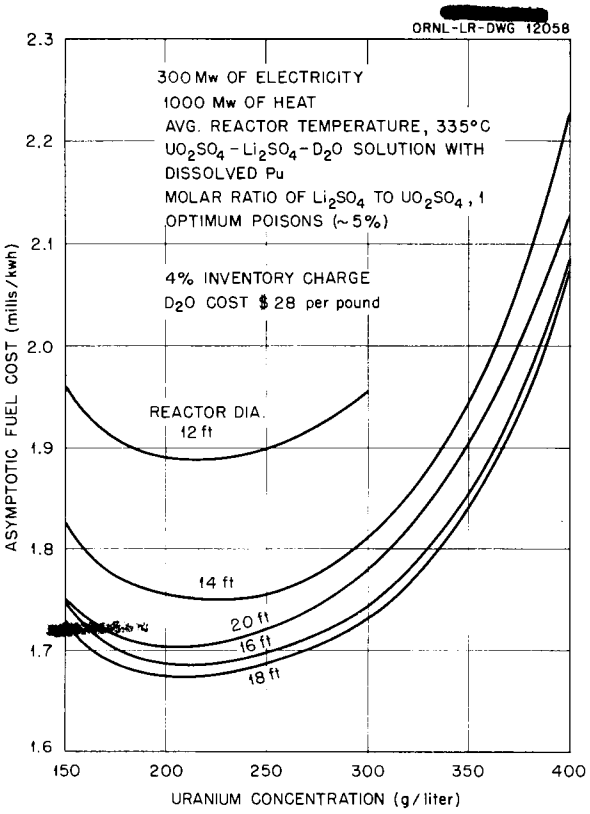

Fig. 7.2. Effect of Uranium Concentration on Fuel Cost.

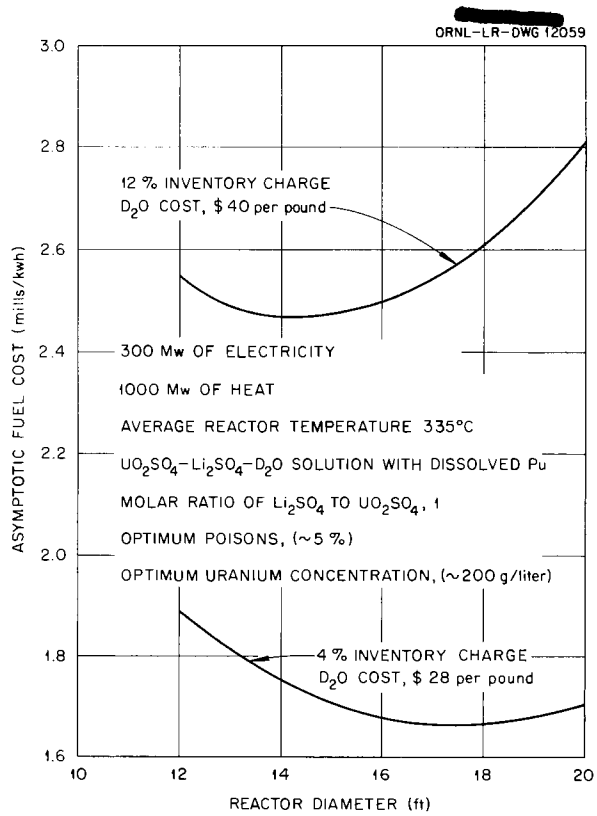

Fig. 7.3. Effect of Diameter on Fuel Cost.

and $28-per-pound D_2O (Fig. 7.2). The study of a plutonium-producing power reactor[3] had indicated that the optimum concentration occurred around 500 g/liter. The main factor contributing to the higher optimum uranium concentration in that study was the premium credit of $40 per gram taken for the plutonium produced, which permitted the investment of larger fuel inventories to increase the production of plutonium.

Figure 7.3 indicates that the optimum diameter is approximately 14 ft for the higher inventory charge and D_2O cost and 17 ft for the lower charge. The difference in fuel cost due to the use of the lower inventory charge and D_2O cost was found to be about 0.8 mill/kwhr.

Table 7.1 lists results for several reactors near optimum conditions as determined in this study. A cost of Li^7 as high as $1000 per pound was found to add only 0.1 to 0.2 mill/kwhr to the power cost, even with the higher inventory charge. The minimum cost of power was about 7.6 mills/kwhr for the higher inventory charge and D_2O cost and 6.8 mills/kwhr for the lower charge. If the fixed charge on plant investment were lowered from 15% to 10.5%, a 1.1 mills/kwhr reduction in cost would result.

The minimum asymptotic fuel cost of 2.5 mills/kwhr (12% inventory charge and $40 per pound for D_2O) was about the same as that found[2] for UO_3-PuO_2-D_2O slurry reactors operating at about 280°C. Within the limitations of this study (no exact evaluation of the effect of reactor size and pressure on the investment cost and net efficiency was made here), it was concluded that the addition of Li_2SO_4 to UO_2SO_4-D_2O fuel solution apparently would make the solution-type fuel reactor operated at 330°C economically competitive with the slurry-fuel reactor operated at 280°C.

TABLE 7.1. RESULTS FOR SEVERAL REACTORS* NEAR OPTIMUM CONDITIONS

Process characteristics					
Reactor diameter, ft	12	14	16	18	20
U^{238} concentration, g/liter	200	200	200	200	200
Feed enrichment, wt % U^{235}	2.11	1.72	1.48	1.33	1.22
Feed rate, g/day of U^{235}	1078	988	923	874	838
Chemical processing cycle, days	359	371	408	466	543
Poisons, %	5	5	5	5	5
Reactor volume, liters	25,620	40,680	60,730	86,470	118,610
Total system volume, liters	88,120	103,180	127,230	148,970	181,110
Power density, kw/liter	39.0	24.6	16.5	11.6	8.4
Isotope concentration, g/liter					
U^{235}	2.11	1.70	1.47	1.31	1.21
U^{236}	0.37	0.30	0.26	0.23	0.21
Pu^{239}	0.97	0.91	0.88	0.85	0.84
Pu^{240}	0.51	0.50	0.50	0.50	0.49
Np^{239}	0.03	0.03	0.02	0.02	0.02
Pu^{241}	0.52	0.48	0.45	0.44	0.43
Conversion ratio	0.667	0.697	0.718	0.733	0.745
Constant unit costs, mills/kwhr					
Reactor plant investment	0.79	0.79	0.79	0.79	0.79
Turbogenerator plant investment	2.78	2.78	2.78	2.78	2.78
Fixed chemical processing	0.87	0.87	0.87	0.87	0.87
Operation and maintenance	0.71	0.71	0.71	0.71	0.71
Total	5.15	5.15	5.15	5.15	5.15
Asymptotic fuel cost, mills/kwhr					
For 12% inventory charge; $40 per pound for D_2O					
Net feed	1.42	1.25	1.12	1.03	0.96
Variable chemical processing	0.11	0.11	0.11	0.11	0.10
Fuel inventory	0.29	0.27	0.27	0.28	0.31
D_2O inventory	0.49	0.57	0.68	0.82	1.00
D_2O losses	0.20	0.24	0.28	0.34	0.42
Lithium losses and inventory	0.014	0.017	0.020	0.024	0.029
Hydroclones	0.04	0.04	0.04	0.04	0.04
Total	2.56	2.49	2.52	2.64	2.86
For 4% inventory charge; $28 per pound for D_2O					
Net feed	1.42	1.25	1.12	1.03	0.96
Variable chemical processing	0.11	0.11	0.11	0.11	0.10
Fuel inventory	0.10	0.09	0.09	0.09	0.10
D_2O inventory	0.11	0.13	0.16	0.19	0.23
D_2O losses	0.14	0.17	0.20	0.24	0.29
Lithium losses and inventory	0.006	0.006	0.008	0.009	0.011
Hydroclones	0.04	0.04	0.04	0.04	0.04
Total	1.93	1.79	1.73	1.71	1.75

TABLE 7.1. (continued)

Total cost of power, mills/kwhr					
For 12% inventory charge, $40 per pound for D_2O	7.71	7.64	7.67	7.79	8.01
For 4% inventory charge, $28 per pound for D_2O	7.08	6.94	6.88	6.86	6.90
Relative neutron absorptions					
U^{235}	0.1685	0.1540	0.1436	0.1360	0.2445
Pu^{249} (thermal)	0.2107	0.2237	0.2328	0.2395	0.2445
Pu^{249} (resonance)	0.0363	0.0348	0.0338	0.0332	0.0328
Pu^{241}	0.0908	0.0949	0.0979	0.1001	0.1017
Pu^{240} (thermal)	0.0310	0.0347	0.0373	0.0392	0.0407
Pu^{240} (resonance)	0.0598	0.0603	0.0607	0.0609	0.0611
Np^{239}	0.0003	0.0003	0.0003	0.0003	0.0002
U^{236}	0.0004	0.0004	0.0003	0.0003	0.0003
U^{238} (thermal)	0.0675	0.0763	0.0828	0.0876	0.0912
U^{238} (resonance)	0.1799	0.1825	0.1842	0.1855	0.1864
Sulfur	0.0237	0.0267	0.0289	0.0306	0.0319
Lithium	0.0110	0.0125	0.0135	0.0143	0.0149
D_2O	0.0029	0.0032	0.0035	0.0037	0.0039
Poisons	0.0182	0.0182	0.0181	0.0181	0.0180
Nonthermal leakage	0.0751	0.0573	0.0451	0.0364	0.0299
Slow leakage	0.0239	0.0203	0.0171	0.0145	0.0124

*1000 Mw of heat; 300 Mw of electricity; average reactor temperature, 330°C.

7.2 CYLINDRICAL-REACTOR STUDIES

D. C. Hamilton

Nuclear calculations for 63 thorium breeder reactors were made on the Oracle, by means of the two-group, two-region cylindrical-reactor code. All calculations were made for a mean reactor temperature of 300°C and a thorium concentration in the blanket of 1000 g/liter. The fuel and moderator used were U^{233} and D_2O, respectively. The parameters were varied over the following ranges: core radius, 2 to 4 ft; blanket thickness, 1 to 3 ft; zirconium-core-tank thickness, ½ to 1 in.; length, 10 to 40 ft; fuel concentration in the blanket, 1 to 5 g of U^{233} per kilogram of Th^{232}; core poisons, 0 to 6% of core fission cross section. The results are being tabulated for use in an evaluation of cylindrical-reactor systems.

7.3 MULTIGROUP, MULTIREGION REACTOR CALCULATIONS

C. W. Nestor, Jr.

Critical concentrations and breeding ratios were calculated, by means of the Eyewash Univac program,[4] for a series of D_2O-moderated thorium breeder reactors. The purposes of this study were (1) to determine the trends in breeding ratio and critical concentration with varying reactor dimensions and blanket compositions; (2) to determine how well the two-group, two-region calculation,[5] currently used for a large number of economic survey calculations, indicates these trends; and (3) to find, if possible, the maximum conversion ratio for a reactor with a U^{235}-D_2O core, a ThO_2-D_2O blanket, and a pressure shell of fixed diameter and thickness.

The reactors studied in the multigroup calculations had the following characteristics:

1. pressure-vessel inside diameter of 6 ft;
2. pressure-vessel thickness of 6 in.;
3. core-tank thickness of approximately ½ in.;
4. four regions: U^{235}-D_2O or U^{233}-D_2O core, Zr core tank, ThO_2-D_2O slurry blanket, and Fe pressure shell;
5. core diameters of 2.5, 3, 3.5, 4, and 4.5 ft;

[4] J. H. Alexander and N. D. Given, *A Machine Multigroup Calculation*, ORNL-1925 (Sept. 6, 1955).

[5] T. B. Fowler, *Oracle Code for a General Two-Region, Two-Group Spherical Homogeneous Reactor Calculation*, ORNL CF-55-9-133 (Sept. 22, 1955).

6. blanket concentrations of 250, 500, and 1000 g of thorium per liter of slurry;
7. reactor computations both for no core poisons and for boron added to the core as a simulated poison.

For comparison purposes, four "clean" reactors with U^{235} in the core were computed by the two-group, two-region methods. Their characteristics were the same as those of the reactors studied in the multigroup calculation, that is, diameters of 2.5, 3, 4, and 4.5 ft and blanket concentration of 1000 g of thorium per liter.

The results for the clean cores were analyzed and are presented in Figs. 7.4 through 7.7. For all reactors, critical concentrations decreased with increasing core sizes and decreasing thorium concentration. For the U^{233} reactors, the breeding ratio decreased with increasing core size and decreasing thorium concentration; for the U^{235}

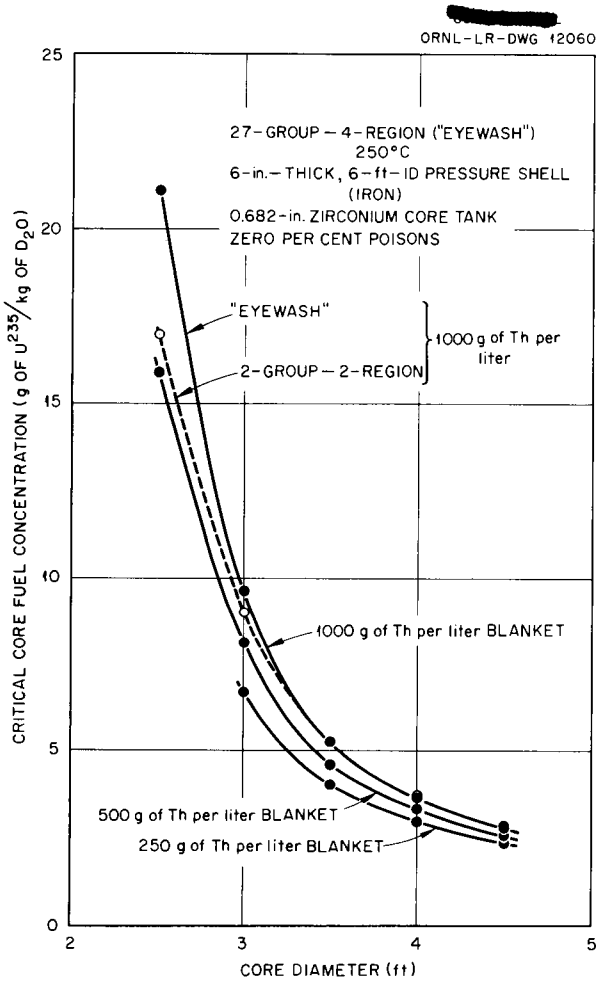

Fig. 7.4. Critical Concentration vs Core Diameter for U^{235}-Fueled Reactors.

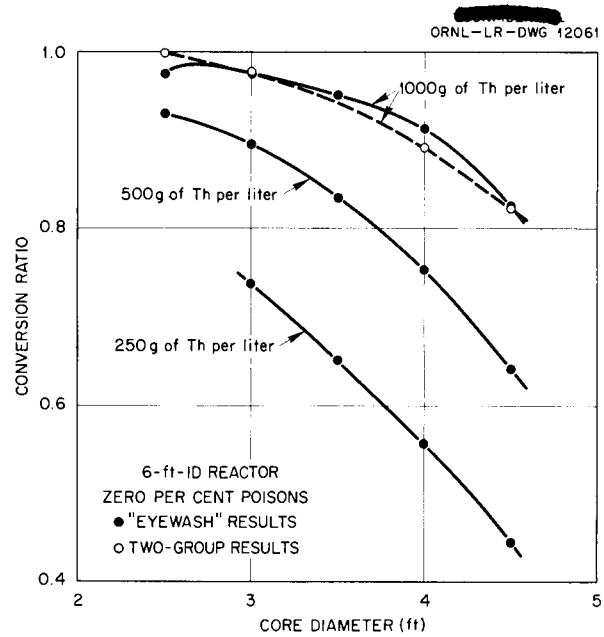

Fig. 7.5. Conversion Ratio vs Core Diameter for U^{235}-Fueled Reactors.

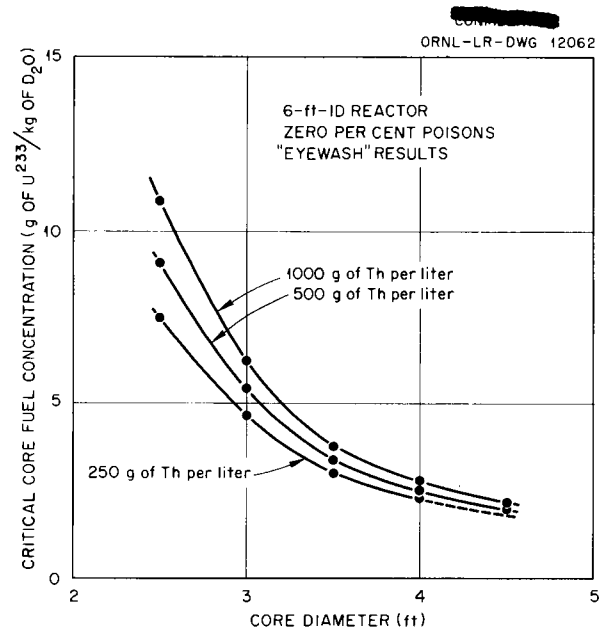

Fig. 7.6. Critical Concentration vs Core Diameter for U^{233}-Fueled Reactors.

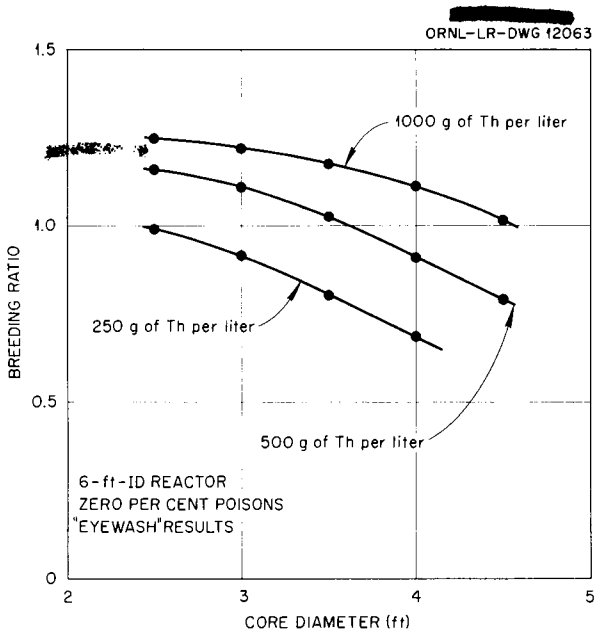

Fig. 7.7. Breeding Ratio vs Core Diameter for U^{233}-Fueled Reactors.

case, however, the reactors with blanket concentrations of 1000 g of thorium per liter showed an apparent maximum in conversion ratio (of about 0.98) at a core diameter of 2.7 ft. The decrease in conversion ratios at smaller core diameters was caused by an increase in energy of the fast-neutron leakage spectrum. Although not shown in the graphs, the maximum in conversion ratio occurred at a smaller core diameter and was displaced downward when poisons were added to the U^{235} reactors.

Results obtained from the two-group, two-region calculations are given in Figs. 7.4 and 7.5. The agreement in critical concentration was excellent for core diameters larger than 3 ft; the agreement in conversion ratio, as shown in Fig. 7.5, was fair for the same core sizes.

7.4 EXTRAPOLATION-DISTANCE ESTIMATES FOR REACTOR CALCULATIONS

M. Tobias

The effective extrapolation distance associated with a pressure vessel was calculated for one-region reactors containing D_2O, U^{235}, and U^{238}. The reactor parameters were varied over the following ranges: inside diameter of pressure vessel, 3 to 15 ft; pressure-vessel thickness, 3 to 20 in.; reactor temperature, 250 to 320°C; U^{238} concentration, 1 to 400 g/liter.

Two-group, two-region calculations were performed in which the pressure vessel was considered a separate region. These results were interpreted on the basis of a bare reactor model so as to give an effective extrapolation distance.[6]

The range of extrapolation distances found was 5 to 36 cm (2 to 14 in.). The extrapolation distance decreased with increasing core diameter and increased with increasing pressure-vessel thickness. The variation of extrapolation distance with temperature and U^{238} concentration was more complex, and no simple interpretation was available for the results obtained.

Since the extrapolation distance is merely a measure of the reflection effect of the pressure vessel, the results can be used to estimate the extrapolation distance associated with the pressure vessel of a two-region spherical reactor. If fuel and fertile materials other than U^{235} and U^{238} are considered, the results can be used if parameters such as reactor size, resonance escape probability, and thermal absorption cross section are matched with those considered here.

7.5 REACTIVITY CHANGES ASSOCIATED WITH SLURRY SETTLING IN THE TBR

H. C. Claiborne P. R. Kasten

The reactivity change associated with settling of the ThO_2 slurry was calculated for the TBR[7] by means of a numerical two-group, two-region, two-dimensional calculation method.[8] The results shown in Table 7.2 are for a 5-ft-dia core, a $2\frac{1}{4}$-ft-thick blanket, and an average temperature of 280°C. Cylindrical geometry (cylinder within a cylinder) was used in the calculations, with the heights of the cylinders equal to their diameters.

Although the reactivity additions obtained were quite large, such additions would not occur instantaneously. Rather, they would be a function of time, the rate of reactivity addition being controlled by the rate at which the slurry settled. Settling data for ThO_2-slurry systems[9] indicate

[6] M. Tobias, *Extrapolation Distance Estimates for Reactor Calculations*, ORNL CF-55-12-97 (Dec. 9, 1955).

[7] R. B. Korsmeyer *et al.*, *HRP Quar. Prog. Rep. April 30, 1955*, ORNL-1895, p 48–65.

[8] C. L. Bradshaw, manuscript to be published.

[9] S. A. Reed, *HRP Quar. Prog. Rep. Jan. 13, 1955*, ORNL-1853, p 83.

TABLE 7.2. REACTIVITY CHANGE AS A FUNCTION OF SLURRY SETTLING

Initial Thorium Concentration in Blanket (g/liter)	Percentage of Reactor Height Slurry Has Settled	Calculated Reactivity Change (% Δk_e)
1000	30	2.8
1000	50	10.2
500	30	2.1
500	50	8.7

that, at 300°C, the free settling rate of the slurry containing 1000 g of thorium per liter is nil and that of the slurry containing 500 g of thorium per liter is about 0.18 cm/sec. Such settling rates correspond to rates of reactivity addition of less than 0.02% Δk_e per second. These rates are well within the permissible rates of reactivity addition, and no reactor safety problem is apparent. However, if appreciable settling took place over a long period of time, the reactor temperature and pressure would eventually reach the point where the fuel system would have to be diluted.

7.6 MATHEMATICS AND COMPUTATIONS

7.6.1 Bessel-Function Code

M. K. Hullings

An Oracle code[10] was written for evaluating the Bessel functions I_0, I_1, J_0, J_1, K_0, K_1. The code is valid for arguments between 0.02 and 50 for I_0 and I_1, between 0.02 and 15 for J_0 and J_1, and between 1 and 50 for K_0 and K_1. It is being used in two-group, two-region cylindrical-reactor calculations.

7.6.2 Estimation of Fermi Age by Numerical Integration

M. Tobias

An Oracle code was prepared for the estimation of Fermi ages by numerical integration. The calculation consists in the evaluation of the integral:

$$\tau = \int_0^{u_{tb}} Z(u)\, du \int_u^{u_{tb}} \left(\frac{D}{\xi \Sigma_T}\right)_{u'} du' ,$$

where

D = diffusion constant,
τ = Fermi age,
ξ = logarithmic energy decrement per collision,
Σ_T = total cross section,
$Z(u)$ = number of neutrons born per unit lethargy at lethargy u,
u, u' = lethargy = ln $10^7/E$,
u_{tb} = thermal lethargy.

The lethargy interval between 10^7 ev and the thermal energy corresponding to 250°C was divided into 27 groups whose widths are those used by the Eyewash Univac code for multigroup reactor calculations. Most of the cross sections used are those employed by the Eyewash code. Provision is made for change of cross sections as improved data become available. The present method makes no provision for special treatment of hydrogen or of inelastic scattering.

7.6.3 Time-Dependence Studies

T. B. Fowler

An Oracle code for obtaining the time-dependent behavior of a batch-operated regenerative homogeneous reactor was completed. Quantities considered as parameters include feed enrichment, hydroclone cycle time, chemical processing cycle time, and unit costs. Cost data or nuclear data or both can be obtained at specified time intervals.

[10] M. K. Hullings, *Oracle Code for Evaluating Bessel Functions*, ORNL CF-56-1-63 (Jan. 10, 1956).

Part III

ENGINEERING DEVELOPMENT

J. A. Lane

8. DEVELOPMENT OF FUEL-SYSTEM COMPONENTS

C. B. Graham

R. Blumberg
C. H. Gabbard
L. F. Goode
B. A. Hannaford
P. H. Harley
P. P. Holz
I. K. Namba
W. L. Ross
I. Spiewak
D. S. Toomb
H. D. Wills

8.1 RECOMBINER DEVELOPMENT

8.1.1 High-Pressure Recombiner Loop

The high-pressure recombiner loop was redesigned and was rebuilt with new pipe. All old piping was removed to eliminate physically those regions shown by earlier tests[1] to have been stress-corroded.

During the last runs with the old loop, entrainment caused depletion of caustic in the gas-generating cells and caustic buildup in the boiler used to keep the system at pressure. Entrainment separators have been installed to prevent such a buildup from occurring in the future. Also, a small amount of liquid will be returned continuously from the boiler to the electrolytic cells during operation of the loop.

Figure 8.1 shows the new loop. The main changes from the previous system[2] are as follows:

1. The boiler pressurizing the system has been placed directly above the electrolytic cells.
2. The inlet of the ORNL pump used indirectly to circulate steam diluent has been attached to the condensate tank.
3. An 0.080-in.-ID recycle line has been installed to prevent caustic buildup in the condensate tank.
4. The condenser has been lengthened to give better temperature control.

The system passed its hydrostatic and helium leak tests. Operation will begin shortly with $Ba(OH)_2$ electrolyte in an effort to obtain a long-term chloride-free run. It is believed that chloride was responsible for the corrosion observed previously.

8.1.2 High-Pressure Flange Test

The purpose of the high-pressure flange test is to determine the effects of thermal and pressure cycling on oval, ring-joint flanges and to develop the techniques of flange assembly (e.g., bolt stresses, gasket loads, leak detection) which assure good performance. The test system includes a 4-in., 1500-psi flange; a 4-in., 2500-psi flange; heaters; a vacuum leak-detection system; and control instruments. The cycling will begin at rates comparable to those expected in the HRT and will increase in severity until leaks occur.

Assembly of the test system is complete except for part of the instrumentation. The torque–bolt stress relationships are being determined for the

[1]C. B. Graham *et al.*, *HRP Quar. Prog. Rep. Oct. 31, 1955*, ORNL-2004, p 64.

[2]C. B. Graham *et al.*, *HRP Quar. Prog. Rep. April 30, 1954*, ORNL-1753, p 54.

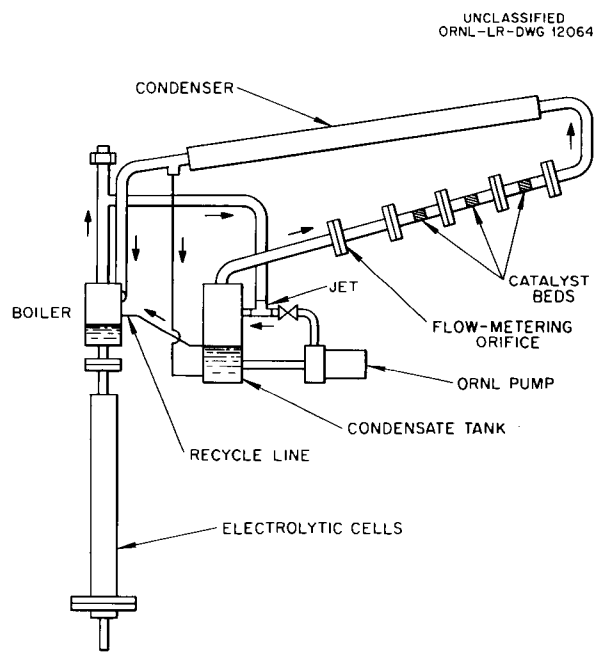

Fig. 8.1. High-Pressure Recombiner Loop, Model III.

flange bolts. After the flanges pass their 3000-psi hydrostatic tests, they will be thermally cycled.

8.1.3 Battelle and Syracuse Subcontracts

Battelle Memorial Institute continues to report low explosion limits[3] of electrolytic gas ($2H_2 + O_2$) in steam when spark-ignited in a 3-in. autoclave. This phase of the investigation will receive future emphasis, such as the following:

1. The reaction limits will be determined precisely by chemical analysis of the vapor.
2. The reaction limits will be obtained over the temperature range 300 to 550° F.
3. The ignition limits will be determined with hot-wire igniters as well as sparks.

Syracuse University is continuing its investigations of detonation pressures, damping of explosion waves, transient loading, and vapor viscosity. The results of the pressure and viscosity work will probably be available during the next quarter.

8.2 SMALL REACTOR COMPONENTS

8.2.1 20-cfm Canned-Rotor Blower

A 20-cfm gas circulator, suitable for operation in the HRT or larger reactors to supply forced circulation in high-pressure recombiner systems (or possibly for blanket stripping), is being built by the Allis-Chalmers Mfg. Co. This unit is designed with pressurized bearings and for "top maintenance." Design of a test loop for this blower was started, and material is on hand or on order. It is anticipated that the blower will be shipped to Oak Ridge in March and that testing will start in May.

8.2.2 Small Circulating Pumps

The 2000-psi, 5-gpm, canned-rotor pump has accumulated over 4000 hr at 300°C with water. Examination of pump parts revealed no excessive wear, defective parts, or corrosion.

A 1000-psi, 5-gpm, ORNL canned-rotor pump has operated for about 11,300 hr at 250°C with water and has accumulated about 6400 hr since the stator was repaired following an electrical failure.

The 5-gpm, canned-rotor pump, with series-connected windings, has accumulated 6600 hr of operation. The system was recently altered to permit studies of water injection to the rotor cavity. The information obtained is applicable to 300- and 400-gpm pumps because of the similarity of the labyrinth seals. Water was injected with the pump in both horizontal and vertical positions and rates of ½ to 1 gph were sufficient to purge the motor chamber during operation. Little difference was noted between vertical and horizontal mounting. An injection rate of 1 to 3 gph was required to prevent mixing during startup.

8.3 LARGE REACTOR COMPONENTS

8.3.1 4000-gpm Loop

Operation of the 4000-gpm loop with a solution of UO_2SO_4 (5 g of uranium per liter) was interrupted when it became impossible to maintain the condensate supply for the seal pump. Condensate is normally obtained from the letdown stream, but the letdown stream flow was reduced for two reasons: the drain valve was leaking because of an undersized valve operator, and the supply of solution injected by the feed pump was inadequate due to excessive corrosion of the Hastelloy D ball checks in this pump. To remedy this situation, Hastelloy C ball checks were installed in the feed pump, pumping rates of the seal pump and feed pump were reduced, and a larger drain-valve operator was installed. To ensure an adequate condensate supply under all operating conditions, a small pump and heat exchanger were added to the loop auxiliary system. These components will also eliminate the necessity of adding water to the system at startup and shutdown.

A short shakedown run on water will be made after installation of the new components (Feb. 1). Completion of the run with UO_2SO_4 solution, to obtain corrosion data on large systems, will be followed by disassembly and inspection of the Byron Jackson pump and the loop.

8.3.2 500-gpm Pump

Specifications were prepared for purchase of a 500-gpm, canned-rotor pump which will be used to evaluate pressurized (all-metal) bearings and "top maintenance" in solution or slurry systems. The capacity of the pump can be reduced to 400 gpm by use of a small impeller. The fabrication will be reactor grade so that the pump may be used in the HRT, or in a similar application, after testing has been completed.

[3] C. B. Graham *et al.*, *HRP Quar. Prog. Rep. Oct. 31, 1955*, ORNL-2004, p 66.

8.4 TITANIUM-LINED EQUIPMENT

The titanium-lined pipe sections and heat exchanger, which are to be fabricated by the Crane Co. and The Pfaudler Co., are in the final design stages. Construction will proceed as soon as the designs are approved. A study of the feasibility of roll-cladding titanium to carbon steel has been in progress at Armour Research Foundation since November 1955. A test rig, to subject the lined equipment to thermal and pressure cycles, is in the preliminary design stage.

9. DEVELOPMENT OF BLANKET-SYSTEM COMPONENTS

R. N. Lyon

P. R. Crowley, D. G. Davis, R. B. Gallaher, W. Q. Hullings, A. S. Kitzes, C. G. Lawson, L. E. McTaggart, I. M. Miller, R. H. Nimmo, L. F. Parsly, M. Richardson, A. N. Smith, D. G. Thomas, R. P. Wichner

9.1 SLURRY BLANKET MOCKUP

L. F. Parsly R. H. Nimmo L. E. McTaggart

Construction of the blanket mockup was substantially complete at the end of this report period. Calibration of the flow elements and testing of the equipment components are under way.

9.2 ATTACK OF CIRCULATING AQUEOUS ThO_2 SLURRIES ON STAINLESS STEEL SYSTEMS

D. G. Thomas

Data on the rate of iron accumulation in thorium oxide slurries when the slurries were circulated in the 100A loops[1] S and T were examined by the use of multiple regression analysis.[2] Combining these results with those from early Chicago experiments[3] and with some preliminary results from the toroid tests[4,5] gave the trend of the effect of certain variables on the attack rate of circulating thorium oxide on stainless steel and permitted an estimate of the relative contributions of the different variables. Thus it should be possible to set the operating conditions for a slurry system to give a minimum attack rate. If, as is entirely probable, conditions giving minimum attack rate are not those found most desirable to minimize the handling or caking problems, the attack rate for various compromise conditions can be estimated and the most satisfactory one chosen.

In a system where the velocity, V, and particle diameter, D_p, are variables, the attack rate can be expected to vary as $(VD_p^2)^n$, where the most likely value of n is 2 to 3. There is also a value of the term (VD_p^2) below which attack is negligible. For the 100A loops S and T, the volumetric flow rate was not varied, and the size of the slurry particles was for the most part unknown, although most of the oxides probably contained 95 wt % of particles less than 25 μ in diameter. Therefore the variables considered in the multiple regression analysis were pH, ThO_2 concentration, ThO_2 calcination temperature, sulfate concentration, and oxygen concentration. It was assumed that the $\log_{10}$ of the attack rate was, to a first approximation, related linearly to these five variables and that it could be expressed by an equation of the form

$$y = b_{y.12345} + b_{y1.2345}X_1 + b_{y2.1345}X_2 + b_{y3.1245}X_3 + b_{y4.1235}X_4 + b_{y5.1234}X_5 ,$$

where

$y = \log_{10}$ (attack rate),

$X_1, \ldots, X_5$ = variables,

$b_{y.12345}$ = the mean value of y minus the contribution to y of the variables X_1, X_2, X_3, X_4, X_5 at their means;

and $b_{y1.2345}$ measures the rate of increasing y with increasing X_1; $X_2, \ldots, X_5$ being constant; $b_{y2.1345}$ measures the rate of increasing y with increasing X_2; X_1, X_3, X_4, X_5 being constant; etc.

The six coefficients which gave the best general fit to the data were determined. This required the solution of six sets of six simultaneous equations. The matrices were inverted[6] on the Oracle, and

[1] R. N. Lyon *et al.*, *HRP Quar. Prog. Reps.* for: *Oct. 31, 1953*, ORNL-1658; *Jan. 31, 1954*, ORNL-1678; *April 30, 1954*, ORNL-1753; *July 31, 1954*, ORNL-1772; *Oct. 31, 1954*, ORNL-1813; *Jan. 31, 1955*, ORNL-1853; *April 30, 1955*, ORNL-1895; and *July 31, 1955*, ORNL-1943.

[2] D. G. Thomas, *Attack of Circulating Aqueous–ThO_2 Slurries on Stainless Steel Systems*, ORNL CF-56-1-21 (Jan. 5, 1956).

[3] C. F. Hiskey *et al.*, *The Heavy-Water Homogeneous Pile: A Review of Chemical Researches and Problems*, CC-1383, A-2024 (Feb. 28, 1944).

[4] D. G. Thomas, *Comments on the Erosiveness of ThO_2 Slurries*, ORNL CF-55-4-36 (April 5, 1955).

[5] G. E. Moore and E. L. Compere, *HRP Quar. Prog. Rep. July 31, 1955*, ORNL-1943, p 147.

[6] A. W. Kimball of the Biometrics Group of the Mathematics Panel arranged for inversion of this matrix on the Oracle.

both an arithmetic relation and a parabolic relation between the attack rate and time were used. The range of variables is given in Table 9.1, and the results of the analysis are presented in Table 9.2.

For the particular conditions under which loops S and T were operated, the following tentative conclusions for stainless steel can be drawn from the results, and even their qualitative confirmation will depend on tests planned specifically to give corrosion-erosion information:

1. The attack rate by aqueous thorium oxide slurries decreases as the oxygen concentration increases, the effect apparently being more important in the first 20 to 300 hr of the run than in times after that.

2. The attack rate by aqueous thorium oxide slurries increases with increasing pH, the effect apparently being more important after the first 20 to 300 hr of the test.

3. The attack rate by aqueous thorium oxide slurries increases with increasing thorium oxide concentration and with thorium oxide calcination temperature.

TABLE 9.1. RANGE OF VARIABLES IN CORRELATIONS

	Variable	Minimum	Mean	Maximum
[Log (10 × linear attack rate)] × 10	y_1	1	13.9	23
[Log (parabolic attack rate)] × 10	y_2	13	36.6	47
pH × 10	X_1	44	59.9	92
Th concentration, g/kg/10	X_2	22	51.8	108
Calcination temperature, °C/10	X_3	65	73.3	95
SO_4^{--} concentration, ppm/100	X_4	1	22.4	81
O_2 concentration, ppm/1000	X_5	0	5.1	10

TABLE 9.2. RESULTS OF STATISTICAL ANALYSIS

Coefficient	Linear Attack Rate		Parabolic Attack Rate	
	Coefficient	Significance Level	Coefficient	Significance Level
$b_{y.12345}$	−5.35		12.78	
$b_{y1.2345}$	0.17 ±0.18	0.082	0.16 ±0.25	0.228
$b_{y2.1345}$	0.04 ±0.08	0.361	0.10 ±0.13	0.083
$b_{y3.1245}$	0.14 ±0.22	0.219	0.24 ±0.30	0.127
$b_{y4.1235}$	0.005 ±0.13	>0.50	−0.06 ±0.18	0.50
$b_{y5.1234}$	−0.62 ±0.71	0.097	−1.38 ±0.97	0.01
$b_{y2.1345} + b_{y4.1235}$		>0.20		
$b_{y1.2345} + b_{y4.1235}$				0.155
Total correlation		0.10		0.02

4. The attack rate by aqueous thorium oxide slurries is independent of sulfate concentration *except* as the sulfate affects the pH of the medium.

Examination of the data from loop tests also showed that (1) the ratio of the weight losses of the impeller to the weight loss of the orifice was a constant and was essentially the same whether the combination was titanium-titanium or stainless steel–stainless steel; (2) the attack rate of aqueous thorium oxide slurries was from two to four times as great on stainless steel as it was on titanium.

The details of the multiple regression analysis and a survey of experimental results of previous investigators were reported.[7]

9.3 SLURRY COMPONENT DEVELOPMENT AND LOOP OPERATION

A. S. Kitzes

P. R. Crowley
R. B. Gallaher
W. Q. Hullings
I. M. Miller
C. G. Lawson
M. Richardson
A. N. Smith
R. P. Wichner

9.3.1 Westinghouse Slurry Pump 200A

W. Q. Hullings

Three basic difficulties have been encountered in the operation of the Westinghouse 200A pump with slurry at 300°C: failure to effect a good seal of the pump flanges, leakage around the thermal barrier, and failure of the Kingsbury bearing. To eliminate the first two difficulties, the pump flanges and thermal barrier will be seal-welded for all slurry runs at 300°C. The pump flanges are designed to be sealed by a weld; the thermal barrier was modified for welding. To facilitate pump disassembly, a custom-made seal weld cutter with an attachment to cut the barrier weld was ordered for delivery February 1.

Failure of the Kingsbury bearing under normal operating conditions is believed to have been due to erosion of the Graphitar ring by thorium oxide slurry. Mixing of the main circulating slurry stream with liquid in the rotor cavity was demonstrated by the presence of thorium oxide in the thermal-barrier and rotor cavities (see Fig. 9.1) at the end of each run, in spite of the injection of a continuous purge of clean condensate at the top of the rotor cavity. Slurry is believed to have passed behind the thermal barrier from the outer edge where the pressure was high, circulated through the thermal-barrier cavity, and passed out through the labyrinth at the hub of the impeller where the pumping action of the ribs on the back of the impeller caused the pressure to be low. Some of the thorium oxide in the thermal-barrier cavity is believed to have been drawn into the lower suction ports in the pump shaft and discharged into the rotor cavity by the secondary impeller. Tests with water containing chromic acid confirmed this circulation of part of the main pumped stream.

In tests with the chromic acid in the circulating stream, with the lower suction ports welded closed, and with the condensate injected at the top of the rotor cavity, but with the thermal barrier unwelded, chromate was found in samples of liquid withdrawn from the thermal-barrier cavity but was not detected in samples taken from the rotor cavity. When the thermal barrier is seal-welded, it is expected that a flow of condensate at 100 cc/min into the top of the motor will be sufficient to prevent the pumped fluid from entering either cavity.

After one slurry run some of the thrust bearing components were found to have been distorted to an extent which implied either total thrust loads above 1000 lb or improper operation of the bearing (possibly caused by packing of thorium oxide around the linkages). There are no pressure equalization holes through the hub of the impeller, but the ribs on the back of the impeller were designed to reduce the thrust. It was found in preliminary tests with water at Westinghouse that the total thrust load was 150 lb. Extension to a pumped fluid with a density of 2 led to a predicted thrust load of 300 lb. Westinghouse technicians at ORNL confirmed these loads by measurements with water and slurry.

Although the loads are considered to be permissible, the length of the impeller ribs has been increased from $3\frac{1}{2}$ to $4\frac{1}{4}$ in. to reduce the thrust load to 120 lb with slurry. Lengthening the ribs also reduces the pressure in the rotor cavity; the lower pressure is expected to result in improved control of injection of condensate.

The feasibility of substituting Al_2O_3 surfaces for Stellite and Graphitar is being investigated. A full set of pads, runners, journals, and radial bearings with Rokite A (sprayed Al_2O_3) surfaces was ordered for pump 200A for testing purposes.

[7] D. G. Thomas, *Attack of Circulating Aqueous–ThO_2 Slurries on Stainless Steel Systems*, ORNL CF-56-1-21 (Jan. 5, 1956).

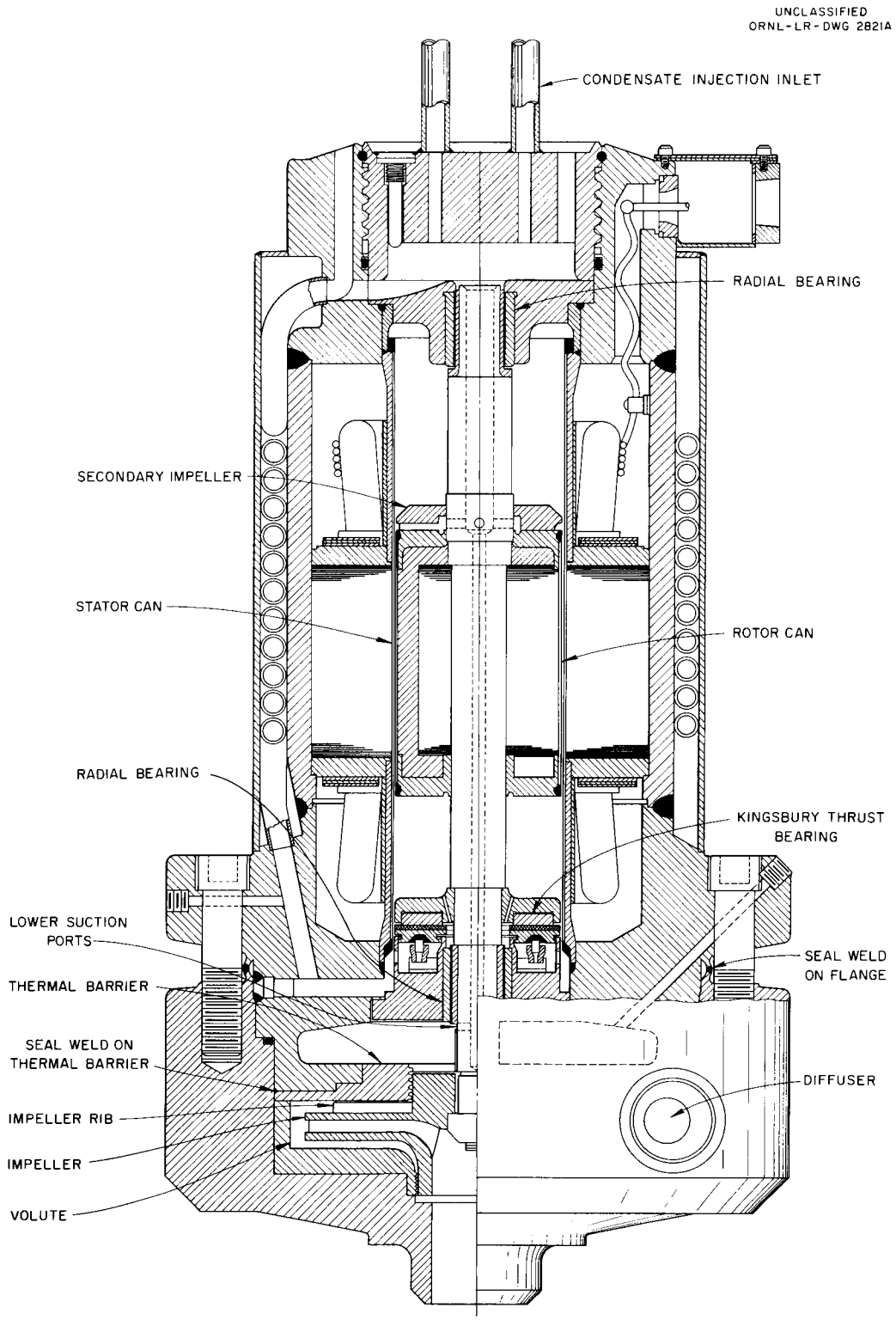

Fig. 9.1. Westinghouse 200A Pump.

9.3.2 Caking During Operation of Slurry Loop 200A

W. Q. Hullings

During the third 200-gpm slurry loop run, approximately 50% of the circulated solids deposited on the pipe walls as a hard, intractable cake[8] from $\frac{1}{8}$ to $\frac{1}{4}$ in. thick and with a density of 5.4 g/cm^3. A single determination of the modulus or rupture (the bending stress at rupture) of a bar of cake $\frac{1}{4} \times \frac{1}{4} \times 2$ in. gave a value of 360 psi compared with an average value of 2850 psi found for samples of Tennessee marble having similar dimensions. Chemical analyses of cakes obtained from various parts of the loop system showed the usual contaminations of iron, nickel, chromium, and sulfate to be present. In addition, aluminum and silica were found. Several steps have been taken to determine the cause of this unprecedented and serious phenomenon.

9.3.3 Dump-Tank Evaporator Tests

M. Richardson A. N. Smith

Two dump-tank systems for use in the HRT blanket being investigated with the use of small steel or glass models are described below.

(a) Combination Race Track–Vertical Gas Lift. – Results with the combination race track–vertical gas lift dump tank[9] continue to look promising. Slurries containing 1000 g of thorium per kilogram of H_2O were circulated for periods of several days to two weeks without an appreciable change in concentration. The system was shut down for varying lengths of time up to ten days and restarted with no difficulty in redispersing the solids.

After the ten-day shutdown, with the bed in each riser leg approximately 18 in. deep, a steam pressure of 3 psig was required to set the bed in motion. Once in motion, 3-psig steam was needed to keep the solids suspended in 100 liters of slurry to evaporate water at the rate of 1 lb/min.

Auxiliary heat, to compensate for heat losses and to maintain concentration, was supplied by a steam coil which was inserted in one of the downcomer legs. In each run, regardless of concentration, a viscous sludge of density 3.7 g/cm^3 was deposited between the steam coil and the downcomer wall, perhaps due to surface boiling in that low-velocity region of the downcomer. Various schemes for supplying the auxiliary heat without sludge formation are being tested.

Slurries containing 1200 g of thorium per kilogram of H_2O were also circulated for 168 hr with no change in concentration. After a 72-hr shutdown, 5-psig steam was required to set the 2-ft-deep bed in motion. Once in motion, only 3-psig steam was needed to keep the solids suspended.

(b) Conical Dump Tank with Vertical Gas Lift. – An inverted-cone-shaped steel tank, approximately 3 ft high and 3 ft in diameter at the top, is being fitted with a gas lift as shown in Fig. 9.2. It is hoped that this type of system will combine the simplicity and effectiveness of the simple gas lift and the capacity of the race-track model. If tests prove successful, it is believed that this type of dump tank can be adapted to handle both large and small amounts of slurry.

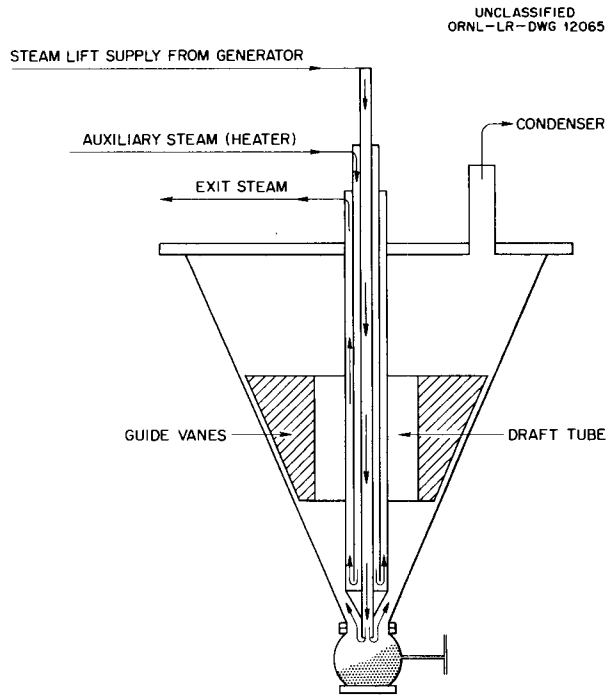

Fig. 9.2. Experimental Dump Tank for ThO_2 Slurry.

[8] R. N. Lyon and D. G. Thomas, *Preliminary Investigation into Cake Formation During Slurry Test 200A-3*, ORNL CF-55-12-32 (Dec. 6, 1955).

[9] R. N. Lyon *et al.*, *HRP Quar. Prog. Rep. Oct. 31, 1955*, ORNL-2004, p 68–71.

9.3.4 Heat-Transfer Studies

C. G. Lawson I. M. Miller

The extent and nature of transitional flow from the laminar to the fully turbulent regions for a typical Bingham-plastic thorium oxide slurry are being determined by means of radial temperature profiles. Preliminary data indicate that plug-type flow, characteristic of laminar flow with Bingham plastics, persisted into the turbulent region for velocities twice those required to initiate measurable turbulence[10,11] for the system studied.

Measurements were made in a 1-in. pipe, 50 pipe diameters downstream from the exit from a 10-ft-long steam-jacketed section. The slurry had a yield stress of 0.15 lb/ft and a modulus of rigidity of 4.5 centipoises as determined in a pipeline viscometer.

---

[10] C. G. Lawson, *A State-of-the-Art Survey on Engineering Calculations for Slurry Systems*, ORNL CF-55-9-165 (Sept. 22, 1955).

[11] B. O. A. Hedström, *Ind. Eng. Chem.* **44**, 651 (1952).

Part IV

CORROSION AND MATERIALS

E. G. Bohlmann

10. SOLUTION CORROSION[1]

J. C. Griess
S. R. Buxton
J. L. English
R. S. Greeley
G. E. Moore
H. C. Savage
R. M. Pierce[2]
J. A. Russell
R. M. Warner
D. B. Weaver[2]

10.1 PUMP LOOPS

J. C. Griess
S. R. Buxton
R. S. Greeley
R. M. Pierce
H. C. Savage
J. A. Russell
R. M. Warner
D. B. Weaver

Tests in the 100A pump loops showed that, if solutions containing 0.04 *m* uranyl sulfate and 0.005 *m* $CuSO_4$ are to be maintained at temperatures as high as 300°C, sulfuric acid must be added to prevent hydrolytic precipitation of copper and uranium. It now seems certain that at least 0.015 *m* H_2SO_4 will be necessary to stabilize the solution at 300°C. Runs with less acid showed that copper and, to a lesser extent, uranium slowly precipitate from the solution. At 300°C with 0.015 *m* sulfuric acid, corrosion of stainless steel was not excessive even at flow rates as high as 45 fps. However, corrosion became much more severe in the above solution in the temperature range of 200 to 250°C, and, in this range, critical velocities as low as 15 to 20 fps were observed. If the critical velocity is not exceeded, corrosion rates of no more than 1 mpy can be expected.

The circulation of 0.04 *m* UO_2SO_4 solutions containing 0.005 *m* $CuSO_4$ with 0.020 *m* H_2SO_4 and with 0.015 *m* H_2SO_4 at 340°C was accomplished, but in both cases two liquid phases were present. Laboratory tests confirmed the loop data and showed that the heavy phase represented no more than 0.1% of the total volume of the solution and that it contained copper. In the loop run the heavy phase was not circulated but apparently collected in crevices or dead ends of the loop. As the temperature was lowered, the two phases became miscible, as evidenced by an increase in the uranium and copper concentrations of the solution. Under the above conditions corrosion damage to stainless steel, titanium, and Zircaloy-2 was minor up to 70 fps.

Other loop runs showed that the presence of copper in 0.04 *m* UO_2SO_4 solutions had no effect on the corrosion rate of stainless steel below the critical velocity; above the critical velocity copper accelerated the corrosion rate. For example, in a 0.04 *m* UO_2SO_4 solution containing 0.02 *m* H_2SO_4 and 0.005 *m* $CuSO_4$, the film-free corrosion rate of type 347 stainless steel was 100 mpy at 250°C. Under identical conditions, but with 0.05 *m* instead of 0.005 *m* $CuSO_4$, the corrosion rate was 300 mpy.

A solution containing 0.03 *m* UO_3 and 0.17 *m* Li_2CO_3, with partial pressures of 600 psi CO_2 and 400 psi oxygen, was circulated in two runs at 250°C, and the solution demonstrated a low degree of corrosiveness. The ferritic stainless steels, carbon steel, and nickel, all of which are corroded heavily by uranyl sulfate solutions, showed low corrosion rates in the carbonate system. The average corrosion rate for carbon steel was 5.7 mpy for a 200-hr exposure. For a 537-hr exposure the corrosion rate was 2.5 mpy, which shows that the corrosion rate was very low after the first 200-hr period. The austenitic stainless steels in all cases showed corrosion rates at least as low as, and in most cases even lower than, in a comparable sulfate system. The Stellites were heavily corroded by both the carbonate and the sulfate system.

Further corrosion tests with uranyl sulfate solutions containing an equimolar concentration of lithium sulfate were completed. The tests made with solutions containing between 300 and 680 g of uranium per liter verified previously reported results. One run made at 350°C with 3.8 *m* UO_2SO_4 showed the absence of a critical velocity up to 70 fps; all stainless steel corrosion specimens developed smooth, adherent films which protected the steel from heavy attack. The average corrosion rate for type 347 stainless steel specimens was 25 mpy for a 143-hr run and undoubtedly would have been lower had the run continued.

[1]This work has been reported in greater detail in ORNL CF-56-1-167 (to be issued).

[2]On loan from TVA.

Solutions containing 300 g of uranium per liter and half the molar equivalent of lithium sulfate were circulated at 300°C. The results obtained in duplicate runs were not in complete agreement, but generally the results indicated that the critical velocity was between 15 and 30 fps. Below the critical velocity, a protective film formed, which minimized the corrosion damage to the stainless steel; above the critical velocity, corrosion was severe, with corrosion rates as high as 1500 mpy. In uranyl sulfate solutions of all concentrations, both with and without added sulfate salts, titanium and zirconium and some of their alloys showed very little corrosion attack.

Loop runs with the highly concentrated UO_2SO_4-Li_2SO_4 solutions failed to demonstrate the low vapor pressure reported in the last quarterly report.[3] Additional autoclave tests also failed to verify the early results. Reasons for the discrepancies have not been obtained.

10.2 TOROIDS

G. E. Moore J. C. Griess

Toroid runs with solutions containing 0.16 *m* UO_2SO_4, both with and without 1.0 *m* Cs_2SO_4, showed that the corrosion of stainless steel was markedly suppressed by the added cesium sulfate. In identical runs (except for the presence or absence of cesium sulfate) at 250°C, the average corrosion rate of type 347 stainless steel in the solutions without the cesium sulfate was 66 mpy, compared with 3.5 mpy for the solutions with the cesium sulfate. Similar toroid runs with 3.8 *m* UO_2SO_4, both with and without 3.3 *m* Li_2SO_4, demonstrated a beneficial effect of the added lithium sulfate. In essence, results obtained with the toroids substantiated the loop data, which showed that the addition of sulfate ions to uranyl sulfate solutions reduced their corrosiveness considerably.

10.3 LABORATORY TESTS

J. L. English J. C. Griess

Preliminary static tests with type 1515N stainless steel showed the alloy to have a corrosion resistance similar to that of type 347 in uranyl sulfate solutions. The alloy was developed by The Babcock & Wilcox Co. specifically for high-temperature steam service in the range of 650 to 800°C. The nominal composition of the alloy is 15% Cr, 15% Ni, 1.5% Mo, 1% Nb, 1% W, balance iron. At boiling temperature all specimens showed very slight weight gains in 1.3 *m* UO_2SO_4 and in 0.04 *m* UO_2SO_4 containing 0.02 *m* H_2SO_4 and 0.005 *m* $CuSO_4$. In the latter solution at 300°C the corrosion rate was 0.3 mpy.

Corrosion studies with an antigalling type of cast alloy, designated as Waukesha Metal No. 88, showed the alloy to have a reasonable corrosion rate, about 0.5 mpy, in boiling 0.04 *m* UO_2SO_4 containing 0.02 *m* H_2SO_4 and 0.005 *m* $CuSO_4$; in the same solution at 300°C, however, the alloy corroded at a rate of 43 mpy. The test samples were supplied by the Allis-Chalmers Mfg. Co. and had a nominal composition of 0.03% C, 12% Cr, 4% Sn, 3.5% Bi, 5% Fe, 3% Mo, 0.8% Mn, balance nickel. In boiling 5% nitric acid, corrosion was severe and averaged 32 mpy for duplicate specimens. Significant pitting attack was apparent.

Studies with Iso-Elastic spring alloy, a material considered for use in the pressurizer liquid-level controller of the HRT, showed the metal to have very poor corrosion resistance to uranyl sulfate solutions, even at room temperature. Corrosion tests with gold-plated specimens showed that if the gold plate contains pinholes corrosion will be severe at these locations, usually severe enough to undercut the gold and allow it to flake off.

In an effort to find a more resistant alloy suitable for use as a spring at 300°C, tests were initiated with Elgiloy, an alloy with a nominal composition of 40% Co, 20% Cr, 15% Ni, 7% Mo, 2% Mn, 0.04% Be, 0.15% C, balance iron. Preliminary tests indicated a corrosion rate of 0.02 mpy in boiling 0.12 *m* UO_2SO_4 and 1.6 mpy in 0.17 *m* UO_2SO_4 at 150°C. In 0.04 *m* UO_2SO_4 containing 0.02 *m* H_2SO_4 and 0.005 *m* $CuSO_4$ at 300°C, the corrosion rate was only 3.5 mpy, and the rate appeared to be decreasing with time. A specimen exposed in the vapor phase at 300°C, which more closely represents the actual service environment, showed negligible corrosion.

Results of preliminary corrosion tests with niobium-zirconium alloys were reported in the last quarterly progress report.[4] Further static testing

[3] H. C. Savage, J. C. Griess, *et al.*, *HRP Quar. Prog. Rep. Oct. 31, 1955*, ORNL-2004, p 98.

[4] J. L. English and J. C. Griess, *HRP Quar. Prog. Rep. Oct. 31, 1955*, ORNL-2004, p 103–105.

with cast alloys containing 2, 5, and 7.5% niobium and with wrought alloys containing 2 and 15% niobium was carried out. During a 500-hr test, in a solution of 0.04 *m* UO_2SO_4 with 0.02 *m* H_2SO_4 and 0.005 *m* $CuSO_4$ at 300°C, the cast alloys containing 2 and 5% niobium exhibited corrosion rates of 37 and 10 mpy, respectively; the 7.5% niobium alloy showed a weight gain corresponding to a corrosion rate of about 4 mpy (assuming no loss of oxide from the specimen). The wrought 2% alloy corroded at a rate of 3.3 mpy, whereas the 15% alloy showed a weight gain, equivalent to a corrosion rate of 2.4 mpy. It should be noted that all alloys contained oxide on their surfaces and that the reported corrosion rates would have been higher had the oxide been removed. All the zirconium-niobium alloys investigated to date have shown a corrosion resistance inferior to Zircaloy-2.

The corrosion rate of sintered aluminum oxide in 0.17 *m* UO_2SO_4 was found to range between 0.5 and 2 mpy in the temperature range of 150 to 250°C. At 300°C the rate ranged between 2.9 and 4.4 mpy and appeared to be increasing with time. It was noted that in 0.17 *m* UO_2SO_4 containing 0.01 *m* $CuSO_4$ a corrosion rate of less than 1 mpy was observed at 200°C; at 250°C, the rate was increasing with time, amounting to 1.1 mpy during the first 100-hr exposure period and 5.3 mpy after 1700 hr. Corrosion tests with three different types of Coors porcelain demonstrated them to be completely unsuitable in 0.17 *m* UO_2SO_4 at 250°C. Corrosion rates between 87 and 200 mpy were observed.

Corrosion tests in which titanium, gold, and Zircaloy-2 were coupled to type 347 stainless steel showed the complete absence of galvanic attack both in boiling 5% HNO_3 and in boiling 0.04 *m* UO_2SO_4 containing 0.005 *m* $CuSO_4$ and 0.02 *m* H_2SO_4.

Stressed specimens of type 347 stainless steel were exposed for 7630 hr both in and above boiling 0.04 *m* UO_2SO_4 containing 0.004 *m* H_2SO_4 and 0.005 *m* $CuSO_4$. No cracking of the specimens was observed either in the vapor or in the solution, and generalized corrosion rates were of the order of 0.01 mpy. At the end of the 7630-hr period 60 ppm of chloride ion as potassium chloride was added to the solution, and the test was continued. In addition to the specimens previously exposed, one new stress assembly of type 347 stainless steel was included in the vapor phase, and one was immersed in the solution. At the end of 500 hr the new specimen exposed in the solution exhibited incipient cracking at several points near the area of maximum applied stress (20,000 psi). The edges also showed random pitting attack and at one point, a blistering of the metal. All pre-exposed specimens and the new specimen exposed in the vapor showed neither cracking nor pitting. A separate, more extensive investigation previously reported[5] showed that specimens of type 347 stainless steel exposed above UO_2SO_4 solutions containing as little as 5 ppm chloride ion can be severely pitted and cracked at areas of residual stresses. These investigations demonstrated the damage that can be done to austenitic stainless steel by low concentrations of chloride ion (or chlorine) either in solution or in the vapor phase.

[5] G. E. Moore, *Summary of Laboratory Corrosion Tests: The Solution and Vapor Phase Corrosion of Type 347 Stainless Steel, Titanium 75A and Zircaloy-2 Exposed to 0.14* m *Uranyl Sulfate in the Absence and Presence of Chlorine or Iodine*, ORNL CF-55-12-70 (Dec. 12, 1955).

11. SLURRY CORROSION

E. L. Compere
S. R. Buxton
G. E. Moore
R. M. Pierce[1]
H. C. Savage
S. A. Reed
R. M. Warner

11.1 PUMP LOOPS

Four short-term runs in 100A loop CS were made during the quarter.[2] Three of the runs were made with thorium oxide slurry; for these runs the loop was charged initially to a concentration of approximately 1200 g of thorium per kilogram of water. Average circulating concentrations ranging from 581 to 1075 g of thorium per kilogram of water were observed. Three different batches of thorium oxide were used. Each of these was a thorium oxalate calcination product, finally calcined at 800°C. One run with water was made to check over-all loop performance. All runs were made at 300°C, with the addition of oxygen to the system.

The first slurry run, CS-18, at a temperature of 300°C in the loop and about 325°C in the pressurizer, was terminated because of excessive pump-bearing wear after 97 hr of operation. The feed of water to the pump rotor cavity was insufficient to keep slurry flushed out of the bearings, and this caused the excessive wear.

Following this run, the condensate system was modified to increase the flow of water to the pump cavity. A water run was then made, and it indicated that the flow had been improved. Subsequent operation with thorium oxide slurry revealed, however, that the condensate system did not operate reliably under all conditions of loop temperature, pressure, and flow. Further revisions to the condensate system and an increase in the size of the bypass line from the pump to the pressurizer have been made.

For run CS-20 the calculated charge concentration was 1180 g of thorium per kilogram of water. The oxide used was produced at the Feed Materials Processing Center at Fernald, Ohio, and was recalcined at 800°C at ORNL. The loop operating temperature was 300°C. Loss of condensate flow, which occurred after 3 hr of operation, required shutdown 3 hr later to avoid pump damage. Subsequent attempts to resuspend the slurry failed, indicating plugging of a sample barrel.

When the loop was dismantled, two kinds of thorium oxide cakes were found. One was a glassy translucent film on many of the pins, the pin holders, and parts of the pump impeller. This hard cake, along with an earlier chalky deposit on the pin holder, appeared to have been formed throughout the course of the run. A softer plug was also noted in a sample barrel. This plug may have resulted from settling of slurry in the pin holder after the aforementioned hard cake constricted the channel. The hard cake probably resulted from impurities in the particular batch of oxide used. No other 100A loop runs with other thorium oxide preparations have produced deposits of this character. Figure 11.1 shows one half of the pin holder.

Run CS-21 was charged with relatively pure ORNL-produced thorium oxide, precipitated by oxalic acid at 70°C and calcined at 800°C. The charge concentration was 1200 g of thorium per kilogram of water, and the loop was operated at 300°C.

A sample barrel, which was restricted downstream so that it allowed a flow rate of 16 fps, apparently was plugged in the upstream header from the beginning of the run. The material of the plug resembled the oxide used in the previous run, CS-20; presumably, the oxide had not been completely washed out after that run.

After 1 hr of operation at 300°C, temperature of the 1-in. bypass mixing line leading from the pump discharge to the top of the pressurizer began to fall, indicating a plug. No subsequent indication of flow was noted for the rest of the run, which had a total duration of 30 hr. During the twenty-second hour of operation, carbon dioxide was added to the loop to a partial pressure of 50 psi in an effort to relieve the plugging, but no effect was noted.

After the loop was water-rinsed, it was opened. The bypass mixing line was found to be entirely open and clear. One sample barrel and its up-

[1]On loan from TVA.

[2]The material in this section has been reported in greater detail in ORNL CF-56-1-168 (to be issued).

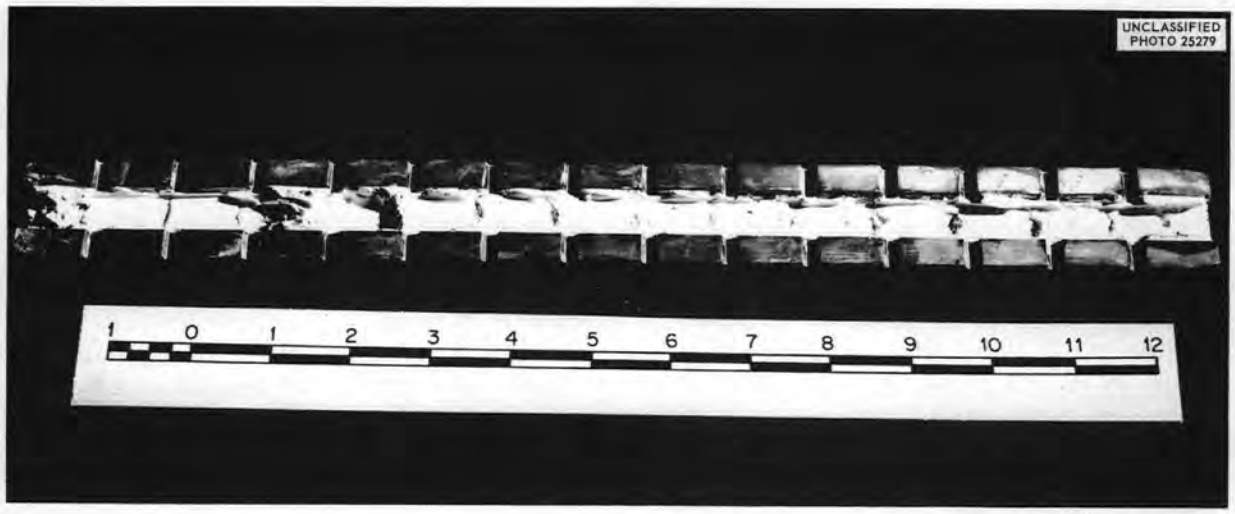

Fig. 11.1. Thorium Oxide Cake in Pin Holder from 100A Pump Loop. Slurry run CS-20 (6 hr); Batch D-47 thorium oxide was used; flow downward (left to right).

stream header were plugged as noted above. A pasty deposit was found in a dead-end pipe cap on the upstream sample-barrel header. In addition, a 6- to 8-in. collar of pasty slurry was found in the tapered pump suction nozzle. A channel had been maintained that was equal to the original pipe diameter.

Corrosion results were observed only on pin specimens in these runs, with flow velocities ranging between 16 and 76 fps. The values given below were observed at 16 and 76 fps, respectively, in separate runs; these values will serve to indicate the levels of attack that were encountered. Respective attack rates in mils per year were: gold, 1–54; platinum, 0–88; Zircaloy-2, 0–68; titanium and its alloys, 0–120; type 347 and other stainless steels, 2–120; and aluminum oxide, up to 4100.

Among the important variables are the slurry concentration and circulation velocity. Graphical correlation of the effects of these variables for type 347 stainless steel indicated a dependence on the square of the velocity and on the first power of the concentration. The data for other materials appeared to be consistent with this behavior, although not necessarily in exact agreement. The correlation provided a good basis for comparing various materials by adjusting the rates observed under various conditions to a common basis. Thus the data from 13 runs at 300°C on the 100A pump loops are summarized in Table 11.1 after having been adjusted to 20 fps and 1000 g of thorium per kilogram of water. In addition, it may be noted that the corrosion rate of stainless steels exhibited a moderate temperature effect, increasing by a factor of 1.7 on going from 250 to 300°C. Platinum

TABLE 11.1. COMPARATIVE CORROSION RATES OF VARIOUS MATERIALS BY CIRCULATING THORIUM OXIDE SLURRY* AT 300°C

Material	Adjusted Corrosion Pin Attack Rate (mpy)
Platinum	2
Gold	2
Zircaloy-2	3
Titanium and alloys	4
Type 347 and other stainless steel	7
Nickel	12
Inconels	24
Stellites	14–40
Aluminum oxide	280
Graphitar; ThO_2 + 0.5% CaO	Consumed

*Adjusted to 20 fps and 1000 g of thorium per kilogram of H_2O.

exhibited a similar temperature effect and a stronger dependence on concentration and velocity. Gold, platinum, and the Stellites appeared to be sensitive to particular batches of oxide, and the Stellites appeared to be undergoing attack by water alone, as well as by flowing slurry.

11.2 TOROIDS

The major portion of the available toroid operating time was devoted to solution runs involving additions of lithium and cesium sulfates to uranyl sulfate solutions. Results of these runs[3] are given in Sec. 10.2.

Replacement variable-speed d-c motors for the remaining three toroid rotators arrived, and installation has begun. Two such motors were in use during the past quarter and proved to be reliable and capable of operating satisfactorily at rotational speeds permitting tests in the range from 5 to 40 fps, where other apparatus strength factors appear to become limiting.

Presently available results permit a consideration[2] of the effects of oxide calcination temperature and flow velocity in toroids on the slurry attack rate on several materials. Interest in aqueous thorium oxide slurries prepared from oxide calcined at high temperature (1000°C or greater) stemmed from observations that at room temperature such slurries handle more easily (i.e., are more fluid) after circulation than slurries prepared from oxide calcined at lower temperatures. The attack of type 347 stainless steel, titanium 75A, and Zircaloy-2 by circulating slurries prepared from thorium oxide calcined at temperatures from 650 to 1600°C was studied over a range of slurry velocities in toroids.

ORNL-produced thorium oxide (batch D-17) originally calcined at 650°C was recalcined at temperatures from 800 to 1600°C. Only a very slight change in the particle-size distribution was observed, as estimated by gravitational sedimentation. In the 1600°C thorium oxide 91 wt % of the material was less than 10 μ in diameter, and the average particle diameter was 2.3 μ; in the original 650°C oxide 85 wt % was less than 10 μ in diameter, and the average diameter was 2.2 μ.

Aqueous slurries of these unsized oxides were circulated at charge concentrations of 1000 g of thorium per kilogram of water in type 347 stainless steel toroids at 250°C and with excess oxygen pressure. Corrosion pin specimens of type 347 stainless steel, titanium 75A, and Zircaloy-2 were used to determine the attack rates at 5, 15, and 26 fps relative slurry velocities. The runs lasted approximately 200 hr at 26 fps and 400 hr at the lower velocities.

The results showed that, for any particular velocity up to 26 fps, the attack rate of any one of the materials by the slurries was independent of the calcination temperature of the oxide. Thus, for example, at 26 fps the attack rates of type 347 stainless steel varied randomly between 2 and 6 mpy for oxides calcined at 650, 800, 1000, 1200, 1400, and 1600°C. Under similar conditions the rates for titanium varied between 0.2 and 8 mpy, while Zircaloy-2 gave rates up to 2 mpy. As a first approximation these rates should probably be doubled in order to put them on the same basis as results from loop tests (due to slug flow in the toroids).

On a few occasions, the attack rates were significantly greater than those generally found. These higher values may be due to inhomogeneities in these particular samples of oxide and emphasize the presence of factors that have not been determined and controlled.

In any event it seems possible to obtain slurries of thorium oxide calcined at high temperature that yield attack rates comparable to those obtained with slurries of oxide calcined at much lower temperatures. The variation in character of the circulated slurries after circulation was pronounced in these experiments. At slurry concentrations of 1000 g of thorium per kilogram of water, the oxides calcined at 650 or 800°C produced a very thick slurry at room temperature after circulation at 15 and 26 fps, whereas slurries of oxides calcined at 1200°C and higher were much more fluid under similar conditions.

Attack rates for both type 347 stainless steel and titanium 75A followed an approximately 1.5-power dependence on the slurry velocity up to 26 fps relative velocity. Approximate values for the stainless steel and titanium, respectively, were: 0.3 and 0.4 mpy at 5 fps, 2.1 and 1.7 mpy at 15 fps, and 3.8 and 3.8 mpy at 26 fps. The rates for Zircaloy-2 were uniformly low for all velocities studied.

[3] ORNL CF-56-1-167 (to be issued).

12. RADIATION CORROSION

G. H. Jenks H. C. Savage

A. L. Bacarella
J. E. Baker
S. E. Bolt
N. C. Bradley
R. J. Davis
H. O. Day
H. A. Fisch
B. O. Heston
D. T. Jones
R. A. Lorenz
T. H. Mauney
J. R. McWherter
A. R. Olsen
J. A. Russell
M. D. Silverman
H. H. Stone
F. J. Walter
R. M. Warner
K. S. Warren
D. B. Weaver[1]
L. F. Woo
W. C. Yee

12.1 IN-PILE LOOPS

G. H. Jenks H. C. Savage

J. E. Baker
S. E. Bolt
N. C. Bradley
D. T. Jones
R. A. Lorenz
T. H. Mauney
J. R. McWherter
A. R. Olsen
J. A. Russell
F. J. Walter
R. M. Warner
D. B. Weaver

12.1.1 Development and Construction

(a) General. – In-pile loop assemblies for radiation-corrosion studies are now being built for operation in beam holes HB-2 and HB-4 at the LITR. Each beam hole has a slightly different geometry as to over-all and tapered section dimensions. In an effort to provide a more versatile in-pile loop package and to reduce the number of components required, a component package suitable for use in either LITR beam hole, through adjustment of the length of two connecting pipes, has been provided.

The loop package previously used in beam hole HB-4 was designed for operation to 1000 psia. The new composite loop is designed for operation to 2000 psia so that radiation-corrosion studies at higher temperatures (up to 300°C) can be made.

(b) HB-4 Mockup. – The fabrication and the performance testing of in-pile loop L-4-12 were completed during the past quarter. This loop was installed and is in operation in beam hole HB-4 of the LITR. The core section[2] of loop L-4-12 was fabricated from titanium, type Ti-75A, and was coupled to the stainless steel loop by means of two special couplings as shown in Fig. 12.1. Results of thermal cycling and pressure tests had indicated that these joints were satisfactory for use at 250°C and 1000 psia. This is the first loop in which such an arrangement has been attempted. All previous in-pile loops were fabricated entirely of type 347 stainless steel with all-welded construction.

The titanium, tapered-channel, corrosion specimen holders, used in the core and line positions of loop L-4-12, contained corrosion coupons of type 347 stainless steel, Zircaloy-2, and titanium type 55AX. Impact specimens of titanium, type RC-A-40, and Zircaloy-2 are included in both the core and line position. Stressed specimens of several titanium alloys, as well as type 17-4 PH stainless steel, were included in the core, line, and pressurizer.

Frequent leak checks with a helium leak detector were made on loop L-4-12 during the operational checkout, particularly after each thermal cycle of the loop, to ensure that the special stainless-steel-to-titanium couplings were satisfactory. These couplings remained leaktight during the checkout and apparently are continuing tight in operation in beam hole HB-4.

(c) HB-2 Loop Package. – In-pile loop L-2-10, designed for operation in beam hole HB-2 of the LITR, was completed and tested. The loop is now ready for installation and operation as soon as facilities at the LITR are completed.

(d) Titanium In-Pile Loop (L-2-14). – The unusual corrosion resistance of titanium to uranyl sulfate solutions, both in and out of nuclear radiations, was demonstrated under a wide variety of conditions. One model 100A dynamic corrosion test loop has already been fabricated of titanium,[3] as have numerous other component parts such as Westinghouse model 100A pump impellers and

[1] On loan from TVA.

[2] G. H. Jenks *et al.*, *HRP Quar. Prog. Rep. April 30, 1954*, ORNL-1753, p 83–84, Figs. 62 and 63.

[3] E. G. Bohlmann *et al.*, *HRP Quar. Prog. Rep. March 31, 1953*, ORNL-1554, p 47.

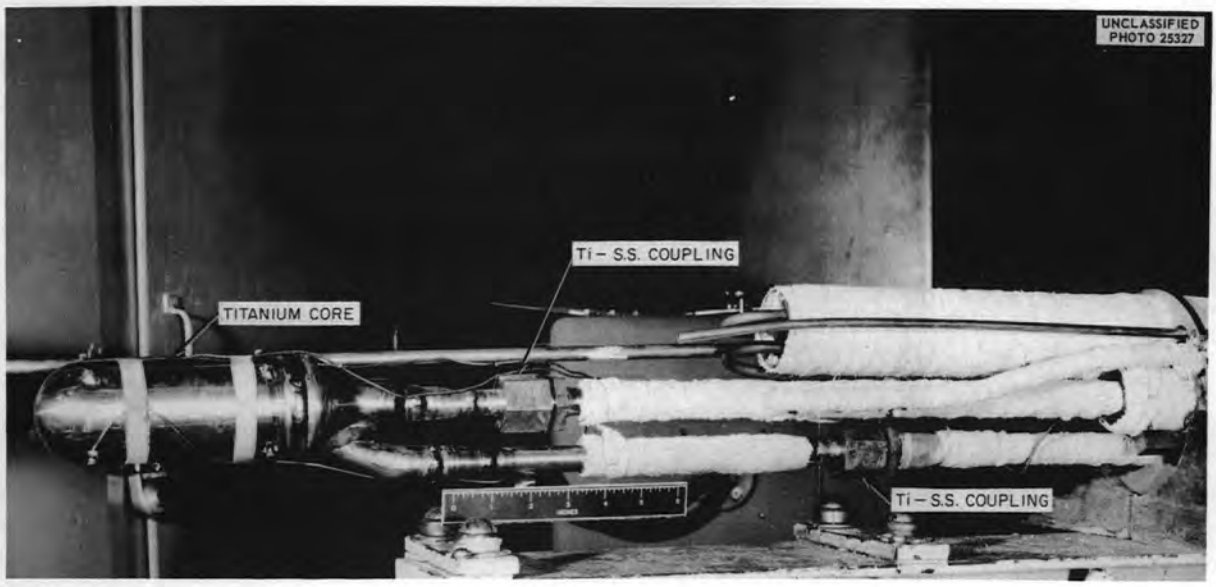

Fig. 12.1. Titanium Core, Loop L-4-12.

volutes, pump thermal spacers, and corrosion-specimen holders.

In view of this experience, an all-titanium in-pile loop, to operate at 300°C and 2000 psia is now under construction to extend the conditions (particularly to higher concentrations of uranyl sulfate solutions) under which radiation corrosion studies can be carried out. The loop is presently scheduled for installation in beam hole HB-2 of the LITR.

At present approximately two-thirds of the individual components of the loop have been constructed. An ORNL, 5-gpm pump, modified for in-pile loops[4] and also made from titanium, should be ready for performance testing within a few weeks. The Metallurgy Group is cooperating in the welding procedures and weld evaluations in this loop.

12.1.2 General Description of In-Pile Loop Experiment, L-4-8

The major portion of the fifth in-pile loop experiment, L-4-8, was completed. Details of this experiment and of the results have been reported.[5] A summary is presented below.

The following list gives information on the specimens that were used.

Specimen Type and Position	Number and Material
Core-holder coupons	8 stainless steel, type 347 8 Zircaloy-2 8 titanium 55AX
Core stress specimen assemblies	2 Zircaloy-2 2 titanium C-130-AM 2 stainless steel, type 17-4 PH
Core sleeve specimens	8 stainless steel, type 347 8 stainless steel, type 309 SCb
In-line holder coupons	8 stainless steel, type 347 8 Zircaloy-2 8 titanium 55AX
Special in-line stress specimen assemblies	1 Zircaloy-2 1 titanium C-130-AM 1 stainless steel, type 17-4 PH

[4] G. H. Jenks *et al.*, *HRP Quar. Prog. Rep. Oct. 31, 1955*, ORNL-2004, p 124, Fig. 12.4.

[5] G. H. Jenks *et al.*, *In-Pile Loop Experiment L-4-8*, ORNL-2042 (in press).

Specimen Type and Position	Number and Material
Pressurizer stress specimen assemblies (one each in vapor and liquid)	2 zircaloy-2 2 titanium C-130-AM 2 stainless steel, type 17-4 PH 2 stainless steel, type 347

Corrosion coupons in Zircaloy-2 tapered holders were installed in both the in-line and core positions. These coupons were of three materials: type 347 stainless steel, Zircaloy-2, and titanium 55AX. The arrangement of the coupons in the holders was identical with that of the coupons for loop EE described previously.[6] Two rod-and-sleeve assemblies containing uncoupled coupons of types 347 and 309 SCb stainless steel were installed in the core position, replacing the coupled specimens used in loop EE. These assemblies were mounted around the coupon holder in the core position along with stressed specimens of Zircaloy-2, hardened type 17-4 PH stainless steel, and type C-130-AM titanium. The type C-130-AM titanium and hardened type 17-4 PH stainless steels are materials with high yield strength that were under consideration for use as bolting material for the fuel-contacting joint between the HRT core and pressure vessel.

In addition to the usual core and in-line corrosion specimens, loop L-4-8 contained stressed specimens in a second in-line holder for comparison with the stressed specimens in the core. This second in-line holder contained three stressed-specimen assemblies: one each of Zircaloy-2, hardened type 17-4 PH stainless steel, and type C-130-AM titanium. A third set of eight stressed-specimen assemblies – two each of Zircaloy-2, type 347 stainless steel, type 17-4 PH stainless steel, and type C-130-AM titanium – was installed in the pressurizer. The assemblies were so arranged that one stressed assembly of each aforementioned material would be exposed to the liquid and one to the vapor phase in the pressurizer. The temperature in the pressurizer is 280°C, whereas the in-line and core temperature is 250°C.

The methods, equipment, and procedures employed in this experiment were similar in most respects to those reported for previous loop experiments.[7,8] The pump employed with the loop was equipped with journals and bearings of sintered alumina. The operating performance of the bearings appeared to be excellent, even though the experiment was terminated by pump failure. Remote examination of the pump indicated that the failure was caused by the pump becoming stalled due to a movement forward of the rear bearing.

The solution charged to the loop for in-pile operation was of the following composition:

UO_2SO_4	0.17 *m* (U^{235}/total U = 0.888)
$CuSO_4$	0.031 *m*
H_2SO_4	0.04 *m*

A solution of the same composition was used to replace liquid withdrawn from the loop during sampling operations. This is the first loop experiment which has been equipped with stainless steel specimens and at the same time has employed a solution of such high acidity. Sulfuric acid concentrations which were smaller by a factor of approximately 5 were previously employed.[8]

Both the total circulating time and the radiation time for this experiment were longer than for any previous experiment. The loop operated in-pile for a total of 1637 hr. The energy output of the LITR during this time was 4377 Mwhr. The average fission power in the loop, as determined from cesium analyses, was 622 w when the LITR was at 3 Mw. As for the previous loop, the power density at a given location in the core was determined from measurements of the induced activities of the Zircaloy and type 347 stainless steel specimens. The power densities thus determined were about the same as those reported for the previous loop, ranging from about 5 w/ml at the position of the forward specimens to about 0.7 w/ml at the rear position.

The nickel and oxygen data obtained during operation indicated the same general corrosion behavior as that observed for previous experiments: a high initial corrosion rate which leveled off to a much lower and fairly constant rate after the first 300 hr of exposure in the reactor.[7,8] As calculated from oxygen data, the corrosion rate

[6] G. H. Jenks *et al.*, *HRP Quar. Prog. Rep. Jan. 31, 1955*, ORNL-1853, p 86–87.

[7] G. H. Jenks *et al.*, *HRP Quar. Prog. Rep. July 31, 1955*, ORNL-1943, p 109.

[8] G. H. Jenks *et al.*, *HRP Quar. Prog. Rep. Oct. 31, 1955*, ORNL-2004, p 123.

during the first 300 hr was 4.0 mpy. During the final 1337 hr, the average rate was 0.7 mpy.

12.1.3 Qualitative Results of Inspection and Evaluation of Loop L-4-8

As with previous loop experiments, all stainless steel surfaces outside the core were covered with a heavy, rustlike scale with no apparent localized attack on any of the components inspected. The quantity of scale in the gas phase of the pressurizer was less than that in the solution phase. There was no visual indication in the pressurizer region of any changes in the scale character other than quantity.

All coupons in the in-line position were covered with a heavy, flaky scale. The stressed specimens in the special in-line position were similar in appearance. Considerable difficulty was again encountered in defilming the in-line coupons by the standard cathodic treatment in an inhibited 5% sulfuric acid solution. The titanium coupons were defilmed more readily than the stainless steel and much more readily than the Zircaloy-2 coupons. The Zircaloy-2 coupons, in fact, were never completely defilmed, as weight gains were recorded after the final defilming. The defilming characteristics of the stressed specimen from the special in-line position and from the pressurizer were similar to those of the in-line coupons.

All stainless steel surfaces in the core were covered with a rustlike scale similar to that in the rest of the loop. With the exception of the core-holder coupons, the apparent thickness of this scale varied inversely with the intensity of radiation to which the surface was exposed. Those core-holder coupons which were in the regions of highest velocity were coated with a thin film. The two rod-and-sleeve stainless steel coupon assemblies were somewhat difficult to disassemble remotely, apparently because an accumulation of corrosion products tended to seal the sleeves to the rod. This sealing was particularly pronounced for the type 309 SCb assembly. After defilming, the stainless steel coupons which were in the higher flux regions of the core holder exhibited a severely pickled appearance. This was particularly true for those which were in the high-velocity regions. The sleeve specimens of type 347 stainless steel which were in the highest flux were marked with longitudinal grooves so that the surface resembled in appearance the bark of a hickory tree. No such grooves were found in the 309 SCb sleeves.

The Zircaloy-2 stress assemblies in the core were covered with a thin, dark film on all surfaces. The coupons in the holder array were coated with a heavier dark film. All titanium coupons in the highest flux regions were coated with a similar dark film, with the exception of the coupon in the highest flux position; this coupon was essentially free of scale. The titanium coupons exposed in the low-flux end of the core array were covered with a rust-colored scale typical of the remainder of the loop. All specimens from the core were defilmed with little difficulty.

12.1.4 Quantitative Results of Inspection and Evaluation of Loop L-4-8

Corrosion-rate values reported in the following were calculated from weight-loss data, with the exposed specimen areas and total radiation time used as a basis for the calculations.

(a) Stress Specimens. – Microscopic examination of the various stress specimens revealed no surface evidence of any stress-corrosion cracking. In addition, there was no evidence from weight-loss determinations that the average corrosion rate of any of the different materials was adversely affected by the stress.

(b) Zircaloy-2. – The corrosion results obtained for Zircaloy-2 in this experiment were nearly in agreement with those obtained in previous loops.[7,8] As before, the corrosion rates of the core specimens were flux-dependent. The corrosion rate for a specimen exposed at a given fission-power density was nearly in agreement with previously determined values. As mentioned above, the Zircaloy-2 specimens which were exposed in portions of the loop outside the core could not be defilmed completely, and, in each case, weight gains were recorded after the final defilming.

(c) Titanium 55AX. – The average corrosion rate of specimens from the core holder was 0.5 mpy; the maximum rate for any specimen was 0.8 mpy. There was no evidence of an effect of solution velocity on the attack of the core specimens. There was also no clear evidence for an effect of power density, although the highest rate found was for the specimen which was in the forward position and, hence, exposed to the highest intensity of radiation. The average corrosion rate for the in-line specimens was 0.2 mpy; the

maximum for any specimen was 0.5 mpy. There was no apparent effect of velocity on the attack of the in-line specimens. The corrosion rates of both the in-line and core specimens are in close agreement with those determined in the previous experiment.[8]

(d) Stainless Steel, Type 347. – The corrosion results for the components fabricated of stainless steel are given below.

(1) Core-Holder Coupons. – The pattern of corrosion among the different stainless steel specimens from the core array of the loop was more complex than that observed for the identical array of specimens in the previous loop.[8] The accelerating effect on corrosion of high-radiation intensities was less pronounced than for the previous loop. However, in contrast with the previous results, the present results indicate a strong accelerating effect of velocity. In this experiment the average corrosion rate determined for each of the three specimens located nearest the front of the core and exposed to a maximum solution velocity of about 17 fps was about 10 mpy. However, the rates determined for the next two steel specimens in the array were 20 and 40 mpy, respectively. The average solution velocities past these specimens were about 29 and 39 fps, respectively. In the previous experiment the corrosion rates determined for the first three specimens were, in each case, about 60 mpy. The rates for the remainder of the specimens were all below 3 mpy.

It can be tentatively postulated that the higher acidity of the solution employed in this experiment was responsible for both differences noted between the results of this and the previous loop. The reduction of the radiation-induced corrosion at low velocities is consistent with the results of in-pile bomb experiments (see Sec. 12.2), and an increase in the velocity effect on corrosion by the addition of sulfuric acid to uranyl sulfate solutions is commonly observed in out-of-pile tests. However, as discussed below, the type 347 stainless steel specimens from the in-line holder did not show any velocity effect. Hence, it is indicated that the observed velocity effect is also dependent on the power density.

(2) Core Sleeve Specimens. – As mentioned previously, it was apparent from visual inspection that most of these specimens were marked with longitudinal grooves and were not uniformly attacked.

The results of weight measurements indicated that the degree of attack of these specimens increased with increasing power density. The average corrosion rate for all specimens, as determined from weight-loss data, was 2.0 mpy. The maximum average rate for a given specimen was 7.7 mpy, and the minimum rate was 0.1 mpy. The maximum rate, which was for the specimen exposed at the highest power density, was out of line with the rates for the other specimens. The rate for the adjacent specimen, which wcs exposed at a slightly lower power density, was 3.2 mpy. It is interesting to note that the average rate of 2.0 mpy determined for these specimens was only slightly higher than the average rate of 1.5 mpy determined for the type 347 in-line holder specimens.

(3) In-Line Holder Coupons. – The average corrosion rate determined for these specimens was 1.5 mpy. The highest rate found for any specimen was 3.5 mpy, and the lowest was 0.2 mpy. There was no apparent correlation between the solution velocity to which a specimen was exposed and the corrosion rate exhibited by that specimen.

(e) Stainless Steel, Type 309 SCb, Core Sleeve Specimens. – The average corrosion rate for these specimens was 1.6 mpy. The highest rate for any specimen was 3.0 mpy, and the lowest rate was 0.8 mpy. As mentioned above, the surface of this specimen appeared to be more uniformly attacked than were the similarly located type 347 sleeve specimens. However, the average corrosion rate was only slightly lower than that for the type 347 specimens.

(f) Correlation Between Nickel and Weight Data. – The total amount of steel oxidized during the loop operation, according to nickel data, was 19.5 g. From the specimen weight data it may be estimated, with certain assumptions as a basis, that the total amount of steel oxidized was 27.4 g.

The basic assumptions are as follows: (1) All steel surfaces in contact with high-temperature solution, excluding the core, corroded uniformly and at an average rate equal to that for the in-line specimens; (2) the attack of a steel surface, which was at a given flux in the core, was the same as that measured for those sleeve specimens which were located outside the core holder and in the same given flux. The rough agreement of the values determined by the two methods suggests that these assumptions are approximately correct. The average corrosion rate for the area in the core

loop was assumed to be twice that determined for the type 347 sleeve specimen which was in the highest flux.

12.2 LITR BOMB TESTS

G. H. Jenks

H. O. Day J. A. Russell
H. A. Fisch F. J. Walter
D. T. Jones K. S. Warren
L. F. Woo

Investigations of the effect of radiation on the corrosion of Zircaloy-2 and type 347 stainless steel by uranyl sulfate solutions continued. Since the last report, two Zircaloy-2 bombs, Z-14 and Z-16, have undergone in-pile exposure, and a third, Z-17, is in progress. An in-pile stainless steel experiment, H-94, was completed, and another one, H-95, is in progress. In addition, a number of previously irradiated bombs, such as Z-15 and H-93, were opened, and the pins from them were inspected for weight loss; they were also employed in the determination of the neutron flux to which the given bomb was exposed by comparing the induced radioactivity of the pins with that of a control specimen which had been irradiated to a known nvt.

A summary of the data which were obtained is presented in Table 12.1. In many cases calculations of the flux from the induced activity data have not been completed. For these cases the value for the power density in solution during exposure, which is calculated from the estimated flux, is indicated by an approximate sign. Values for radiation time are those obtained by setting 3 Mwhr of LITR energy equivalent to 1 hr. All corrosion rate values were calculated with radiation time as a basis. Each HB-5 bomb was equipped with six pin corrosion specimens, and each HB-6 bomb was equipped with four. Unless otherwise noted, the pin material was the same as the bomb material. The plus-minus value assigned to a given corrosion-rate or power-density value is the most probable error in the usual statistical meaning and is not to be taken as a measure of the absolute accuracy. Some of the data listed in Table 12.1 repeat those given in earlier reports, but are given for convenience and clarity.

Although many of the experiments are incomplete, some preliminary discussion is worth while.

The results of the steel experiments H-93 and H-94 confirm the result of the similar experiment H-85, which was previously reported.[9] For each experiment the observed rate was less than 1 mpy over long periods of exposure, and there was no indication of a marked change in rate during exposure. In contrast, early steel experiments, which contained no added acid and were generally at an initial oxygen pressure of 250 to 350 psi at the test temperature, exhibited an increase in the rate of attack after one to seven days of exposure.[10] The lowest initial oxygen pressure employed with the present experiments was roughly 500 psi, measured at 250°C, in experiment H-94. The observed corrosion rate for H-94 was little different from that of H-93, for which the initial oxygen pressure was greater by a factor of about 3. These results indicate that the high oxygen pressures have little effect on the corrosion. An experiment is planned at a lower oxygen pressure to enable a more direct comparison with the previous experiments.

The steel experiment H-95 which is in progress is, in part, designed to furnish information necessary to the design of a test of a stainless steel bomb at high power density in the MTR.

The results of experiments Z-14, Z-15, and Z-16 demonstrate that the solution concentration may strongly influence the degree of attack of Zircaloy-2 by uranyl sulfate solutions under irradiation. The test conditions for each of these three experiments were essentially the same except for the uranyl sulfate concentration employed; with Z-15 it was 0.17 *m*, and with Z-14 and Z-16 it was about 1.4 *m*. The corrosion rate observed for both Z-14 and Z-16 was about 8 mpy, but that observed for Z-15 was about 15 mpy; for all three experiments these rates occurred at the exposure temperature of 280°C. The explanation for the difference in corrosion rate between the two solutions is unknown.

In experiment Z-15 the corrosion rate determined from weight-loss measurements for the titanium 75A pins, which were mounted along with pins of other materials in the rack, was 5.2 mpy. This value represents an appreciably greater rate of attack than the 1.5 mpy determined for the same material in experiment H-76, in which the exposure

[9] G. H. Jenks *et al.*, *HRP Quar. Prog. Rep. July 31, 1955*, ORNL-1943, p 129.

[10] S. F. Clark *et al.*, *HRP Quar. Prog. Rep. July 31, 1954*, ORNL-1772, p 161.

TABLE 12.1. LITR BOMB CORROSION STUDIES

Bomb No.	LITR Beam Hole	Bomb Material	Solution Composition (*m*) UO_2SO_4	$CuSO_4$	H_2SO_4	Enrichment (% U^{235})	Starting O_2 Pressure at 100°C (psi) Before Pretreatment	Exposure Temperature (°C)	Fission Power Density (w/ml)	Irradiation Time (days)	Corrosion Rate (mpy) From O_2 Data	Over-all Corrosion Rates (mpy) for Pins; Includes Pretreatment
H-76	HB-6	Titanium-75A	0.178	0.021	0.046	93.2	452	250	~10[a]	26.0	1.7 ± 0.3	1.49 ± 0.09
H-57	HB-6	Zircaloy-2	0.162	0.020	0	93.2	171	250	5.9 ± 0.1	4.4	10.4 ± 0.1	9.6
H-58	HB-6	Zircaloy-2	0.154	0.019	0	93.2	336	250	5.3 ± 0.1	11.1	8.3 ± 0.1	8.5 ± 0.2
Z-5	HB-6	Zircaloy-2 (with two Zircaloy-3 type pins)[b]	0.173	0.021	0	44.1	487	250 280	4.5 ± 0.1 4.3 ± 0.1	17.8 2.9	4.8 ± 0.1 10.8 ± 0.8 (over-all = 5.6)	5.6 (Zr-2) 6.0 (Zr-3)[b]
Z-8	HB-6	Zircaloy-2	0.178 plus 0.004 *m* CrO_3	0.021	0.046	93.2	420	250	~10[a]	15.3	5.0 ± 0.1 5.6 ± 0.5[c]	6.4 ± 0.1
Z-9	HB-6	Zircaloy-2 (with two Zircaloy-3 type pins)[d]	0.172	0.007	0	93.2	310	250 280	~9.7[a] ~9.1[a]	4.3 2.5	8.3 ± 0.3 15.8 ± 0.5 (over-all = 11.5)	11.1 ± 0.0 (Zr-2) 10.9 ± 0.0[d] (Zr-3)
Z-10	HB-6	Zircaloy-2	0.173	0.021	0	44.1	489	225 250 280 290	5.0 ± 0.1 4.8 ± 0.1 4.5 ± 0.1 4.4 ± 0.1	7.9 4.6 6.6 1.7	3.1 ± 0.2 5.7 ± 0.1 10.1 ± 0.2 12.2 ± 0.2 (over-all = 6.6)	5.8 ± 0.1
Z-12	HB-5	Zircaloy-2	0.043[e]	0.050	0.020	93.2	580	280 300	4.2 ± 0.1 4.0 ± 0.1	9.7 5.4	10.3 ± 0.2 10.3 ± 0.2	9.0 ± 0.1
Z-13	HB-5	Zircaloy-2	0.170	0.020	0	0.05_4	540	250 280 300 250	~0.01[g] ~0.01 ~0.009 ~0.01	23.5 11.7 12.5 19.6	3.2 →1.2 4.3 →0.7 1.9 →1.2 0.1 →0.8 (over-all = 1.5)	[f]
Z-14	HB-5	Zircaloy-2	1.363	0.043	0.043	14.0	303	250 280	~17.1[h] ~16.4	0.1 4.3	[f]	7.8 ± 0.1[i]
Z-15	HB-5	Zircaloy-2 (with two titanium-75A and two platinum pins)	0.173	0.041	0.040	93.2	313	280	~17[g]	4.2	14.6 ± 0.1[j] (Zr-2)	15.6 ± 0.7 (Zr-2) 5.2 (titanium) 0.4 (platinum)
Z-16	HB-5	Zircaloy-2	1.355	0.043	0.043	14.0	312	250 280	~17.0[h] ~16.3	5.2 1.7	6.1 ± 0.1 7.5 ± 0.2 (over-all = 6.5)	[f]
Z-17	HB-5	Zircaloy-2	0.169	0	0.040	6.0	302	250	~1.2[g]	Continuing		
H-93	HB-6	Type 347 stainless steel	0.174	0.010	0.030	93.2	~830	250	~9.8[a]	38.4	0.7	0.87 ± 0.03
H-94	HB-6	Type 347 stainless steel	0.167	0.010	0.030	93.2	~300	250	~9.4[a]	32.9	[f]	0.69 ± 0.02
H-95	HB-6	Type 347 stainless steel	0.042	0.049	0.039	93.2	333	250 280	~2.4[a] ~2.3	24.2 6.6 Continuing	~0.3	

[a]Estimated from the flux measured in Z-5 and Z-10.
[b]The Zircaloy-3 pins contained 0.45% Sn, 0.72% Fe, and 0.73% Cr besides Zr.
[c]This rate occurred after a long reactor shutdown and prevailed for 106 radiation hours.
[d]The Zircaloy-3 pins contained 0.50% Sn and 1.50% Cr besides Zr.
[e]Solution analysis at the end of the experiment indicated that UO_2SO_4 concentration was about 0.03 *m*, and that $CuSO_4$ was about 0.03 *m*.
[f]To be determined and/or evaluated.
[g]Estimated from the flux obtained in Z-12.
[h]Estimated, assuming flux = 1.0×10^{13} neutrons/cm^2/sec.
[i]Average of five pins; the sixth pin had pits and a corrosion rate of 14.2 mpy.
[j]Calculated, assuming that the titanium area corroded 2.0 mpy and that the platinum surface had no attack.

temperature and the power density were lower than in Z-15. These results indicate that the radiation corrosion of titanium 75A increases with increasing power density and/or system temperature. Further experiments with titanium are planned.

The Zircaloy-2 experiment Z-17, which is in progress, is designed as a determination of corrosion under irradiation in the absence of copper.

12.3 MTR BOMB TESTS

G. H. Jenks

R. J. Davis, J. R. McWherter, D. T. Jones, A. R. Olsen, R. A. Lorenz, H. H. Stone

Experiments ORNL-15-3 and -4 have been completed at the MTR. These experiments were of the same general type as ORNL-15-1 and -2, which were previously reported.[11,12] The operating power at the MTR has been increased from 30 to 40 Mw. This increase took place between the 15-2 and the 15-3 experiments.

Experiment 15-3 employed a titanium autoclave, which was charged with a solution 0.04 *m* in UO_2SO_4 (93.2% enriched), 0.05 *m* in $CuSO_4$, and 0.02 *m* H_2SO_4. The autoclave was exposed in the high-flux region for approximately 41 hr. The estimated exposure temperature was 290°C, and the estimated total power density in solution due to the absorption of radiation was 48 w/ml. The results of the pressure measurements for this experiment are not unequivocal. However, the best estimate of the maximum corrosion rate based on the pressure data is 7 mpy. It is expected that a better value for the corrosion will be available after the autoclave and specimens are inspected.

Experiment 15-4 was designed as a test of the effect of reactor radiations alone on the corrosion of Zircaloy-2. The autoclave for this experiment was of Zircaloy-2. The solution employed was 0.04 *m* in UO_2SO_4 (0.03% enriched) and 0.02 *m* in H_2SO_4. No copper was added. The enrichment was such that the contribution of fission fragments to the total intensity of radiation was less than 0.02 w/ml. The estimated average power density in the solution due to the absorption of fast neutrons and gamma-ray energy was 8 w/ml – 4 w/ml from neutrons and 4 w/ml from gamma rays. Exposure to radiation was for a period of 50 hr at the test temperature of 280°C. The average corrosion rate during this time, based on measurements of over-all oxygen consumption, was 11 mpy. This rate is about the same as that observed in the LITR experiment Z-12, in which the fission power density in solution was about 4 w/ml but the neutron and gamma-ray intensities were relatively small. The other test conditions for Z-12 were the same as those described for this MTR experiment, except that the solution was 0.05 *m* in $CuSO_4$ (see Sec. 12.2).

12.4 SUPPORTING RESEARCH

G. H. Jenks

A. L. Bacarella, B. O. Heston, M. D. Silverman

12.4.1 Van de Graaff Accelerator Tests

A determination of the effect of fast electrons from a Van de Graaff accelerator on the corrosion of Zircaloy-2 by uranyl sulfate solutions has been reported.[13] The equipment and techniques employed in this study were previously used and reported by Ghormley and Hochanadel[14] for a similar study of stainless steel. Three foil-type specimens of Zircaloy-2 were positioned vertically in the small thermal-convection loop and exposed to a circulating UO_2SO_4 solution. Only the center specimen was irradiated. The other specimens served as up- and downstream controls. The loop was constructed of type 347 stainless steel, and the solution employed was 0.17 *m* UO_2SO_4 and 0.02 *m* $CuSO_4$. Irradiation was carried out intermittently for a total of 104 hr with the test temperature at 250°C. During irradiation the estimated power density in the solution adjacent to the exposed specimen was 20 to 30 w/ml.

The specimens were examined and weighed after 32 hr of irradiation and then examined again after 54 hr; at the termination of exposure they were removed and weighed and examined in a detailed manner. They were then submitted for electron diffraction and electron microscopy studies. Following these studies the irradiated specimens were

[11] G. H. Jenks *et al.*, *HRP Quar. Prog. Rep. July 31, 1955*, ORNL-1943, p 130.

[12] G. H. Jenks *et al.*, *HRP Quar. Prog. Rep. Oct. 31, 1955*, ORNL-2004, p 152.

[13] B. O. Heston and M. D. Silverman, *Van de Graaff Accelerator Tests of the Radiation Induced Corrosion of Zircaloy-2*, ORNL CF-56-2-2 (in press).

[14] J. A. Ghormley and C. J. Hochanadel, *Chem. Semiann. Prog. Rep. Dec. 20, 1953*, ORNL-1674, p 76.

stripped by cathodic defilming in a corrosion-inhibited 5% solution of sulfuric acid. No significant weight change was observed for any of the specimens as removed from the loop. A small weight loss for the irradiated specimen resulted from the defilming. If uniform corrosion of the specimen is assumed, a penetration of 0.007 mil is calculated from the weight loss. The estimated probable error of the weight determination corresponds to a probable error in this penetration value of ±0.004 mil. This value is comparable with values of 0.005 to 0.01 mil which have been determined for the penetration of Zircaloy-2 during similar exposure periods and under similar conditions in out-of-pile bomb tests.[15]

These weight data indicate that the beta irradiation effected no significant increase in the corrosion of Zircaloy-2 in this experiment. However, the results of the electron microscope observation suggest a greater attack of the irradiated specimen than of the unirradiated downstream specimen.

In order to eliminate the possibility that stainless steel corrosion products in solution would affect the corrosion of Zircaloy-2, a titanium thermal-convection loop was fabricated and will be used for further beta-irradiation studies.

12.4.2 Corrosion of Stainless Steel by Uranyl Sulfate Solutions Free of Stainless Steel Corrosion Products

The corrosion of metals of interest to the HRP has been investigated in the loop, rocking bomb, and static autoclave facilities. These are closed systems; in them the concentrations of the products of corrosion increase with time. There has been much speculation concerning the role of the corrosion product Cr^{6+} in the corrosion behavior of stainless steel. This product will probably not be present with in-pile systems because Cr^{6+} in acid solution under irradiation is in general reduced to insoluble Cr^{3+}. Experimental confirmation of this expectation is available from the in-pile loop experiments. In general, only traces of chromium are detected in the loop solutions after exposure.[16–19] The out-of-pile rocking-bomb experiments have demonstrated that the total corrosive penetration at 250°C is decreased and also that the initial rate of corrosion is substantially lessened by the addition of CrO_4^{--} to the UO_2SO_4 solution.[20] Loop experiments[21] have also demonstrated an inhibition of corrosion by Cr^{6+}. A study of the corrosion of stainless steel in a system in which the products of corrosion do not accumulate was initiated to determine to what extent the soluble products affect the corrosion behavior.[22]

Equipment for this study has been designed and constructed; it permits a rod-type corrosion specimen to be continuously exposed to fresh solution by passing fresh solution from a reservoir through a titanium capillary and then through a titanium sleeve, inside which the type 347 stainless steel specimen is positioned in a Teflon holder. The reservoir is at room temperature, and the solution is heated to the test temperature as it passes through a section of the capillary directly upstream from the sleeve.

Initial experiments were carried out with uranyl sulfate solutions with a concentration in the neighborhood of 40 g of uranium per liter. The solutions contained dissolved oxygen at an approximate pressure of 400 psi at the test temperature of 250°C. The solution flow rates employed were adequate to maintain the concentrations of nickel and chromium in solution in the sleeve at less than 2 ppm.

A total of seven experimental exposures at these conditions was completed. The exposure time for a given experiment ranged from about 26 to 221 hr. Specimen weight data from these experiments were obtained. Values for the corrosion penetration calculated from these data are plotted in Fig. 12.2. The numbers adjacent to each experimental point

[15] G. H. Jenks *et al.*, *HRP Quar. Prog. Rep. Oct. 31, 1954*, ORNL-1813, p 83.

[16] G. H. Jenks *et al.*, *HRP Quar. Prog. Rep. April 30, 1955*, ORNL-1895, p 102.

[17] G. H. Jenks *et al.*, *HRP Quar. Prog. Rep. July 31, 1955*, ORNL-1943, p 112.

[18] G. H. Jenks *et al.*, *HRP Quar. Prog. Rep. Oct. 31, 1955*, ORNL-2004, p 127.

[19] G. H. Jenks *et al.*, *In-Pile Loop Experiment L-4-8*, ORNL-2042 (in press).

[20] S. F. Clark *et al.*, *HRP Quar. Prog. Rep. July 31, 1954*, ORNL-1772, p 161.

[21] J. C. Griess and R. S. Greeley, *HRP Quar. Prog. Rep. Jan. 31, 1955*, ORNL-1853, p 76.

[22] A. L. Bacarella, *Corrosion of Stainless Steel by Uranyl Sulfate Solutions Which Are Free of Stainless Steel Corrosion Products*, ORNL CF-56-2-3 (in press).

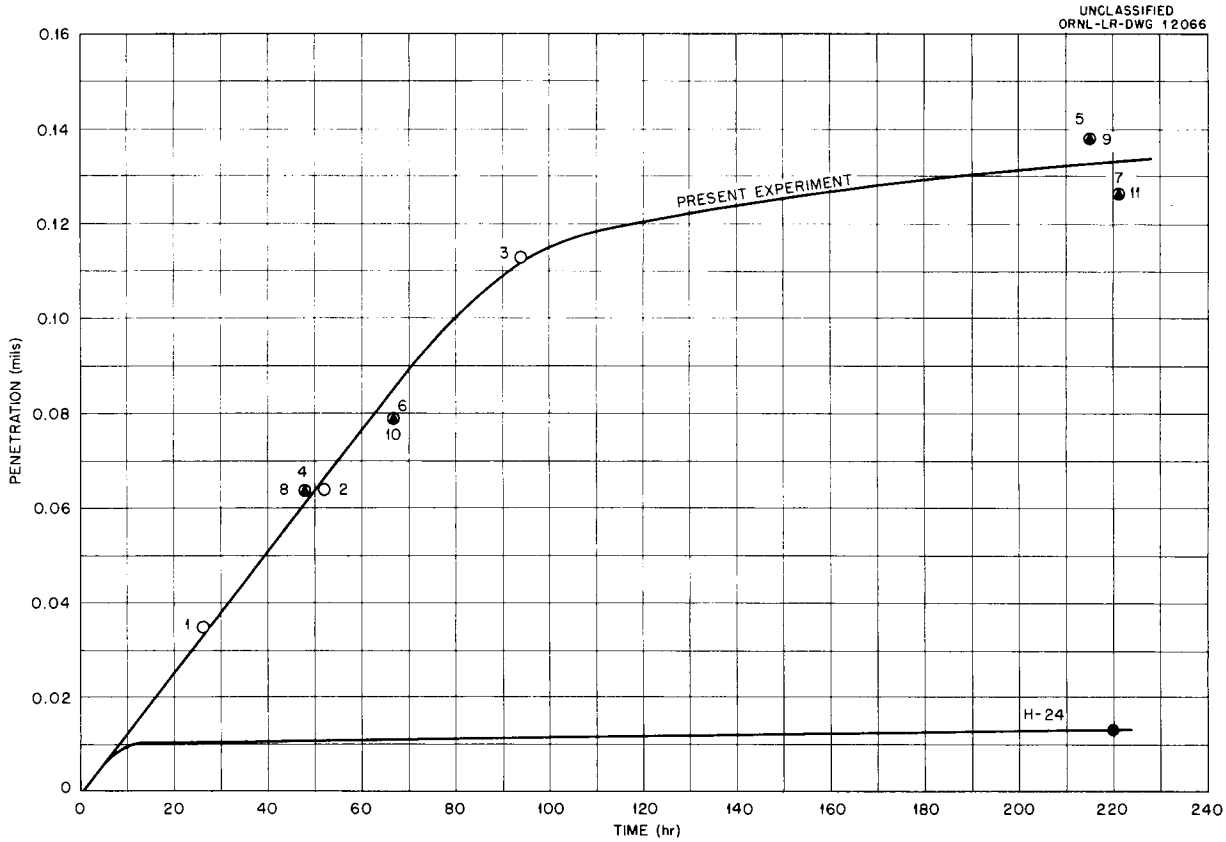

Fig. 12.2. Corrosion of Type 347 Stainless Steel at 250°C in UO_2SO_4 Solution Free from Corrosion Products.

indicate the order in which the experiments were run. For comparison, a representative plot for the corrosion of type 347 stainless steel in the out-of-pile rocking-bomb facility is also given.

In the rocking-bomb experiment the corrosion was inhibited after 10 to 12 hr with a total penetration of about 0.01 mil, but the corrosion in this system did not decrease until after 96 hr and a penetration of about 0.1 mil.

These results are regarded as preliminary. Further experiments are required before it can be established that the concentration of corrosion products is responsible for the effect, and not some other solution variable.

13. METALLURGY

G. M. Adamson

R. G. Berggren
W. J. Fretague
W. J. Leonard
M. L. Picklesimer
G. B. Wadsworth
J. C. Wilson

13.1 PHYSICAL METALLURGY

M. L. Picklesimer G. B. Wadsworth

13.1.1 Effects of Hydrogen on Zirconium and Its Alloys

To provide information on basic mechanisms in the important zirconium-hydrogen system and also to serve as metallographic standards for loop work, specimens of Zircaloy-2, crystal-bar zirconium, and WAPD's Zircaloy-2W and Zircaloy-3A were hydrogenated to contents of less than 5, 10, 50, 100, 150, 500, and 1000 ppm hydrogen. All specimens were outgassed at 900°C for 24 hr, hydrogenated at 900°C, homogeneized at 900°C for 1 hr, step-cooled in 100°C intervals every 30 min to 300°C, and furnace-cooled to room temperature. Vacuum-fusion hydrogen analyses of the specimens indicated final concentrations within 2% of the intended levels. Metallographic examination of the specimens is in progress. The examinations that have been made permit the following conclusions:

1. The hydride needles in the zirconium-base alloys investigated do not precipitate within the grains as in crystal-bar zirconium but seem to have a decided preference for the grain boundaries and grain corners, Fig. 13.1.
2. No fat needles such as form in the pure zirconium were observed in the alloys.
3. At the lower concentrations of hydrogen the alloys seem to precipitate the hydride as a film in the grain boundary (no positive proof as yet).

A metallographic method for the identification of the hydride needles in the metal specimens was developed. The specimens, after being etched, are anodized electrolytically at approximately 20 v dc in a solution of 35 ml of water, 60 ml of ethyl alcohol, 5 ml of phosphoric acid, 10 ml of lactic acid, 20 ml of glycerine, and 2 g of citric acid. Neither the time nor the voltage of anodizing is critical. The hydride needles are colored a golden yellow, while the zirconium matrix is colored blue-to-purple. Etching difficulties prevented the use of this method for locating and positively identifying the very small, almost irresolvable, needles or pits that are also thought to be hydride.

While it is known that the physical properties of zirconium alloys are greatly altered when hydrogen is picked up, it is not known that such a pickup will take place at the 300°C temperatures encountered in reactors. To determine whether hydrogen will diffuse into zirconium when nascent hydrogen is present at low or moderate temperatures, attempts are being made to charge zirconium and Zircaloy-2 with hydrogen cathodically at 30

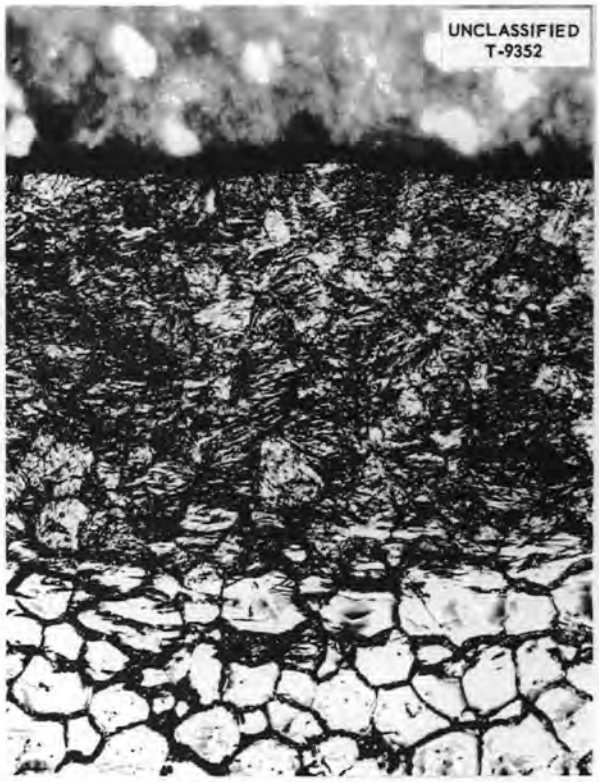

Fig. 13.1. Distribution of Hydrides in Zircaloy-2. Shows hydride surface layer typical of H_2 additions at low temperatures and hydrides concentrated in the grain boundaries. Zircaloy-2 with 1400 ppm H_2 added at 450°C, followed by homogeneization at 500°C. Bright field, 400X. Reduced 11%.

and 250°C in 1 *N* sulfuric acid. This work is still in the preliminary stages, and considerable difficulty is being encountered with the equipment.

Poor reproducibility was obtained with the hydrogen analyses of the first two as-received samples, but within the limits imposed by the poor precision no increase in hydrogen content was found after three Zircaloy-2 samples were treated for 100 hr at 30°C. After three other samples were charged for 100 hr at 250°C, increases of from 50 to 100 ppm were found. Values are not yet available for crystal-bar zirconium samples.

13.1.2 Development of Zirconium Alloys

The purpose of the zirconium-alloy development program is to obtain a complete understanding of the Zircaloy-2 material used for the HRT core tank and to determine any desirable changes in alloy composition or fabricating practice for the cores of future reactors.

It was found that incorrect values were previously reported[1] for the Zircaloy-2 alpha-to-(alpha-plus-beta) and beta-to-(alpha-plus-beta) temperatures; the correct temperatures are 810 and 970°C, respectively.

Zircaloy-2 specimens were heat treated to determine (1) grain-growth rates in the alpha, alpha-plus-beta, and beta fields; (2) the effect of quenching rates on the martensitic (alpha-prime) structure; and (3) the effects of time and temperature on the annealing of the quenched beta (alpha-prime) structure. Metallographic examination of the specimens permits the following conclusions to be drawn:

1. The rate of grain growth of equiaxed annealed alpha grains is very slow at any temperature in the alpha range. Figure 13.2 shows the fine-grained, but oriented, structure of as-received Zircaloy-2 which had been alpha annealed after rolling.

2. The beta grain size is apparently established during the heating through the alpha-beta field to the beta temperatures. Specimens containing more than 75% beta have essentially the same large grain size as those held for 30 min at 1050°C, which is well within the beta field, Fig. 13.3. While the beta grains are large, growth in the all-beta field is very slow and is not affected appreciably by increasing the temperature up to 1080°C. Specimens held for 2 hr at 1080°C had a grain size not more than 10% larger than that of one held at 980°C for 30 min.

3. The effect of different quenching rates on the alpha-prime structure is seemingly only that

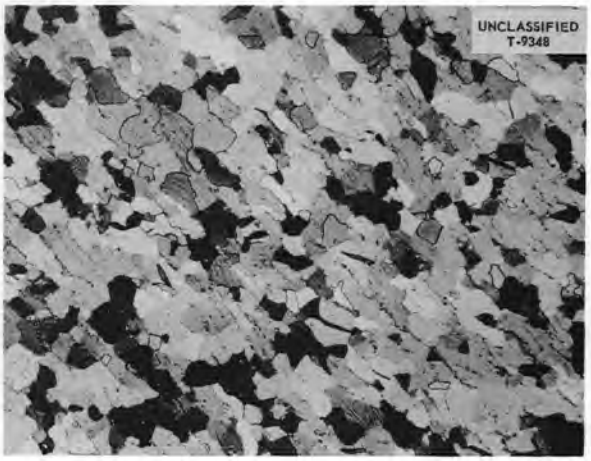

Fig. 13.2. As-Received Structure of Zircaloy-2. Annealed at 650°C after hot-rolling, causing a high degree of preferred orientation and a small grain size (ASTM 8 to 10), with one continuous stringer and many broken ones. Polarized light, 400X. Reduced 32%.

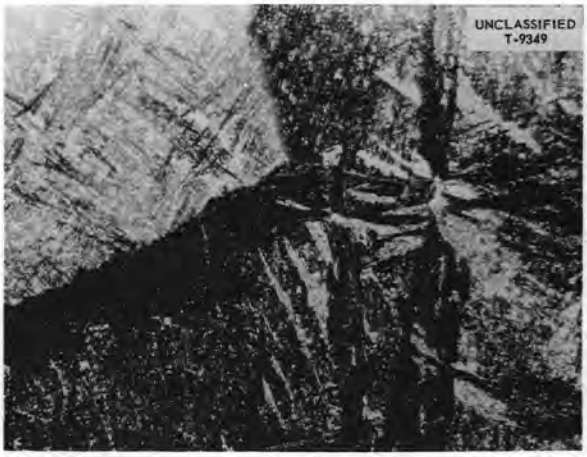

Fig. 13.3. Structure of Beta-Quenched Zircaloy-2. Annealed at 1050°C for 30 min and water-quenched. Shows quenched beta or alpha-prime martensitic structure and prior beta grain size (1 to 2 mm). Polarized light, 400X. Reduced 32%.

[1] M. L. Picklesimer, *HRP Quar. Prog. Rep. Oct. 31, 1955*, ORNL-2004, p 156.

of changing the size of the needles of the alpha-prime structure. Water-quenching produces a very fine martensitic needle structure, Fig. 13.3; air-cooling produces a coarser needle structure, usually called "basket weave"; and furnace-cooling yields a very coarse, fat, needle structure.

4. Beta-treated specimens have a grain orientation as highly preferred as that found in the starting material. Annealing of the beta-quenched structure produces first a sharpening of the needle structure of the alpha prime, Fig. 13.4, and then a secondary recrystallization to essentially equiaxed alpha grains, the size of which depends on the annealing temperature and time. Annealing at 700°C gives a very large alpha grain size, while at 800°C a smaller equilibrium grain size is obtained in a much shorter time interval, Fig. 13.5. After annealing at any of the lower temperatures within the alpha-plus-beta field, a retention of the fine basket-weave structure is noted, even after 2 hr at 900°C. Tests in the upper temperature range of the alpha-plus-beta field have not been performed. The equiaxed alpha grains resulting from the alpha-annealing treatments seem to be almost randomly oriented, but are of relatively coarse size. Cold-working of the beta-quenched structure to as much as 20% reduction results in very small, apparently randomly oriented, equiaxed alpha grains when annealed at 800 and 820°C for 15 to 30 min, Fig. 13.6. Reductions of 5, 10, and 15% are scheduled in order to determine whether

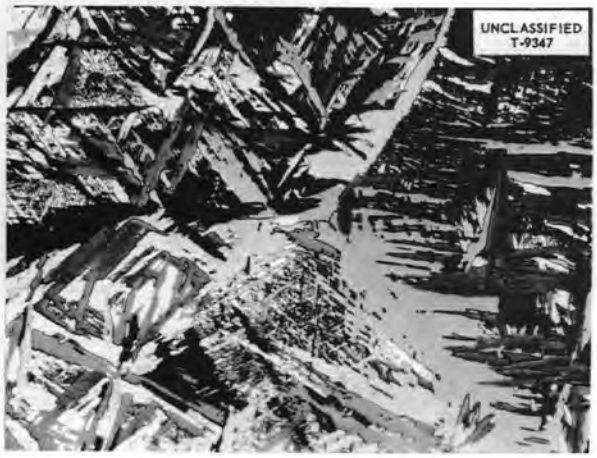

Fig. 13.4. Structure of Beta-Quenched, 600°C-Aged, Zircaloy-2. Shows coarsening of alpha-prime structure after being annealed at 1000°C for 30 min, water-quenched, aged at 600°C for 2 hr, and water-quenched. Structure compares with what would be expected in a multipass weld. Polarized light, 400X. Reduced 32%.

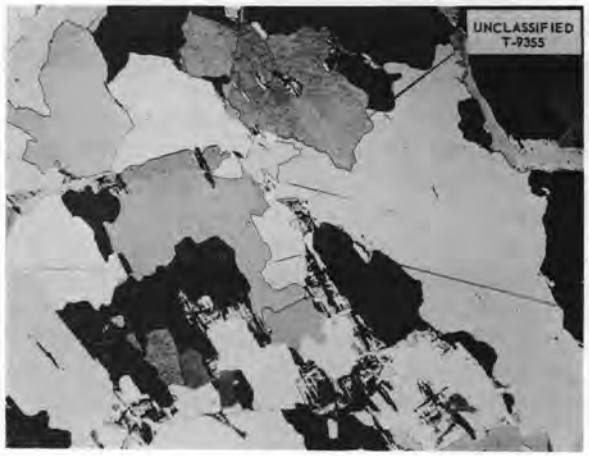

Fig. 13.5. Recrystallized Alpha-Prime Zircaloy-2 Structure. Annealed at 1000°C for 30 min, water-quenched, aged at 800°C for 15 min, and water-quenched. Shows the secondary recrystallization of alpha-prime structure almost complete. Polarized light, 100X. Reduced 33%.

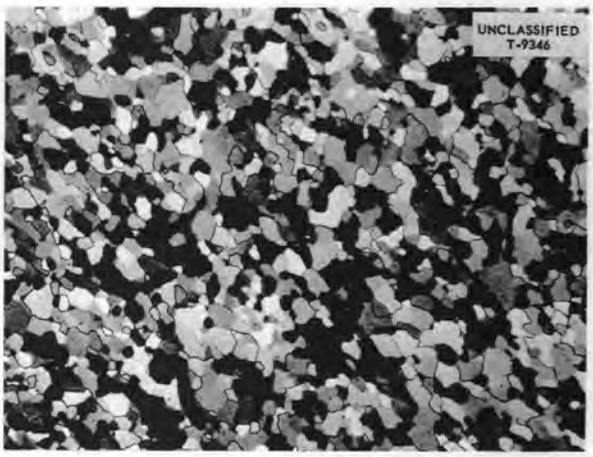

Fig. 13.6. Fine-Grained Equiaxed Alpha Grains in Zircaloy-2. Annealed at 1000°C for 30 min, water-quenched, cold-rolled 20%, annealed at 820°C for 30 min, and water-quenched. Compared with Fig. 13.2, shows desired fine-grained equiaxed alpha grains (ASTM 8 to 10) with almost random orientation. Polarized light, 400X. Reduced 32%.

the relatively large cold reduction is necessary. X-ray determinations of the preferred orientation of the annealed specimens will be made.

The x-ray group of the Metallurgy Division completed the determination of the preferred orientation of the core-tank material. The highly perfected texture is such that the most preferred crystallographic direction of the rolling direction is 14 deg from the {1010} poles and 18 deg from the {1120} poles. The normal direction is 14 deg from the {0001} poles and 80 deg from the {1210} poles. The transverse direction is 90 deg from each of the above positions. Analysis of the slip and twin planes available for deformation suggests that the mechanical properties, in the plane of the rolled sheet, will be quite similar, regardless of direction, and will show good ductility. However, there will probably be only very little ductility in the direction normal to the sheet. Thus it is expected that the yield strength in a direction perpendicular to the sheet will be close to the ultimate strength; brittle fracture would be expected to occur for any deformation perpendicular to the plane of the rolled sheet. These properties are not particularly detrimental in the core tank, since any expected tensile forces will be tangent to the surface of the tank.

13.1.3 Nature of Zirconium Oxide Films

A final report[2] was received from the Battelle Memorial Institute on their study of the nature of ZrO_2 films. All the selected corroded alloys were examined; cubic ZrO_2 was found only on the 10 wt % Mo and the 6, 8, and 10 wt % Nb binary zirconium alloys. The major phase in all cases was monoclinic. No further work with BMI samples is planned. All BMI samples tested were corroded to "failure" in high-temperature water and steam.

13.1.4 Stress-Corrosion Testing

Stress-corrosion testing of spring-tempered Inconel-X in boiling 42% $MgCl_2$ (154°C) was completed. Specimen No. 1 was stressed at 70,000 psi in $MgCl_2$ for 194.5 hr. Specimen No. 2 was stressed at 70,000 psi for 316 hr and then at 90,000 psi for 196.5 hr. Both tests were terminated by equipment failure. No evidence of stress corrosion of the specimens was found, and neither specimen failed.

[2]C. M. Schwartz, letter to M. L. Picklesimer, dated Dec. 9, 1955.

Previous reports[3–5] have presented evidence that a safe threshold stress exists below which there is no stress-corrosion cracking of types 309 and 310 stainless steel in magnesium chloride. The same apparatus has been used in an effort to find similar safe levels for types 304L and 347 stainless steel. The results are indicative only of a wide scatter in fracture times at the necessarily low stress levels. These results are summarized in Table 13.1. This scatter was not eliminated by changes in specimen preparation, such as different electropolishing techniques or annealing treatments.

TABLE 13.1 VARIATIONS IN TIME-TO-FAILURE IN STRESS-CORROSION TESTING OF STAINLESS STEELS

Type of Stainless Steel	Stress (psi)	Time-to-Failure (hr)
304L	16,000	3.4 to 29.5
304L	14,000	6.6 to 56.5
347	20,000	24.9 to 33.4
347	15,000	24 to 103

13.2 MECHANICAL METALLURGY OF TITANIUM AND ZIRCONIUM AND THEIR RESPECTIVE ALLOYS

W. J. Fretague

13.2.1 Commercial Titanium

Two specimens of C-130-AM titanium alloy (4% Mn, 4% Al, balance titanium), a proposed bolting material for use in the HRT, were tested in tension at room temperature and at 600°F. A crosshead speed of 0.05 in./min was used for these tests.

Results of the room-temperature test show a yield strength (0.2% offset) of 153,500 psi, a tensile strength of 156,400 psi, and an elongation of 22.5%. The specimen tested at 600°F had a yield strength of 102,600 psi, a tensile strength of 120,900 psi, and an elongation of 15%.

[3]J. I. Federer *et al.*, *HRP Quar. Prog. Rep. Oct. 31, 1955*, ORNL-2004, p 159.

[4]W. O. Harms, J. I. Federer, and G. B. Wadsworth, *HRP Quar. Prog. Rep. Jan. 31, 1955*, ORNL-1853, p 155–157.

[5]W. O. Harms, J. I. Federer, and G. B. Wadsworth, *HRP Quar. Prog. Rep. April 30, 1955*, ORNL-1895, p 161.

13.2.2 Zircaloy-2

To determine whether the embrittlement found in Zircaloy-2 impact samples irradiated in the corrosion loops[6] could be due simply to aging, a series of subsize tensile and impact specimens were aged for various times at 250°C. The tensile specimens, 0.180 in. in diameter with a $1\frac{1}{4}$-in. gage length, were pulled at strain rates of 0.01 and 0.1 in./in./min at 250°C and at room temperature. No systematic variations were found in yield strength, tensile strength, or elongation of samples aged for 0, 500, 1085, and 1585 hr. The impact samples were aged, along with the tensile specimens, but they have not yet been broken.

13.3 WELDING DEVELOPMENT

W. J. Leonard

13.3.1 Titanium Welding Development

In conjunction with the welding departments at the X-10 and Y-12 sites, welding procedures for titanium sheet and plate (up to $\frac{3}{8}$ in. in thickness) and pipe (up to 3 in. in diameter with a $\frac{3}{4}$-in. wall) have been developed. Three different welding methods were tried: (1) inert-atmosphere or dry-box welding; (2) protective trailers enclosing the torch and heated area; and (3) air-welding, or no protection other than that provided by the torch and the purging gas. Successful welds with essentially the same high quality were made by all three methods. Representative samples of each type were checked both by metallography and by mechanical testing.

If titanium is to be used for a reactor system, it is highly advisable, and possibly even necessary, that procedures for welding it in air be developed. The major effort was therefore placed upon the air-welding techniques. By use of this method an all-titanium loop was fabricated at X-10 for the Chemical Technology Division; a canned-rotor pump and a pressurizer for an all-titanium in-pile corrosion loop were fabricated at Y-12. At both sites air-welding was used, and the welds appear to be of high quality. From the experience gained on these loops, a titanium welding procedure is being prepared.

[6]W. J. Fretague, *HRP Quar. Prog. Rep. July 31, 1955*, ORNL-1943, p 167.

13.3.2 Welding of Stainless Steel By Using Preplaced Inserts for the Root Pass

A method of welding stainless steel by using preplaced inserts and the inert-gas-shielded arc-welding process were modified for HRP welding. The insert or ring is suitably placed in the root of the weld groove, and the root pass is made without adding filler metal. The balance of the weld is completed by using standard HRP welding procedures. The advantages of this method of making root passes over the conventional method of adding filler metal by hand are a closer geometrical control of the resulting weld bead and the high-quality root passes, which are obtained with less welding skill required of the operator. A tentative HRP welding specification was written for this process.

13.3.3 Inert-Gas-Shielded Arc Welding of Type 347 Stainless Steel with Fully Austenitic Filler Metal

To minimize weld-cracking, most inert-gas welding procedures, including HRP-2, using type 347 filler wire, are designed to produce a deposit containing 5 to 10% ferrite. In highly corrosive conditions the presence of this second phase may be harmful. A modified type 347 welding wire is now available which will produce sound, fully austenitic, weld deposits. A tentative HRP welding specification was developed to permit the use of this rod where service requirements are so severe that an austenitic deposit is desired.

13.3.4 Inert-Gas-Shielded Arc Welding of Carbon Steel

The composite structures of carbon steel and stainless steel found in most HRP designs require the development of suitable carbon-steel welding procedures. Inert-gas-shielded arc welding of carbon steels usually results in a weld that is poor because of its excessive porosity. This difficulty was also encountered in sigma welding procedures but was overcome by modifications in the filler wire. An inert-gas-shielded arc-welding procedure that will produce acceptable welds was worked out by using the wire from the sigma welding method. This wire is a fully killed steel which contains small amounts of silicon and chromium. Satisfactory welds were made in a $\frac{3}{4}$-in. carbon-steel plate.

13.4 EFFECTS OF RADIATION ON STRUCTURAL METALS AND ALLOYS

R. C. Berggren J. C. Wilson

Construction of an apparatus for irradiation of impact and tensile specimens at temperatures below 300°F in a beam hole of the MTR was completed, and the experiment was shipped to the MTR. Design of an elevated-temperature apparatus for use in the MTR was completed, and construction will start soon. Redesign of the specimen chamber of an apparatus for use in the MTR was started to permit, at an early date, irradiation at 575°F of RC-A-40 titanium, Zircaloy-2, Zircaloy-3A, Zircaloy-3B, and Zircaloy-3C. All the components, except the specimen chamber, were fabricated, and the completed apparatus should be ready within three months.

Impact tests are in progress on irradiated steels that are on hand; the results will be reported when this series of tests is completed.

Part V

CHEMICAL ENGINEERING DEVELOPMENT

F. R. Bruce

14. THORIUM OXIDE SLURRY DEVELOPMENT

D. E. Ferguson
V. D. Allred
A. R. Jones
E. V. Jones
N. A. Krohn
J. P. McBride
L. E. Morse
C. E. Schilling
W. M. Woods

14.1 THORIUM OXIDE SLURRY IRRADIATION STUDIES

A. R. Jones
N. A. Krohn
J. P. McBride
C. E. Schilling
W. M. Woods

14.1.1 Slurry Irradiations in the LITR

Four thorium oxide slurries containing 0.5 mole % UO_3 were irradiated in the LITR at 300°C and at a thermal-neutron flux of 3×10^{13} neutrons/cm^2·sec in the dash-pot-stirred irradiation bomb. The irradiation times were 151, 68, 172, and 200 hr. The slurries were stirred without difficulty while under irradiation. The irradiated slurries were readily removed from the bombs and appeared to be visually unchanged by the irradiation.

The slurries each contained 1000 g of thorium per kilogram of H_2O; the thorium oxide had been calcined at 650°C, wet-autoclaved at 300°C with the uranium as $UO_3 \cdot H_2O$, and then recalcined at 900°C. One thousand parts of PdO per million parts of thorium was added to each slurry as a catalyst for radiolytic-gas recombination. All slurries were mixed before insertion in the bombs, and the experimental setups were pretested at 300°C. During the last irradiation an oxygen overpressure was used (300 psi at room temperature).

14.1.2 Slurry Irradiations in the Graphite Reactor

Three ThO_2 slurries (1000 g of thorium per kilogram of H_2O) containing 0.5 mole % of 93.14% U^{235} as the oxide were irradiated in the ORNL Graphite Reactor at 300°C and at a thermal-neutron flux of 7×10^{11} neutrons/cm^2·sec. One slurry was prepared (as described above) from a 650°C calcined thorium oxide which had been pumped as an aqueous slurry for 200 hr at 250 to 300°C and then dried at 110°C. The other two slurries were prepared from unpumped 650°C calcined oxide. One thousand parts of PdO per million parts of thorium was added to each slurry before the irradiation. The irradiation times were 318, 313, and 480 hr, respectively, the last irradiation being carried out with an oxygen overpressure (250 psi at room temperature). The stirrer ceased operating in the slurry prepared from pumped oxide after only 8.5 hr of irradiation. No difficulty was encountered with stirring one slurry prepared from unpumped oxide, but stirring ceased in the other slurry after 187 hr of irradiation. No gas pressure in excess of steam was observed in any of the experiments. The slurry prepared from the pumped oxide could not be rinsed from the irradiation bomb. The other two slurries were readily removed and appeared to be visually unchanged by the irradiation.

Drying of the pumped oxide at 110°C, previous to its use in preparing the slurry for irradiation, resulted in a grainy solid. This physical characteristic was retained in the mixed oxide prepared from it and may account for the difficulties encountered in handling the slurry of mixed oxide during and after the irradiation.

14.1.3 Postirradiation Examination of Slurries

All slurries irradiated to date have been recovered for at least visual determination of any irradiation effect. Contamination of the laboratory now in use has precluded more precise determinations of radiation damage, except in a limited number of cases. The data are summarized in Table 14.1. Within the limitations of the measurements, no gross changes in the physical characteristics of the slurry solids appear to have taken place.

A cell of the High-Radiation-Level Analytical Facility is being modified for use in the postirradiation examination of slurries.

14.1.4 Slurry Viscosity Measurements in the Irradiation Bombs

A Thyratron-operated timer obtained for use with the dash-pot-stirred irradiation bombs (Fig. 14.1) has made it possible to obtain relative viscosity measurements on thorium oxide slurries in these bombs. In the irradiation bomb the stirrer is

TABLE 14.1. SUMMARY OF EFFECT OF IRRADIATION ON THORIUM OXIDE SLURRIES

Experiment No.*	Oxide** Preparation (from Thorium Oxalate)	Slurry Concentration (g of Th per kg of H_2O)	X-Ray Crystallite Size (Å)			Average Particle Size (μ)			Settled Concentration (g of Th per liter)			Final pH	
			Original	Control	Irradiated	Original	Control	Irradiated	Original	Control	Irradiated	Slurry	Supernatant
GR-1	650°C calcined	750			205								
GR-3	Pyrohydrolyzed + 8% U^{235}	500		250	220		0.6			900	500		
GR-4	Pyrohydrolyzed + 8% U^{235} + 1% Cu	500		200	180		2			1300	400		
GR-5	650°C calcined (D-12)	500	110		230			5			1100		
GR-6	650°C calcined (D-16)	Settled	123		175	2		2	1300		1200		
GR-7	650°C calcined + 3400 ppm Ag	Settled			120			1			1250	9.0	9.1
GR-8	900°C calcined (D-30, pumped)	Settled			410			0.5			1400	9.0	9.2
LITR-2	900°C calcined (Lindsay 8)	500			900			2			1200		
LITR-3	650°C calcined (D-16)	500		200	195			1		1000	1500		
LITR-4	650°C calcined (D-16)	500									1600		
LITR-5	900°C calcined (D-16)	500	474	650	285	2	1	1	1500	1100	1400	9.5	9.5
LITR-8	650°C calcined (D-16)	500			260	2		2				9.3	9.3
LITR-9	900°C calcined (D-30, pumped)	500	450		200	0.6	2	0.6	900	800	1100	9.3	9.3

*GR, Graphite Reactor: flux = 7×10^{11} neutrons/cm^2·sec; LITR: flux = 3×10^{13} neutrons/cm^2·sec; all experiments carried out at 300°C.

**D-oxides prepared from Thorex-product thorium nitrate.

actuated by two solenoids, which are alternately energized to pull the stirrer up and down. The Thyratron power supply is so designed that the solenoid current, stirring cycle frequency, and load division between the two solenoids (fractional cycle time on upper coil) can be varied independently. Hence, if any two of these variables are kept constant, the third may be calibrated against solutions of known viscosities and then used in obtaining an estimate of the viscosity of a thorium oxide slurry.

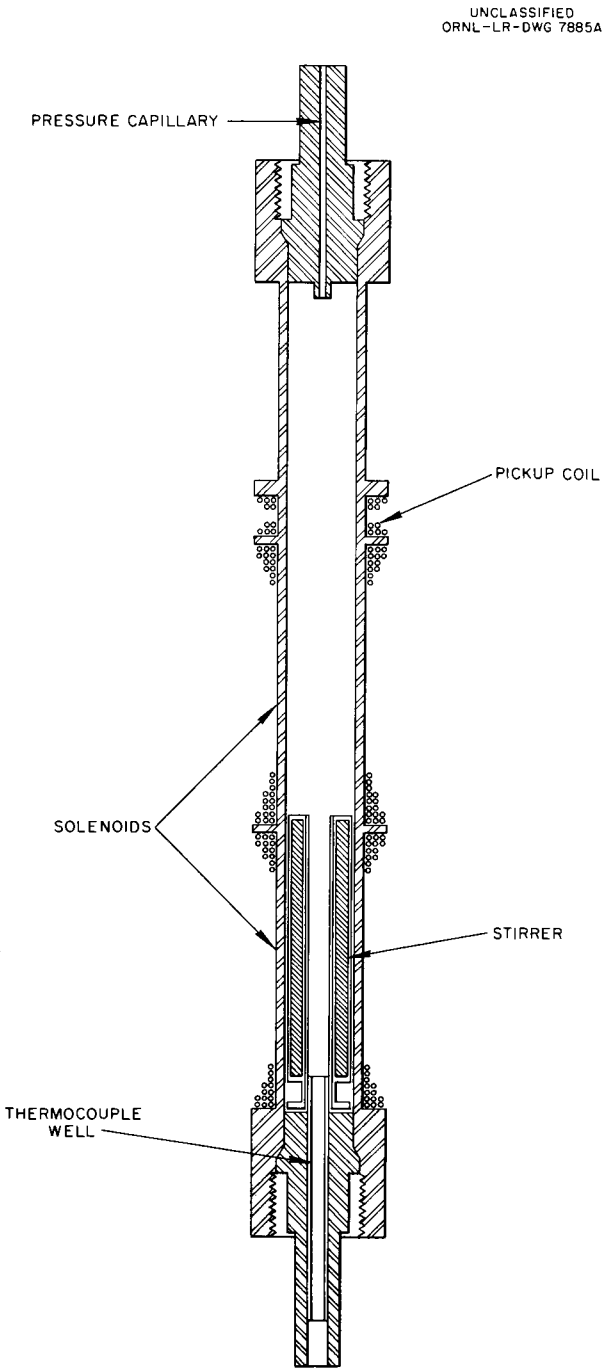

Fig. 14.1. Dash-Pot Irradiation Bomb No. 5.

Four calibration curves were prepared from a 75% glycerol–water mixture and a Dow Corning 200 fluid, for which the viscosity-temperature curves are known. They were: (1) the minimum current required to stir the fluids at 50% load division and 4-cps stirring rate; (2) the maximum frequency at which the fluids could be stirred at 50% load division with 8 amp of current to the solenoid; (3) the minimum per cent load on the top coil required for stirring at 4 cps with a solenoid current of 8 amp; and (4) same as curve 3, except with a solenoid current of 10 amp. From the calibration curves the viscosity, in centistokes, of a 900°C calcined thorium oxide slurry (1000 g of thorium per kilogram of H_2O) was measured at several different temperatures and for various pretreatments of the oxide. A measurement was also obtained for a slurry of a 900°C oxide which had been pumped for 100 hr at 250°C (X-28). The results are summarized in Table 14.2. The last column shows the average of the viscosities obtained by use of the four calibration curves. The limits are based on a 95% confidence interval.

The slurry viscosity does not appear to change markedly with increasing temperature up to 200°C and increases only moderately with prolonged stirring in the radiation bomb. Particle degradation causes a significant increase in viscosity, as shown by the data for the pumped slurry.

While the precision of the method is not good, it does permit the relative measurement of slurry viscosity at high temperatures and pressures and the detection of viscosity changes that may occur in slurries under irradiation. A new model of the irradiation bomb for in-pile slurry viscosity measurements, having a coaxial cylinder and a viscosity-sensitive, electromagnetically operated plunger, is under laboratory test with slurries. The slurry is caused to flow back and forth through the outer annulus, and relative viscosity is measured by determining the stirring frequency of the plunger for a given electrical load.

TABLE 14.2. VISCOSITIES OF THORIUM OXIDE SLURRIES

Slurry concentration: 1000 g of thorium per kilogram of H_2O

Slurry	History	Temperature (°C)	Average Viscosity* (centistokes)
900°C D-16	Freshly prepared	30	5.9 ± 4.1
900°C D-16	Freshly prepared	100	6.9 ± 3.5
900°C D-16	Freshly prepared	190	6.4 ± 3.6
900°C D-16	Stirred 4 hr in bomb	190	9.3 ± 4.1
900°C D-16	Stirred 23 hr in bomb	190	18.1 ± 8.8
900°C D-16	Stirred 32 hr in bomb	170	15.1 ± 7.5
900°C D-16	Stirred 32 hr in bomb	90	16.9 ± 7.1
X-28	Pumped slurry	200	57 ± 9

*Average of viscosities obtained by use of the four calibration curves (see text); the limits are based on a 95% confidence interval.

14.1.5 Preparation of Thorium-Uranium Mixed Oxides

Thorium-uranium mixed oxides were prepared by two different methods in attempts to simulate material which would result from neutron irradiation of a thorium oxide slurry under actual breeder blanket conditions. In one method an aqueous suspension of thorium and uranium oxides was autoclaved at 300°C to give a cream-colored solid in which the uranium was apparently homogeneously distributed; in the second, thorium and uranous oxalates were coprecipitated and the recovered solids calcined to the oxide. The materials produced by the two methods had a characteristic orange color after firing but differed in their specific surface areas, average x-ray crystallite sizes, and time-temperature dependence for crystallite growth.

In the autoclave preparation method a mixture of D-16 oxide and 0.5% uranium as $UO_3 \cdot H_2O$ was autoclaved as a slurry for 19 hr at 300°C. The material was then dried and was calcined in air at 900°C from 1 to 67 hr. A log-log plot of the crystallite size vs calcination time gave a straight line with a slope identical to that of the D-16 curves (Fig. 14.3). Specific-surface-area–crystallite-size relations were similar to those obtained with pure oxide (Table 14.3). The amount of uranium leached in 17 hr by tumbling with 8 *M* HNO_3 decreased linearly with calcination time from 36.8% at 1 hr to 8.0% after 16 hr. Only 4.3% of the uranium dissolved after 67 hr calcination. The amount of tetravalent uranium in the calcined solids varied from 0 to 15% of the total uranium but showed no relation to calcination time. In a similar mixture of ThO_2 and $UO_3 \cdot H_2O$ which had not been autoclaved, a decrease in the amount of tetravalent uranium with calcination time was noted. An attempt to reduce the uranium in the dried solid (not calcined at 900°C) with hydrogen at 700°C was only partially successful. Only 50 to 60% of the uranium was reduced in 8 hr, and no further reduction was noted after an additional 5 hr.

The thorium and uranous oxalates (0.5 to 5 wt % uranium based on thorium) were coprecipitated by adding to a thorium nitrate solution an oxalic acid solution containing tetravalent uranium. The oxalic acid solution was prepared by adding to it a saturated ammonium oxalate solution of uranous oxalate[1] just prior to its use in the precipitation step. The first precipitation was carried out at room temperature in 0.3 to 0.6 *M* $Th(NO_3)_4$ solution. About 40% of the uranium failed to precipitate because of oxidation by nitric acid. In subsequent precipitations uranium losses were minimized: first, by diluting the thorium nitrate

[1] L. E. Marchi, "Uranium(IV) Oxalate," p 166 in *Inorganic Syntheses*, Collective Vol. III, ed. by L. F. Audrieth, McGraw-Hill, New York, 1950.

TABLE 14.3. CHARACTERISTIC PROPERTIES OF THORIUM-URANIUM MIXED OXIDES

Preparation Method	Uranium (mole %)	Calcination Conditions		Surface Area, S (m^2/g)	Crystallite Size, D (Å)	$S \times D$* ($\times 10^{-3}$)
		Time (hr)	Temperature (°C)			
D-16 ThO_2–$UO_3 \cdot H_2O$ wet-autoclaved at 300°C	0.5	18	750	18.9	195	3.69
		1	900	19.1	222	4.24
		8	900	13.5	306	4.13
		15.5	900	11.7	335	3.92
		29	900	11.3	362	4.09
		18	1000	5.8	483	2.80
Oxalates coprecipitated at 25°C; calcined at 375, 500, 650°C	0.29	21	800	4.7	375	1.76
Oxalates coprecipitated at 250°C; calcined at 375°C	0.57	3	500	23.0	74	1.70
		3	650	8.0	173	1.38
		16	800	5.5	243	1.34
Oxalates coprecipitated at 40°C (0.3 M H_2NNH_2); calcined at 375°C	0.42	3	500	20.5	84	1.72
		3	650	9.5	100	0.95
		16	800	3.0	239	0.72
		64	800	2.0	354	0.71
	5.6	3.4	500	17.3	54	0.93
		20	800	1.8	123	0.22

*$S \times D = 3.6 \times 10^3$ for oxides prepared by thermal decomposition of thorium oxalate (V. D. Allred and S. R. Buxton, *HRP Quar. Prog. Rep. July 31, 1955*, ORNL-1943, p 186).

solution and, second, by adding 0.3 M hydrazine when the precipitation temperature was increased to 40°C.

The mixed oxides prepared by calcining the coprecipitated oxalates had much smaller surface areas than would be predicted from their x-ray crystallite sizes, based on the experience with pure oxide.[2] In addition, the specific-surface-area–crystallite-diameter products obtained with these mixed oxides were lower than those obtained with the pure oxide or the autoclaved mixed oxide and were not constant for a given preparation carried through a multistage firing (Table 14.3).

It may be concluded from the above that, in the mixed oxides prepared by simple autoclaving of the thorium-uranium oxide, the uranium, although seemingly homogeneous with the thorium, is probably only on the thorium oxide surface.

[2]V. D. Allred and S. R. Buxton, *HRP Quar. Prog. Rep. July 31, 1955*, ORNL-1943, p 186.

14.2 GAS-RECOMBINATION STUDIES

L. E. Morse J. P. McBride

Development of a catalyst for use in thorium oxide slurries to recombine the radiolytic gases has continued, with further work being done on oxides of palladium, molybdenum, vanadium, and cerium and on copper chromite. The palladium was by far the most effective; at 830 ppm concentration based on thorium it gave a combination rate more than sufficient to recombine the radiolytic gases expected in the TBR blanket. Molybdenum and vanadium at 0.1 m concentration also gave rates sufficiently fast for TBR use. Cerium oxide showed negligible catalytic activity. Copper chromite[3] was not significantly better than copper oxide as a catalyst.

The experiments were carried out with slurries

[3]A. H. Blatt (ed.), *Organic Syntheses*, p 142, Collective Vol. II, John Wiley, New York, 1944.

of 900°C calcined thorium oxide containing 660 to 1000 g of thorium per kilogram of H_2O. The slurry solids were mixed and tumbled dry for 1 hr before they were formed into an aqueous suspension and then heated for 3 hr at 285°C in the reaction bombs under an oxygen overpressure. Experimental details and methods of analysis have been described previously.[4,5] The observed reaction rate, k_π, and the rate of hydrogen combination with oxygen in moles per hour per liter of slurry are listed in Table 14.4; these rates were obtained from the observed decrease in gas pressure with time, perfect gas behavior being assumed.

The palladium oxide used in the catalytic study was prepared by precipitating the hydrous oxide from nitrate solution and drying it at 120°C. At 830 ppm palladium concentration and 116°C in a slurry of thorium oxide (1000 g of thorium per kilogram of H_2O) containing 0.5% uranium, the combination rate was 12 moles of hydrogen per hour per liter of slurry at a hydrogen partial pressure of 500 psi (Table 14.4). As in previous studies, it was necessary to preheat the slurry containing the PdO to a temperature above 120°C in the presence of the stoichiometric gas mixture to obtain the high catalytic activity. With 550 ppm of palladium, based on thorium, high combination rates were obtained above 120°C, but below this temperature the catalyst appeared to be poisoned readily.

The molybdenum oxide catalyst was prepared by calcining ammonium molybdate in a covered crucible

[4] D. E. Ferguson *et al.*, *HRP Quar. Prog. Rep. Oct. 31, 1954*, ORNL-1813, p 143–144.

[5] H. F. McDuffie *et al.*, *Reactor Sci. Technol.* 4, No. 2, 23 (1954), TID-2013.

TABLE 14.4. COMBINATION RATES OF STOICHIOMETRIC HYDROGEN AND OXYGEN MIXTURES IN THORIUM OXIDE SLURRIES CONTAINING VARIOUS CATALYSTS

900°C calcined oxide
660 to 1000 g of thorium per kilogram of H_2O
Heated as slurry 3 hr at 285°C under oxygen (250 to 300 psi at room temperature)

Catalyst	Catalyst Concentration	Conditions	Temperature (°C)	k_π (hr^{-1})	H_2 Combination Rate, P_{H_2} = 500 psi (moles/hr/liter)
PdO	830 ppm	As prepared	116	17	12
	1000 ppm	As prepared	115	26	21
MoO_3	0.1 *m*	As prepared	255	67	25
		Heated under H_2 at 250°C*	135	16	12
		Reheated reduced slurry under O_2 at 250°C**	158	33	22
V_2O_5	0.1 *m*	As prepared	280	0.3	0.1
		Heated under H_2 at 280°C*	182	31	17
		Reheated reduced slurry under O_2 at 285°C**	195	10	5
CeO_2	0.1 *m*	As prepared	275	0.1	0.03
$CuCr_2O_4$	0.1 *m*	As prepared	280	18	5

*1000-psi H_2 at room temperature.
**500-psi O_2 at room temperature.

at 480°C for 18 hr. Although a very active catalyst (25 moles of hydrogen per hour per liter at 255°C and a P_{H_2} of 500 psi) was obtained by simply adding the oxide at 0.1 *m* concentration to the slurry solids, the activity was markedly increased by heating the slurry containing the molybdenum oxide at 250°C with a hydrogen overpressure.

The vanadium was precipitated with peroxide from an aqua regia solution, dried, and calcined at 300 to 350°C. As-prepared vanadium oxide showed negligible activity as a catalyst at 0.1 *m* concentration in a thorium oxide slurry. Subjecting the slurry containing the vanadium to a hydrogen overpressure (1000 psi at room temperature) at 280°C resulted in a partial reduction of the vanadium (probably from V_2O_5 to V_2O_3) and a considerable increase in catalytic activity (17 moles of hydrogen per hour per liter at 182°C and P_{H_2} = 500 psi; Table 14.4). Reheating the reduced catalyst at 285°C with oxygen (500 psi at room temperature) decreased its catalytic activity by a factor of about 3.

The rate of hydrogen consumption with the 0.1 *m* copper chromite catalyst was 5 moles/hr per liter of slurry at 280°C. The presence of soluble chromate in the aqueous phase at the completion of the experiment and the color of the solid phase of the slurry suggested that the copper chromite had been partially oxidized and hydrolyzed.

14.3 LABORATORY STUDIES ON THORIUM OXIDE SLURRIES

V. D. Allred E. V. Jones
J. P. McBride

14.3.1 Properties of Pumped Oxides

The effect of pumping (at 250°C for 100 hr in the 5-gpm loops) upon the average crystallite size, sedimentation particle-size distribution, hindered-settling rate, and settled concentration of three different oxide preparations was determined. The oxides were prepared by firing at 900°C for 24 hr (1) the standard pilot-plant oxide, D-16 (D-16-900-24); (2) an oxide prepared by a multistage calcination of thorium oxalate precipitated at 10°C (TO-10-900-24); and (3) an oxide prepared by the pyrohydrolysis,[6] at 300°C, of this precipitated thorium oxalate and a multistage calcination of the product (PO-10-900-24). The data are summarized in Table 14.5, which shows the characteristic properties of the oxides before and after pumping. The effect of pumping on the particulate properties of the oxides is further illustrated by electron micrographs (Fig. 14.2).

The average x-ray crystallite sizes appear to be only slightly affected, if at all, by the pumping. The larger particles (>1 μ) in all preparations were degraded, with a pronounced decrease in the hindered settling rates of the slurries prepared from the standard oxide and the pyrohydrolyzed material. The hindered settling rate, except at 27°C (Table 14.5), and the particle-size distribution of the slurry of oxide prepared by thermal decomposition from oxalate precipitated at 10°C were relatively unaffected by the pumping. The electron micrographs of this material also show relatively little change in the shape of the particles. The lack of change in these characteristics when the slurry was pumped may be desirable in a blanket slurry.

14.3.2 Crystallite Growth in Thorium Oxide

In a previous report[7] it was shown that the average x-ray crystallite diameter of an oxide prepared by the thermal decomposition of thorium oxalate increases exponentially with both calcination time and calcination temperature. Growth curves have now been evaluated for the standard D-16 oxide,[8] a series of oxides prepared in the laboratory, and two oxides prepared at the Feed Materials Processing Center at Fernald, Ohio (Fig. 14.3).

The crystallite diameter of a D-16 oxide is related to time and temperature of calcination by the equation

$$D \approx t^{0.14} e^{10.3513 - (5482/T)} ,$$

where D is the average crystallite diameter in angstroms, t is the time in hours, and T is the absolute temperature in degrees Kelvin. The time-dependent variable, $t^{0.14}$, appears to be characteristic of thorium oxide prepared by the thermal decomposition of the oxalate. The temperature-dependent function, $e^{A-(B/T)}$, on

[6] D. E. Ferguson *et al.*, *HRP Quar. Prog. Rep. Jan. 31, 1954*, ORNL-1678, p 87.

[7] V. D. Allred and S. R. Buxton, *HRP Quar. Prog. Rep. July 31, 1955*, ORNL-1943, p 181.

[8] W. H. Carr, *HRP Quar. Prog. Rep. July 31, 1955*, ORNL-1943, p 198.

TABLE 14.5. EFFECT OF PUMPING ON PROPERTIES OF THORIUM OXIDE SLURRIES

Material	X-Ray Crystallite Size (Å)	Specific Surface Area (m^2/g)	Mean Particle Size (μ)	Hindered Settling Rate, 500 g of Th per kg of H_2O (cm/sec)				Settled Concentration (g of Th per liter)	pH of Supernatant
				27°C	50°C	75°C	98°C		
D-16-900-24[a]	618; 680	6[b]	2.8	0.064	0.085	0.116	0.146	1480	10.1
D-16-900-24 pumped 100 hr at 250°C, X-28	613		0.8	0.004	0.010	0.014	0.018	1165	8.0
D-16-900-24 + 1000 ppm SO_4^{--} pumped 100 hr at 250°C, X-27	653		0.8	0.013	0.014	0.020	0.032	1310	6.0
TO-10-900-24[c]	536	5.2	0.7	0.0001	0.009	0.033	0.047	1090	9.8
TO-10-900-24 pumped 100 hr at 250°C, V-8	660		0.8	0.010	0.015	0.025	0.025	1170	7.0
PO-10-900-24[d]	228	18.3	0.9	0.005	0.022	0.131	0.205	985	10.1
PO-10-900-24 pumped 100 hr at 250°C, U-37	243		0.6	0.0003	0.0006	0.0010	0.0014	975	8.0

[a]Prepared by refiring D-16 standard oxide at 900°C for 24 hr.
[b]Estimated.
[c]Prepared by a multistage calcination of 10°C precipitated thorium oxalate, with the final firing at 900°C for 24 hr.
[d]Prepared by autoclaving an aqueous suspension of 10°C precipitated thorium oxalate at 300°C for 24 hr and a multistage calcination of the product, with the final firing at 900°C for 24 hr.

the other hand, must be evaluated for a given source material.

Oxides prepared by the wet-autoclaving of thorium oxalate at 250 to 300°C (pyrohydrolysis) are unique in that they do not show crystallite growth even upon prolonged heating at temperatures up to 900°C.[9] This phenomenon most probably results from the absence of an ordered or relic structure (random orientation of the crystallites) and the small size of the ultimate particles.

Mechanical or chemical degradation, such as that which an oxide undergoes when it is pumped as a slurry, could also result in a loss of relic structure. The crystallite-growth characteristic should give an indication of the degree of degradation which has occurred. To test this hypothesis, aliquots of the original charge (800°C oxide), the pumped slurry, and the cake from the 200A-3 loop run at Y-12 were heated for 24 hr at 900°C. The original charge showed the normal crystallite growth expected in an oxide with relic structure (Fig. 14.4). The crystallites in the pumped and caked oxide increased only slightly in size, indicating nearly complete absence of relic structure and that, on pumping, degradation of the oxide particles to crystallite dimensions had occurred. Electron micrographs of the pumped slurry and the cake substantiated this conclusion. Since the average particle size of the pumped oxide, as measured by sedimentation, was between 0.5 and 1 μ, it may be further concluded from the above that the sedimenting particles were agglomerates of fine particles. Furthermore, it follows that those properties which depend on the nature and the shape of the "working particle," such as hindered settling, viscosity, and abrasion, will be different in the pumped slurry than in the slurry as originally prepared. A possible exception may be the oxide prepared by the thermal decomposition of oxalate precipitated at 10°C, whose particulate and slurry properties appear to be slightly affected, if at all, by pumping (see Sec. 14.3.1).

[9]V. D. Allred, *HRP Quar. Prog. Rep. Oct. 31, 1955*, ORNL-2004, p 172.

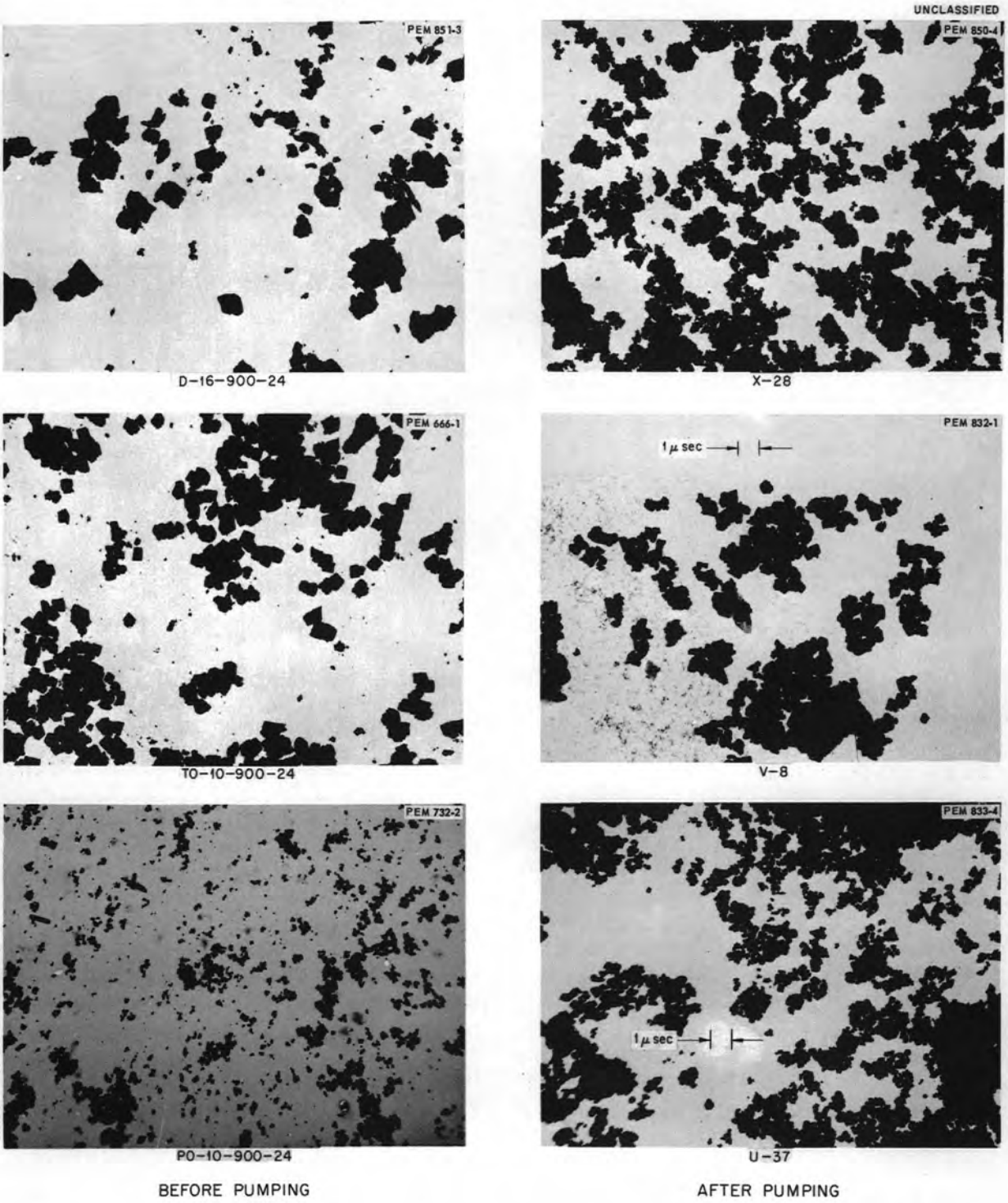

Fig. 14.2. Electron Micrographs of Selected Thorium Oxides Before and After Pumping for 100 hr at 250°C. (See Table 14.5 and text for preparation methods.)

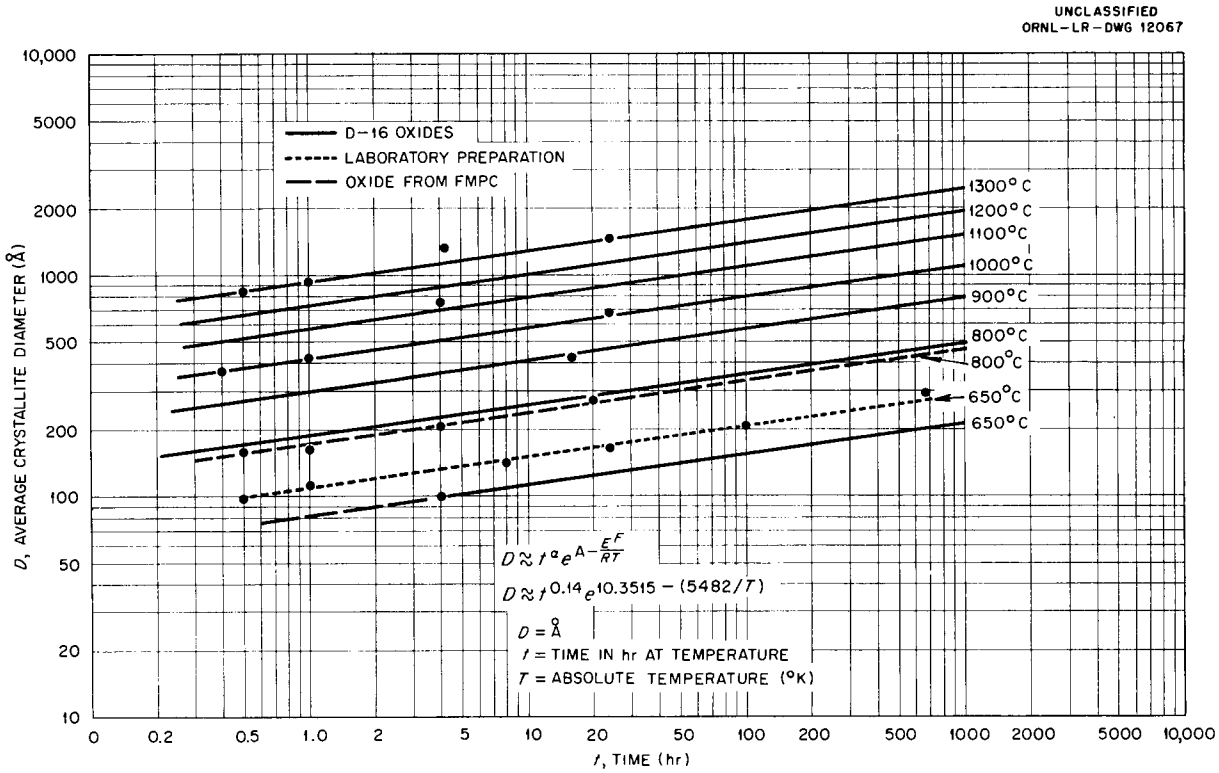

Fig. 14.3. Growth of ThO_2 Crystallites with Firing Time and Temperature.

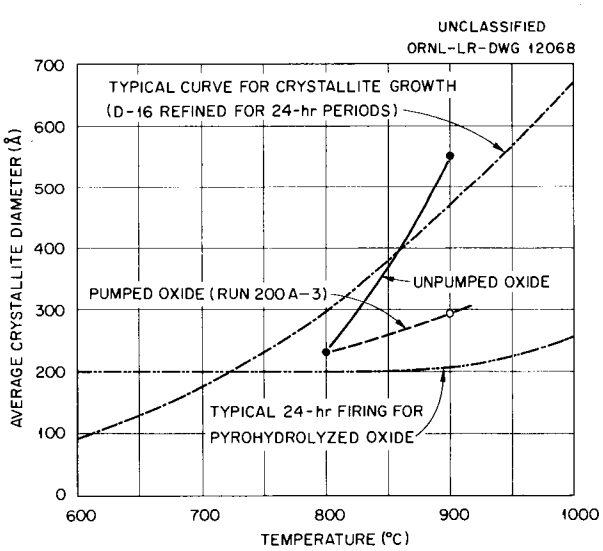

Fig. 14.4. Effect of Pumping on Crystallite Growth in Thorium Oxide (Original Oxide Fired at 800°C; Pumped and Unpumped Material Refired at 900°C for 24 hr).

14.3.3 Hindered-Settling Properties of Thorium Oxide Slurries

Studies of the hindered-settling properties of thorium oxide slurries have continued, with further work on the effect of sulfate on the settling rate of slurries of the 800°C fired oxide and an investigation of the temperature dependence, up to 98°C, of the hindered-settling characteristics of slurries fired at 650 to 1300°C. The objective is to determine the effect of various chemical environments on the dispersion properties of thorium oxide, to develop hindered-settling techniques as a means of characterizing thorium oxide preparations, and to provide background information for settling studies to be carried out at 300°C.

The hindered-settling characteristics of ThO_2 slurries, containing 500 g of thorium per kilogram of H_2O, of an 800°C fired oxide to which 0.005 *M* $Na_2O{\cdot}3SiO_2$ and 0 to 20,000 ppm of sulfate as H_2SO_4 had been added showed a pH dependence

similar to that obtained with H_2SO_4 alone in a 900°C fired oxide slurry[10] (Fig. 14.5). The data are summarized in Table 14.6. The use of an 800°C oxide precludes a direct comparison with a similar study carried out with 0.005 *M* $Na_4P_2O_7$ and a 900°C fired oxide,[10] but the markedly higher settling rates and lower bulk densities obtained in the present study indicate that the silicate is less effective than the pyrophosphate as a dispersant in slurries containing sulfate.

Hindered-settling studies were carried out at 27, 50, 75, and 98°C on slurries (500 g of thorium per kilogram of H_2O) of D-16 oxide (650°C fired) and oxides prepared by refiring the D-16 oxide at 800, 900, 1000, and 1300°C. In general, the settling rate increased with increasing slurry temperature and increasing temperature of calcination up to 1000°C. Unusually high dispersion characteristics were obtained at the higher slurry temperatures for the oxide calcined at 1300°C. These have not been satisfactorily explained as yet but tend to substantiate the conclusion that oxides calcined at 1000°C or above have slurry properties markedly different from those of oxides calcined at lower temperatures.

The hindered-settling data are summarized in Table 14.7, where U_0 is the hindered-settling

[10] E. V. Jones, *HRP Quar. Prog. Rep. Oct. 31, 1955*, ORNL-2004, p 172–178.

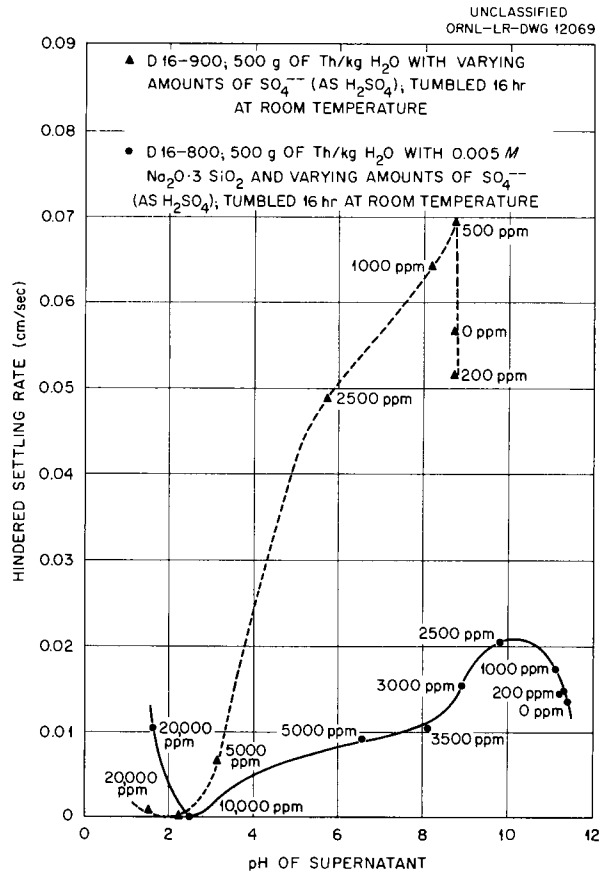

Fig. 14.5. Effect of Sulfate on Settling Rates of ThO_2 Slurries.

TABLE 14.6. EFFECT OF H_2SO_4 PLUS 0.005 *M* $Na_2O \cdot 3SiO_2$ ON SETTLING PROPERTIES OF ThO_2 SLURRIES

Sulfate Concentration (ppm)	pH of Supernatant	Hindered Settling Rate, U_0 (cm/sec)	Settled Concentration (g of Th per liter)
0	11.4	0.0135	1800
200	11.3	0.0149	1785
500	11.2	0.0143	1770
1,000	11.1	0.0173	1695
2,500	9.8	0.0204	1680
3,000	8.9	0.0154	1710
3,500	8.1	0.0105	1725
5,000	6.5	0.0091	1695
10,000	2.5	*	1785
20,000	1.6	0.0105	1850

*Too slow to be read.

TABLE 14.7. EFFECT OF SLURRY TEMPERATURE AND OXIDE CALCINATION TEMPERATURE ON SETTLING CHARACTERISTICS OF ThO_2 SLURRIES

U_0 = hindered settling rate, cm/sec

Slurry Temperature (°C)	Viscosity of H_2O, μ (centipoises)	Settling Characteristics of Oxides Calcined at Indicated Temperature									
		650°C		800°C		900°C		1000°C		1300°C	
		U_0	$U_0\mu$	U_0	$U_0\mu$	U_0	$U_0\mu$	U_0	$U_0\mu$	U_0	$U_0\mu$
27	0.8545	0.031	0.029	0.038	0.032	0.06	0.05	0.10	0.08	0.032	0.027
50	0.5494	0.045	0.025	0.07	0.036	0.09	0.047	0.15	0.08	0.07	0.041
75	0.3799	0.07	0.027	0.12	0.044	0.12	0.044	0.27	0.10	0.16	0.06
98	0.2899	0.10	0.028	0.16	0.048	0.15	0.042	0.34	0.10	0.20	0.06
			0.027		0.040		0.047		0.09		0.046

rate and μ is the viscosity of water at the temperature of the settling slurry. From theoretical considerations the product $U_0\mu$ should remain constant for an oxide over a series of settling temperatures, provided that no change has occurred in the particulate or dispersive characteristics. As shown by data in Table 14.7, $U_0\mu$ does remain fairly constant over the temperature range 27 to 98°C. Changes do occur in oxide properties with increasing calcination temperature up to 1000°C, as shown by the progressive increase in the $U_0\mu$ product. The trend reverses with the 1300°C material, which shows a high dispersive characteristic (low value of $U_0\mu$) and marked changes in $U_0\mu$ with increasing slurry temperature.

An apparent particle diameter, D_s, in microns, corresponding to that obtained by usual permeability techniques, was calculated from $U_0\mu$ by the equation[11]

$$D_s = 13\left[\frac{U_0\mu}{\Delta\rho g_c}\left(\frac{1-e}{e^3}\right)\right]^{1/2} ,$$

when $\Delta\rho$ is the difference in the densities of the oxide and the water, g_c is the gravitational constant, and e is the porosity factor. For a ThO_2 slurry containing 500 g of thorium per kilogram of H_2O, the equation becomes

$$D_s = 3.73 \times 10^{-3}(U_0\mu)^{1/2} .$$

The calculated diameters are given in Table 14.8, along with other characteristic properties of the oxides used in the hindered-settling studies. Data obtained with the slurries in the pumping studies reported in Sec. 14.3.1 are also summarized in Table 14.8.

[11] J. M. Dalla Valle, private communication.

TABLE 14.8. CHARACTERISTIC PROPERTIES OF VARIOUS THORIUM OXIDES AND THEIR AQUEOUS SLURRIES

Slurry concentration: 500 g of thorium per kilogram of H_2O

Oxide	Average X-Ray Crystallite Size (Å)	Sedimentation Particle Size (μ)	Particle Size Calculated* from Settling Rates (μ)	Settled Concentration (g of Th per liter)	pH of Supernatant
D-16 calcined at 650°C for 4 hr	110	2–3	6.1	1215	8.4
D-16 calcined at 800°C for 24 hr	263	2–3	7.3	1355	9.8
D-16 calcined at 900°C for 24 hr	619	2–3	8.1	1480	10.1
D-16 calcined at 1000°C for 24 hr	745	2–3	11.4	1735	9.2
D-16 calcined at 1300°C for 24 hr	1483	2–3	8.0	1840	7.5
D-16 calcined at 900°C for 24 hr plus 1000 ppm SO_4^{--}, pumped 100 hr at 250°C, X-27	613	0.8	2.6	1165	8.0
D-16 calcined at 900°C for 24 hr pumped 100 hr at 250°C, X-28	653	0.8	3.6	1310	6.0
TO-10-900-24**	536	0.7	4.3	1090	9.8
TO-10-900-24 pumped 100 hr at 250°C, V-8	660	0.8	3.5	1170	7.0
PO-10-900-24**	228	0.9	8.6	985	10.1
PO-10-900-24 pumped 100 hr at 250°C, U-37	243	0.6	0.7	975	8.0

*Calculated from $3.73 \times 10^{-3}(U_0\mu)^{1/2}$, where U_0 = hindered settling rate and μ is the viscosity of water (see Table 14.7 and ref. 11).

**See footnote *c*, Table 14.5.

15. FUEL PROCESSING

15.1 FISSION- AND CORROSION-PRODUCT CHEMISTRY

D. E. Ferguson E. O. Nurmi
R. W. Horton R. P. McNees
S. S. Kirslis S. Peterson

15.1.1 Rare Earths

(a) Praseodymium. – The effect of various solutes on the solubility of praseodymium sulfate was similar to that previously reported[1] for neodymium sulfate. In 0.02, 0.04, and 0.05 *m* UO_2SO_4 the praseodymium sulfate solubility was 160, 190, and 320 mg per kilogram of H_2O, respectively, when it was the only rare earth present. When other rare earths were present, so that praseodymium sulfate was only 32, 11, and 6% of the total rare earths, the praseodymium sulfate solubility in 0.02 *m* UO_2SO_4–0.005 *m* H_2SO_4 at 280°C decreased to 48, 16, and 13 mg per kilogram of H_2O, respectively. With other fission and corrosion products present, the solubility dropped further to 6 mg per kilogram of H_2O.

Extrapolation of these and similar data for cerium and neodymium indicates that some of the heavier rare earths, which will be produced in only very small amounts, will be scavenged from the reactor fuel by the other materials precipitating.

(b) Neodymium. – In loop A the apparent solubility of neodymium sulfate in simulated fuel solution (0.04 *m* UO_2SO_4) at 325°C was 65 to 70 mg per kilogram of H_2O. The amount of neodymium sulfate added above that required to maintain this concentration precipitated in the preheater; about 80% of the precipitate remained in the heater and filter, while 20% went to the underflow pot of the hydroclone attached to the loop. The loops were operated at 2000 psi and 300°C.

In quartz tubes the behavior of precipitating neodymium sulfate from 0.02 *m* UO_2SO_4–0.005 *m* H_2SO_4 in the presence of a Zircaloy-2-clad iron pin was not reproducible. In some cases a large part of the precipitating salt adhered to the metal surface, but in others it remained suspended in the solution as finely divided solids. In the latter case there was no marked tendency for the solids already formed to adhere to the hot metal surface. In these experiments the solution was heated by the metal pin, which was in turn heated by hysteresis effects (3000 kc).

15.1.2 Zirconium

In high-temperature loop studies with simulated fuel, containing fission and corrosion products approximately as expected in the HRT-CP, zirconium sulfate hydrolyzed to the oxide. Seventy-five per cent of the oxide accumulated in the preheater and the rest in the hydroclone underflow pot. Underflow-pot zirconium concentrations, of the order of 30,000 mg per kilogram of H_2O, were higher than the loop concentrations by factors of about 4000. Of the total weight of oxide and sulfate solids recovered, 45 and 75% were found in the preheater and filter and the rest in the underflow pot. When the hydroclone was cleaned at the end of the tests, about half the solids were removed from the underflow pot by draining; the rest adhered so tightly that vigorous agitation with rinse water was required for their removal.

15.1.3 Ruthenium

When 0.02 *m* UO_2SO_4–0.005 *m* H_2SO_4 solutions, containing 5 and 10 mg of ruthenium, as ruthenium sulfate, per kilogram of H_2O, were heated to 300°C in quartz tubes with air present, a black precipitate rapidly formed. The precipitate did not redissolve on cooling; it presumably was an oxide of tetravalent ruthenium. When the solutions were saturated with oxygen and an atmosphere of oxygen was maintained in the quartz tubes, no precipitate formed. In one case, in which an oxygenated solution contained a small fleck of cellulose, a small amount of ruthenium precipitated on the cellulose.

The ruthenium sulfate for these experiments was prepared by fuming ruthenium tetrachloride with sulfuric acid to dryness several times. The black solid formed was soluble in water, was hygroscopic, and corresponded in composition to $Ru(SO_4)_2 \cdot H_2SO_4$.

15.1.4 Molybdenum

The solubility, at room temperature, of molybdic acid in 0.02 *m* UO_2SO_4–0.005 *m* H_2SO_4 is less than 100 mg of molybdenum per kilogram of H_2O. At 265°C the solubility is between 300 and 400

[1] D. E. Ferguson *et al.*, *HRP Quar. Prog. Rep. Oct. 31, 1955*, ORNL-2004, p 186.

mg per kilogram of H_2O. When a uranyl sulfate solution containing 900 mg of molybdenum per kilogram of H_2O, as a molybdic acid slurry, was heated to 265°C, the flocculent particles rapidly agglomerated and then changed into a crystalline material of indefinite structure. This crystalline material was slowly transformed into massive crystals of definite, although unrecognizable, form. When cooled, the massive crystals disintegrated into a fine granular material. Precipitates heated to 250 to 300°C, but not held there long enough for the massive crystals to form, were granular when cooled, in contrast to their flocculent nature before being heated.

15.1.5 Iodine

Improved techniques increased the material balances usually obtained in iodine studies from 40–60% to 85–95%. With the new techniques the elemental/oxidized iodine ratio was shown to be 9/1 at 250°C and 6/1 at 300°C. The data were obtained in a stainless steel system. Preliminary results indicated that the presence of precipitating fission and corrosion products lowered these values markedly.

Laboratory studies[2] are under way to evaluate various possible solutions as a means of scrubbing iodine from a circulating gas stream of D_2O vapor and oxygen. Water shows an efficient absorption for a limited amount of iodine, but its capacity is so low that its use in a plant operation seems, at this time, inadvisable. A dilute solution of silver sulfate proved to be an efficient absorbing solution with a capacity, before any iodine broke through, probably in excess of 10% of the stoichiometric amount of iodine. Using such a solution at 300°C has the advantage of efficiently trapping iodine in a fixed form, which permits a simple concentration process, but the disadvantage of being a potential source of neutron poison for the reactor if any solution should be carried to the fuel system by the recirculating gas stream.

Engineering and design efforts were directed toward the development of a liquid jet ejector to serve the dual purpose of a single-stage contactor for pumped fuel solution and stripping gas (D_2O vapor and oxygen) and a high-capacity, low-head compressor for circulating the stripping gas through an iodine absorption cycle. A working model of such an ejector was fabricated and was installed in a 5-gpm, 1000-psi loop. Installation of heaters and other auxiliaries is in progress.

[2]This work done by Vitro and reported in more detail in KLX-10020.

15.2 REACTOR SOLIDS DISSOLUTION

Dissolution of the fission-product and corrosion-product solids expected from the operation of the HRT and collected in the chemical processing plant will be desirable in order to obviate the need for handling radioactive solids and to provide a representative sample. Since the exact composition of the solids to be encountered is not known, the dissolution of materials of various compositions was studied.

Solids simulating those expected from reactor operation, provided that excessive corrosion is not encountered, were prepared by heating, to 285°C, a uranyl sulfate solution containing various metal sulfates in the proportions expected from fission. These solids could be dissolved almost completely (>98%) by 70% HNO_3 containing 0.1% HF, provided that the solids had not been heated excessively while dry. The reactivity of solids heated to 300°C was less than that of unheated solids, while solids heated to 900°C were attacked only slightly (less than 10% dissolved) by the above treatment.

Solids simulating those expected in the case of extensive corrosion to the reactor system were prepared. These solids contained 90% stainless steel and Zircaloy-2 corrosion products and 10% mixed fission products. Larger amounts of HF in nitric acid were needed and dissolutions were slower and less complete than when only fission products were present. The adverse effect of heating the dry solids was again noted.

Stainless steel corrosion product solids obtained from the corrosion test loops have been studied. These solids differ from those prepared in the laboratory in that they have been "aged" for several hundred hours at the operating temperature of the loops. These solids showed extreme resistance to attack by HNO_3 and HNO_3-HF mixtures; better dissolution (70–83%) was obtained when HCl and HCl-HF mixtures were used. A solution of stannous chloride in concentrated HCl gave better dissolution (87%), and when followed by nitric acid, a total dissolution of 93% was obtained.

Sulfuric acid, 10.8 *M*, at 165 to 170°C has proved to be the best solvent thus far tried for various synthetic reactor solids. It is equally effective

for solids consisting of fission products only, for solids which contain as much as 90% by weight of Zircaloy-2 and stainless steel corrosion products, and for "aged" solids from the corrosion test loops. The efficiency of the sulfuric acid solution was not appreciably lowered by heating the solids to 300°C prior to dissolution. This same treatment sharply reduced the dissolving power of the other acids tested. In one test 0.5 g of a high ZrO_2 content sample which had been fired at 900°C for 16 hr was 70% dissolved in a single treatment with 30 ml of 10.8 *M* sulfuric acid.

15.3 TEST EQUIPMENT

15.3.1 Irradiation Bombs

A theoretical treatment indicated that, in the LITR with downflow cooling air, the plug closure at the bottom of a standard irradiation bomb would be the hottest part of the system. Temperatures measured in such a bomb in the LITR agreed with those theoretically predicted. A new irradiation bomb was designed which should allow the movable metal pin in the bomb to be the hottest part of the system.

15.3.2 Circulating Loop

The heat-transfer coefficient of the preheater in experimental loop A was dependent on the amount of deposited fission and corrosion products. The coefficient, based on internal surface area, dropped to as low as 200 $Btu/ft^2 \cdot hr \cdot °F$ at the end of the precipitation runs but consistently returned to about 400 $Btu/ft^2 \cdot hr \cdot °F$ after each cleanup.

16. PLUTONIUM-PRODUCER BLANKET PROCESSING

D. E. Ferguson E. O. Nurmi
J. M. Chilton R. E. Leuze
P. A. Haas R. H. Rainey

The study of plutonium chemistry during the last quarter continued[1] to include adsorption of plutonium on metals, concentration of PuO_2 by a hydroclone, effect of Li_2SO_4 on plutonium solubility, and in-pile studies.

16.1 ADSORPTION OF PLUTONIUM ON METALS

Since previous studies[1] had indicated that plutonium adsorption on Zircaloy-2 and on titanium from uranyl sulfate under simulated reactor conditions is essentially nonreversible, the rate of adsorption must be known for the amount of plutonium adsorbed per day on the walls of the reactor system to be calculated. Both plutonium concentration and temperature have large effects on the rate of plutonium adsorption.

From 1.26 *m* UO_2SO_4 containing 100 mg of plutonium per kilogram of H_2O, the rates of plutonium adsorption on Zircaloy-2 and on titanium at 250°C were 22 and 11 $\mu g/cm^2/hr$, respectively (Fig. 16.1). Several rates determined in the same equipment at 250°C but with 1.4 *m* UO_2SO_4 containing 3 to 6 mg of plutonium per kilogram of H_2O were not consistent but varied from 0.008 to 0.04 $\mu g/cm^2/hr$ for both titanium and Zircaloy-2. Based on these rates of adsorption, 0.3 to 1.4% of the plutonium produced in a two-region reactor would adsorb on the metal walls. Since the latter conditions are expected in the blanket of the plutonium producer, emphasis will be placed on a more thorough study under these conditions.

The adsorption rate was also affected by temperature. The rate of plutonium adsorption at 150°C from 1.4 *m* UO_2SO_4 containing 4 to 6 mg of plutonium per kilogram of H_2O was 0.008 $\mu g/cm^2/hr$ on titanium and 0.012 $\mu g/cm^2/hr$ on Zircaloy-2. Adsorption rates at 80°C from 1.4 *m* UO_2SO_4 containing 13 mg of plutonium per kilogram of H_2O were only 9×10^{-5} $\mu g/cm^2/hr$ on titanium and 2×10^{-5} $\mu g/cm^2/hr$ on Zircaloy-2 (Fig. 16.2). As can be noted, at 150 and 250°C, plutonium adsorption was greater on Zircaloy-2 than on titanium, but at 80°C it was less.

[1]D. E. Ferguson, R. E. Leuze, and R. H. Rainey, *HRP Quar. Prog. Rep. Oct. 31, 1955*, ORNL-2004, p 189.

The nature of plutonium adsorption at room temperature was different from that at elevated temperatures. At room temperature, titanium and Zircaloy-2 in contact with uranyl sulfate solutions exhibited equilibrium adsorption values that depended on the plutonium concentration in solution. At 80°C, metal in contact with 1.4 *m* UO_2SO_4 containing 13 mg of plutonium per kilogram of H_2O showed no indication of approaching an equilibrium value in 1000 hr (Fig. 16.2). At 23°C, plutonium adsorption on Zircaloy-2 from 1.4 *m* UO_2SO_4 containing 12, 60, and 110 mg of plutonium per kilogram of H_2O reached equilibrium values of 0.007, 0.048, and 0.18 $\mu g/cm^2$, respectively, but plutonium adsorption on titanium from these same solutions reached equilibrium values of 0.007, 0.12, and 0.31 $\mu g/cm^2$, respectively. The time required to reach equilibrium was dependent on the plutonium concentration. For uranyl sulfate solutions

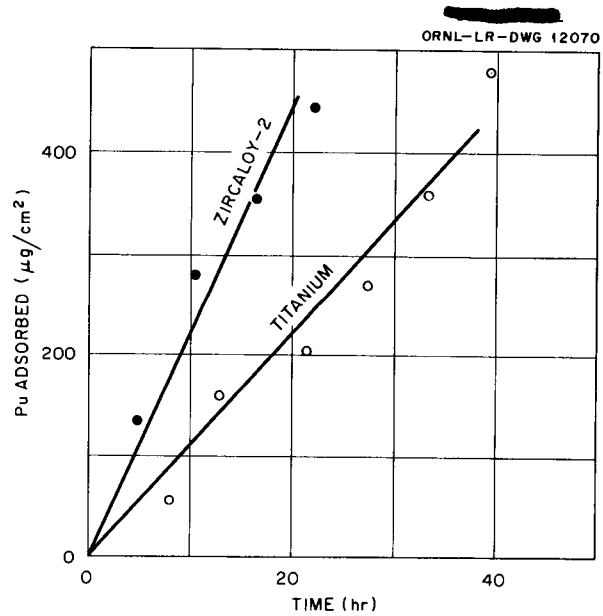

Fig. 16.1. Rate of Plutonium Adsorption at 250°C on Zircaloy-2 and Titanium from 1.26 *m* UO_2SO_4 Solution Containing 100 mg of Plutonium per kilogram of H_2O.

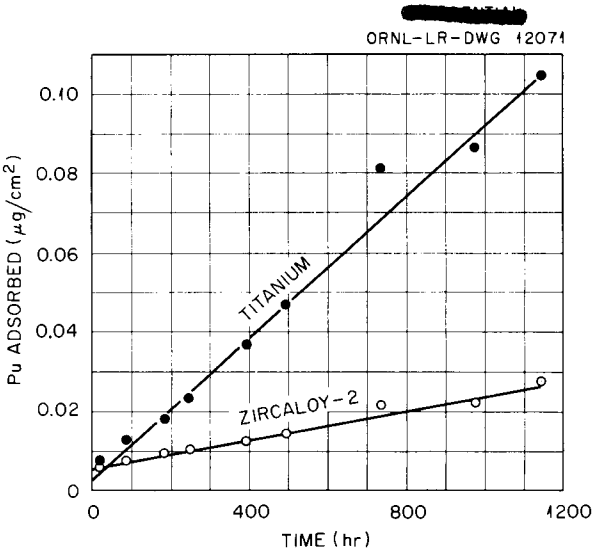

Fig. 16.2. Rate of Plutonium Adsorption at 80°C on Zircaloy-2 and Titanium from 1.4 *m* UO_2SO_4 Solution Containing 13 mg of Plutonium per kilogram of H_2O.

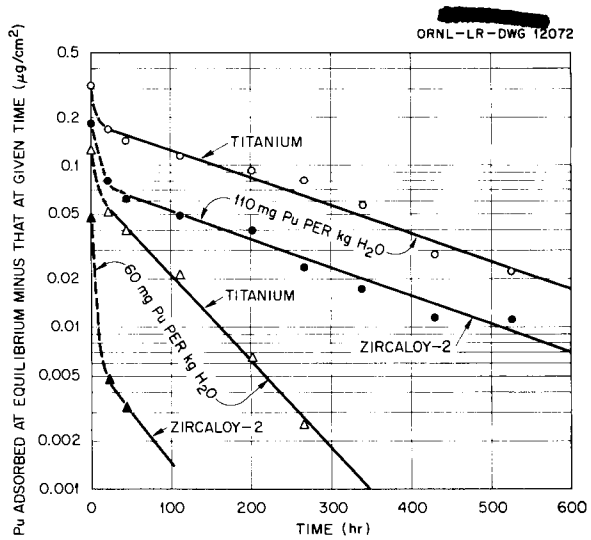

Fig. 16.3. Rate of Plutonium Adsorption at 23°C on Titanium and Zircaloy-2 from 1.4 *m* UO_2SO_4 Solution Containing 60 and 110 mg of Plutonium per kilogram of H_2O.

containing 12, 60, and 110 mg of plutonium per kilogram of H_2O, the times required to reach equilibrium were 22, 100, and 500 hr, respectively. It can be seen in Fig. 16.3 that after an initial rapid adsorption the plutonium adsorption behaved as a first-order reaction.

X-ray diffraction analysis of plutonium adsorbed at room temperature gave no indication of PuO_2, as was found in adsorption at 250°C. Uranyl sulfate solutions, containing *no* plutonium, partially desorbed plutonium that had been adsorbed previously at room temperature but did not desorb plutonium previously adsorbed at 250°C.

16.2 SEPARATION OF PuO_2 BY A HYDROCLONE

Studies of the concentration of PuO_2 in water slurries at room temperature by centrifugation in a ¼-in.-dia hydroclone with a 35-ml underflow pot were encouraging; however, material balances were consistently low. When plutonium slurries of about 1 liter were circulated through the hydroclone at 0.2 gpm until steady-state conditions were reached, the concentration factor in seven tests varied from 2.6 to 8.8, and material balances were 40 to 72%. Greater concentration factors can be expected at 250°C. The PuO_2 used in these experiments had been precipitated from uranyl sulfate at 250°C, centrifuged, washed free of uranyl sulfate, and reslurried in water.

For comparison, the concentration of ThO_2 (with a particle-size distribution of 100 wt % less than 26 μ, 50 wt % less than 7 μ, and 18 wt % less than 0.6 μ) was determined under the same conditions. In 14 tests, concentration factors varied from 21 to 32, and material balances were 67 to 85%.

16.3 IN-PILE CHEMISTRY OF PLUTONIUM AND NEPTUNIUM

When a 1.4 *m* UO_2SO_4 (0.03% U^{235}) solution containing no copper catalyst was irradiated in the LITR at 200 to 250°C, there was no significant buildup of pressure as a result of radiolytic gas formation; nor was there evidence of radiolytic gas buildup when 1.4 *m* UO_2SO_4 (0.3% U^{235}) was irradiated at 250°C. Since an overpressure of hydrogen and oxygen is required to obtain the proper reduction-oxidation conditions for studying plutonium chemistry, the use of slightly enriched uranium for in-pile studies will be investigated.

16.4 SOLUBILITY OF PLUTONIUM IN URANYL SULFATE–LITHIUM SULFATE SOLUTIONS

The solubility of tetravalent plutonium in 1.3 *m* UO_2SO_4–1.3 *m* Li_2SO_4 solutions under 50 psi H_2

and 25 psi O_2 at 250°C was 2 to 3 mg per kilogram of H_2O when determined in gold tubes and was 5 to 6 mg per kilogram of H_2O when determined in pyrex tubes. A control test with 1.3 *m* UO_2SO_4 solution in pyrex showed the previously determined solubility of 3 mg per kilogram of H_2O. Apparently the addition of lithium sulfate approximately doubled the solubility of Pu(IV).

When a solution containing 4.0 *m* UO_2SO_4, 4.0 *m* Li_2SO_4, and 4.77 g of Pu(IV) per kilogram of H_2O was heated for 12 hr under air in a pyrex tube, only 7.8 mg of Pu(IV) per kilogram of H_2O remained in solution. When a fivefold excess of chromate was added to the feed solution at room temperature, the plutonium was oxidized to Pu(VI). When this solution was heated at 250°C for 12 hr, 415 mg of Pu(VI) per kilogram of H_2O remained in solution. Both tests were made in a sealed, pyrex glass tube with an air overpressure.

Further experiments are planned for studying plutonium valence and solubility in these solutions in the presence of chromium, oxygen, and hydrogen.

16.5 TEST EQUIPMENT

16.5.1 Loop T-1

Shop fabrication of loop T-1, which is to be used for plutonium-producer-reactor equipment development studies, was completed; field installation is expected to be completed by February 1. All components that contact high-temperature fuel, except the labyrinth backup plate and a small part of the scroll case in the pump, are titanium. The low-temperature parts of this loop, including valves and the back of the pump, are type 347 stainless steel.

16.5.2 Loop P-1

Loop P-1 for the out-of-pile study of the chemical processing required for the removal of plutonium from concentrated uranyl sulfate solutions (300 g of uranium per kilogram of H_2O) will be constructed of type 347 stainless steel. This loop will use a Westinghouse A-150 canned-rotor pump with the simplest piping configuration possible for installation in a pressure tank of about 3 ft in diameter and 5 ft in height. The large pump will give heating without external heaters and will thus avoid possible hot-wall precipitation.

17. EQUIPMENT DECONTAMINATION

D. E. Ferguson
R. D. Baybarz R. E. Leuze

The object of the equipment-decontamination program is to develop methods for removing fission products and plutonium deposited on metal surfaces under reactor conditions. Strong inorganic reducing agents were tested for removal of oxide film and plutonium from type 347 stainless steel, titanium, and Zircaloy-2.

17.1 OXIDE SCALE REMOVAL

Strong reducing agents such as chromous sulfate, titanous chloride, stannous chloride, and nascent hydrogen effectively removed the oxide film deposited on type 347 stainless steel by 1.4 *m* UO_2SO_4 at 250°C. A solution of chromous sulfate in dilute sulfuric acid appears to be the one best suited for decontamination of homogeneous reactor and process equipment, since it converts the oxide to a soluble form and does not add foreign materials to the reactor system.

Chromous sulfate solutions were prepared by reducing $CrK(SO_4)_2$ solutions with zinc amalgam. A solution containing 0.4 *M* $CrSO_4$–0.2 *M* K_2SO_4–1.0 *M* H_2SO_4 (under CO_2) at 87°C effectively reduced and dissolved the oxide corrosion film from type 347 stainless steel in 2 hr. At 23°C, the oxide film was converted to a loosely held oxide in 4 hr and was completely dissolved in 24 hr.

Oxide films deposited on titanium and Zircaloy-2 by uranyl sulfate at 250°C are more difficult to remove than the oxides on type 347 stainless steel. Several types of oxide films were observed on titanium, varying from a heavy golden oxide to a thin bluish coloration. The heavy golden oxide film was removed from titanium by 0.4 *M* $CrSO_4$–0.2 *M* K_2SO_4–1.0 *M* H_2SO_4 (under CO_2) at 87°C in 10 hr. No effort has yet been made to remove the thin bluish film.

17.2 PLUTONIUM REMOVAL FROM METAL WALLS

It may be necessary to remove plutonium periodically from the walls of the plutonium producer blanket system, since laboratory tests[1] indicate that plutonium continues to be adsorbed indefinitely under operating conditions. Plutonium has been effectively removed, from the oxide film deposited on type 347 stainless steel by UO_2SO_4 solutions at 250°C, by three different solutions: 3.0 *M* HNO_3–0.1 *M* $(NH_4)_2Ce(NO_3)_6$; 3.0 *M* HNO_3–0.0025 *M* HF; and 0.4 *M* $CrSO_4$–0.2 *M* K_2SO_4–1.0 *M* H_2SO_4 under CO_2. A solution containing 0.2 *M* $CrSO_4$–0.1 *M* K_2SO_4–0.5 *M* H_2SO_4 was not very effective as a removal agent. Of the three solutions removing plutonium effectively, the 0.4 *M* $CrSO_4$ solution appears to be the most applicable for homogeneous reactor and process equipment, since it completely dissolves the oxide film and does not add foreign materials to the reactor system. This solution was also effective in removing plutonium from titanium and Zircaloy-2 oxide films.

With stainless steel, the nitric acid–cerate solution at 87°C gave a plutonium decontamination factor of 8×10^2 in 4 hr and 2×10^3 in 24 hr. The nitric acid–hydrofluoric acid solution at 71°C gave a plutonium decontamination factor of 3×10^3 in 24 hr. The 0.4 *M* $CrSO_4$–0.2 *M* K_2SO_4–1.0 *M* H_2SO_4 solution at 87°C (under a CO_2 pressure of 5 psig) gave plutonium removal factors from type 347 stainless steel of 1.4×10^3 in 3 hr and 6×10^4 in 7 hr, from Zircaloy-2 of 1.9×10^3 in 3 hr, and from titanium of 1.7×10^3 in 4 hr. The solution containing 0.2 *M* $CrSO_4$–0.1 *M* K_2SO_4–0.5 *M* H_2SO_4 in 7 hr removed only 60% of the plutonium from type 347 stainless steel at 87°C and only 32% at 23°C.

Neither the nitric acid–cerate nor the nitric acid–hydrofluoric acid solutions dissolved the iron oxide corrosion film, but they both caused considerable flaking of the film. The chromous sulfate solution reduced the iron oxide films to a soluble form.

Scouting tests showed that 3 *M* HNO_3–0.1 *M* $(NH_4)_2Ce(NO_3)_6$ is moderately corrosive to type 347 stainless steel. Corrosion rates determined by weight loss were 50 mpy at 23°C and 75 mpy at 87°C. However, there was evidence of pitting and intergranular corrosion. Titanium and Zircaloy-2 corrosion rates were low in this solution: 1 and 0.4 mpy, respectively, at 23°C and 1.4 and 0.6 mpy at 87°C. Corrosion rates for type 347 stainless steel, titanium, and Zircaloy-2 in 0.4 *M* $CrSO_4$–0.2 *M* K_2SO_4–1.0 *M* H_2SO_4 at 87°C were 10, 7, and 2 mpy, respectively.

[1] D. E. Ferguson, R. E. Leuze, and R. H. Rainey, *HRP Quar. Prog. Rep. Oct. 31, 1955*, ORNL-2004, p 189.

Part VI

SUPPORTING CHEMICAL RESEARCH

E. H. Taylor

18. AQUEOUS SYSTEMS AT ELEVATED TEMPERATURES

C. H. Secoy

F. E. Clark
J. S. Gill
F. J. Loprest
W. L. Marshall
D. M. Richardson
R. Slusher
F. H. Sweeton

18.1 ALKALI METAL CARBONATE–URANIUM TRIOXIDE SYSTEMS

W. L. Marshall F. J. Loprest

The investigation of the system lithium oxide–uranium trioxide–carbon dioxide–water was continued during the quarter. Experimental methods were the same as those described previously,[1] except for the analytical technique for determining lithium, which consisted in removing the uranium and carbonate quantitatively by means of Dowex A-1 ion exchange resin in the hydroxide form and determining the eluent lithium hydroxide by acid-base titration. This method was found to be considerably more precise than the flame spectrophotometric method used previously.

Seven new experiments were completed which were designed to fix with greater certainty the liquid phase solubility surfaces when lithium carbonate is the stable solid phase and when a lithium uranyl carbonate complex is the stable solid phase. These experiments confirmed the finding that, at 250°C and with 1000 to 2000 psi total pressure, the two solubility surfaces are very close to each other and the suspicion that maintenance of an unsaturated solution with more than about 10 g of uranium per liter would be difficult (see Fig. 18.1).

Additional experiments were performed on that portion of the system in which Li_2CO_3 is the solid phase. These experiments involved the measurement of the solubility of Li_2CO_3 in water and in UO_3-CO_2-H_2O solutions as a function of temperature and carbon dioxide pressure. A study of the data from these experiments and from previous experiments disclosed the following relationships:

1. A straight line is obtained if the molality of lithium in the saturated solution is plotted as a function of the molality of uranium at a fixed carbon dioxide partial pressure. Furthermore, the family of lines obtained by plotting several such isobars all have the same slope equal to 3.37 at 250°C (Fig. 18.2). These isobars terminate by intersection with the isobaric invariant, which is also approximately linear with a slope of about 4 at 250°C.

2. From the data for the solubility of $LiHCO_3$ in water, plots of the logarithm of carbon dioxide pressure as a function of the logarithm of the lithium concentration, expressed as molality of $LiHCO_3$, at each of several temperatures yield parallel straight lines with a slope of 4 (Fig. 18.3). The linearity does not hold at low CO_2 pressures, presumably because of the hydrolysis of the carbonate ion. Thus the quotient, m^4/P_{CO_2}, is a constant at a constant temperature. This relation follows readily from the solubility product constant of Li_2CO_3, the carbonate-bicarbonate equilibrium constant, and Henry's law constant for CO_2 if it is assumed that the lithium ion concentration and

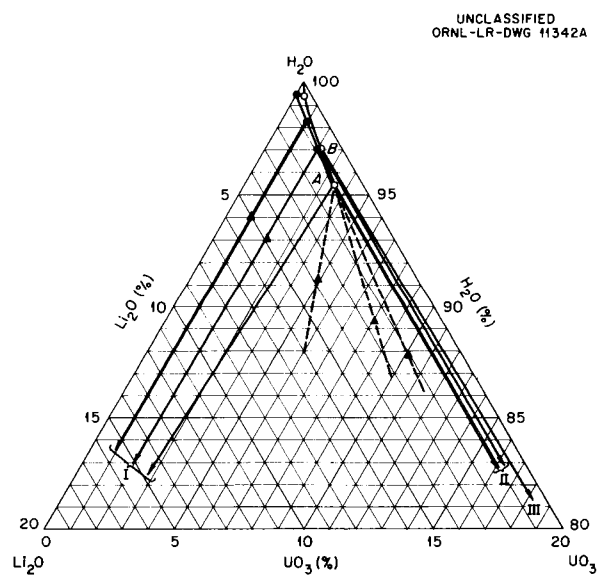

Fig. 18.1. The System Li_2O-UO_3-CO_2-H_2O at 250°C and 1500 psi Total Pressure, Where $P_{total} = P_{H_2O} + P_{CO_2}$. Jänecke projection; A, B = invariant points; I = Li_2CO_3 solid; II, III = lithium-uranium solids.

[1] F. J. Loprest, W. L. Marshall, and C. H. Secoy, *Chem. Semiann. Prog. Rep.* Oct. 10, 1955, ORNL-1940, p 70–79.

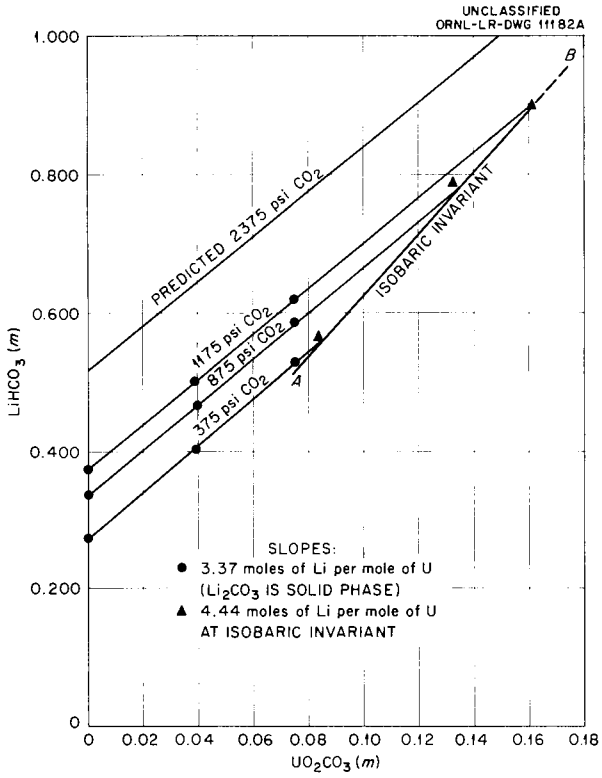

Fig. 18.2. Variation of Li_2CO_3 Solubility (Expressed as Molality of $LiHCO_3$) with UO_2CO_3 Concentration at Constant CO_2 Pressure (250°C).

the bicarbonate ion concentration are equal. Figure 18.4 shows the dependence of the quotient, $m^4_{LiHCO_3}/P_{CO_2}$ (called K_6), on temperature.

From these observations the principal ionic species existing in solution may be postulated to be Li^+, HCO_3^-, $UO_2(HCO_3)(CO_3)_2^{3-}$, and $UO_2(HCO_3)_2(CO_3)_2^{4-}$. The presence of these ions would account for all the observed facts, and their existence does not seem to be unreasonable.

Exploratory studies were made with several cations other than lithium. The results indicated a negligible solubility of uranium in the thallous, magnesium, and ammonium systems at 250°C. The solid phases appear to be uranates in these cases rather than carbonates, and, presumably, much higher CO_2 pressures would be required to attain an appreciable uranium solubility. In the rubidium system, however, solutions containing about 2.5% UO_3 at a rubidium-to-uranium mole ratio of about 15 were obtained at 250°C and total pressures between 1200 and 1900 psi.

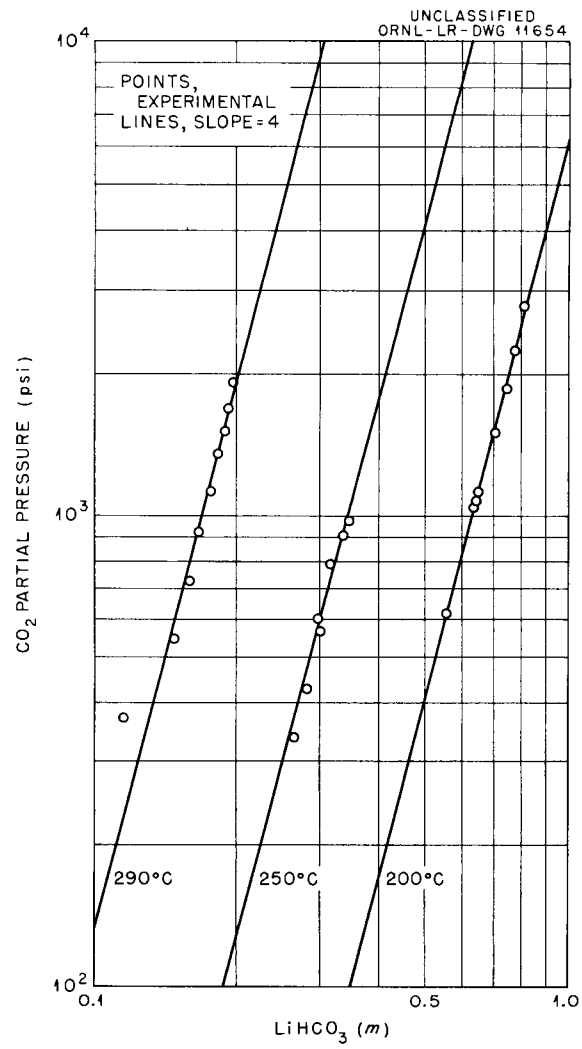

Fig. 18.3. Solubility of Li_2CO_3 as a Function of CO_2 Pressure.

18.2 THE QUATERNARY SYSTEMS $CuO-UO_3-SO_3-H_2O$ AND $NiO-UO_3-SO_3-H_2O$

F. E. Clark J. S. Gill
R. Slusher

The 100°C isotherm for the base (CuO and/or UO_3) saturated region of the system $CuO-UO_3-SO_3-H_2O$ was completed. The identity and range of stable existence for all solid phases which occur were established, with the possible exception of those appearing from very dilute solutions (low SO_3 content). The liquidus surface was quantitatively defined, thus making possible the pre-

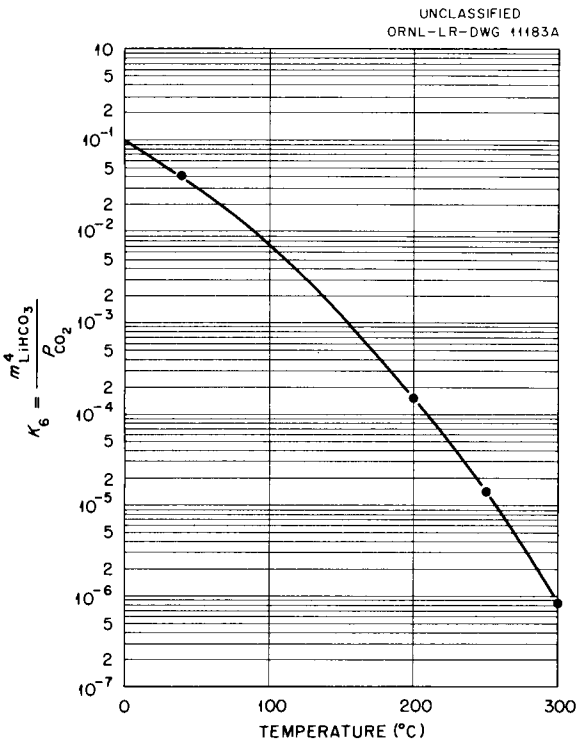

Fig. 18.4. Variation of K_6 with Temperature.

diction of any precipitation phenomena if CuO or UO_3 or any mixture of the two is added to a homogeneous unsaturated solution at this temperature. Details of the work and the experimental data will appear in a forthcoming ORNL report.

The determination of higher temperature isotherms was postponed in deference to a nonisothermal exploration of the very dilute solution region of more immediate interest to the reactor project. This work has not advanced sufficiently to permit any general conclusions to be made.

A study of the base-saturated region in the system NiO-UO_3-SO_3-H_2O at 100°C has continued but has not yielded unambiguous data. Combined analytic, microscopic, and diffraction studies of solid phases indicated the probable existence of several complex nickel-uranyl basic sulfates or several hydrates of such a complex. A reasonably pure sample of any one of these has not been obtained. It would appear that the probability of obtaining a complete unequivocal phase diagram at 100°C is slight, since various techniques have been tried without success.

18.3 STABILIZATION OF ThO_2 Sols – Sol E

F. H. Sweeton

A general study of the stabilization of ThO_2 sols was started. One sample, designated as sol E, was prepared and some of its properties were determined.

18.3.1 Preparation

The method used was, in general, that outlined by Szilard.[2] Hydrous ThO_2 was precipitated by the addition of an excess of a solution of NH_4OH to a solution of $Th(NO_3)_4$. The precipitate was washed by several decantations in order to remove the resulting NH_4NO_3 and the excess NH_4OH. Some of the hydrous ThO_2 suspension was heated to boiling during two of the decantations in an effort to get more effective removal of the impurities. Peptization was carried out by adding this washed hydrous ThO_2, in steps, to a hot solution of $Th(NO_3)_4$. After each addition the hydrous oxide slurry went into suspension within a few minutes, giving a sol that looked like water except for a slight amount of opalescence.

18.3.2 Composition

Analysis of sol E by the Analytical Chemistry Division showed that its total concentration of thorium was 2.5_0 *M* (moles per liter) and that the total concentration of nitrate radical was 0.9_7 *M*. This concentration of nitrate was higher by approximately 0.4_1 *M* than that equivalent to the $Th(NO_3)_4$ used for peptization; the difference was supposedly due to adsorption of nitrate radical on the washed hydrous ThO_2 used to prepare the sol. The total concentration of NH_3, according to analyses, was below 0.006 *M*, showing the effectiveness with which the hydrous ThO_2 used in preparing the sol was washed.

18.3.3 Description

The pH of the sol appeared to be about 3.3, but theoretical problems involved in measuring such a sol make this value uncertain by 0.5 or possibly more. An x-ray analysis was performed (by the Metallurgy Division) directly on the sol in its liquid state; ThO_2 was the only crystalline material found. The width of the ThO_2 lines corresponded to an average crystallite size of 56 Å, with a relative uncertainty of about 5 Å and an absolute

[2] B. Szilard, *J. chim. phys.* 5, 488–494 (1907).

uncertainty several times as large. Electron micrographs prepared by the Analytical Chemistry Division showed that the sol particles were small, and gave an indication that the average particle size was probably in the range of 50 to 100 Å. The specific gravity of the sol was found to be 1.64_5 at room temperature (25°C). The viscosity of sol E relative to water was found to be 1.4_8 at 25°C.

18.3.4 Properties

It was found that when the sol was diluted with water to one-hundredth its original concentration it could be precipitated by the addition of an equal volume of 0.003_5 *M* Na_2SO_4 solution or of 0.007_5 *M* $(NH_4)_2SO_4$. In the first case analyses showed that not all of the thorium was precipitated, the soluble amount corresponding within experimental error to the thorium nitrate used in preparing the sol. With $(NH_4)_2SO_4$, however, all the thorium in the sol appeared to be precipitated.

In order to study the thermal stability of sol E as a function of the addition of further $Th(NO_3)_4$, several portions of the sol were diluted to two-thirds their original concentrations by the addition of thorium nitrate solutions of various concentrations. The samples were then sealed in small pyrex glass tubes and were heated at a rate of about 6°C per minute in an apparatus designed and assembled by W. L. Marshall and described elsewhere.[3] The temperature was noted at which each sample started to turn yellow by transmitted light. These transitions occurred very sharply; within an interval of only 3 to 5°C the color would change from clear to yellow, then to dark brown, and so on until the sample was opaque. Figure 18.5 gives the results of these tests. It can be seen that the addition of $Th(NO_3)_4$ reduced the thermal stability of the sol throughout the range covered.

18.3.5 Discussion

That the so-called "sol E" is actually a true sol is believed to be firmly established. The sol has the slight opalescence to be expected of a sol with particles that are considerably smaller than a wave length of light, and the x-ray analysis proves the presence of crystalline ThO_2. From x-ray data and electron micrography it appears fairly well established that the individual sol

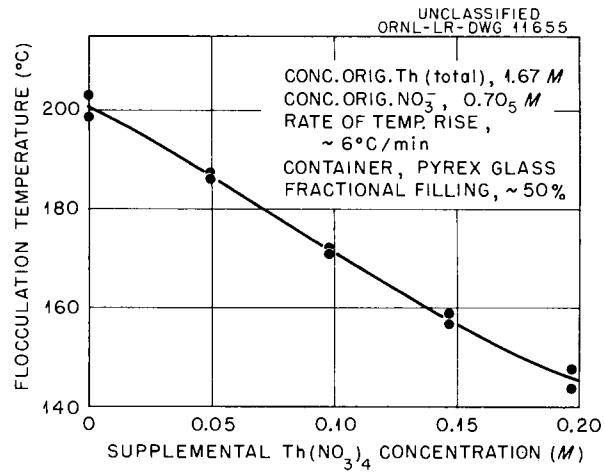

Fig. 18.5. Thermal Stability of Sol E with Supplemental $Th(NO_3)_4$.

particles contained, at most, only a relatively few crystallites. The relative viscosity of this sol (1.4_8) is definitely less than that of several preparations described by Dhar and Mittra,[4] who report sols that were similar but with lower concentrations of total thorium and of nitrate radical.

The fact that Na_2SO_4 and $(NH_4)_2SO_4$ precipitated the thorium in the sol to varying degrees demonstrates the specificity of the reactions of the sol. Although the Na_2SO_4 appeared to precipitate only that fraction of total thorium corresponding to the hydrous ThO_2 used in preparing the sol, it seems best to regard this correspondence as coincidence until more such data are available.

The thermal stability of this particular sol was found to be far below that necessary for a reactor blanket. The method used in the test is thought to be general for studying sol stability; it has the advantage that the more stable sols are tested at higher temperatures and thus closer to the desired operating conditions. Since the further addition of $Th(NO_3)_4$ to this sol decreased its stability, sols with a smaller original concentration of $Th(NO_3)_4$ might be expected to be more stable.

The fact that this sol will repeptize after being slightly flocculated and recooled is of interest because it emphasizes the admitted incompleteness of the theory of stabilization as outlined by

[3] W. L. Marshall, H. W. Wright, and C. H. Secoy, *J. Chem. Educ.* **31**, 34 (1954).

[4] N. R. Dhar and R. N. Mittra, *Kolloid-Z.* **71**, 172–6 (1935).

Verwey and Overbeek[5] for application to flocculated colloid systems.

Work will continue on determining the properties of this particular sol preparation. The preparation of other sols having lower concentrations of $Th(NO_3)_4$ will be attempted.

18.4 ADSORPTION OF H_2O BY ThO_2 AT ELEVATED TEMPERATURES

D. M. Richardson

The experimental method employed to measure the adsorption of water by thorium dioxide was described in previous reports.[6,7] Tentative isotherms from 260 to 360°C can be drawn based on the present experimental data. There is no evidence that a hydrate ($ThO_2 \cdot xH_2O$) exists. The slow rise in pressure observed at temperatures above 300°C is attributed to small amounts of CO_2 and H_2O present in the thoria studied. In the volumetric method used, these impurities would also have the effect of lowering the apparent amount of H_2O adsorbed. The present status of this study is reported in greater detail elsewhere.[8]

[5] E. J. W. Verwey and J. T. G. Overbeek, *Theory of the Stability of Lyophobic Colloids*, Elsevier, New York, 1948.

[6] D. M. Richardson, *HRP Quar. Prog. Rep. April 30, 1955*, ORNL-1895, p 195–196.

[7] D. M. Richardson, *HRP Quar. Prog. Rep. July 31, 1955*, ORNL-1943, p 244–245.

[8] D. M. Richardson, *Adsorption of H_2O by ThO_2 at High Temperatures*, ORNL CF-56-1-109 (Jan. 20, 1956).

19. ADSORPTION ON INORGANIC MATERIALS

K. A. Kraus

T. A. Carlson J. S. Johnson
D. J. Coombe H. O. Phillips

19.1 CATION-EXCHANGE PROPERTIES OF ZIRCONIUM TUNGSTATE

19.1.1 Adsorptive Properties as a Function of Drying Temperature

The effect of drying or firing temperature on the adsorbability of cesium (tracer) by zirconium tungstate was investigated. The material was prepared in the usual way by precipitation of Zr(IV) with a large excess of sodium tungstate solution previously adjusted to pH 1.2. After being dried at room temperature, the material was washed with 0.2 *M* HCl, rewashed, dried, and fired overnight at various temperatures up to 950°C. The room-temperature-dried material had a distribution coefficient $D \approx 60$ for cesium tracer in 0.1 *M* NH_4Cl. When the material was fired at temperatures above about 110°C, the values of D became first negligibly small but became appreciable again ($D \approx 20$) for firing temperatures above about 600°C. The decrease in distribution coefficients with firing temperature was accompanied by a decrease in uptake of cesium, which became less than about 1% of the uptake of room-temperature-dried material (0.45 mole of cesium per kilogram) when firing was carried out above about 110°C. Materials fired above about 600°C showed cesium uptake amounting to about 2% of the uptake of room-temperature-dried material.

19.1.2 Acid-Base Titrations: Uptake of Cesium and Stability as a Function of pH

It had been observed earlier[1] that the uptake of cesium on zirconium tungstate is dependent on the acidity of the solutions; this behavior is reminiscent of weak-acid cation exchangers. Acid-base titrations of the materials were therefore carried out in an attempt to estimate the "capacity" for cations. At the same time, the stability of the tungstate was investigated, since loss of tungstate from the precipitate was expected at high pH. Zirconium tungstate was prepared in the usual manner, except that it contained W^{185} to permit radiometric determination of dissolution of tungstate in the various media. Small portions of the tungstate were treated with varying amounts of ammonia solutions in 1 *M* NH_4Cl. After ½ hr of shaking, the pH was measured, dissolved tungstate in the solution was determined radiometrically, and cesium uptake was determined by repeated equilibration with 0.1 *M* CsCl solutions containing tracer Cs^{134}. The results are summarized in Fig. 19.1. It may be noticed that loss of tungstate is essentially negligible up to about pH 6 but becomes relatively serious at higher pH. Further, cesium uptake, which is about 0.65 mole per kilogram near pH 2, rises considerably with

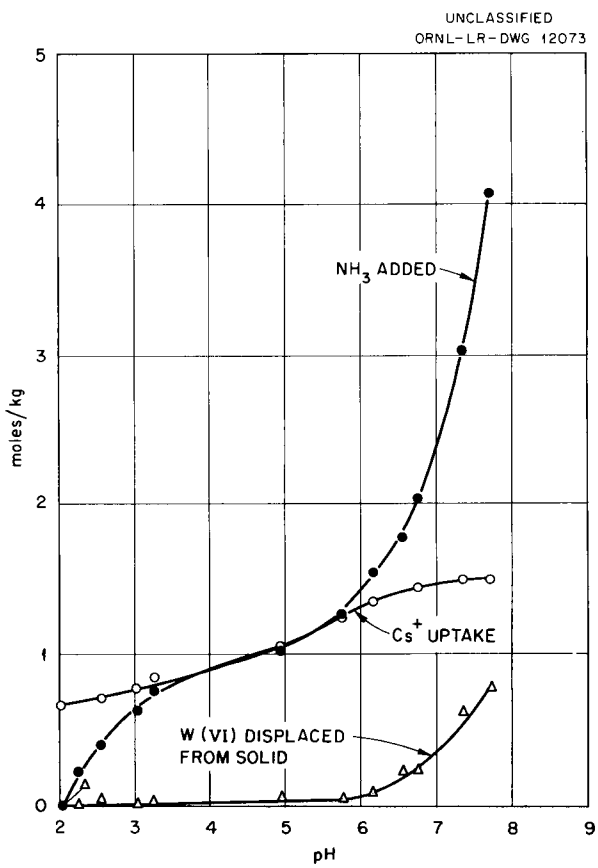

Fig. 19.1. Zirconium Tungstate – Acid-Base Titration and Cs^+ Uptake.

[1] K. A. Kraus *et al.*, *HRP Quar. Prog. Rep. Oct. 31, 1955*, ORNL-2004, p 208–212.

increasing pH and reaches about 1.5 moles per kilogram near pH 7. Since loss of tungstate appears at about the same pH where cesium uptake levels off, the capacity of the material is presumably larger than the maximum uptake determined here, although present data do not permit unambiguous determination of this capacity.

19.2 CATION-EXCHANGE PROPERTIES OF ZIRCONIUM PHOSPHATE

19.2.1 Stability in a Number of Media

The stability of zirconium phosphate was determined in a number of acidic and basic media by the use of a radiometric method of analysis. In the preparation, a solution of Zr(IV) was added to 3.4 *M* H_3PO_4 containing P^{32}. The precipitate was dried at 120°C overnight, washed with 1 *M* HCl, with water, and again dried at room temperature. It contained 6.1 moles of phosphate per kilogram and a PO_4^{3-}/Zr(IV) ratio of about 2.

Portions of this material were shaken in various media for usually 21 to 24 hr, and the supernatant was analyzed for phosphorus. Essentially negligible attack of the solid occurred in the following media: 1, 4, and 12 *M* HCl; 1, 4, and 15.7 *M* HNO_3; 1, 4, and 17.4 *M* HOAc. In these media less than 2% of the phosphate activity appeared in solution. Although this might imply some attack, it could also arise from insufficient washing of the original phosphate. Similarly, little attack was shown in 1 and 4 *M* H_2SO_4, although severe attack occurred in 18 *M* H_2SO_4 (33% of phosphate appeared in solution).

Severe attack occurred in fluoride solutions. The solid lost 62% of the phosphate in 1 *M* KF, 1 *M* HF, and 1 *M* HF – 1 *M* HCl. In 5 and 10 *M* KF essentially all the phosphate was lost from the solid. Even in 0.1 *M* HF almost 10% of the phosphate was lost, although in this case the fluoride-to-phosphate ratio was only 0.2.

The phosphate was found to be surprisingly stable in ammonia solutions, with phosphate losses of 2, 5, and 7% occurring in 0.1, 1, and 3.8 *M* NH_3 solutions. Severe phosphate losses occurred in carbonate solutions (50% in 1 *M* Na_2CO_3) and sodium hydroxide (50 to 90% in 1 *M* NaOH). Only moderate loss occurred in bicarbonate solutions (less than 10% in 1 *M* $NaHCO_3$).

19.2.2 Acid-Base Titrations: Cation Uptake and Stability as a Function of pH

In an attempt to evaluate the inherent cation-exchange capacity of zirconium phosphate and its stability with respect to loss of phosphate as a function of pH, acid-base titrations of the zirconium phosphate, containing tracer P^{32}, were carried out. Approximately 2½ moles of sodium hydroxide could be added per kilogram of the phosphate before pH 4 was reached in 1 *M* NaCl solutions. At this pH, loss of phosphate was essentially negligible (less than 2%). At higher pH, loss of phosphate became serious: At pH 7 about 0.9 mole of phosphate was liberated per kilogram of solid; this value rose essentially linearly with pH to 3.1 moles PO_4^{3-} per kilogram at pH 11. This latter value represents more than 50% of the phosphate in the solid. It thus appears that a large fraction of the phosphate can readily be displaced by hydroxide ions in what might be termed a typical anion-exchange manner, or metathesis.

19.3 HYDROUS ZIRCONIUM OXIDE

19.3.1 Apparent Solubility in a Number of Media

The stability of hydrous zirconium oxide, which earlier had been shown[1] to have interesting anion-exchange properties, was determined in a number of media. The hydrous oxide, containing Zr^{95} tracer, was prepared in the usual manner by ammonia precipitation and dried at 200°C overnight. Apparent solubilities were determined radiometrically by counting the supernatant after 27 hr of shaking. Surprisingly high "solubilities" were found in acidic solutions. They were: 18, 32, and 63% in 1, 2, and 4 *M* H_2SO_4; 4, 8, and 17% in 1, 2, and 4 *M* HCl; and 4, 6, and 11% in 1, 2, and 4 *M* HNO_3. At present it is not clear whether these data represent dispersions of the solid or actual dissolution. Stability in basic solutions was excellent, less than 0.05% "dissolving" in 1 *M* NaOH.

19.3.2 Stability in Fluoride Solutions: Fluoride Uptake

In order to evaluate the usefulness of hydrous zirconium oxide as an adsorbent for fluoride, the preparation containing tracer Zr^{95} was treated with various HF and KF solutions. The results,

summarized in Table 19.1, indicate that the material is reasonably stable in HF solution, provided that the amount of fluoride added per kilogram of solid remains moderate. On the other hand, excellent stability was found for the oxide in KF solutions even at very large ratios of fluoride to zirconium oxide.

TABLE 19.1. STABILITY OF HYDROUS ZIRCONIUM OXIDE (FIRING TEMPERATURE 200°C) IN FLUORIDE SOLUTIONS

Medium	F^- (moles/kg)	Time (hr)	% Dissolved
0.1 *M* HF	1.16	0.25	2.2
0.1 *M* HF	1.01	1.0	1.8
0.1 *M* HF	0.83	20	2.7
0.1 *M* HF	0.72	44	3.2
1 *M* HF	12	0.25	34
1 *M* HF	10.4	1.0	38
0.5 *M* KF	4.24	8	0.05
1.0 *M* KF	8.5	16	0.05
2.5 *M* KF	21	16	0.05

Hydrous zirconium oxide was found to have an enormous "capacity" for fluoride. This was illustrated by the following experiment. A small column was prepared containing 0.635 g of the oxide (firing temperature 200°C). The column was prewashed with ammonia and water, after which a 0.1 *M* HF solution was added. Fluoride breakthrough occurred only after addition of 49 ml of this solution; this addition corresponds to an uptake of 7.7 moles F^- per kilogram. Only when fluoride breakthrough occurred did the effluent also contain zirconium, as determined radiometrically.

19.3.3 Use of Hydrous Zirconium Oxide in Chromate Analysis

It had been found earlier[1] that chromate adsorption on zirconium oxide is rapid, that the apparent capacity is high, and that, furthermore, chromate can be eluted relatively efficiently with base. In a typical experiment, 2 ml of a 0.01 *M* Cr(VI) solution in 1 *M* HCl was added to a 0.12 $cm^2 \times 2.2$ cm column of hydrous oxide. Chromium(VI) adsorbed in a relatively narrow, sharp, yellow band at the top of the column. After washing with water, elution was carried out with 1 *M* NaOH. Within 0.7 ml of effluent more than 95% of the Cr(VI) was removed. It might therefore be expected that hydrous zirconium oxide would be an acceptable adsorbent for chromates and that it could be used in chromate analysis. The anion-exchanging oxides such as hydrous ZrO_2 might have some advantages over standard organic anion exchangers in chromate analyses, since they should be insensitive to attack by this oxidizing agent and errors from reduction of Cr(VI) to Cr(III) should be small. Further, they should also withstand attack from more powerful oxidizing agents which might be added to effect oxidation of Cr(III) to Cr(VI) in preparation for the analysis.

The problem of analyzing for Cr(VI) in the presence of large amounts of Zr(IV) was presented by the Analytical Chemistry Division. The use of hydrous zirconium oxide for this analysis was investigated. Using 0.1 *M* Zr(IV) solutions containing 0.01 *M* Cr(VI), it was found that in 1 *M* HCl all the Cr(VI) could be adsorbed, together with considerable amounts of Zr(IV). However, the Zr(IV) did not elute with base, affording a clean separation of Cr(VI) from Zr(IV). More than 95% of the Cr(VI) could be recovered in 3 column volumes of 1 *M* NaOH. There was tailing of the remaining Cr(VI).

Preliminary work with hydrous titanium and tin oxides showed similar results: good separation from Zr(IV), good elution of the bulk of the Cr(VI), and tailing of the last few per cent of Cr(VI). At present, these oxides show no obvious advantage over zirconium oxide in the analysis for chromate.

19.3.4 Acid-Base Titrations: Anion-Exchange and Cation-Exchange Properties

As shown in earlier quarterly reports,[1,2] zirconium oxide shows interesting anion-exchange properties in acidic solutions and cation-exchange properties in basic solutions. In an attempt to evaluate the importance of these two phenomena as a function of pH, acid-base titrations of the oxides were carried out, together with radiometric measurements of sodium uptake (Na^{22}). At the same time it was hoped that this type of titration might become useful for the characterization of various oxides. It was found that the uptake of

[2] K. A. Kraus *et al.*, *HRP Quar. Prog. Rep. July 31, 1955*, ORNL-1943, p 246–251.

chloride ions decreased relatively rapidly with increasing pH and essentially vanished near pH 8. Sodium uptake, on the other hand, became noticeable near pH 6 and increased continuously to pH 12, the highest pH investigated. Near pH 7 sodium uptake and chloride uptake appeared to be approximately equal, although small, suggesting that this is the isoelectric point of the solid.

19.4 HYDROUS STANNIC AND THORIUM OXIDES

19.4.1 Acid-Base Titrations: Anion-Exchange and Cation-Exchange Properties

Acid-base titrations in the presence of sodium tracer were also carried out for hydrous oxides of Sn(IV) (firing temperature 105°C) and Th(IV) (firing temperature 105°C). The technique was essentially the same as that described for zirconium oxide. The results for SnO_2 were very similar to those for ZrO_2; that is, there was decreasing adsorption of chloride ions with increasing pH and increasing adsorption of Na^+. However, the curves differed in significant detail, most striking being the fact that chloride uptake became equal to sodium uptake near pH 4.8 for Sn(IV), in contrast to pH 7 for Zr(IV).

The titration curves for thorium oxide differed widely from those for the oxides of Zr(IV) and Sn(IV). Loss of chloride with increasing pH was slower for Th(IV), and sodium uptake was quite small, even at pH 12. Presumably this type of titration curve reflects the differences in the amphoteric properties of these oxides; the results are in agreement with the usual assumption that Th(IV) tends much less towards amphoteric character than either Zr(IV) or Sn(IV).

19.4.2 Dispersions of Hydrous Thorium Oxides: Degree of Polymerization

In an earlier quarterly report,[3] preparation of a Th(IV) oxide quite soluble in water (of the order of 1 kg or more of Th(IV) per kilogram of water) was discussed. The material was prepared by precipitating hydrous thorium oxide from thorium chloride solutions, filtering with little washing, and heating the precipitate overnight at 300°C. Heating at higher or lower temperatures (e.g., 200 or 400°C) or modifying the procedure in other ways (e.g., precipitating from excess thorium chloride) drastically decreased dispersibility. Similar materials can be prepared from Th(IV) nitrate solutions at somewhat lower drying temperatures. Although none of these dispersions was stable under prolonged heating at 250°C, further study seemed warranted.

Equilibrium ultracentrifugations of "solutions" [0.025 *M* Th(IV)] containing the very soluble material prepared from chloride were carried out in water and 1 *M* NaCl. The results indicated a polydisperse distribution of polymers, the average degree of polymerization being in the neighborhood of 700. Since results were only slightly higher in the NaCl solution, the charge on the polymer does not seem to be great. Preliminary light scattering measurements in 0.6 *M* NaCl indicated a weight average degree of polymerization of about 1200, in better agreement with equilibrium ultracentrifugation than could be expected at this time.

It seemed of interest to compare the molecular weight of the soluble material with the molecular weights of oxides which were less readily dispersed. Comparisons were made by velocity ultracentrifugations. The sedimentation constant of the "soluble" material was compared with those of oxides (1) prepared from the nitrate, heated to 250°C, and (2) prepared in the presence of excess thorium chloride and heated to 300°C. All sedimentation constants were found to be about the same (about 5×10^{-12}). The range of error in this figure is large, since these systems are not ideal for this type of study, but there does not seem to be any great dependence of dispersibility on average molecular weights.

[3] K. A. Kraus *et al.*, *HRP Quar. Prog. Rep. April 30, 1955*, ORNL-1895, p 197–200.

20. RADIATION STUDIES OF THORIUM NITRATE SOLUTIONS

C. J. Hochanadel

J. W. Boyle H. A. Mahlman

Gas yields[1,2] of hydrogen, oxygen, and nitrogen from reactor-irradiated thorium nitrate solutions have been reported previously. The extent of the radiation-induced back reaction between nitrogen and oxygen to re-form nitrate is now under study with the use of a metal bomb[3] similar to the bombs used by the HRP Radiation Corrosion Group. If a steady-state pressure exists below 3000 psi, it will be evident from the measurement of the total pressure during the first week of reactor irradiation. Studies will be made at 150, 200, and 250°C to determine the effect of temperature on the back reaction.

The bomb will be platinum-lined, with platinum-rhodium tubing leading from the bomb to eliminate corrosion. The platinum also serves as a catalyst for the recombination of hydrogen and oxygen arising from the radiation decomposition of water. The solution used will be 7 *m* $Th(NO_3)_4 \cdot 2HNO_3$. The excess nitric acid is required to prevent hydrolytic precipitation[4] at the temperatures contemplated.

The necessary measurements[5] of density as a function of temperature and thermal recombination of hydrogen and oxygen in a platinum-lined bomb were completed. Solutions of 7 *m* $Th(NO_3)_4 \cdot 2HNO_3$ are thermally unstable. Red oxides of nitrogen were visible above the liquid when the solution was heated in a sealed glass container. This thermal decomposition resulted in pressures greater than the pressure of pure water and seemed to be reversible on cooling back to room temperature. Additional experiments are necessary to determine the extent of the thermal decomposition.

[1] J. W. Boyle and H. A. Mahlman, *Chem. Semiann. Prog. Rep. Dec. 20, 1954*, ORNL-1832, p 69.

[2] J. W. Boyle and H. A. Mahlman, *Chem. Semiann. Prog. Rep. June 20, 1955*, ORNL-1940, p 61.

[3] F. H. Sweeton, "Effect of Reactor Radiation on the Corrosion of Stainless Steel by Fissioning Solutions," *Radiation Damage Conference, March 23–24, 1953*, ORNL-CF-53-3-276, p 144.

[4] M. H. Lietzke and W. L. Marshall, *Present Status of the Investigation of Aqueous Solutions Suitable for Use in a Thorium Breeder Blanket*, ORNL-1711 (May 15, 1954), p 2.

[5] J. W. Boyle and H. A. Mahlmon, *Chem. Semiann. Prog. Rep. Dec. 20, 1955*, ORNL-2046 (in press).

[redacted]

21. PROTACTINIUM CHEMISTRY

B. Weaver F. M. Scheitlin

21.1 EXTRACTION OF PROTACTINIUM

Extraction of tracer Pa^{233} from HCl solutions by diisobutyl carbinol was compared with previous data, as shown in Table 21.1, for extraction from HNO_3 solutions.

Data were obtained for the extraction of tracer Pa^{233} from various aqueous solutions by 0.1 *M* di(2-ethylhexyl)phosphoric acid in kerosene, which is a good extractant for uranium and also an extractant for thorium; the distribution coefficients are shown below:

Aqueous Solvent	*D* (org/aq)
0.1 *M* HNO_3	31.8
2.0 *M* HNO_3	111
1.0 *M* $Al(NO_3)_3$ (pH 1.7)	267
0.5 *M* citric acid	77
2.0 *M* citric acid	3.9

21.2 COLLODIAL BEHAVIOR OF PROTACTINIUM

Preliminary work was done on investigating the collodial behavior of protactinium at very low concentrations. The concentration levels attainable with tracer Pa^{233} may be too low for separation of colloidal particles. Therefore it may be necessary to use small quantities of Pa^{231} for this investigation. One series of experiments involved filtration of various solutions of tracer Pa^{233} through millipore HA filter papers, which are supposed to retain all particles of greater than 0.5-μ diameter. The following media were used: (1) 0.04 *M* Th and 0.1 *M* HNO_3 at room temperature; (2) solution 1 heated at 80°C for 1 hr and cooled; (3) 1 *M* HCl at room temperature; and (4) solution 3 heated at 80°C for 1 hr and cooled. In no case was there any significant retention on the filter, but in every case there was considerable adsorption of Pa^{233} on glassware.

TABLE 21.1. DISTRIBUTION COEFFICIENTS [*D* (org/aq)] PROTACTINIUM INTO DIBC (100%) FROM HCl AND HNO_3

Molarity of Acid	*D* (org/aq)	
	HCl	HNO_3[a]
1	0.005	0.9
3.5	0.86	32
6	105	160

[a] A. T. Gresky *et al.*, *Progress Report: Laboratory Development of the Thorex Process*, ORNL-1367, p 77 (Dec. 17, 1952).

[redacted]